

MR-HIFU mediated local drug delivery using temperature-sensitive liposomes

Citation for published version (APA):

Smet, de, M. (2013). *MR-HIFU mediated local drug delivery using temperature-sensitive liposomes*. [Phd Thesis 1 (Research TU/e / Graduation TU/e), Biomedical Engineering]. Technische Universiteit Eindhoven.
<https://doi.org/10.6100/IR750278>

DOI:

[10.6100/IR750278](https://doi.org/10.6100/IR750278)

Document status and date:

Published: 01/01/2013

Document Version:

Publisher's PDF, also known as Version of Record (includes final page, issue and volume numbers)

Please check the document version of this publication:

- A submitted manuscript is the version of the article upon submission and before peer-review. There can be important differences between the submitted version and the official published version of record. People interested in the research are advised to contact the author for the final version of the publication, or visit the DOI to the publisher's website.
- The final author version and the galley proof are versions of the publication after peer review.
- The final published version features the final layout of the paper including the volume, issue and page numbers.

[Link to publication](#)

General rights

Copyright and moral rights for the publications made accessible in the public portal are retained by the authors and/or other copyright owners and it is a condition of accessing publications that users recognise and abide by the legal requirements associated with these rights.

- Users may download and print one copy of any publication from the public portal for the purpose of private study or research.
- You may not further distribute the material or use it for any profit-making activity or commercial gain
- You may freely distribute the URL identifying the publication in the public portal.

If the publication is distributed under the terms of Article 25fa of the Dutch Copyright Act, indicated by the "Taverne" license above, please follow below link for the End User Agreement:

www.tue.nl/taverne

Take down policy

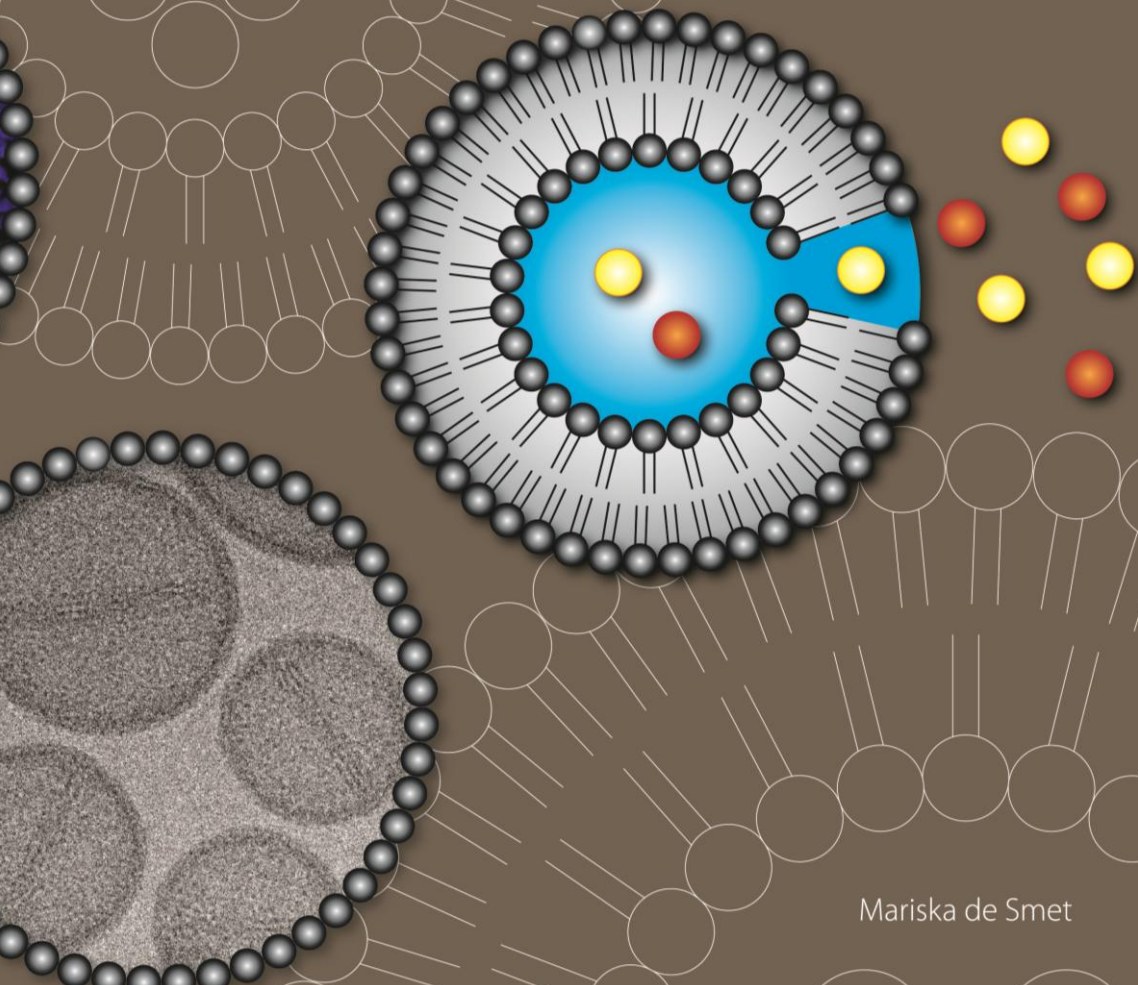
If you believe that this document breaches copyright please contact us at:

openaccess@tue.nl

providing details and we will investigate your claim.

MR-HIFU mediated local drug delivery

using temperature-sensitive liposomes



MR-HIFU mediated local drug delivery using temperature-sensitive liposomes

PROEFSCHRIFT

ter verkrijging van de graad van doctor aan de
Technische Universiteit Eindhoven, op gezag van de
rector magnificus, prof.dr.ir. C.J. van Duijn, voor een
commissie aangewezen door het College voor
Promoties in het openbaar te verdedigen
op donderdag 14 maart 2013 om 16.00 uur

door

Mariska de Smet

geboren te Oostburg

Dit proefschrift is goedgekeurd door de promotor:

prof.dr. H. Grill

Copromotor:

dr. S. Langereis

Committee:

prof.dr. H. Grüll

dr. S. Langereis

prof.dr. C.T.W. Moonen

dr. M.R. Dreher

prof.dr. S. Aime

prof.dr. K. Nicolay

prof.dr. G.C. van Rhoon

prof.dr. P.A.J. Hilbers (chairman)

The financial support by Philips Healthcare and Lipoid for the publication of this thesis is gratefully acknowledged.

This project was funded in part by the EU Project Sonodrugs (NMP4-LA-2008-213706).

Cover design: b-deSign grafische vormgeving

Printed by: Wöhrmann Print Service, Zutphen

A catalogue record is available from the Eindhoven University of Technology Library

ISBN: 978-90-386-3336-7

Contents

Chapter 1:

Introduction: Image-guided local drug delivery using temperature-sensitive liposomes **1**

Chapter 2:

Temperature-sensitive liposomes for doxorubicin delivery under MRI guidance **25**

Chapter 3:

Validation of doxorubicin quantification methods in tissue and blood samples **47**
– a multi-centre comparison

Chapter 4:

Blood kinetics and biodistribution of temperature-sensitive liposomes for MR-image guided drug delivery with High Intensity Focused Ultrasound **71**

Chapter 5:

Magnetic Resonance Imaging of High Intensity Focused Ultrasound mediated drug delivery from temperature-sensitive liposomes; an *in vivo* proof-of-concept study **95**

Chapter 6:

MR-HIFU mediated hyperthermia improves the intratumoral distribution of temperature-sensitive liposomal doxorubicin **117**

Chapter 7:

Therapeutic effect of MR-HIFU mediated local drug delivery using temperature-sensitive liposomes **137**

Chapter 8:

General discussion **153**

Ethical paragraph 167

Summary 168

Acknowledgements 170

List of Publications 173

Curriculum Vitae 177

Chapter 1

Introduction

Image-guided local drug delivery using temperature-sensitive liposomes

1.1 Cancer treatment

Cancer is one of the leading causes of death worldwide and demographic changes towards an aging society will increase its prevalence even further. As a consequence, there is a strong clinical need for improved therapies that have less impact on the patient and/or offer higher therapeutic efficacy. Standard treatments for cancer consist of surgery, radiotherapy, chemotherapy, or a combination hereof, depending on the type and staging of cancer.¹

Surgical removal of a tumor is first line treatment for localized tumors. Surgical resection of solid tumors provides excellent local control and is currently the only curative option for most solid tumors. To minimize the chance for recurrence, the surgeon removes not only the tumor, but also a wide margin of normal tissue. Often surgery is combined with neo-adjuvant or adjuvant chemotherapy and/or radiotherapy, to reduce tumor size before resection or to treat possible residual tumor cells after the surgical procedure. In some cases, surgical removal of the tumor is not feasible, for example for lesions invading into surrounding vital structures or for tumors at places that are impossible to reach by conventional surgery.

Radiotherapy uses high-energy radiation to destroy cancer cells, either delivered by external beams, or by implanted radioactive material. Treatment planning aims to maximize the dose to the tumor, while keeping radiation exposure of healthy tissue minimal to limit side effects. Yet, radiation therapy is in many cases associated with a significant burden to the patient. Additionally, the radiation can also increase the risk for the development of other cancers.

Chemotherapy is a therapeutic option for cancers that are difficult to remove surgically or have metastasized to the rest of the body. The treatment typically involves chemotherapeutic agents that kill cells by interfering for example with cell division and act therefore both on cancerous and normal cells. However, as cancer cells divide more rapidly, tumors are more susceptible to chemotherapy than normal tissue. As cytotoxic chemotherapy usually affects cells that grow and die rapidly such as hair follicles, intestinal cells, and bone marrow cells, considerable side effects arise. Cancer patients may appear bald, experience gastrointestinal symptoms and are prone to infections, bleeding, and anemia, because of reduced counts in white blood cells, red blood cells, and platelets.

Although remarkable progress has been made in cancer therapy, many cancers are still untreatable by these conventional therapies. New cancer treatments to improve the treatment possibilities, treatment efficacy, and reduce the treatment burden on patients need to be investigated. In this thesis a new treatment of tumors using a temperature-sensitive drug delivery system was investigated. The aim was to locally deliver chemotherapeutic drugs at the tumor site, thereby increasing the efficacy and/or reducing the side effects in the rest of the body.

1.2 Local drug delivery

In classical chemotherapy the therapeutic window of low molecular weight cytostatics is limited by the undesired high drug uptake in vital organs. For example, doxorubicin (Figure 1.1) is a widely used chemotherapeutic drug with significant antitumor activity against several human malignancies, including leukemia and breast cancer.^{2, 3} Doxorubicin rapidly redistributes after intravenous injection across the whole body leading to toxicity in healthy organs. The clinical utility of doxorubicin is hampered by cumulative and irreversible cardiotoxicity, myelosuppression, and the occurrence of drug resistance.^{4, 5}

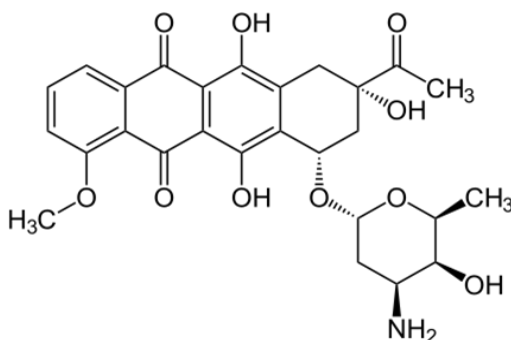


Figure 1.1. Chemical structure of doxorubicin.

New nanomedicines, where the active drug is encapsulated into liposomal nanovesicles of sizes around 100 nm, show significantly reduced acute toxicity by preventing drug uptake in normal tissue.^{6, 7} For instance, sterically-stabilized liposomal doxorubicin formulations (e.g. Caelyx[®]/Doxil[®]) have shown to greatly reduce cardiac toxicity when compared to unencapsulated doxorubicin.^{8, 9} These long-circulating liposomes accumulate in tumor tissue due to extravasation through the leaky vasculature of tumors in combination with the poorly operating lymphatic system exploiting the so-called enhanced permeability and retention (EPR) effect.¹⁰⁻¹² For Caelyx[®], the final drug concentration in the tumor is mainly determined by the plasma concentration, circulation time of the liposomal drug carrier, passive diffusion of the encapsulated doxorubicin through the liposomal bilayer and the pharmacokinetic properties of doxorubicin itself.^{13, 14} Preclinical studies comparing free doxorubicin with liposomal doxorubicin, showed 3- to 15-fold greater peak doxorubicin levels in tumors and enhanced antitumor activity for the liposomal formulations.^{13, 15-17} Clinical studies in patients with Caelyx[®] showed a 16-fold increase in doxorubicin levels in the tumor for liposomal doxorubicin in comparison with the unencapsulated drug.^{10, 18} The liposomal encapsulation consistently showed reduced cardiotoxicity and increased drug uptake in the tumor. However, the anti-tumor activity of Caelyx[®] in the clinical setting seems to be dependent on the kind of tumor and the treatment protocol. Some clinical studies observed an increase in

anti-tumor activity,¹⁹ while others found a comparable efficacy for liposomal doxorubicin versus the unencapsulated cytostatic.²⁰⁻²² Obviously, the increased drug concentration does not directly translate into an improvement of antitumor efficacy due to the limited bioavailability, as doxorubicin stays within the liposomal nanocarrier.

1.3 Temperature-sensitive liposomes

Localized triggered drug delivery from responsive liposomal formulations holds great promise to further increase the drug concentration and its bioavailability in the tumor. For instance, temperature-sensitive liposomes (TSLs) are able to release encapsulated molecules near their phase transition temperature (T_m), where the lipid membrane shows a transition from a gel to a liquid crystalline phase.²³⁻²⁵ The first pioneering work to prove the function and utility of TSLs as drug carriers for triggered delivery was reported by Yatvin, Weinstein and coworkers.^{23,26} After the intravenous injection of TSLs, release of the liposomal contents could occur during passage of liposomes through the heated tumor region (Figure 1.2). Using TSLs containing methotrexate and microwave induced hyperthermia of subcutaneous Lewis lung tumors on mouse flanks they found a 3.6 times increase in drug concentration in the heated tumors relative to the unheated controls. With these early experiments they demonstrated the potential for TSLs in localized drug delivery.

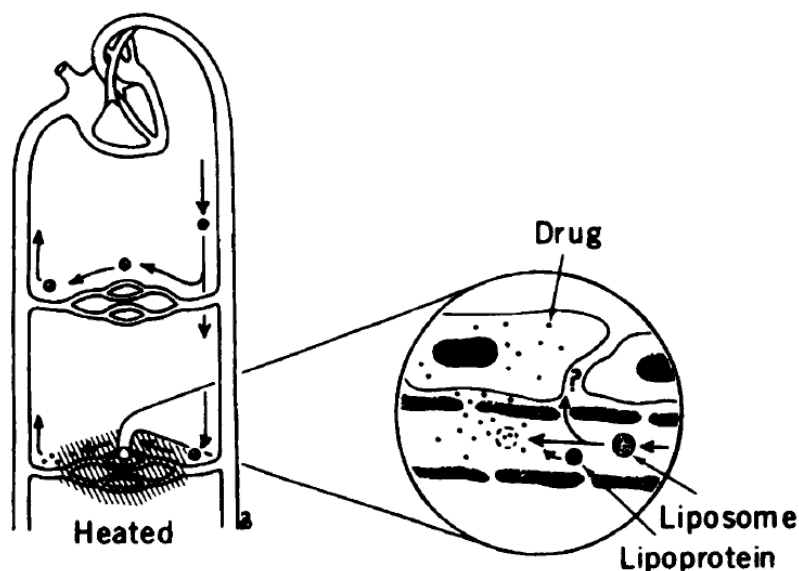


Figure 1.2. Principle of local drug delivery using temperature-sensitive liposomes.

Reprinted with permission from reference.²⁶

The liposomes used by Yatvin and Weinstein were prepared from two lipid components: DPPC (dipalmitoyl phosphatidylcholine) and DSPC (distearoyl phosphatidylcholine) (Figure 1.3). DPPC was responsible for the temperature sensitivity, because of its phase transition temperature at 41.5 °C, while DSPC was used to improve its stability at 37 °C and to fine tune the transition temperature of the liposomal membrane. Using a DPPC: DSPC ratio of 3:1 resulted in release in the range of 42.5-44.5 °C. However, this formulation was not yet optimal, because of poor blood circulation times and slow release kinetics.

Various strategies have been developed to prevent the fast clearance by the reticuloendothelial system (RES) by coating the surface of the liposomes.^{13, 27} The basic concept is to hinder access and binding of blood plasma opsonins to the liposome surface, and therefore to prevent interactions of the liposomes with the RES macrophages. The first strategy studied was the preparation of liposomes modified with gangliosides, such as monosialoganglioside (G_{M1}).²⁸ Inclusion of 6 mol% G_{M1} significantly increased blood levels of DPPC/DSPC liposomes, with 80 % found in the blood after 0.5 h versus 10% for the same formulation without G_{M1} .²⁹ Another investigated polymer for increasing the blood circulation time of liposomes is poly(ethylene glycol) (PEG) (Figure 1.3).³⁰ The advantages of PEG are that the molecular weight and structure can be modulated for specific purposes and it is easy to conjugate with the liposomal phospholipids. Therefore, it has been widely used as polymeric steric stabilizer on different liposomal systems.

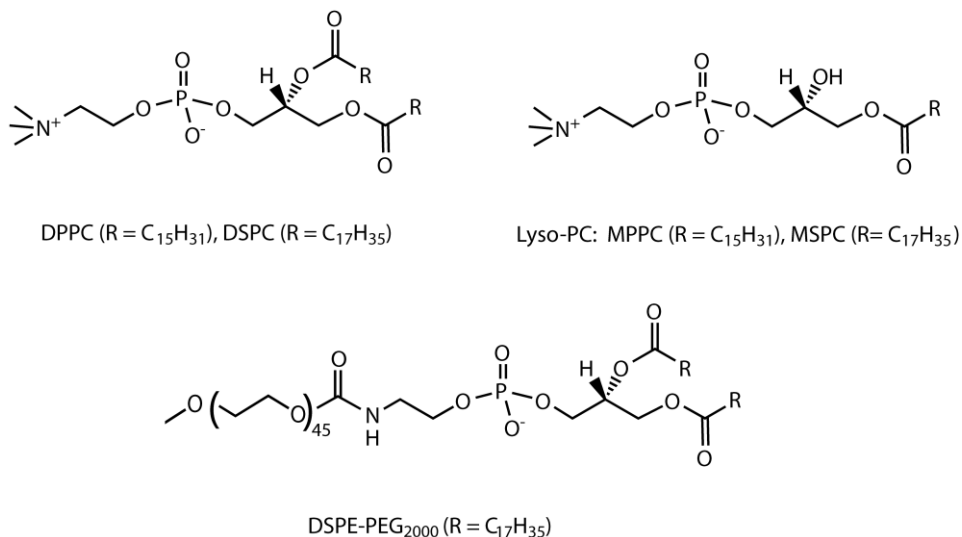


Figure 1.3. Chemical structures of phospholipids used for preparation of TSLs.

Another interesting finding for the improvement of temperature-sensitive liposomes was that the incorporation of lysolipids into the liposomal membrane, such as MPPC (1-palmitoyl-*sn*-glycero-3-phospho-choline) or MSPC (1-stearoyl-*sn*-glycero-3-phospho-choline) (Figure 1.3),

leads to a more rapid release of the encapsulated contents.³¹⁻³⁴ Traditional temperature-sensitive liposomal formulations without lysolipids, *e.g.* consisting of only DPPC, show a slight increased permeability at T_m , due to mismatches between liquid and solid chains at the grain boundaries (Figure 1.4 and 1.5).³⁴ Grain boundaries in lipid bilayers are planar defects due to the imperfect crystalline arrangement of the molecules. Continued heating past T_m leads to, after a slight drop, further increased membrane permeability, due to high permeability of the purely melted bilayer (Figure 1.5).³³ When the temperature of a lysolipid containing liposome, *e.g.* DPPC:MSPC (90:10), is raised to T_m , the lysolipids are free to diffuse into the grain boundary regions. Due to the tendency of these lysolipids to form highly curved micelles, this presumably results in the formation of transient pores in the lipid bilayer. These pores formed by lysolipids can also be stabilized by PEG-lipids present in the liposomal formulation (Figure 1.4B). Due to this mechanism, the drug release from lysolipid-containing TSLs around T_m is extremely fast (Figure 1.5), showing complete release within a few seconds. However, at temperatures above T_m , the permeability of the purely melted bilayer is recovered.

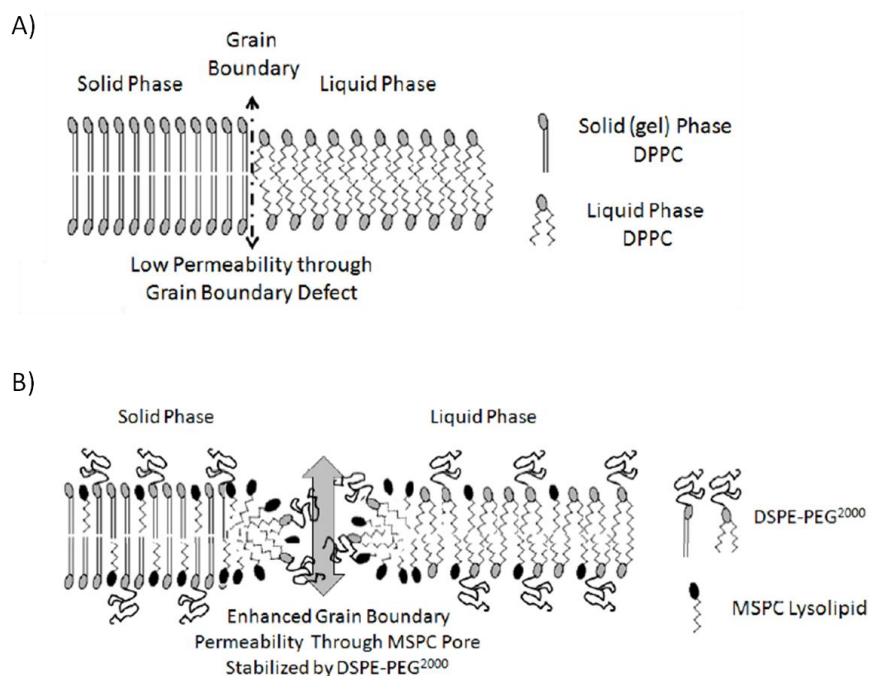


Figure 1.4. Schematic representation of effects that result in membrane permeability upon heating. A) DPPC bilayer in phase transition region. B) DPPC:MSPC:DSPE-PEG bilayer in phase transition region with enhanced permeability through MSPC pore stabilized by DSPE-PEG. Figure adjusted from Landon *et al.*³⁴

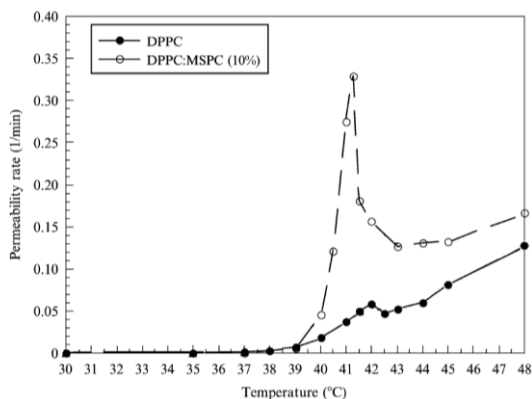


Figure 1.5. Dithionite ion permeability rates at different temperatures for liposomes with and without lysolipids: DPPC:DSPE-PEG2000 (96:4) and DPPC:MSPC:DSPE-PEG2000 (86:10:4). Figure adjusted from Mills and Needham.³³

To compare traditional temperature sensitive liposomes (TTSL) with lysolipid-containing low-temperature sensitive liposomes (LTSL), preclinical studies were performed to investigate tumor drug uptake after liposome injection combined with heating. Kong *et al.* found that LTSL achieved a 3.6-fold higher doxorubicin concentration of 25.6 ng/mg, versus 7.2 ng/mg for the TTSL, in homozygous NCr athymic nude mice, immediately after heating of the subcutaneous FaDu tumor-bearing leg for 1 hour to 42 °C.³² More recently, Al Jamal *et al.* compared the two liposomal formulations by studying the doxorubicin concentrations in B16F10 tumors at 1 and 24 hours after TSL injection followed by water bath heating of the tumor bearing leg.³⁵ In this study, a higher doxorubicin concentration for the LTSL was found at 1h after injection of 6.7 %ID/g in comparison with 2.8 %ID/g for TTSL. However after 24h, the TTSL resulted in a high doxorubicin uptake of 13.5 %ID/g, while the LTSL only had 2.8 %ID/g in the tumor.

Various liposomal formulations were tested in preclinical studies investigating the therapeutic effect of hyperthermia-mediated doxorubicin delivery with TSLs (Table 1.2). The majority of these studies were performed with the LTSL formulation. In seminal work by Kong and Needham, the therapeutic effect was investigated using a single dose of 5 mg/kg doxorubicin encapsulated by LTSL. One study showed local control for 6 out of 9 treated tumors, while in the second study 100% of the 11 treated tumors showed complete regression.^{32,36} Other studies using a similar liposomal formulation but different heating methods and tumor models showed smaller effects on the tumor growth.^{37,38} Yarmolenko *et al.* tested the therapeutic effect of LTSL + heat in five different tumormodels.³⁹ SKOV-3 was the most sensitive tumor model; 50% of the tumors reached 5x the initial volume in 60 days. In this study, the FaDu tumor model as used by Kong and Needham in previous

studies was tested as well, but although the injected dose was higher (6-7 mg/kg vs 5 mg/kg) the 100% complete regression (11 out of 11) was not achieved in this study. Slight modifications of the LTSL formulation and/or resistance to doxorubicin of the FaDu tumor evolved through successive passages were mentioned as possible explanations for this different result.

Table 1.2. Overview of preclinical therapeutic studies performed with doxorubicin-loaded temperature sensitive liposomes. STI = Survival Time Increase is defined as the difference in survival time between treated (TSL+hyperthermia) and control tumors (saline injection or no treatment). TGD = Tumor Growth Delay is defined as the difference in time to reach a certain tumor size between treated (TSL+hyperthermia) and control tumors (saline injection or no treatment). Table partly based on the review from Kong *et al.* ⁴⁰

Ref.	Liposomal Formulation	Tumor model	Hyperthermia protocol	Therapeutic effect
Zou <i>et al.</i> ⁴¹ 1993	DPPC	W256 carcino-sarcoma (rat liver)	42 °C for 6 min, 2h after injection (emission plate)	STI ≈25%
Marayuma <i>et al.</i> ²⁹ 1993	DPPC/DSPC GM1/DPPC/DSPC	C26 tumor (mouse)	42 °C for 20 min	STI ≈11 days STI ≈ 17 days
Ning <i>et al.</i> ⁴² 1994	HSPC/Chol/ α-tocopherol	RIF-1 (mouse)	42 °C for 30 min (waterbath and ultrasound)	TGD ≈ 6 days
Huang <i>et al.</i> ⁴³ 1994	PEG/DSPE/HSPC/ Chol/ α-tocopherol	C26 tumor (mouse)	42 °C for 30 min (MW ring radiator)	STI ≈27%
Unezaki <i>et al.</i> ⁴⁴ 1994	DPPC/DSPC DPPC/DSPC/ PEG1000 DPPC/DSPC/ PEG5000	C26 tumor (mouse)	42 °C for 20 min (RF oscillator)	STI ≈ 11 days STI ≈ 17 days STI ≈ 15 days
Kong <i>et al.</i> ³² 2000	LTSL TTSL	FaDu tumor (mouse)	42 °C for 1h (waterbath)	66% cure (6/9) 8% cure (1/12)
Needham <i>et al.</i> ³⁶ 2000	LTSL TTSL	FaDu tumor (mouse)	42 °C for 1h (waterbath)	100% cure (11/11) 10% cure (1/10)
Dromi <i>et al.</i> ³⁷ 2007	LTSL	JC adenocarcinoma (mouse)	41-42 °C for 15-20 min (pulsed-HIFU)	TGD ≈ 6 days
Ponce <i>et al.</i> ³⁸ 2007	LTSL (Mn + dox)	FSA-1 tumor (rats)	38.5-46 °C for 1h (catheter with heated water)	29% cure (2/7) TGD ≈ 26 days
Hauck <i>et al.</i> ⁴⁵ 2006	LTSL	Spontaneous tumors (dogs)	44 °C (median T) for 1.5h (MW applicator)	Response rate = 30%
Yarmolenko <i>et al.</i> ³⁹ 2010	LTSL	4T07 (mouse) HCT116 (mouse) FaDu (mouse) PC-3 (mouse) SKOV-3 (mouse)	42 °C for 1h (waterbath)	TGD≈12days (0% cure) TGD≈17days (5% cure) TGD≈27days (10% cure) TGD≈34days (33% cure) TGD≈37days (20% cure)
Tagami <i>et al.</i> ⁴⁶ 2011	Brij-liposomes LTSL	EMT-6 tumor (mouse)	40-43 °C for 1h (waterbath)	50% cure 25% cure

Nowadays, the lysolipid-containing liposomal formulation produced under the trade name Thermadox[®] (Celsion) is investigated in ongoing clinical trials. The Celsion phase I clinical trial for patients with primary and metastatic tumors of the liver is now completed. In this study, patients were treated with a combination of RF ablation and Thermadox[®].^{34,47,48} The trial outcome shows that the combination of RF ablation and Thermadox[®] was safe and likely more efficacious than RF ablation alone. As a result, a global phase III clinical trial was initiated treating hepatocellular carcinoma patients with RF ablation and Thermadox[®]. Additionally, in ongoing phase I and phase II clinical trials, Thermadox[®] is combined with superficial microwave hyperthermia for local breast cancer recurrence.³⁴

1.4 Hyperthermia

Besides the use of heat to trigger the drug release from temperature-sensitive liposomes, local mild hyperthermia of tumor tissue has more favorable effects. Several studies demonstrated a significant enhancement in the tumor treatment efficacy when hyperthermia was combined with chemotherapy. *In vitro*, for some drugs (e.g. cisplatin) enhanced responses were found to be linear with increasing temperatures from 39 to 43 °C.⁴⁹ Another class of drugs, under which doxorubicin, became more effective only above a threshold temperature of 42 °C.⁵⁰ Additionally, the order in which the drug and heat are administered can have an effect on this interaction, with the optimum enhancement occurring when heat and drug are given simultaneously.⁵¹ *In vivo*, Overgaard has demonstrated that simultaneous heat and doxorubicin increases doxorubicin antitumor effect at 41.5 °C in a mouse model.⁵² A major contribution to the field was the clinical study from Issels *et al.*, showing that regional hyperthermia acts synergistically with neo-adjuvant chemotherapy for the treatment of localized soft tissue sarcoma.⁵³ Patients showed an increased response rate (28.8% vs 12.7%) and were less likely to experience progression (6.8% vs 20.6%) with chemotherapy (EIA: etoposide, ifosfamide, adriamycin (=doxorubicin)) and hyperthermia in comparison with chemotherapy alone. These findings are promoting the action of hyperthermia as an adjuvant to the chemotherapeutic drug. The observed synergistic effects may originate from an increased blood flow, an enhanced permeability of the tumor (micro) vasculature, enhanced extravasation of drugs, the expression of heat shock proteins, inhibition of DNA repair and/or the stimulation of immune responses.^{11, 34, 54-58} However, these studies are not a targeted delivery approach, therefore the systemic exposure to the drugs is not reduced and a similar level of toxicity may be expected.

In the case of liposomal chemotherapy, some additional aspects of hyperthermia may have a positive contribution. Figure 1.6 gives an overview of all the different aspects how hyperthermia may contribute to the therapeutic effects when combined with temperature-sensitive as well as non-temperature sensitive liposomes. Non-temperature sensitive liposomal formulations benefit from hyperthermia thanks to an increased

extravasation from the vascular compartment and subsequent accumulation into the interstitial space.^{40,56,59} These accumulated liposomes will slowly release the drug throughout the tumor over a longer time period, resulting in higher drug concentrations present at the tumor site. For temperature sensitive liposomes, hyperthermia triggers intravascular release of the drug payload, leading to high peak concentrations with directly bioavailable drugs. Preclinical experiments with doxorubicin-loaded temperature-sensitive systems in combination with an externally applied regional temperature increase clearly showed an improved efficacy of temperature-induced drug delivery.^{29,32,36-38,44,46,60-63} In these studies, hyperthermia was applied during the first hour after injection of the temperature-sensitive liposomal formulation of doxorubicin, resulting in a rapid release of the drug in the tumor microvasculature and subsequent uptake by the tumor cells. Both the intravascular release of doxorubicin from temperature-sensitive liposomes and the increased accumulation of doxorubicin-filled liposomes may have an important contribution to the therapeutic outcome of temperature-triggered local drug delivery.

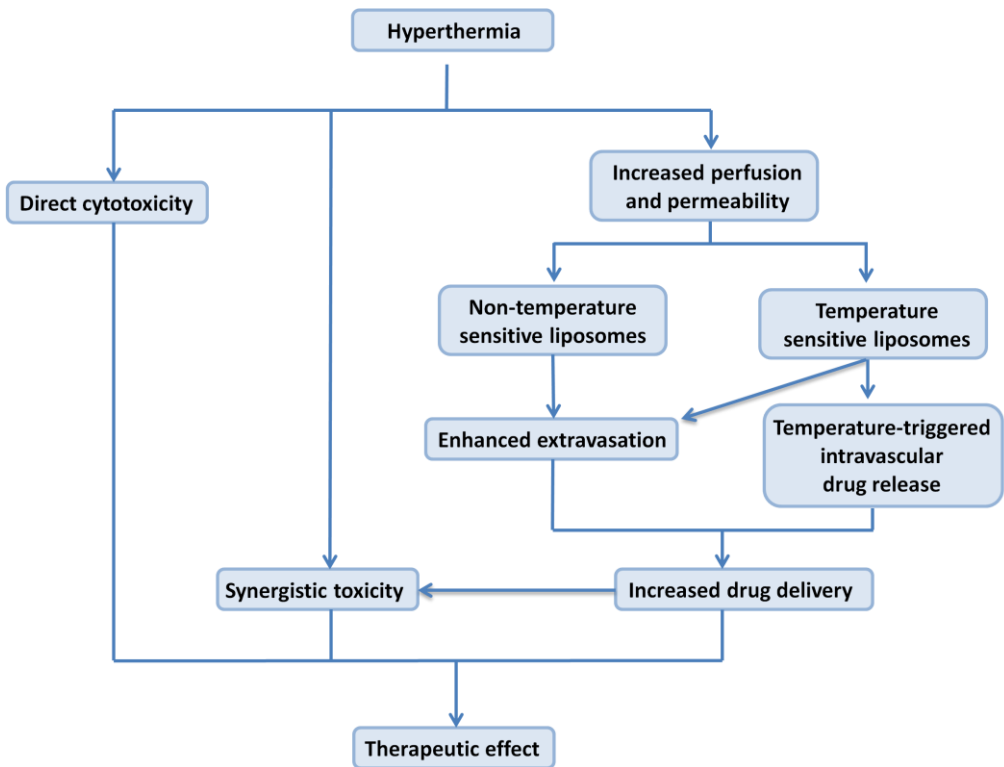


Figure 1.6. Flow diagram depicting the multifactorial therapeutic benefits of hyperthermia. Based on Kong and Dewhirst.⁴⁰

1.5 High Intensity Focused Ultrasound (HIFU) for drug delivery

In the clinic, different methods are available to induce hyperthermia, under which the use of radiofrequency applicators,^{64,65} microwave applicators^{66,67} and hot water baths.^{68,69} Drawbacks of these methods are the lack of spatial and temporal accuracy and/or the limited penetration depth. Several of these shortcomings can be addressed with Magnetic Resonance-guided High Intensity Focused Ultrasound (MR-HIFU), which is an emerging non-invasive technology to apply accurate deep local thermal therapies in oncology (Figure 1.7). Here, a therapeutic ultrasound transducer is used to focus ultrasound into a small focal volume at the specific target locations inside the body. The ultrasound transducer is integrated into the patient bed of an MRI scanner, enabling the acquisition of MR images with excellent soft tissue contrast for therapy planning and spatial guidance. Additionally, MR-based temperature maps serve as an input for providing direct feedback to the ultrasound control unit.⁷⁰⁻⁷² This MR-HIFU technology platform is currently clinically evaluated for thermal ablation of uterine fibroids and for palliative treatment of bone metastasis, but has potential applications in temperature-induced local drug delivery at mild hyperthermia ($T \approx 42\text{ }^{\circ}\text{C}$).^{37, 73, 74}

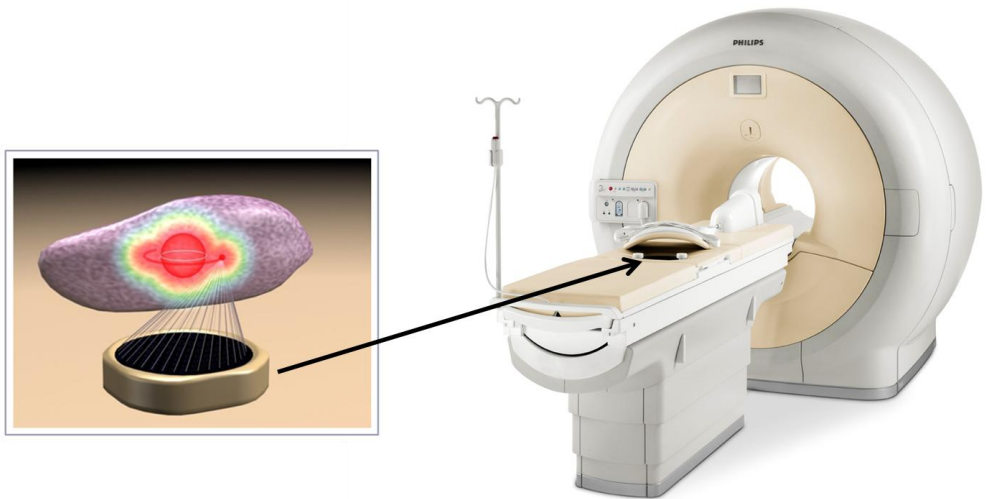


Figure 1.7. High Intensity Focused Ultrasound for local heating of tissue. MRI can be used for therapy planning as well as for dynamic mapping of the temperature change, providing direct feedback to the ultrasound control unit.

Various preclinical studies were published showing HIFU-induced drug delivery in different animal models (Table 1.3). The first study, reported in 2007, used pulsed HIFU for temperature-triggered drug delivery.³⁷ Ultrasound-induced hyperthermia was performed for 2 min per raster point (a typical exposure for an entire tumor was 15 to 20 min), either directly or 24h after the injection of ThermoDox®. When HIFU-induced hyperthermia was performed 24h after the injection, no increase of the doxorubicin concentration in the tumor could be detected in comparison with the unheated tumors. This implies that the liposomes were cleared from the blood within 24 hours and/or that drug release from these liposomal systems already occurred at physiological temperatures. On the other hand, HIFU-induced heating directly after injection resulted in a 3 to 4-fold increased doxorubicin concentration in the tumor in comparison to the experiment without hyperthermia. Additionally, this treatment schedule significantly reduced tumor growth compared to non-temperature sensitive liposomal doxorubicin and saline control groups.

Staruch *et al.* published three studies about temperature-induced drug delivery of doxorubicin using ThermoDox® in New Zealand rabbits; in muscle, in bone and in VX2 tumors. For heating, a focused US transducer was used that was mechanically scanned to cover the entire target region.⁷⁵ MRI provided temperature maps as a feedback for power control to maintain a target temperature of 43 ± 1 °C over a time span of 25 min. A 15-fold increase of doxorubicin was observed in heated compared with unheated muscle. In 4 out of 10 studies, however, partial thermal ablation of the muscle tissue was observed, due to imperfect temperature control. In a follow-up study they demonstrated the feasibility of localized drug delivery in bone. Temperatures of 43 °C were generated in a 10-mm-diameter circular region at a bone interface and were maintained for 20 min based on MR imaging temperature measurements in adjacent soft tissue. With this method they achieved a 8.2-fold drug increase in heated versus unheated bone marrow.⁷⁶ Finally, they found a 26.7 times doxorubicin increase in VX2 tumors due to heating.⁷⁷ However, the adjacent muscle showed an increase in doxorubicin uptake with a factor of 22.2. The enhancement in heated over unheated muscle stresses the importance of localized hyperthermia to prevent unwanted drug release in normal tissues. Interestingly, Ranjan *et al.* performed drug delivery in the same rabbit tumor model using the same liposomal formulation, but with a clinical MR-HIFU system. They found only a 3.4 fold increase in doxorubicin within the heated compared to unheated tumors.⁷⁸ A reasonable explanation for this discrepancy is that they only heated a 4 mm diameter tumor region to 40-41 °C, while Staruch *et al.* heated 10 mm regions to 43 °C.

Overall, all the reported preclinical studies performing HIFU-mediated drug delivery using temperature-sensitive liposomes provide promising data, showing significant increase in drug concentrations within the target tissue.

Table 1.3. Overview of tissue concentration of doxorubicin (dox) in temperature-induced drug delivery from ThermoDox[®] using HIFU. In most cases, exact dox concentrations were not reported, therefore the numbers are extracted from the published graphs. Table adapted from Gröll *et al.*⁷⁹ ID=injected doxorubicin dose in mg/kg.

Ref.	Tissue	Hyperthermia protocol	ID	[dox] ($\mu\text{g/g}$ tissue)			
				Time p.i	+ HIFU	- HIFU	Factor
Dromi <i>et al.</i> ³⁷	Mouse tumor (mammary adenocarcinoma)	15-20min, temp.elevation 4-5°C	2.0	15-20 min 24h	3.5 1.8	1.5 1.8	2.3 1.0
Staruch <i>et al.</i> ⁷⁵	Rabbit muscle	20 min at 43°C	2.5	2h	8.3	0.5	17
Ranjan <i>et al.</i> ⁷⁸	Rabbit tumor (VX2)	3×10 min at 40.5±0.1 °C	5.0	4h	30	8.8	3.4
Staruch <i>et al.</i> ⁷⁶	Rabbit muscle & bone marrow	20 min at 43°C	2.5	2h	30 40	2 5	16.8 8.2
Staruch <i>et al.</i> ⁷⁷	Rabbit tumor Rabbit muscle	20 min at 43°C	2.5	2h	75 15	3 0.7	26.7 22.2

1.6 Image-guided drug delivery

Besides improving the TSL systems and local heating strategies, monitoring of the drug release process during the treatment can provide useful information. Therefore, the encapsulation of MRI contrast agents (CAs) in the aqueous lumen of TSLs together with the drug holds great promise for drug delivery under MR image guidance (Figure 1.8). The release of the CAs at temperatures near T_m provides a distinct change in the MR signal that enables the visualization of the CA release.⁸⁰⁻⁸⁶ When drug and CA release occurs simultaneously, the observed MRI contrast change can be used for quantification of the drug release. This concept is termed 'chemodosimetry' or 'dose painting'.

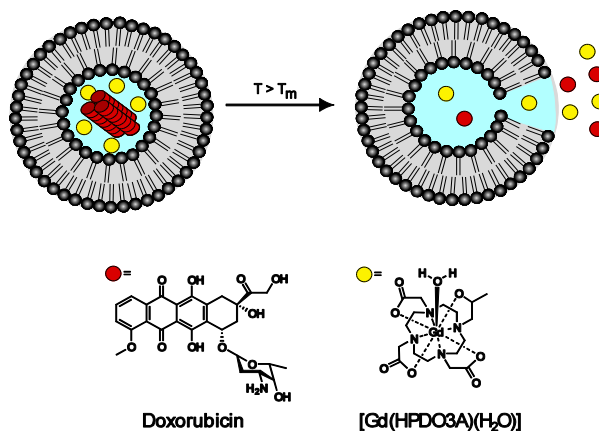


Figure 1.8. TSLs for MR image guided drug delivery, co-encapsulating the chemotherapeutic drug doxorubicin and the MRI contrast agent [Gd(HPDO3A)(H₂O)].

Temperature-sensitive liposomes encapsulating both doxorubicin and manganese have been reported previously^{87, 88} and were investigated for MR image-guided drug delivery *in vivo*.^{38, 89, 90} The advantages of this approach are that Mn^{2+} forms a non-covalent dimer with doxorubicin inside the liposomes, resulting in a decrease of the apparent longitudinal relaxivity r_1 and ensuring the simultaneous release with the drug. After release from the TSL, Mn^{2+} interacts with negatively charged phospholipids in tissue leading to an increase in the r_1 .⁹¹ Additionally, this interaction of Mn^{2+} with tissue prevents washout of the contrast agent, creating a large time span for imaging after the local release has occurred. Viglianti *et al.* demonstrated the co-release of Mn^{2+} with doxorubicin from TSLs in a subcutaneous rat tumor model, where the tumor was heated invasively using a catheter.⁹⁰ The change in T_1 according to MRI showed a good correlation with the doxorubicin concentration in the tissue as determined with HPLC, thereby demonstrating MRI-based quantification of doxorubicin release (Figure 1.9). Although Mn^{2+} was the first MRI contrast agent proposed for use in image guided drug delivery, a major drawback is its cellular toxicity, which slowed down the development of Mn^{2+} -based MRI contrast agents.⁹²

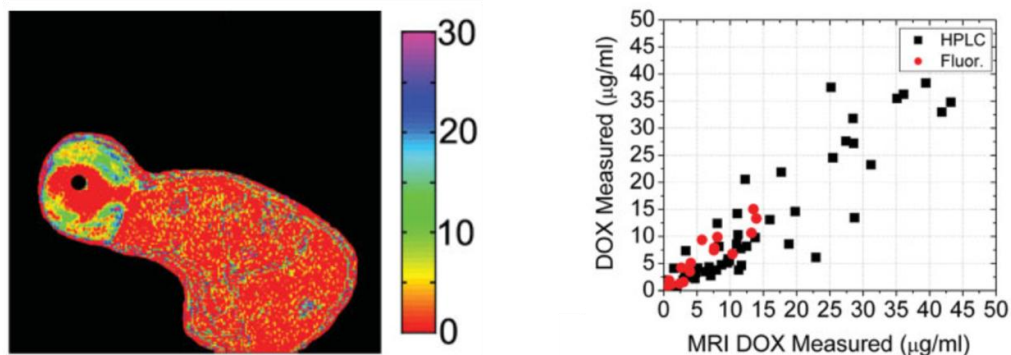


Figure 1.9. MRI-based quantification of temperature-induced release of doxorubicin from temperature-sensitive liposomes based on co-release of paramagnetic Mn^{2+} . Left: The calculated doxorubicin concentration (ng/mg) on a pixel-by-pixel basis. Right: Dox concentrations measured with HPLC vs MRI. Reprinted with permission from reference.⁹⁰

Alternatively, clinically approved paramagnetic MRI contrast agents have been co-encapsulated with doxorubicin in TSLs. Negussie *et al.* studied the temperature-dependent release kinetics *in vitro* in buffer, plasma and gel phantoms of imageable TSLs (iTSLs) loaded with doxorubicin and [Gd(HPDO3A)(H₂O)] (Prohance[®]).⁹³ *In vivo*, MR signal increase was observed after iTSL injection and MR-HIFU-heating in a VX2 tumor model, however, no doxorubicin was quantified in the HIFU-treated tissue. Another temperature-sensitive liposomal formulation consisting of DPPC and Brij78 and co-encapsulating Gd-DTPA and doxorubicin was investigated by Tagami *et al.*⁶⁰ Also for these liposomes, T_1 response after injection combined with waterbath heating of the tumor-bearing leg quantitatively correlated with the doxorubicin uptake of the tumors. Furthermore, the extent of T_1 relaxation enhancement in the heated tumor successfully predicted the antitumor efficacy in a EMT-6 tumor model in mice (Figure 1.10).

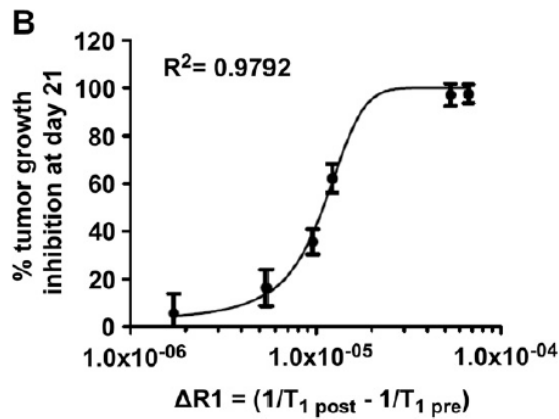


Figure 1.10. Correlation between antitumor efficacy and tumor T_1 immediately after the treatment.⁶⁰

1.7 Aim of this thesis

In this thesis, temperature-sensitive liposomes co-encapsulating doxorubicin and $[Gd(HPDO3A)(H_2O)]$ are investigated for the use of MR image-guided HIFU-mediated local drug delivery. A schematic representation of this approach is shown in Figure 1.11.

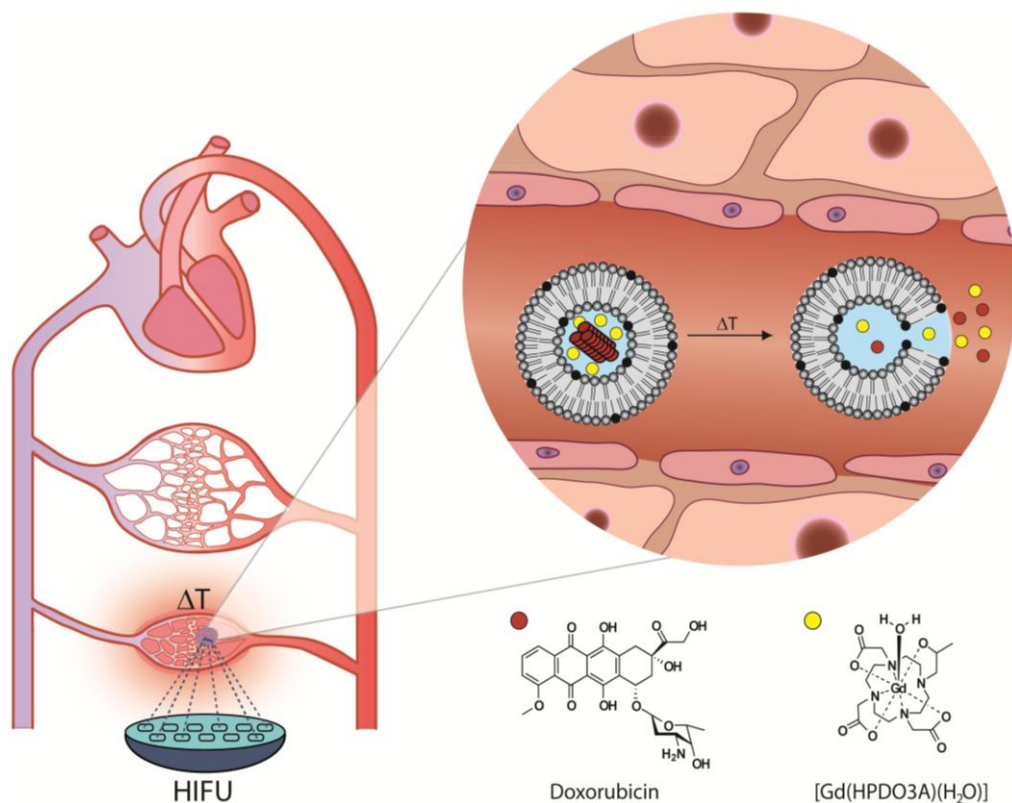


Figure 1.11. MR image-guided HIFU-induced hyperthermia-triggered drug delivery using temperature-sensitive liposomes encapsulating doxorubicin and $[Gd(HPDO3A)(H_2O)]$.

In Chapter 2, the preparation and *in vitro* characterization of three different liposomal formulations co-encapsulating doxorubicin and [Gd(HPDO3A)(H₂O)] are discussed. The stability and temperature-induced release of the contents from the aqueous lumen of liposomes were studied *in vitro* in great detail.

In Chapter 3, two different methods for quantification of doxorubicin in blood and tissue samples were setup and compared. One is based on the quantification of doxorubicin fluorescence with High Performance Liquid Chromatography (HPLC) after chemical extraction. The other method requires the use of ¹⁴C-labeled doxorubicin, which is a β -emitter that can be quantified with Liquid Scintillation Counting.

In Chapter 4, the blood kinetics and biodistribution of TSL and their encapsulated compounds, doxorubicin and [Gd(HPDO3A)(H₂O)] were investigated. The biodistribution of free doxorubicin and [Gd(HPDO3A)(H₂O)] are well known, however encapsulation into liposomes changes the biodistribution of these compounds radically. Altered drug and contrast agent distribution, coupled with tissue-dependent differences in metabolism of these compounds, could play an important role in therapeutic effects and toxicity to healthy organs motivating a thorough study of the biodistribution of all injected compounds. Subsequently, the influence of HIFU-mediated local hyperthermia of the tumor on the biodistribution was studied using SPECT/CT imaging.

In Chapter 5, hyperthermia-mediated doxorubicin delivery from TSLs under MR image guidance was explored *in vivo*. In a proof-of-concept study, local hyperthermia has been applied for 30 minutes in tumor bearing rats using a clinical MR-HIFU system at 3T. The local temperature-triggered release of [Gd(HPDO3A)(H₂O)] was monitored with interleaved T_1 mapping of the tumor tissue and correlated with the co-release of doxorubicin.

In Chapter 6, the intratumoral distribution of the temperature-sensitive liposomal carrier and its encapsulated compounds was investigated, after HIFU-mediated hyperthermia induced local drug release. The presence of the liposomal carriers and the intratumoral distribution of doxorubicin were imaged *ex vivo* with autoradiography and fluorescence microscopy, respectively.

In Chapter 7, the therapeutic effect of the HIFU-mediated hyperthermia treatment with administration of TSLs was studied and compared with saline, doxorubicin and clinically available non-temperature sensitive liposomal doxorubicin (Caelyx[®]). Additionally, the potential of MR imaging to predict and monitor the response to the treatment was investigated.

References

1. Govindan R. The Washington manual of oncology, second edition, 2008.
2. Bonadonna G, Monfardini S, de Lena M, et al. Clinical evaluation of adriamycin, a new antitumour antibiotic. *British Medical Journal*. 1969;3:503-6.
3. Lown JW. Discovery and development of anthracycline antitumour antibiotics. *Chemical Society Reviews*. 1993;22(3):165-76.
4. Licata S, Saponiero A, Mordente A, et al. Doxorubicin metabolism and toxicity in human myocardium: Role of cytoplasmic deglycosidation and carbonyl reduction. *Chem Res Toxicol* 2000;13:414-20.
5. Olson RD, Mushlin PS. Doxorubicin cardiotoxicity: analysis of prevailing hypotheses. *The FASEB Journal*. 1990;4(13):3076-86.
6. Allen TM, P.R. Cullis. *Drug Delivery Systems: Entering the Mainstream*. Science. 2004;303:1818-22.
7. Torchilin VP. Targeted Pharmaceutical Nanocarriers for Cancer Therapy and Imaging. *AAPS J*. 2007;9(2):E128-E47.
8. Gabizon A. Pharmacokinetics of PEGylated liposomal doxorubicin. *Clinical Pharmacokinetics*. 2003;42:419-36.
9. Abraham SA, D.N. Waterhouse, D. Lawrence, D. Mayer, P.R. Cullis, T.D. Madden, M.B. Bally. The liposomal formulation of doxorubicin. *Methods Enzymol*. 2005;391:71-97.
10. Gabizon A, R. Catane, B. Uziely, B. Kaufman, T. Safra, R. Cohen, F. Martin, A. Huang, Y. Barenholz. Prolonged circulation time and enhanced accumulation in malignant exudates of doxorubicin encapsulated in poly-ethylene-glycol coated liposomes. *Cancer Res*. 1994;54:987-92.
11. Gaber MH, Wu NZ, Hong K, et al. Thermosensitive liposomes: extravasation and release of contents in tumor microvascular networks. *Int J Radiat Oncol Biol Phys* 1996;36(5):1177-87.
12. Matsumura Y, H. Maeda. A new concept for macromolecular therapeutics in cancer chemotherapy: mechanism of tumoritropic accumulation of proteins and the antitumor agent smancs. *Cancer Res*. 1986;46:6387-92.
13. Drummond DC, Meyer O, Hong KL, et al. Optimizing liposomes for delivery of chemotherapeutic agents to solid tumors. *Pharmacological Reviews*. 1999;51(4):691-743.
14. Drummond DC, C.O. Noble, M.E. Hayes, J.W. Park, D.B. Kirpotin. Pharmacokinetics and In Vivo drug release rates in liposomal nanocarrier development. *J Pharm Sci*. 2008;97(11):4696-740.
15. Siegal T, Horowitz A, Gabizon A. Doxorubicin encapsulated in sterically stabilized liposomes for the treatment of a brain tumor model: biodistribution and therapeutic efficacy. *J Neurosurg*. 1995;83(6):1029-37.
16. Gabizon A. Selective tumor localization and improved therapeutic index of anthracyclines encapsulated in long-circulating liposomes. *Cancer Res*. 1992;52:891-6.
17. Gabizon A, Catane R, Uziely B, et al. Prolonged circulation time and enhanced accumulation in malignant exudates of doxorubicin encapsulated in polyethylene-glycol coated liposomes. . *Cancer Research*. 1994;54(4):987-92.
18. Northfelt DW, F.J. Martin, P. Working, P.A. Volberding, J. Russell, M. Newman, M.A. Amantea, L.D. Kaplan. Doxorubicin encapsulated in liposomes containing surface-bound polyethylene glycol: pharmacokinetics, tumor localization, and safety in patients with AIDS-related Kaposi's Sarcoma. *J Clin Pharmacol*. 1996;36:55-63.

19. Northfelt DW, B.J. Dezube, J.A. Thommes, B.J. Miller, M.A. Fischl, A. Friedman-Kien, L.D. Kaplan, C. Du Mond, R.D. Mamelok, D.H. Henry. Pegylated-liposomal doxorubicin versus doxorubicin, bleomycin and vincristine in the treatment of AIDS-related Kaposi's Sarcoma: results of a randomized phase III clinical trial. *J Clin Oncol.* 1998;16(7):2445-51.
20. Judson I, Radford JA, Harris M, et al. Randomised phase II trial of pegylated liposomal doxorubicin (DOXIL^(R)/CAELYX^(R)) versus doxorubicin in the treatment of advanced or metastatic soft tissue sarcoma: a study by the EORTC Soft Tissue and Bone Sarcoma Group. *Eur J Cancer.* 2001;37:870-7.
21. Harris L, Batist G, Belt R, et al. Liposome-encapsulated doxorubicin compared with conventional doxorubicin in a randomized multicenter trial as first-line therapy of metastatic breast carcinoma. *Cancer.* 2002;94(1):25-36.
22. O'Brien MER, Wigler N, Inbar M, et al. Reduced cardiotoxicity and comparable efficacy in a phase III trial of pegylated liposomal doxorubicin HCl (CAELYXTM/Doxil^(R)) versus conventional doxorubicin for first-line treatment of metastatic breast cancer. *Ann Oncol.* 2004;15:440-9.
23. Yatvin MB, Weinstein JN, Dennis WH, et al. Design of liposomes for enhanced local release of drugs by hyperthermia. *Science.* 1978;202:1290-3.
24. Gaber MH, K. Hong, S.K. Huang, D. Papahadjopoulos. Thermosensitive sterically stabilized liposomes: formulation and in vitro studies on mechanism of doxorubicin release by bovine serum and human plasma. *Pharm Res.* 1995;12(10):1407-16.
25. Lindner JR. Microbubbles in medical imaging: current applications and future directions. *Nature Reviews Drug Discovery.* 2004;3(6):527-32.
26. Weinstein JN, Magin RL, Yatvin MB, et al. Liposomes and local hyperthermia- selective delivery of methotrexate to heated tumors. *Science.* 1979;204(4389):188-91.
27. Immordino ML, Dosio F, Cattel L. Stealth liposomes: review of the basic science, rationale, and clinical applications, existing and potential. *International Journal of Nanomedicine.* 2006;1(3):297-315.
28. Gabizon A, Papahadjopoulos D. Liposome formulations with prolonged circulation time in blood and enhanced uptake by tumors. *Proc Natl Acad Sci USA.* 1988;85:6949-53.
29. Maruyama K, S. Unezaki, N. Takahashi, M. Iwatsuru. Enhanced delivery of doxorubicin to tumor by long-circulating thermosensitive liposomes and local hyperthermia. *Biochimica et Biophysica Acta - Biomembranes.* 1993;1149:209-16.
30. Allen TM, Hansen C. Pharmacokinetics of stealth versus conventional liposomes: effect of dose. *Biochimica et Biophysica Acta.* 1991;1068:133-41.
31. Anyarambhatla GR, D. Needham. Enhancement of the phase transition permeability of DPPC liposomes by incorporation of MPPC: A new temperature-sensitive liposome for use with mild hyperthermia. *J Liposome Res.* 1999;9(4):491-506.
32. Kong G, Anyarambhatla G, Petros WP, et al. Efficacy of liposomes and hyperthermia in a human tumor xenograft model: importance of triggered drug release. *Cancer Res.* 2000;60:6950-7.
33. Mills JK, Needham D. The materials engineering of temperature-sensitive liposomes. *Methods Enzymol.* 2004;387:82-113.
34. Landon CD, Park J, Needham D, et al. Nanoscale drug delivery and hyperthermia: The materials design and preclinical and clinical testing of low temperature-sensitive liposomes used in combination with mild hyperthermia in the treatment of local cancer. *The Open Nanomedicine Journal.* 2011;3:38-64.

35. Al-Jamal WT, Al-Ahmady ZS, Kostarelos K. Pharmacokinetics & tissue distribution of temperature-sensitive liposomal doxorubicin in tumor-bearing mice triggered with mild hyperthermia. *Biomaterials*. 2012;33:4608-17.
36. Needham D, Anyarambhatla G, Kong G, et al. A new temperature-sensitive liposome for use with mild hyperthermia: characterization and testing in a human tumor xenograft model. *Cancer Res*. 2000;60:1197-201.
37. Dromi S, Frenkel V, Luk A, et al. Pulsed-High Intensity Focused Ultrasound and Low Temperature-Sensitive Liposomes for enhanced targeted drug delivery and antitumor effect. *Clin Cancer Res*. 2007;13(9):2722-7.
38. Ponce AM, Viglianti BL, Yu D, et al. Magnetic Resonance Imaging of temperature-sensitive liposome release: Drug dose painting and antitumor effects. *J Natl Cancer Inst* 2007;99:53-63.
39. Yarmolenko PS, Zhao Y, Landon C, et al. Comparative effects of thermosensitive doxorubicin-containing liposomes and hyperthermia in human and murine tumors. *International Journal of Hyperthermia*. 2010;26(5):485-98.
40. Kong G, M.W. Dewhirst. Review Hyperthermia and liposomes. *Int J Hyperthermia*. 1999;15(5):345-70.
41. Zou Y, Yamagishi M, Horikoshi I, et al. Enhanced therapeutic effect against liver W256 carcinosarcoma with temperature-sensitive liposomal adriamycin administered into the hepatic artery. *Cancer Research*. 1993;53:3046-51.
42. Ning S, Macleod K, Abra RM, et al. Hyperthermia induces doxorubicin release from long-circulating liposomes and enhances their anti-tumor efficacy. *Int J Radiation Oncology Biol Phys*. 1994;29(4):827-34.
43. Huang SK, P.R. Stauffer, K. Hong, J.W.H. Guo, T.L. Philips, A. Huang, D. Papahadjopoulos. Liposomes and Hyperthermia in Mice: Increased Tumor Uptake and Therapeutic Efficacy of Doxorubicin in Sterically Stabilized Liposomes. *Cancer Res*. 1994;54:2186-91.
44. Unezaki S, K. Maruyama, N. Takahashi, M. Koyama, T. Yuda, A. Suginaka, M. Iwatsuru. Enhanced Delivery and Antitumor Activity of Doxorubicin Using Long-Circulating Thermosensitive Liposomes Containing Amphipathic Polyethylene Glycol in Combination with Local Hyperthermia. *Pharmaceutical Research*. 1994;11(8):1180-5.
45. Hauck ML, Larue SM, Petros WP, et al. Phase I trial of doxorubicin-containing low temperature sensitive liposomes in spontaneous canine tumors. *Clinical Cancer Research*. 2006;12(13):4004-10.
46. Tagami T, Ernsting MJ, Li S-D. Efficient tumor regression by a single and low dose treatment with a novel and enhanced formulation of thermosensitive liposomal doxorubicin. *Journal of Controlled Release*. 2011;152(2):303-9.
47. Poon RTP, Borys N. Lyso-thermosensitive liposomal doxorubicin: a novel approach to enhance efficacy of thermal ablation of liver cancer. *Expert Opinion on Pharmacotherapy*. 2009;10(2):333-43.
48. Poon RTP, Borys N. Lyso-thermosensitive liposomal doxorubicin: an adjuvant to increase the cure rate of radiofrequency ablation in liver cancer. *Future Oncology*. 2011;7(8):937-45.
49. Bull JMC. An update on the anticancer effects of a combination of chemotherapy and hyperthermia. *Cancer Research*. 1984;44:4853s-6s.
50. Hahn GM, Braun J, Har-Kedar I. Thermochemotherapy: Synergism between hyperthermia (42-43°) and Adriamycin (or Bleomycin) in mammalian cell inactivation *Proc Natl Acad Sci USA*. 1975;72(3):937-40.

51. Storm FK. Clinical hyperthermia and chemotherapy. *Radiologic Clinics of North America*. 1989;27(3):621-7.
52. Overgaard J. Combined adriamycin and hyperthermia treatment of a murine mammary carcinoma *in vivo*. *Cancer Research*. 1976;36:3077-81.
53. Issels RD, Lindner LH, Verweij J, et al. Neo-adjuvant chemotherapy alone with regional hyperthermia for localised high-risk soft-tissue sarcoma: a randomised phase 3 multicentre study. *Lancet oncology*. 2010;11(6):561-70.
54. Roti Roti JL. Cellular responses to hyperthermia (40-46 degrees C): cell killing and molecular events. *International Journal of Hyperthermia*. 2008;24(1):3-15.
55. Skitzki JJ, Repasky EA, Evans SS. Hyperthermia as an immunotherapy strategy for cancer. *Curr Opin Invest Drugs*. 2009;10(6):550-8.
56. Kong G, Braun RD, Dewhirst MW. Characterisation of the effect of hyperthermia on nanoparticle extravasation from tumor vasculature. *Cancer Research*. 2001;61:3027-32.
57. Koning GA, Eggermont AMM, Lindner LH, et al. Hyperthermia and thermosensitive liposomes for improved delivery of chemotherapeutic drugs to solid tumors. *Pharm Res*. 2010;27:1750-4.
58. Krawczyk PM, Eppink B, Essers J, et al. Mild hyperthermia inhibits homologous recombination, induces BRCA2 degradation, and sensitizes cancer cells to poly (ADP-ribose) polymerase-1 inhibition. *Proc Natl Acad Sci*. 2011;108:9851-6.
59. van Bree C, Krooshoop JJ, Rietbroek RC, et al. Hyperthermia enhances tumor uptake and antitumor efficacy of thermostable liposomal daunorubicin in a rat solid tumor. *Cancer Research*. 1996;56:563-8.
60. Tagami T, Foltz WD, Ernsting MJ, et al. MRI monitoring of intratumoral drug delivery and prediction of the therapeutic effect with a multifunctional thermosensitive liposome. *Biomaterials*. 2011;32(27):6570-8.
61. Han HD, Shin BC, Choi HS. Doxorubicin-encapsulated thermosensitive liposomes modified with poly(N-isopropylacrylamide-co-acrylamide): Drug release behavior and stability in the presence of serum. *Eur J Pharm Biopharm* 2006;62(1):110-6.
62. Morita K, Zywiets F, Kakinuma K, et al. Efficacy of doxorubicin thermosensitive liposomes (40°C) and local hyperthermia on rat rhabdomyosarcoma. *Oncology reports*. 2008;20:365-72.
63. Yarmolenko PS, Moon EJ, Landon C, et al. Thresholds for thermal damage to normal tissues: An update. *International Journal of Hyperthermia*. 2011;27(4):320-43.
64. Paulides MM, Bakker JF, Neufeld E, et al. The HYPERcollar: A novel applicator for hyperthermia in the head and neck. *International Journal of Hyperthermia*. 2007;23(7):567-76.
65. Fatehi D, van der Zee J, de Bruijne M, et al. RF-power and temperature data analysis of 444 patients with primary cervical cancer: Deep hyperthermia using the Sigma-60 applicator is reproducible. *International Journal of Hyperthermia*. 2007;23(8):623-43.
66. Johnson JE, Neuman DG, Maccarini PF, et al. Evaluation of a dual-arm Archimedean spiral array for microwave hyperthermia. *International Journal of Hyperthermia*. 2006;22(6):475-90.
67. Juang T, Stauffer PR, Neuman DG, et al. Multilayer conformal applicator for microwave heating and brachytherapy treatment of superficial tissue disease. *International Journal of Hyperthermia*. 2006;22(7):527-44.

68. Boreham DR, Gasmann HC, Mitchel REJ. Water bath hyperthermia is a simple therapy for psoriasis and also stimulates skin tanning in response to sunlight. *International Journal of Hyperthermia*. 1995;11(6):745-54.
69. Markovic M, Majkic-Singh N, Ignjatovic S. Beneficial effects of cellular stress response in traditional spa treatment of rheumatoid arthritis. *Clin Lab*. 2009;55(5-6):235-41.
70. Cline HE, Hynynen K, Hardy CJ, et al. MR temperature mapping of focused ultrasound surgery. *Magnetic Resonance in Medicine*. 1994;31(6):628-36.
71. Ishihara Y, Calderon A, Watanabe H, et al. A precise and fast temperature mapping using water proton chemical shift. *Magn Reson Med*. 1995;34(6):814-23.
72. Hynynen K, Darkazanli A, Unger E, et al. MRI-guided noninvasive ultrasound surgery. *Medical Physics*. 1993;20(1):107-15.
73. Hokland SL, Pedersen M, Salomir R, et al. MRI-Guided focused ultrasound: Methodology and applications. *IEEE Transactions on Medical Imaging*. 2006;25(6):723-31.
74. Partanen A, Yarmolenko PS, Viitala A, et al. Mild hyperthermia with magnetic resonance-guided high-intensity focused ultrasound for applications in drug delivery. *International Journal of Hyperthermia*. 2012;28(4):320-36.
75. Staruch R, Chopra R, Hynynen K. Localised drug release using MRI-controlled focused ultrasound hyperthermia. *International Journal of Hyperthermia*. 2011;27(2):156-71.
76. Staruch R, Chopra R, Hynynen K. Hyperthermia in bone generated with MR imaging-controlled focused ultrasound: control strategies and drug delivery. *Radiology*. 2012;263(1):117-27.
77. Staruch RM, Ganguly M, Tannock IF, et al. Enhanced drug delivery in rabbit VX2 tumours using thermosensitive liposomes and MRI-controlled focused ultrasound hyperthermia. *International Journal of Hyperthermia*. 2012;28(8):776-87.
78. Ranjan A, Jacobs GC, Woods DL, et al. Image-guided drug delivery with magnetic resonance guided high intensity focused ultrasound and temperature sensitive liposomes in a rabbit Vx2 tumor model. *Journal of Controlled Release*. 2012;158:487-94.
79. Grüll H, Langereis S. Temperature-triggered drug delivery using MRI-guided high intensity focused ultrasound. *Journal of Controlled Release*. 2012;161(2):317-27.
80. McDannold N, S.L. Fossheim, H. Rasmussen, H. Martin, N. Vykhodtseva, K. Hynynen. Heat-activated liposomal MR contrast agent: initial in vivo results in rabbit liver and kidney. *Radiology*. 2004;230:743-52.
81. Salomir R, Palussiere J, Fossheim SL, et al. Local delivery of magnetic resonance (MR) contrast agent in kidney using thermosensitive liposomes and MR imaging-guided local hyperthermia: A feasibility study in vivo. *Journal of Magnetic Resonance Imaging*. 2005;22(4):534-40.
82. Peller M, A. Schwerdt, M. Hossann, H.M. Reinl, T. Wang, S. Sourbron, M. Ogris, L.H. Lindner. MR characterization of mild hyperthermia-induced gadodiamide release from thermosensitive liposomes in solid tumors. *Investigative Radiology*. 2008;43(12):877-92.
83. Langereis S, Keupp J, van Veldhoven JIJ, et al. A temperature-sensitive liposomal 1H CEST and 19F contrast agent for MR Image-guided drug delivery. *J Am Chem Soc*. 2009;131:1380-1.
84. Bos C, M. Lepetit-Coiffé, B. Quesson, C.T.W. Moonen. Simultaneous monitoring of temperature and T1: methods and preliminary results of application to drug delivery using thermosensitive liposomes. *Magn Reson Med*. 2005;54:1020-4.

85. Fossheim SL, K.A. Il'yasov, J. Hennig, A. Bjørnerud. Thermosensitive paramagnetic liposomes for temperature control during MR Imaging-guided hyperthermia: In vitro feasibility studies. *Acad Radiol.* 2000;7(12):1107-15.
86. de Zwart JA, Salomir R, Vimeux F, et al. On The Feasibility Of Local Drug Delivery Using Thermo-Sensitive Liposomes and MR-Guided Focused Ultrasound. *Proc Intl Sot Mag Reson Med.* 2000;8:43.
87. Abraham SA, K. Edwards, G. Karlsson, S. MacIntosh, L.D. Mayer, C. McKenzie, M.B. Bally. Formation of transition metal-doxorubicin complexes inside liposomes. *Biochim Biophys Acta.* 2002;1565:41-54.
88. Chiu GNC, S.A. Abraham, L.M. Ickenstein, R. Ng, G. Karlsson, K. Edwards, E.K. Wasan, M.B. Bally. Encapsulation of doxorubicin into thermosensitive liposomes via complexation with the transition metal manganese. *J Control Release.* 2005;104:271-88.
89. Viglianti BL, S.A. Abraham, C.R. Michelich, P.S. Yarmolenko, J.R. MacFall, M.B. Bally, M.W. Dewhirst. In vivo monitoring of tissue pharmacokinetics of liposome/drug using MRI: illustration of targeted delivery. *Magn Reson Med.* 2004;51:1153-62.
90. Viglianti BL, A.M. Ponce, C.R. Michelich, D. Yu, S.A. Abraham, L. Sanders, P.S. Yarmolenko, T. Schroeder, J.R. MacFall, D.P. Barboriak, O.M. Colvin, M.B. Bally, M.W. Dewhirst. Chemodosimetry of in vivo tumor liposomal drug concentration using MRI. *Magn Reson Med.* 2006;56:1011-8.
91. Koenig SH, G.F. Ahkong, R.D. Brown, M. Lafleur, M. Spiller, E. Unger, C. Tilcock. Permeability of liposomal membranes to water: results from the magnetic field dependence of t_1 of solvent protons in suspensions of vesicles with entrapped paramagnetic ions. *Magn Reson Med.* 1992;23(2):275-86.
92. Koretsky AP, A.C. Silva. Manganese-enhanced magnetic resonance imaging (MEMRI). *NMR Biomed.* 2004;17:527-31.
93. Negussie AH, Yarmolenko PS, Partanen A, et al. Formulation and characterisation of magnetic resonance imageable thermally sensitive liposomes for use with magnetic resonance-guided high intensity focused ultrasound. *International Journal of Hyperthermia.* 2011;27(2):140-55.

Chapter 2

Temperature-sensitive liposomes for doxorubicin delivery under MRI guidance

Abstract

In this Chapter, the release of doxorubicin and [Gd(HPDO3A)(H₂O)] from different temperature sensitive liposomal formulations was investigated *in vitro* for applications in temperature-induced drug delivery under magnetic resonance image guidance. In particular, two temperature sensitive systems composed of DPPC:MPPC:DPPE-PEG2000 (low temperature sensitive liposomes, LTSL) and DPPC:HSPC:cholesterol:DPPE-PEG2000 (traditional temperature sensitive liposomes, TTSL) were investigated. The co-encapsulation of [Gd(HPDO3A)(H₂O)], a clinically approved MRI contrast agent, did not influence the encapsulation and release of doxorubicin. The LTSL system showed a faster release of doxorubicin at 42 °C, but a higher leakage at 37 °C, compared to the TTSL system. Furthermore, the rapid release of both doxorubicin and the MRI contrast agent from the liposomes occurred near the melting phase transition temperature, making it possible to image the release of doxorubicin using MRI.

Based on:

M. de Smet, S. Langereis, S. van den Bosch and H. Grüll. *Temperature-sensitive liposomes for doxorubicin delivery under MRI guidance*, Journal of Controlled Release 2010; 143(1); 120-127

2.1 Introduction

The application of temperature-sensitive liposomes (TSLs) for local drug delivery was first proposed by Yatvin and Weinstein.^{1,2} These systems are able to release encapsulated molecules near their melting phase transition temperature (T_m), where the lipid membrane shows a transition from a gel to a liquid crystalline phase. Since then, different TSLs have been described and by careful selection of the lipid composition their temperature sensitivity can be tuned between 39 to 42 °C.³⁻⁹ The incorporation of lysolipids into the liposomal membrane presumably facilitates the formation of transient pores in the lipid bilayer around T_m leading to a more rapid release of the encapsulated contents.⁹⁻¹² The most clinically advanced TSL system, known as Thermodox[®], is composed of DPPC:MSPC:DSPE-PEG2000. This lysolipid containing formulation is currently in Phase III clinical trials for the treatment of liver cancer and Phase II for the treatment of breast cancer recurrence at the chest wall.¹³

For drug delivery *in vivo*, the amount of delivered drug scales with the time where hyperthermia is applied, the plasma concentration of the liposomal drug carrier, the drug-payload per carrier, and the perfusion of the tumor tissue. Therefore, drug release from the liposomal carrier and subsequent uptake into the tumor tissue needs to be relatively fast to compete against downstream wash-out. Ideally, this approach requires TSLs that do not show leakage at body temperature, but rapidly release their drug payload at mild hyperthermia (39-42 °C). Besides improving the TSL systems as such, quantification and monitoring of the drug release process is crucial. In particular for ultrasound induced drug delivery under MR image guidance, the incorporation of MRI contrast agents into the TSL system offers the possibility to visualize and quantify the drug delivery process.¹⁴⁻²¹

In this Chapter, we report on the preparation and characterization of temperature-sensitive liposomal contrast agents for MR image guided release of doxorubicin. Two temperature sensitive liposomal systems were investigated. One system, the low temperature-sensitive liposomes (LTSL), is a lysolipid-containing liposomal formulation composed of DPPC, MPPC and DPPE-PEG2000. The second system is a traditional temperature-sensitive liposomal (TTSL) formulation containing DPPC, HSPC, cholesterol and DPPE-PEG2000. For comparison NTSL (Non-Temperature-Sensitive Liposomes) containing HSPC, cholesterol and DPPE-PEG2000 were prepared using identical procedures. The LTSL and TTSL formulations have been earlier investigated by other researchers,²²⁻²⁵ while the chemical composition of the NTSL formulation is similar to Doxil[®] (Caelyx[®]).²⁶ The *in vitro* leakage of doxorubicin at body temperature as well as the release kinetic at elevated temperatures was studied for these different liposomal systems. The MRI contrast of these paramagnetic liposomes was investigated as a function of temperature to test whether these liposomes are suitable for monitoring the release of the doxorubicin with MRI.

2.2 Materials and Methods

2.2.1 Materials

1,2-Dipalmitoyl-*sn*-glycero-3-phosphocholine (DPPC), 1-palmitoyl-*sn*-glycero-3-phosphocholine (MPPC), 1,2-dipalmitoyl-*sn*-glycero-3-phosphoethanolamine-*N*-[methoxy-(polyethyleneglycol)-2000] (DPPE-PEG2000), hydrogenated-*L*- α -phosphatidyl-choline (HSPC) and cholesterol were purchased from Avanti Polar Lipids. Doxorubicin hydrochloride was purchased from Sigma Aldrich and [Gd(HPDO3A)(H₂O)] (ProHance[®]) was obtained from Bracco Diagnostics.

2.2.2 Preparation of liposomes

Three different liposomal formulations were prepared; LTSL composed of DPPC:MPPC:DPPE-PEG2000 = 86:10:4 (molar ratio), TTSL composed of DPPC:HSPC:Chol:DPPE-PEG2000 = 50:25:15:3 (molar ratio) and NTSL composed of HSPC:Chol:DPPE-PEG2000 = 75:50:3 (molar ratio). A total amount of 115 μ mol of phospholipids and cholesterol were dissolved in a solution of chloroform/ methanol (4:1 v/v). The organic solvents were removed *in vacuo* until a thin lipid film was formed, which was further dried overnight under a nitrogen flow. The lipid film was hydrated at 60 °C with a 240 mM (NH₄)₂SO₄ buffer (pH 5.4) containing 60 mM [Gd(HPDO3A)(H₂O)]. The suspension was extruded successively at 60 °C through a 400 nm filter (two times), a 200 nm filter (two times), and a 100 nm filter (five times). After extrusion, the extraliposomal buffer was replaced by HEPES Buffered Saline (HBS), pH 7.4 (20 mM HEPES, 137 mM NaCl) by gel filtration through a PD-10 column (GE Healthcare). Subsequently, a doxorubicin solution in HBS (5 mg/mL) was added to the liposomes at a 20:1 phospholipid to doxorubicin weight ratio and incubated at 37 °C for 90 minutes. Finally, the liposomes were passed through another PD-10 column to remove traces of unencapsulated doxorubicin.

2.2.3 Determination of the phosphorus, gadolinium and doxorubicin concentrations

The intraliposomal doxorubicin concentration was determined using fluorescence measurements (Perkin Elmer LS55, $\lambda_{\text{ex}} = 485$ nm and $\lambda_{\text{em}} = 590$ nm) after destruction of the liposomes with Triton X-100. Phosphorus and gadolinium concentrations were determined by means of Inductively Coupled Plasma-Mass Spectrometry (ICP-MS, DRCII, Perkin Elmer) after the destruction of the liposomes with nitric acid and perchloric acid at 180 °C.

2.2.4 Dynamic Light Scattering

The hydrodynamic radius of the liposomes was determined using dynamic light scattering (ALV/CGS-3 Compact Goniometer System, ALV-GmbH, Langen, Germany). Intensity correlation functions were measured at a scattering angle of $\theta=90^\circ$ using a wavelength of 632.8 nm. The diffusion coefficient (D) was obtained from cumulant fits of the intensity correlation function using ALV software. All reported hydrodynamic radii were calculated

using Stokes–Einstein equation $r_h = kT/(6\theta\eta D)$, where k is the Boltzmann constant, T is the temperature and η is the solvent viscosity.

2.2.5 Differential Scanning Calorimetry

The phase transition temperatures of the lipid membranes were determined with differential scanning calorimetry (Q2000 differential scanning calorimeter, TA Instruments, USA) during heating with 5 K/min from 20 °C to 70 °C.

2.2.6 Cryo- Transmission Electron Microscopy

Cryogenic transmission electron microscopy (cryo-TEM) was used to investigate the morphology of the doxorubicin loaded liposomes in their natural hydrated state. Sample preparation was performed by applying the liposome solution (2 μ L) to a lacey carbon film and subsequently plunge-freezing into liquid ethane using a Vitrobot. Subsequently, cryo-TEM studies were performed using a FEI TECNAI F30ST at 300kV and the cryo-TEM sample was maintained at -167 °C. Cryo-TEM images were recorded in low-dose mode on a CCD camera (1k \times 1k). In order to visualize the ordered structure of the doxorubicin crystal, an intensity profile, averaged over 30 lines of pixels, was calculated over a line perpendicular to the doxorubicin fiber bundle in the high resolution image.

2.2.7 Release of doxorubicin from liposomes

The release of doxorubicin from the LTSL, TTSL and NTSL was determined by measuring the intensity of fluorescence ($\lambda_{ex} = 485$ nm and $\lambda_{em} = 590$ nm) as a function of the temperature. At the end of each measurement, 5 μ L of a 10% v/v solution of Triton X-100 was added to 2 mL of the solution, to afford quantitative release of doxorubicin. The percentage of doxorubicin release was calculated according to: $(I_t - I_0)/(I_{100} - I_0) \times 100\%$, in which I_t is the intensity of the fluorescence at a specific time (t), I_0 is the intensity of the fluorescence at $t=0$, I_{100} is the intensity of the fluorescence after the addition of Triton X-100. The release of doxorubicin from the liposomes (5 μ L) in 2 mL fully supplemented Dulbecco's Modified Eagle's Medium (DMEM, Invitrogen) was determined at 37 °C and 42 °C.

2.2.8 Cell viability assay

A431 squamous carcinoma cells were maintained in a humidified CO₂ (5%) cell incubator at 37 °C in DMEM supplemented with heat-inactivated fetal bovine serum (10% v/v), glutamax (1% v/v) and penicillin/streptomycin (1% v/v). One day after seeding the cells in 96-wells plates (4000 cells/well), incubation experiments with solutions of the three different liposomal formulations of co-encapsulated doxorubicin and [Gd(HPDO3A)(H₂O)] were performed and unencapsulated doxorubicin was used as a reference. The liposomes and the reference doxorubicin solution were diluted in fully supplemented DMEM to a doxorubicin concentration of 10 μ M. All four samples were kept for 30 minutes at either 37 °C or 42 °C

respectively before they were added to the cells. After removal of the medium, the cells were incubated with 150 μL of the preheated samples for 4 hours at 37 $^{\circ}\text{C}$. After the incubation, the samples were removed and the cells were gently washed with Dulbecco's Phosphate Buffered Saline (DPBS) and incubated in 150 μL fresh medium for 2 days at 37 $^{\circ}\text{C}$. The cell proliferation was determined by means of a methylthiazolyldiphenyl tetrazolium bromide (MTT) colorimetric assay. To this end, MTT was dissolved in medium (5 mg/mL), passed through a 0.22 μm filter, and 17 μL was added to each well. Following an incubation period of 120 min, the medium was gently aspirated. The formed formazan crystals were dissolved in DMSO (100 μL), and the UV absorbance was measured with a plate reader (BMG labtech) at 570 nm, with a reference absorbance at 690 nm. The average value and the standard deviation for cell proliferation were calculated from data obtained with five wells for each sample. As a control, the same procedure was performed with NTSL, TTSL and LTSL encapsulating only [Gd(HPDO3A)(H₂O)].

2.2.9 Nuclear Magnetic Resonance spectroscopy

The release of [Gd(HPDO3A)(H₂O)] from the liposomes was studied by measuring the longitudinal relaxation time (T_1) as a function of the temperature at 300 MHz (Bruker Avance 300). The experiments were performed from 25 < T/ $^{\circ}\text{C}$ < 50 (heating rate = 0.5 K/min), followed by cooling down from 50 > T/ $^{\circ}\text{C}$ > 25 (-0.5 K/min). The longitudinal relaxivity (r_1) was calculated according to $r_1 = [(1/T_1) - (1/T_{1,0})]/[\text{Gd}]$, in which T_1 is the longitudinal relaxation time, $T_{1,0}$ is the longitudinal relaxation time of the HBS buffer, and [Gd] is the concentration of [Gd(HPDO3A)(H₂O)] in mM.

2.2.10 Calculation of the water exchange rate across the lipids bilayer

From the three paramagnetic liposomal solutions (LTSL, TTSL and NTSL), the extraliposomal buffer (HBS) and the intraliposomal buffer (HBS with 60 mM [Gd(HPDO3A)(H₂O)]), T_1 measurements were performed at different temperatures at 300 MHz (Bruker Avance 300). The volume fraction of the intraliposomal space f was calculated by dividing the Gd concentrations of the liposomal solutions, $[\text{Gd}]_{\text{sol}}$, by the Gd concentration of the intraliposomal buffer $[\text{Gd}]_{\text{in}}$; $f = [\text{Gd}]_{\text{sol}}/[\text{Gd}]_{\text{in}}$. The water exchange rate k_{ex} over the liposomal membrane was calculated according to the two-compartment model^{27, 28}

$$k_{\text{ex}} = \frac{1}{\tau_{\text{in}}} \quad \text{and} \quad \tau_{\text{in}} = \frac{f}{R_{1,\text{eff}} - R_{1,\text{bulk}}} - \frac{1}{R_{1,\text{in}}}$$

where k_{ex} is the transmembrane water exchange rate, τ_{in} is the average residence time of water inside the liposomes, $R_{1,\text{eff}}$ is the longitudinal relaxation rate of the paramagnetic liposomal solution, $R_{1,\text{bulk}}$ is the longitudinal relaxation rate of the extraliposomal buffer, $R_{1,\text{in}}$ is the longitudinal relaxation rate of the intraliposomal water protons and f is the volume

fraction of the intraliposomal space. For a given liposomal formulation, k_{ex} is also directly correlated to the liposome size.

2.2.11 Magnetic Resonance Imaging

Magnetic Resonance Imaging was performed at 3T (Achieva, Philips Healthcare, The Netherlands). The T_1 and T_2 measurements on the liposomes (*i.e.* LTSL, TTSL, NTSL) containing 60 mM [Gd(HPDO3A)(H₂O)] intraliposomal were performed at 25 °C, in which three of the six samples were heated for 30 minutes at 45 °C. The total concentration of [Gd(HPDO3A)(H₂O)] was adjusted to 0.45 mM for all the six samples. The samples were placed in a sample holder containing a standard phantom solution (0.77 g/L CuSO₄·5H₂O, 2 g/L NaCl, 0.1 % (v/v) arquad (Akzo Nobel) and 15 µN H₂SO₄). T_1 -weighted MR images were obtained using an inversion recovery pulse sequence (TE = 7.7 ms, TR = 10 s, FOV = 70 × 70 mm², slice thickness = 4 mm, voxel size = 0.5 × 0.5 mm², NSA = 5). A T_1 map was calculated from the T_1 -weighted MR images with 13 different inversion times, varying from 17 ms until 6000 ms. T_2 -weighted MR images were obtained with a turbo spin echo sequence (TE = 40 ms, TR = 6000 ms, FOV = 70 × 70 mm², slice thickness = 4 mm, voxel size = 0.5 × 0.5 mm², NSA = 3, TSE-factor = 32), of which a T_2 -map was calculated. The average T_1 and T_2 values and standard deviations of the different samples were calculated from the pixels within a manually traced ROI.

2.3. Results

2.3.1 Preparation and characterization of TSL

Two temperature sensitive liposomal formulations encapsulating doxorubicin and [Gd(HPDO3A)(H₂O)], a clinically used MRI contrast agent, denoted LTSL (Low Temperature-Sensitive Liposomes) and TTSL (Traditional Temperature-Sensitive Liposomes) and for comparison NTSL (Non-Temperature-Sensitive Liposomes) were prepared using identical procedures. The difference between the three different liposomal formulations is the phospholipid composition of the liposomal membranes reported in Table 2.1. The different liposomal formulations were prepared by using the same protocol for the encapsulation of 60 mM [Gd(HPDO3A)(H₂O)] followed by the active loading of doxorubicin with the (NH₄)₂SO₄ gradient method.²⁹ All three systems showed a hydrodynamic radius of around 70 nm as evidenced from dynamic light scattering (Table 2.1). The concentrations of phosphorus, gadolinium and doxorubicin of the three systems are shown in Table 2.1. The DSC data (Figure 2.2) showed that the phospholipid composition has a strong influence on the phase transition temperature (T_m). The offset of the DSC peak is here defined as the T_m , which is 38.8 °C for the LTSL, while it is at 40.9 °C for the TTSL. Larger differences were seen when looking at the maximum of the peak, which was found to be at 41.6 °C for the LTSL and 46.7 °C for the TTSL.

No phase transition was found for the NTSL within the temperature range between 20 °C to 60 °C, therefore this formulation is called non-temperature sensitive as the T_m is outside the temperature range relevant for clinical applications.

Table 2.1. Overview of the properties of the three liposomal formulations containing doxorubicin and [Gd(HPDO3A)(H₂O)]. LTSL (Low Temperature-sensitive Liposomes), TTSL (Traditional Temperature-sensitive Liposomes) and NTSL (Non-Temperature-sensitive Liposomes); the composition of the liposomes (molar ratio), hydrodynamic radius (r_h) with polydispersity index (PDI), phosphorus, gadolinium and doxorubicin concentrations, the phase transition temperature (T_m) and temperature at the maximum of the peak on the DSC results. All three liposomal formulations were filled with 60 mM [Gd(HPDO3A)(H₂O)] and loaded with doxorubicin for 90 min. at 37 °C in a 20:1 phospholipid:doxorubicin weight ratio. *) The T_m and DSC peak maximum was not determined (N.D.) for the NTSL, since no phase transition was found within the measured temperature range (20 °C to 60 °C).

Nomenclature	Composition (molar ratio)	r_h (nm) (PDI)	[P] (mM) ± st.dev.	[Gd] (mM) ± st.dev.	[dox] (mM) ± st.dev.	T_m (°C)	DSC peak max. (°C)
LTSL	DPPC:MPPC:DPPE-PEG (86:10:4)	64 (0.26)	4.4 ± 0.2	0.47 ± 0.02	0.63 ± 0.03	38.8	41.6
TTSL	DPPC:HSPC:Chol:DPPE-PEG (50:25:15:3)	68 (0.33)	3.4 ± 0.2	0.39 ± 0.02	0.59 ± 0.03	40.9	46.7
NTSL	HSPC:Chol:DPPE-PEG (75:50:3)	73 (0.15)	2.6 ± 0.1	0.34 ± 0.02	0.13 ± 0.01	N.D. *)	N.D. *)

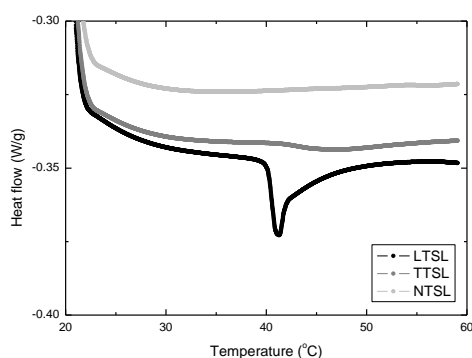


Figure 2.2. DSC results of the three liposomal formulations (LTSL, TTSL, NTSL). A sharp phase transition was observed for the LTSL, while the TTSL showed a much weaker phase transition peak. For the NTSL no phase transition was observed between 20 °C and 60 °C.

The active loading of doxorubicin into the liposomes using the ammonium sulphate gradient resulted in a quantitative accumulation of doxorubicin inside the liposomal aqueous space. The intraliposomal doxorubicin was found as crystalline self-assembled fiber-like structures as evidenced from high resolution cryo-TEM (Figure 2.3). The doxorubicin crystals showed a similar structure observed earlier on doxorubicin-loaded liposomes without [Gd(HPDO3A)(H₂O)], where the formation of doxorubicin fiber bundles was shown.³⁰ The individual fibers of stacked doxorubicin molecules aggregated together into bundles. In order to visualize the ordered structure of the doxorubicin crystal, an intensity profile averaged over 30 lines of pixels was calculated over a line perpendicular to the doxorubicin fiber bundle in the high resolution cryo-TEM image. This intensity profile showed a separation between doxorubicin fibers of approximately 3 nm, which was also seen in the doxorubicin liposomes without [Gd(HPDO3A)(H₂O)]. Moreover, the presence of [Gd(HPDO3A)(H₂O)] in the intraliposomal space did not affect the loading of doxorubicin and the formation of doxorubicin crystals inside the liposomes.

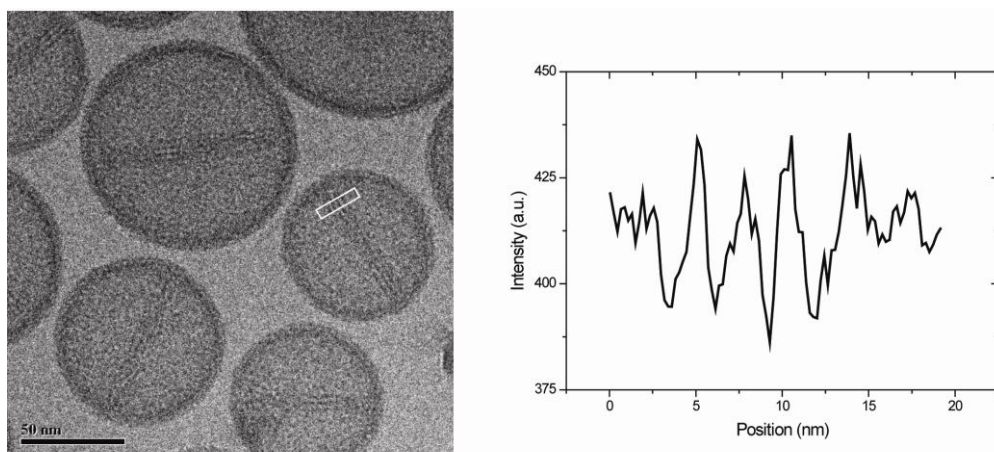


Figure 2.3. High resolution Cryo-TEM image (left) of NTSL containing 60 mM [Gd(HPDO3A)(H₂O)] and doxorubicin crystals. The white rectangle indicates the region of which the intensity profile was calculated (right). The presence of [Gd(HPDO3A)(H₂O)] did not effect the structure of the doxorubicin crystals inside the liposomes.

2.3.2 Stability and release of doxorubicin from TSL

The fluorescence of the intraliposomal doxorubicin is quenched, due to the high concentration. Release of doxorubicin from the aqueous interior of the liposomes will result in a dilution of the doxorubicin in the extraliposomal buffer to concentrations below its self-quenching concentration leading to an increase in fluorescence intensity. The latter is

proportional to the concentration of doxorubicin in the solution. Figure 2.4 shows the release of doxorubicin from the three different liposomes (LTSL, TTSL and NTSL), which was determined by measuring the increase of the fluorescence intensity of the different liposomal formulations in fully supplemented DMEM at 37 °C and 42 °C.

For the LTSL a fast release was observed at 42 °C with quantitative release of doxorubicin within one minute. However, these low temperature-sensitive liposomes showed leakage of doxorubicin at 37 °C leading to a doxorubicin release of approximately 30% after 1 hour. The TTSL showed a slower release of doxorubicin than the LTSL formulation at 42 °C, but still all doxorubicin was released within a few minutes. In contrast to the LTSL, the TTSL showed at 37 °C no release of doxorubicin over 1 hour. The NTSL did not show any doxorubicin release at both temperatures.

Figure 2.5 shows the doxorubicin leakage at 37 °C from LTSL in fully supplemented DMEM containing 10% Fetal Bovine Serum (FBS), as well as in pure HBS solution and a 1:1 mixture of DMEM:HBS. The observed dox leakage in DMEM was still observed in the 1:1 mixture of DMEM:HBS, while in pure HBS no dox leakage was observed.

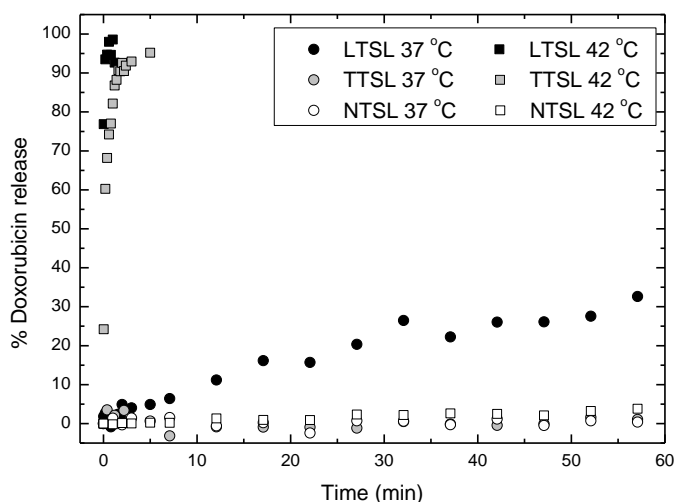


Figure 2.4. Release of doxorubicin from the three liposomal systems encapsulating doxorubicin and $[Gd(HPDO3A)(H_2O)]$, in fully supplemented DMEM at 37 °C and 42 °C. The percentage of doxorubicin released was calculated from the fluorescence intensities which were measured over time.

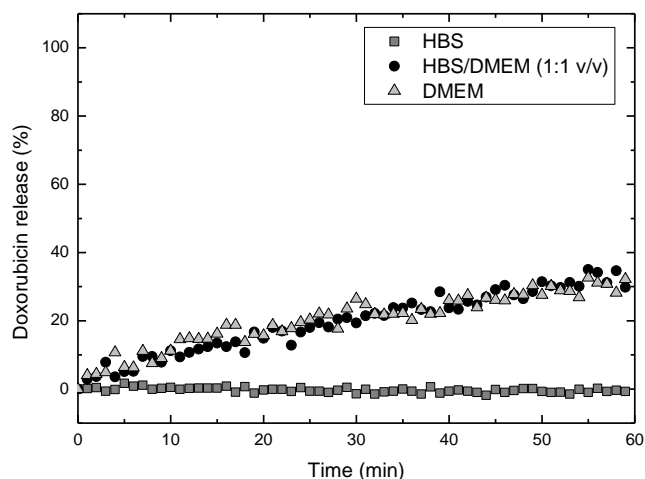


Figure 2.5. Release of doxorubicin from LTSL in HBS, HBS/DMEM (1:1 v/v) and DMEM at 37 °C.

2.3.3 Cell viability

A MTT cell viability assay was performed after 4 hour incubation with preheated (30 min. at 37 °C or 42 °C) samples of the three different liposomes in fully supplemented DMEM (Figure 2.6). The incubation of cells with the LTSL and TTSL preheated at 42 °C resulted in a low cell viability (<5%), which is a similar effect as obtained with the incubation of unencapsulated doxorubicin (Figure 2.6). These data indicate that doxorubicin was released from the temperature sensitive liposomes at 42 °C, which corresponds with the fluorescence measurements (Figure 2.4). In comparison, the NTSL showed strongly reduced cytotoxicity with cell viabilities >75%. In the cell viability studies with preheated samples at 37 °C, the LTSL system showed a reduced but still significant cytotoxicity with cell viabilities around 30%. The latter reflects the considerable leakage of doxorubicin from LTSL at 37 °C (Figure 2.4). The TTSL showed a strongly reduced cytotoxicity compared to viability studies using the 42 °C preheated TTSL, as expected based on the release data shown in Figure 2.4. Cell viability after incubation with the TTSL with preheated samples at 37 °C was comparable to the NTSL system. For the latter, cell viabilities were found to be unchanged when samples were preheated at 37 °C or 42 °C. NTSL did not show any release of doxorubicin at 42 °C or at 37 °C (Figure 2.4). The observed increase in cytotoxicity for the NTSL compared to medium is assumed to be due to uptake of doxorubicin-loaded liposomes in the cells by endocytosis. Liposomes encapsulating [Gd(HPDO3A)(H₂O)] without doxorubicin showed no toxicity.

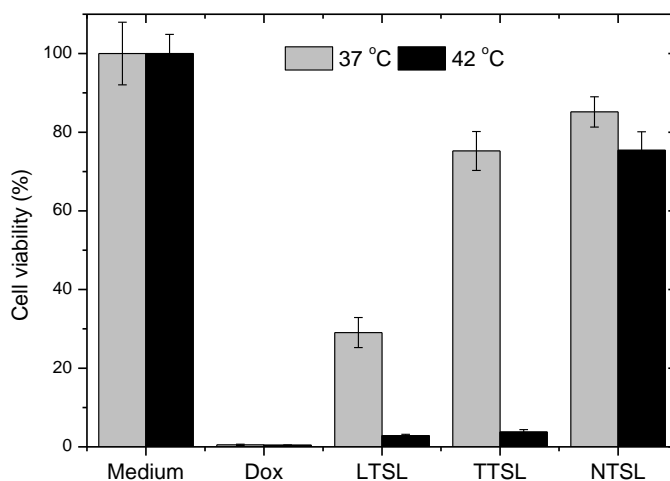


Figure 2.6: MTT viability assay on A431 cells, incubated with cell medium (DMEM), 10 μM doxorubicin in DMEM, or one of the three liposomal formulations (LTSL, TTSL, NTSL) in DMEM containing 10 μM doxorubicin. The solutions were preheated for 30 min. at either 37 °C or 42 °C.

2.3.4 Release of doxorubicin and $[\text{Gd}(\text{HPDO3A})(\text{H}_2\text{O})]$

In order to study the co-release of doxorubicin and $[\text{Gd}(\text{HPDO3A})(\text{H}_2\text{O})]$ from the liposomes during heating, fluorescence and NMR measurements were performed on the three liposomal solutions in HBS over a temperature range of $25 < T / ^\circ\text{C} < 50$, with a heating rate of 0.5 K/min. The graphs in Figure 2.7 show the fluorescence of the three liposomal formulations during heating, and the T_1 relaxivity during heating and subsequent cooling. The fluorescence measurements showed a fast release of doxorubicin from the LTSL starting around 38 °C, which is near the melting phase transition of these liposomes as found by the DSC measurements (Table 2.1). In this case, all doxorubicin was released within a few minutes.

The TTSL showed a slower release starting around 40 °C, which is also when the T_m was approached. For these liposomes it took about 10 minutes to release almost 100% of the doxorubicin. No doxorubicin release was observed for the NTSL during heating. However after the addition of Triton X-100, a quantitative release of the doxorubicin was obtained.

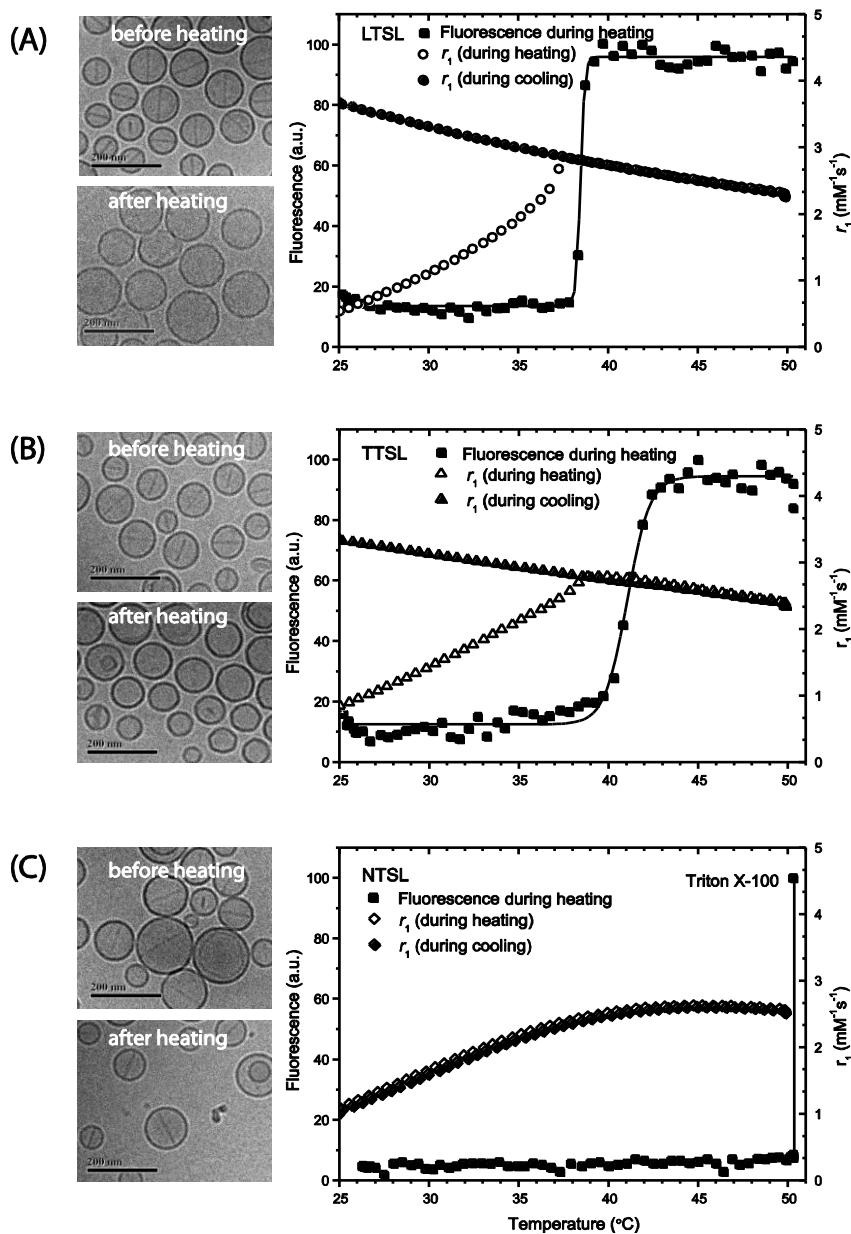


Figure 2.7. Fluorescence and T_1 relaxivity of liposomes (LTSL (A), TTSL (B), and NTSL (C)) during a linear temperature increase (0.5 K/min) from 25 °C to 50 °C. The cryo-TEM images of the liposomes were recorded before and after heating. The release of doxorubicin from inner aqueous interior determined from the intensity of the fluorescence, whereas the release of $[Gd(HPDO3A)(H_2O)]$ was probed with the longitudinal relaxivity (r_1).

Subsequently, the morphology of the liposomes and the encapsulated doxorubicin crystals were studied with cryo-TEM before and after heating and cooling. Before heating, the doxorubicin crystals were observed inside all different liposomes on cryo-TEM images. No morphological differences can be observed between the three different formulations, based on cryo-TEM results. However, after heating to 50 °C and cooling back down to 25 °C with a heating rate of 0.5 K/min, a distinct difference between the three different liposomal compositions was noticed. For the LTSL, no doxorubicin crystals were seen anymore inside the liposomes, which is in agreement with the complete release as observed with fluorescence measurements. After heating and cooling of the TTSL, few liposomes were observed still containing doxorubicin crystals compared to the initial picture before heating, where every single liposome contained a doxorubicin crystal, implying a near quantitative release. This is in agreement with the fluorescence measurements that indicate about 95% release. For the NTSL no difference was observed before and after the heating treatment, with doxorubicin crystals remaining inside the liposomes. These observations are consistent with the fluorescence measurements shown in Figure 2.7.

The encapsulation of [Gd(HPDO3A)(H₂O)] inside the liposomes reduced the observed longitudinal relaxivity (r_1) compared to free [Gd(HPDO3A)(H₂O)], as the water exchange between the bulk water outside and the [Gd(HPDO3A)(H₂O)] inside the liposomes is reduced by the lipid bilayer.³¹ Measuring the T_1 relaxivity allows therefore to calculate the water permeability of the liposome membrane using a two compartment model, where water molecules are distributed in the extra- and intraliposomal compartments, separated by the liposome membrane^{28, 32} (Figure 2.8). Upon release from the inner lumen of the liposomes, the relaxivity of free [Gd(HPDO3A)(H₂O)] is recovered.

All NMR measurements showed an increase in T_1 relaxivity during heating, at temperatures below the phase transition temperature due to an increase in water permeability of the lipid bilayer. The calculated trans-membrane water exchange rates at 37 °C are about one order of magnitude higher compared to water exchange rates at 26 °C (Table 2.2). For the LTSL and TTSL the [Gd(HPDO3A)(H₂O)] was released when heated above the phase transition temperature and the relaxivity curve corresponds with the relaxivity of the free [Gd(HPDO3A)(H₂O)] (Figures 2.7 and 2.9). Upon cooling, the T_1 relaxivity remains identical to the relaxivity of free [Gd(HPDO3A)(H₂O)] which is taken as experimental evidence for the complete release of the paramagnetic contrast agent from the liposomes. For the NTSL, T_1 relaxivities observed during heating and cooling were found to be identical, which is consistent with no release of [Gd(HPDO3A)(H₂O)]. Below T_m , the T_1 measurements as a function of temperature show a reversible behavior during heating and cooling, implying that [Gd(HPDO3A)(H₂O)] remains intraliposomal at these temperatures (Figure 2.10).

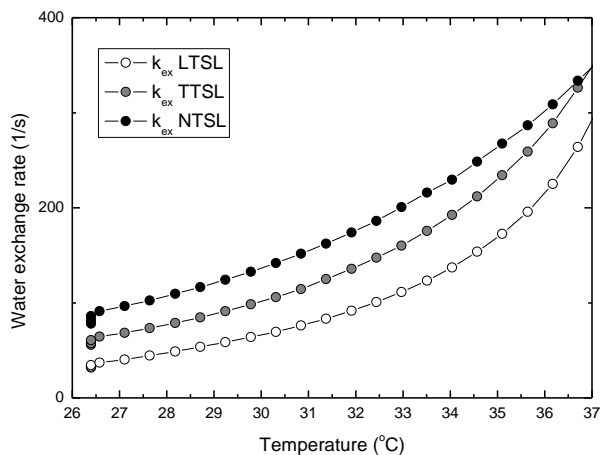


Figure 2.8. Water exchange rates as a function of the temperature for the three liposomal systems; LTSL, TTSL and NTSL.

Table 2.2. Water exchange rates (\pm error) for the three liposomes at 26 °C and 37 °C.

Nomenclature	k_{ex} (1/s) at 26 °C	k_{ex} (1/s) at 37 °C
LTSL	32 ± 2	293 ± 37
TTSL	56 ± 4	348 ± 65
NTSL	78 ± 7	349 ± 74

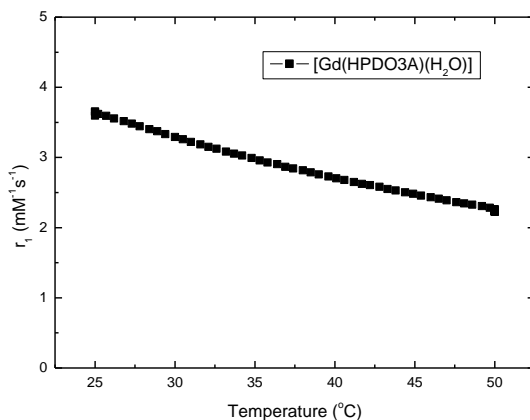


Figure 2.9. Longitudinal relaxivity of $[\text{Gd}(\text{HPDO3A})(\text{H}_2\text{O})]$ during heating and cooling from 25 °C to 50 °C with 0.5 K/min.

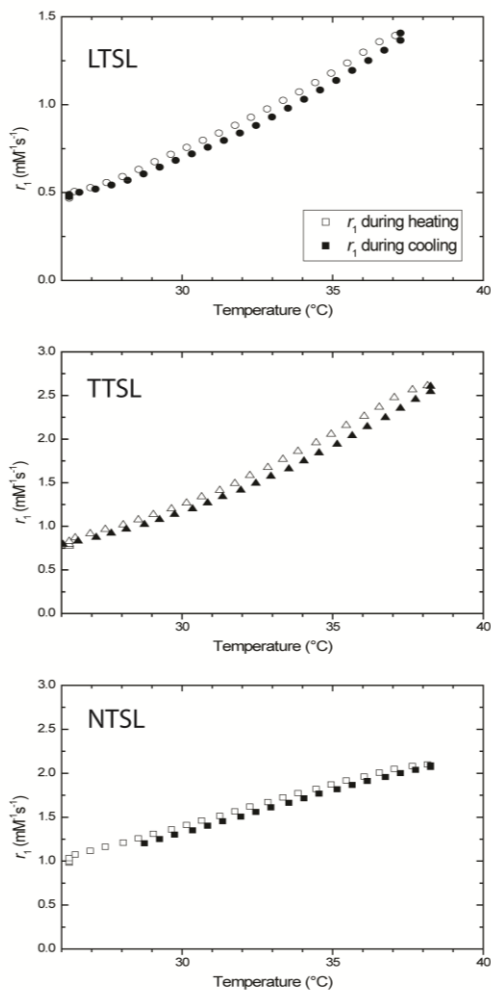


Figure 2.10. The longitudinal relaxivity of LTSL, TTSL and NTSL containing $[\text{Gd}(\text{HPDO3A})(\text{H}_2\text{O})]$ and doxorubicin in HBS during heating from 25 $^{\circ}\text{C}$ to 37 $^{\circ}\text{C}$ (0.5 K/min) and cooling.

2.3.5 Magnetic Resonance Imaging

Next, T_1 and T_2 relaxation times for all liposomal formulations, before and after heating to a temperature of $T = 45^{\circ}\text{C}$ for 30 minutes, were measured and imaged on a human 3T MRI scanner. A T_1 -weighted image, T_2 -weighted image, T_1 map and T_2 map of heated and unheated samples of the LTSL, TTSL and NTSL are shown in Figure 2.11. Table 2.3 gives the corresponding T_1 and T_2 values.

Table 2.3: T_1 and T_2 values (\pm standard deviation) of LTSL, TTSL and NTSL, before and after heating. The average and standard deviation were calculated from all the pixels within an ROI on the T_1 and T_2 maps.

Formulation	T_1 (ms) unheated	T_1 (ms) heated	T_2 (ms) unheated	T_2 (ms) heated
LTSL	1828 \pm 11	394 \pm 2	772 \pm 4	270 \pm 2
TTSL	1763 \pm 16	409 \pm 3	993 \pm 7	293 \pm 2
NTSL	1559 \pm 30	1522 \pm 14	928 \pm 6	909 \pm 13

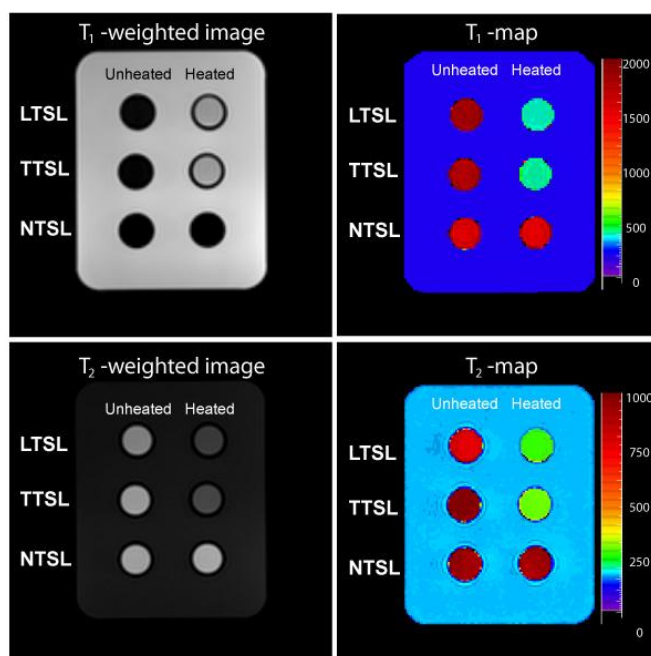


Figure 2.11. T_1 -weighted image ($TI = 1500$ ms) (top left), T_1 map (top right), T_2 -weighted image ($TE = 320$ ms) (bottom left) and T_2 map (bottom right) of LTSL, TTSL and NTSL, before and after heating. The Gd concentration was 0.45 mM for all samples. The sample holder contains a standard phantom solution.

Before heating, the three different paramagnetic liposomes showed similar T_1 values, while after heating a decrease in T_1 was observed for the LTSL and TTSL due to the complete release of $[\text{Gd}(\text{HPDO3A})(\text{H}_2\text{O})]$. No significant difference was measured between the heated and unheated sample of the NTSL. The same behavior is observed in the corresponding T_2 measurements. This experiment shows the potential for MR imaging in combination with these temperature-sensitive liposomal formulations, as an indicator for contrast agent release.

2.4. Discussion

The stability, release kinetic and cytotoxicity of two temperature sensitive liposomal formulations of doxorubicin co-encapsulated with [Gd(HPDO3A)(H₂O)] have been investigated and compared to a non-temperature sensitive liposomal formulation. The T_1 measurements as a function of temperature imply that [Gd(HPDO3A)(H₂O)] remains intraliposomal at $T < T_m$. At these conditions, the transport of the hydrophilic MRI contrast agent across the lipid bilayer by diffusion is unlikely due to the unfavorable lipid/water partition coefficient. At $T < T_m$, the longitudinal relaxivity of the liposome encapsulated paramagnetic MRI contrast agents is modulated by the water diffusion across the phospholipid bilayer that increases with increasing temperature. At temperatures close to T_m , an increasing permeability of the lipid bilayer allows rapid release of this compound as well as doxorubicin. These findings correspond with the results published by Fossheim *et al.*, who studied the *in vitro* feasibility of liposomal Gd-DTPA-BMA without additional co-encapsulation of a drug.¹⁴ In their work, a sharp increase in r_1 was observed as the temperature approached the T_m of the lipid bilayer. For temperatures above T_m , the longitudinal relaxivities of liposomal Gd-DTPA-BMA were found to be identical to free Gd-DTPA-BMA.

The LTSL and TTSL showed a rapid release of encapsulated doxorubicin and MRI contrast agents at $T \geq T_m$. It is important to note that the onset of release of the hydrophilic [Gd(HPDO3A)(H₂O)] and the aggregated doxorubicin appears to occur at the same temperature. The fast release of [Gd(HPDO3A)(H₂O)] at $T \geq T_m$ might be explained in terms of pore formation, which allows the release of hydrophilic structures from the aqueous lumen of the liposome. The LTSL shows considerable doxorubicin leakage in fully supplemented DMEM containing 10% Fetal Bovine Serum (FBS) at 37 °C, while it was found stable in pure HBS solution. Apparently, the interaction of the LTSL with compounds present in the fully supplemented DMEM, such as albumin, alters the release properties. The doxorubicin release is more rapid for the LTSL compared to the TTSL, which may originate from the lysolipids present in LTSL formulation. The lysolipids are also known for their ability to leave the liposomal bilayer to interact with *e.g.* albumin or exchange and incorporate into cellular membranes.³³ The latter effect leads most likely to a reduction in phase transition temperature and a much enhanced leakage at 37 °C in DMEM compared to buffer solution. However, the presented experimental data do not allow any quantitative assessment of the exact release mechanism, like differences in number of pores, pore diameters or temporal effects.

The *in vitro* data presented here show that the LTSL and TTSL systems encapsulating both doxorubicin and [Gd(HPDO3A)(H₂O)] present promising formulations for *in vivo* use. In the next Chapters, these systems will be investigated *in vivo* for temperature induced drug delivery under MR image guidance using high intensity focused ultrasound to locally heat the target tissue.

2.5. Conclusion

A novel methodology for the preparation of liposomal systems encapsulating doxorubicin and a clinically approved T_1 MRI contrast agent, [Gd(HPDO3A)(H₂O)], has been developed for application in temperature-induced drug delivery under MRI guidance. The presence of [Gd(HPDO3A)(H₂O)] in the intraliposomal space did not affect the loading of doxorubicin and the formation of doxorubicin crystals inside the liposomes. The release kinetics of the encapsulated contrast agents and drugs strongly depends on the composition of the liposomal membrane and needs to be tuned with respect to the drug delivery aspect and the MRI contrast generation. For the former, stability at 37 °C is important to avoid rapid drug leakage, but on the other hand, rapid drug release at hyperthermic conditions is required. The *in vitro* experiments shown in this publication indicate the TTSL formulation as the most promising candidate, as it meets these specific requirements, while the drug leakage of LTSL system at body temperature might be too high. The lipid membrane acts as a diffusion barrier below T_m and modulates the water diffusion and therefore also the T_1 and T_2 contrast generation. Imaging of the drug release of temperature-sensitive liposomes will be an important tool in order to be able to monitor and control the drug delivery process. The here presented combination of a chemotherapeutic drug with a clinically approved MRI contrast agent will provide the ability of *in vivo* MR monitoring of a temperature-controlled drug delivery process.

2.6 Acknowledgements

We thank dr. Marcel Verheijen and Monja Kaiser, Material Analysis, Philips Research Eindhoven, for the cryo-TEM measurements, dr. Jeroen Pikkemaat, Material Analysis, Philips Research Eindhoven, for the NMR measurements at 300 MHz, Roland van de Molengraaf, Life Science Facility, Philips Research Eindhoven, for help with the MRI measurements and Martijn Lijbers for the fruitful discussions on the transmembrane water exchange rate.

2.7 References

1. Yatvin MB, Weinstein JN, Dennis WH, et al. Design of liposomes for enhanced local release of drugs by hyperthermia. *Science*. 1978;202:1290-3.
2. Weinstein JN, Magin RL, Yatvin MB, et al. Liposomes and local hyperthermia- selective delivery of methotrexate to heated tumors. *Science*. 1979;204(4389):188-91.
3. Kong G, M.W. Dewhirst. Review Hyperthermia and liposomes. *Int J Hyperthermia*. 1999;15(5):345-70.
4. Maruyama K, S. Unezaki, N. Takahashi, M. Iwatsuru. Enhanced delivery of doxorubicin to tumor by long-circulating thermosensitive liposomes and local hyperthermia. *Biochimica et Biophysica Acta - Biomembranes*. 1993;1149:209-16.
5. Hossann M, Wiggernhorn M, Schwerdt A, et al. In vitro stability and content release properties of phosphatidylglyceroglycerol containing thermosensitive liposomes. *Biochim Biophys Acta*. 2007;1768:2491-9.
6. Hossann M, Wang T, Wiggernhorn M, et al. Size of thermosensitive liposomes influences content release. *Journal of Controlled Release*. 2010;147:436-43.
7. Li L, T.L.M. ten Hagen, D. Schipper, T.M. Wijnberg, G. van Rhoon, A.M.M. Eggermont, L.H. Lindner, G.A. Koning. Triggered content release from optimized stealth thermosensitive liposomes using mild hyperthermia. *J Control Release*. 2010.
8. Lindner LH, Eichhorn ME, Eibl H, et al. Novel temperature-sensitive liposomes with prolonged circulation time. *Clin Cancer Res*. 2004;10:2168-78.
9. Mills JK, Needham D. The materials engineering of temperature-sensitive liposomes. *Methods Enzymol*. 2004;387:82-113.
10. Anyarambhatla GR, D. Needham. Enhancement of the phase transition permeability of DPPC liposomes by incorporation of MPPC: A new temperature-sensitive liposome for use with mild hyperthermia. *J Liposome Res*. 1999;9(4):491-506.
11. Kong G, Anyarambhatla G, Petros WP, et al. Efficacy of liposomes and hyperthermia in a human tumor xenograft model: importance of triggered drug release. *Cancer Res*. 2000;60:6950-7.
12. Needham D, Anyarambhatla G, Kong G, et al. A new temperature-sensitive liposome for use with mild hyperthermia: characterization and testing in a human tumor xenograft model. *Cancer Res*. 2000;60:1197-201.
13. Landon CD, Park J, Needham D, et al. Nanoscale drug delivery and hyperthermia: The materials design and preclinical and clinical testing of low temperature-sensitive liposomes used in combination with mild hyperthermia in the treatment of local cancer. *The Open Nanomedicine Journal*. 2011;3:38-64.
14. Fossheim SL, K.A. Il'yasov, J. Hennig, A. Bjørnerud. Thermosensitive paramagnetic liposomes for temperature control during MR Imaging-guided hyperthermia: In vitro feasibility studies. *Acad Radiol*. 2000;7(12):1107-15.
15. Frich L, A. Bjørnerud, S. Fossheim, T. Tillung, I. Gladhaug. Experimental application of thermosensitive paramagnetic liposomes for monitoring magnetic resonance imaging guided thermal ablation. *Magn Reson Med*. 2004;52:1302-9.
16. McDannold N, S.L. Fossheim, H. Rasmussen, H. Martin, N. Vykhodtseva, K. Hynynen. Heat-activated liposomal MR contrast agent: initial in vivo results in rabbit liver and kidney. *Radiology*. 2004;230:743-52.

17. Bos C, M. Lepetit-Coiffé, B. Quesson, C.T.W. Moonen. Simultaneous monitoring of temperature and T1: methods and preliminary results of application to drug delivery using thermosensitive liposomes. *Magn Reson Med.* 2005;54:1020-4.
18. Salomir R, J. Palussière, S.L. Fossheim, A. Rogstad, U.N. Wiggen, N. Grenier, C.T.W. Moonen. Local delivery of Magnetic Resonance (MR) contrast agent in kidney using thermosensitive liposomes and MR Imaging-guided local hyperthermia: a feasibility study in vivo. *J Magn Reson Imaging.* 2005;22:534-40.
19. Peller M, A. Schwerdt, M. Hossann, H.M. Reinl, T. Wang, S. Sourbron, M. Ogris, L.H. Lindner. MR characterization of mild hyperthermia-induced gadodiamide release from thermosensitive liposomes in solid tumors. *Investigative Radiology.* 2008;43(12):877-92.
20. Langereis S, Keupp J, van Veldhoven JLJ, et al. A temperature-sensitive liposomal ¹H CEST and ¹⁹F contrast agent for MR Image-guided drug delivery. *J Am Chem Soc.* 2009;131:1380-1.
21. Wang T, M. Hossann, H.M. Reinl, M. Peller, H. Eibl, M. Reiser, R.D. Issels, L.H. Lindner In vitro characterization of phosphatidylglycerol-based thermosensitive liposomes with encapsulated ¹H MR T₁-shortening gadodiamide. *Contrast Media Mol Imaging.* 2008;3:19-26.
22. Gaber MH, K. Hong, S.K. Huang, D. Papahadjopoulos. Thermosensitive Sterically Stabilized Liposomes: Formulation and in Vitro Studies on Mechanism of Doxorubicin Release by Bovine Serum and Human Plasma. *Pharm Res.* 1995;12(10):1407-16.
23. Anyarambhatla GR, D. Needham. Enhancement of the Phase Transition Permeability of DPPC Liposomes by Incorporation of MPPC: A New Temperature-Sensitive Liposome for Use with Mild Hyperthermia. *J Liposome Res.* 1999;9(4):491-506.
24. Needham D, G. Anyarambhatla, G. Kong, M.W. Dewhirst. A new temperature-sensitive liposome for use with mild hyperthermia: characterization and testing in a human tumor xenograft model. . *Cancer Res.* 2000;60:1197-201.
25. Kong G, G. Anyarambhatla, W.P. Petros, R.D. Braun, O.M. Colvin, D. Needham, M.W. Dewhirst. Efficacy of liposomes and hyperthermia in a human tumor xenograft model: importance of triggered drug release. . *Cancer Res.* 2000;60:6950-7.
26. Abraham SA, D.N. Waterhouse, D. Lawrence, D. Mayer, P.R. Cullis, T.D. Madden, M.B. Bally. The liposomal formulation of doxorubicin. *Methods Enzymol.* 2005;391:71-97.
27. Koenig SH, G.F. Ahkong, R.D. Brown, M. Lafleur, M. Spiller, E. Unger, C. Tilcock. Permeability of liposomal membranes to water: results from the magnetic field dependence of t₁ of solvent protons in suspensions of vesicles with entrapped paramagnetic ions. *Magn Reson Med.* 1992;23(2):275-86.
28. Terreno E, A. Sanino, C. Carrera, D. Delli Castelli, G.B. Giovanzana, A. Lombardi, R. Mazzon, L. Milone, M. Visigalli, S. Aime. Determination of water permeability of paramagnetic liposomes of interest in MRI field. *J Inorg Biochem.* 2008;102(5-6):1112-9.
29. Haran G, R. Cohen, L.K. Bar, Y. Barenholz. Transmembrane ammonium sulfate gradients in liposomes produce efficient and stable entrapment of amphipathic weak bases. *Biochimica et Biophysica Acta - Biomembranes.* 1993;1151:201-15.
30. Li X, D.J. Hirsh, D. Cabral-Lilly, A. Zirkel, S.M. Gruner, A.S. Janoff, W.R. Perkins. Doxorubicin physical state in solution and inside liposomes loaded via a pH gradient. *Biochim Biophys Acta.* 1998;1415:23-40.
31. Unger E, D.K. Shen, G.L. Wu, T. Fritz. Liposomes as MR contrast agents: pros and cons. *Magn Reson Med.* 1991;22(2):304-8.

32. Mulkern RV, A.R. Bleier, I.K. Adzami, R.G. Spencer, T. Sandor, F.A. Jolesz. Two-site exchange revisited: a new method for extracting exchange parameters in biological systems. *Biophys J* 1989;55(2):221-32.
33. Sandstrom MC, Ickenstein LM, Mayer LD, et al. Effects of lipid segregation and lysolipid dissociation on drug release from thermosensitive liposomes. *J Control Release*. 2005;107:131-42.

Chapter 3

Validation of doxorubicin quantification methods in tissue and blood samples – a multi-centre comparison

Abstract

Two different protocols for quantification of doxorubicin in tissue and blood samples were compared. One is based on the quantification of doxorubicin fluorescence with High Performance Liquid Chromatography (HPLC) after chemical extraction from tissue and blood samples. The other method requires the use of ^{14}C -labeled doxorubicin, which is a β -emitter that can be quantified with Liquid Scintillation Counting (LSC). In this study, both methods were used to quantify doxorubicin in tissue and blood samples obtained from rats after *i.v.* injection with ^{14}C -doxorubicin encapsulated in temperature-sensitive liposomes. For spiked samples, the two quantification methods showed reliable results. For blood and tissue samples from the *in vivo* experiments, LSC showed 13-42 % higher ^{14}C -doxorubicin concentrations than HPLC. Advantages and disadvantages of both methods are discussed. A multi-centre comparison of doxorubicin quantification using HPLC showed a good correspondence of the obtained results between different labs.

Based on:

M. de Smet, S. van den Bosch, K. Donato, K. Bitter, M. Hossann, A.H. Negussie, M.R. Dreher, S. Langereis, B.J. Wood, L.H. Lindner and H. Gröll. *Validation of doxorubicin quantification methods in tissue and blood samples – a multi-centre comparison*. In preparation

3.1 Introduction

Doxorubicin is a widely used chemotherapeutic drug in clinical practice with significant antitumor activity against several human malignancies, including leukemia and breast cancer.^{1,2} The clinical utility of doxorubicin is hampered by cumulative and irreversible cardiotoxicity, myelosuppression, and the occurrence of drug resistance.^{3,4} Emerging drug delivery approaches can alter doxorubicin biodistribution radically and reduce the toxicity profiles of this chemotherapeutic drug. For example, long circulating, sterically stabilized liposomes containing doxorubicin have shown to reduce cardiac toxicity compared to unencapsulated doxorubicin.^{5,6} Using these formulations, drug deposition in the tumor can be increased due to the enhanced permeability and retention (EPR) effect.⁷⁻⁹ To further enhance the amount of doxorubicin delivered to the tumor, trigger-responsive nanoparticles have been investigated, for instance, temperature-sensitive liposomes (TSLs) that are able to release encapsulated drugs upon heating.¹⁰⁻¹⁴ However, the radical change in biodistribution profiles of the drug due to the encapsulation into liposomal carriers requires a careful investigation. Coupled with tissue-dependent differences in metabolism, the altered biodistribution could play an important role in the toxicity profiles of the drug. Each different liposomal formulation may lead to a different biodistribution. For example, Charrois *et al.* showed that drug leakage rates from TSLs play an important role in the therapeutic activity as well as in the toxicity of liposomal drug formulations. Pegylated liposomes with fast, intermediate and slow rates of doxorubicin leakage were formulated by altering the fatty acyl chain length and degree of saturation of phosphatidylcholine, the bilayer-forming element in the liposomes.¹⁵ In order to detect these subtle changes, a reliable method enabling the quantification of doxorubicin is essential and would assist the optimization of carrier-based strategies for local drug delivery.

A variety of procedures to extract and quantify doxorubicin and its metabolites using High Performance Liquid Chromatography (HPLC) with subsequent fluorescence detection have been published.¹⁶⁻³⁴ Validation of these methods is usually performed using spiked blood or tissue samples with known amounts of doxorubicin. However, *in vivo* many other processes can occur and doxorubicin may be taken up by cells differently than in case of spiked samples. Since extraction efficiencies might be different for doxorubicin internalized by cells than for the extracellular drug, validation of extraction protocols using spiked samples may not be representative for the quantification of the drug after *in vivo* administration.

Israel *et al.* compared two different protocols for quantification of ¹⁴C-labeled N-trifluoroacetyl Adriamycin-14-valerate (AD32). They measured levels of radioactivity as well as total anthracycline fluorescence in mouse serum, urine and organs after *i.v.* administration of ¹⁴C-labeled AD32.^{35,36} AD32 is a semisynthetic analog of doxorubicin, which, in contrast to doxorubicin, does not bind to isolated DNA preparations. Comparison of

the levels of metabolites as determined by radioactivity with those detected by fluorescence was used as a methodology for detecting, quantifying, and isolating possible nonfluorescent metabolites of AD32. Verdun *et al.* studied the tissue distribution of doxorubicin and doxorubicinol 1h after *i.v.* injection of ^{14}C -doxorubicin linked to polyisohexylcyanoacrylate nanoparticles.³⁷ Although the amount of doxorubicin was reduced, the total anthracycline concentration (doxorubicin + doxorubicinol) showed a good correlation with ^{14}C -liquid scintillation counting.

In the study presented here, two different protocols for quantification of doxorubicin in tissue and blood samples were compared. One is based on the quantification of doxorubicin fluorescence with HPLC after chemical extraction from tissue and blood samples with an organic solvent, using daunorubicin as an internal standard (Figure 3.1B). The other method requires the use of ^{14}C -labeled doxorubicin (Figure 3.1A), which is a β -emitter that can be quantified with Liquid Scintillation Counting (LSC). Both methods are used to quantify doxorubicin in tissue and blood samples obtained from rats after intravenous injection with ^{14}C -doxorubicin encapsulated in temperature-sensitive liposomes. The results of the two quantification methods were compared and the advantages and disadvantages are discussed. In order to test the reproducibility of the HPLC protocol, a multi-centre comparison was performed by analysis of the same samples in three different labs. Furthermore, a dual labeling method was discussed, where the liposomes were labeled with ^{111}In , to quantify the liposomal carrier as well as the encapsulated doxorubicin.

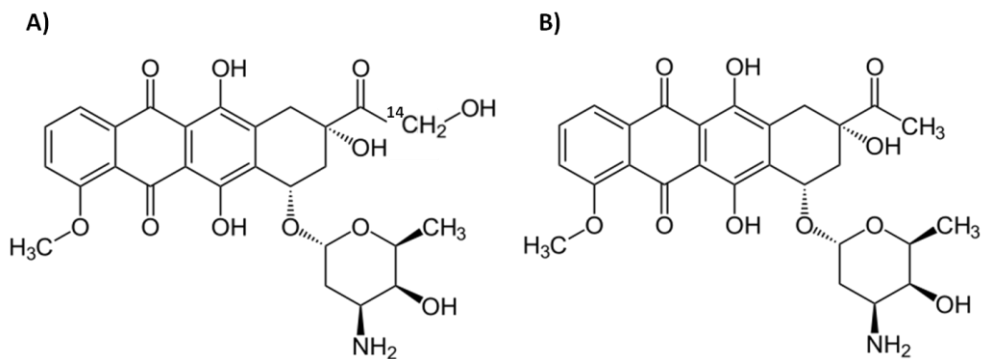


Figure 3.1. Structural formulas of A) ^{14}C -labeled doxorubicin and B) daunorubicin, which is used as an internal standard for the HPLC quantification.

3.2. Materials and methods

3.2.1 Materials

1,2-Dipalmitoyl-*sn*-glycero-3-phosphocholine (DPPC) and hydrogenated-*L*- α -phosphatidylcholine (HSPC) were kindly provided by Lipoid. 1,2-Dipalmitoyl-*sn*-glycero-3-phosphoethanolamine-*N*-[methoxy(polyethyleneglycol)-2000] (DPPE-PEG2000) and cholesterol were purchased from Avanti Polar Lipids. DOTA-DSPE was synthesized according to the procedure described by Hak *et al.*³⁸ [Gd(HPDO3A)(H₂O)] (ProHance[®]) was obtained from Bracco Diagnostics (Italy). Doxorubicin hydrochloride was purchased from AvaChem Scientific (USA). ¹⁴C-doxorubicin hydrochloride, ¹¹¹InCl₃, SOLVABLE™ and Ultima Gold™ scintillation fluid were purchased from Perkin Elmer (USA).

3.2.2 Temperature-sensitive liposomes

For comparison of the different quantification methods three different groups were defined. Animals of the first group received an injection of doxorubicin loaded TSLs. The rats of the second and third group were injected with TSLs loaded with ¹⁴C-doxorubicin. Subsequently, the TSLs of the third group were radiolabeled with ¹¹¹In as described in section 3.2.3. Figure 3.2 represents a schematic overview of the three different formulations.

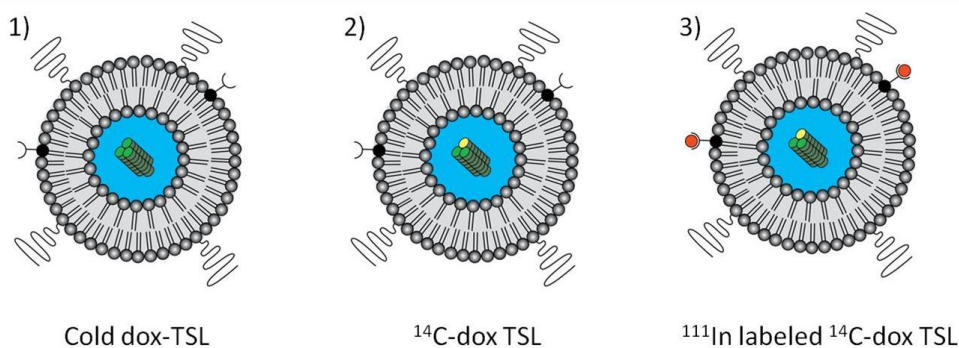


Figure 3.2. Schematic overview of the three groups used in this study; 1) TSL loaded with cold doxorubicin, 2) TSL loaded with ¹⁴C-doxorubicin and 3) TSL loaded with ¹⁴C-doxorubicin and labeled with ¹¹¹In.

Preparation and characterization of temperature-sensitive liposomes was performed in a similar fashion as described in Chapter 2. DPPC:HSPC:Chol:DPPE-PEG2000:DOTA-DSPE (50:25:15:3:1 molar ratio) were dissolved in a solution of chloroform:methanol (4:1 v/v). The organic solvents were removed *in vacuo* until a thin lipid film was formed, which was further dried under nitrogen flow. The lipid film was hydrated at 60 °C in 120 mM (NH₄)₂SO₄

buffer (pH 5.4) containing 250 mM [Gd(HPDO3A)(H₂O)]. The suspension was extruded at 60 °C successively through a polycarbonate filter of 200 nm (two times), and 100 nm (six times). Subsequently, the extraliposomal buffer was replaced by HEPES Buffered Saline (HBS) (20 mM HEPES and 137 mM NaCl at pH 7.4) by gel filtration through a PD-10 column. A solution of doxorubicin in HBS (5 mg/mL) was added to the liposomes at a phospholipid to doxorubicin molar ratio of 17.5:1 and the TSLs were incubated at 37 °C overnight. For TSLs loaded with ¹⁴C-doxorubicin (group 2 and 3), 110 kBq/mL ¹⁴C-doxorubicin was added to the 5 mg/mL cold doxorubicin in HBS solution prior to the addition to the liposomal solution. Finally, the TSLs were passed through a 0.22 µm filter and a second PD-10 column in order to remove any unencapsulated doxorubicin. The liposomes were concentrated using an Amicon Ultra-15 Centrifugal Filter Unit (50 kDa MWCO, Millipore).

For characterization of the cold dox-TSLs, the hydrodynamic radius of the liposomes was determined in HBS using Dynamic Light Scattering (DLS; ALV/CGS-3 Compact Goniometer System, ALV-GmbH, Langen, Germany). The melting phase transition temperature (T_m) of the liposomal membrane was determined with Differential Scanning Calorimetry (DSC; Q2000 differential scanning calorimeter, TA Instruments, USA) during heating with 5 K/min from 20 °C to 60 °C. The T_m was defined as the onset of the melting peak in the DSC thermogram. The doxorubicin concentration was determined fluorimetrically in an isopropyl alcohol:H₂O (1:1 v/v) solution using a spectrophotometer (Perkin Elmer LS55, λ_{ex} = 485 nm and λ_{em} = 590 nm). The phospholipid concentration was measured by phosphate determination according to Rouser *et al.*³⁹ and the gadolinium concentration was determined by Inductively Coupled Plasma-Mass Spectrometry (ICP-MS, DRCII, Perkin Elmer) after the destruction of the sample with nitric acid and perchloric acid at 180 °C. For the samples containing ¹⁴C-dox these characterization assays could not be performed due to radiosafety regulations.

3.2.3 ¹¹¹In labeling of TSLs

For group 3 (Figure 3.2), TSLs were radiolabeled by overnight incubation at 30 °C with ¹¹¹InCl₃ in ammonium acetate buffer (pH 4.5, 95 mM). The radiolabeling yield was tested with radio-TLC (running buffer: 200 mM EDTA in saline) before and after 10 minutes of incubation with 0.1 mM DTPA. Subsequently, the sample was passed through a Zeba Desalt Spin column (7 kDa) pre-equilibrated with HBS (pH7.4) in order to remove the ammonium acetate and unbound ¹¹¹In, resulting in a 4 MBq/mL TSL solution with a radiolabeling yield of > 95%.

3.2.4 *Blood kinetics and biodistribution*

The blood circulation and biodistribution of the liposomes was investigated by injecting TSLs (5 mg doxorubicin/ kg bodyweight) via the tail vein of Fisher 344 rats (Charles River, age 5-7 weeks, weight 125-151 g, n=4/group). Blood samples were taken via the vena saphena at 2, 10, 30, 60, 90 and 240 minutes and 24 hours after injection. At 48 h after injection, blood was collected with heart puncture under anesthesia and the rats were euthanized by cervical dislocation. Subsequently pieces of various organs were dissected (average sample weight = 81 ± 34 mg, max = 151 mg, min = 35 mg). The weights of the collected blood samples varied between 21 and 244 mg, with an average of 80 ± 55 mg. All blood and organ samples were collected in preweighed 2 mL eppendorf cups, weighed and stored at -80 °C until further processing.

3.2.5 *Quantification of ^{111}In with γ -counting*

For the blood and organs collected from the rats injected with ^{111}In -labeled TSLs (group 3, see Figure 3.2), the samples and standards of ^{111}In -labeled TSLs were weighed and their radioactivity was counted with a 1480 Automatic Gamma Counter (Wizard™ 3", Perkin Elmer). The percentage of the injected dose was calculated per gram blood or tissue as well as for the total blood and organs, assuming a total blood volume of 7% of the body weight.

3.2.6 *Homogenisation and sample distribution*

After ^{111}In quantification of the samples of group 3 (Figure 3.2), 1.5 mL water containing 0.5 $\mu\text{g}/\text{mL}$ daunorubicin was added to the weighed blood and organ samples of all groups. Also, standards were prepared from the injected liposome solutions. Subsequently, the samples were homogenized at 4 °C with a stainless steel ball for 5-20 min at 30 Hz with a Qiagen TissueLyser. The homogenized samples of group 1 were used for the multi-centre comparison of the doxorubicin concentration by HPLC and were therefore divided in three aliquots. One of the aliquots was analysed with HPLC in our own lab and the other two aliquots were shipped on dry ice to the different labs. Lab B was the Department of Internal Medicine III, University Hospital Munich, Ludwig Maximilians-University, Munich, Germany, and lab C was the Center for Interventional Oncology, Radiology and Imaging Sciences, Clinical Center, National Institutes of Health, Bethesda, Maryland. Both labs are experienced in the quantification of doxorubicin using HPLC.^{40, 41}

The homogenized samples of group 2 and 3 were divided in two aliquots, which were used for: I) the determination of the doxorubicin concentration by HPLC and II) the determination of the doxorubicin concentration by liquid scintillation counting (LSC). A schematic overview of the sample processing is shown in Figure 3.3.

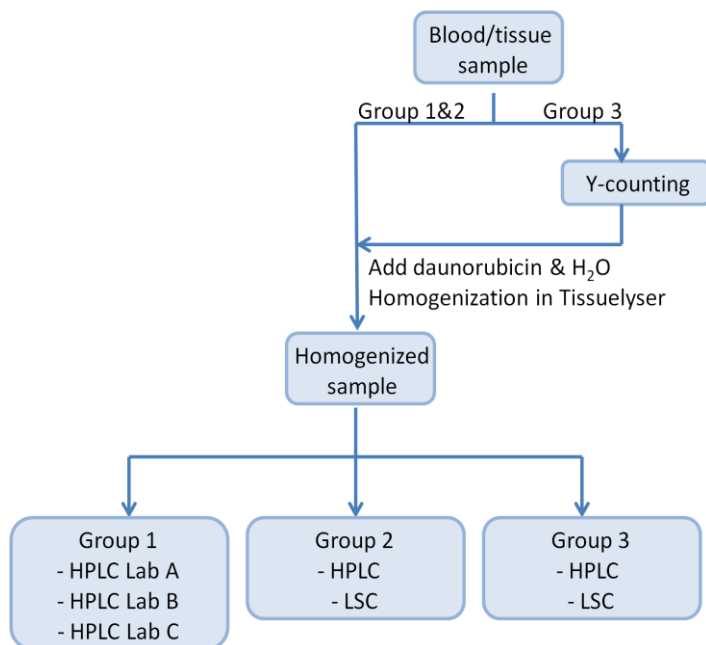


Figure 3.3. Overview of the processing and analysis of the samples from the different groups. Gamma-counting was used to quantify ^{111}In , while HPLC and LSC were used for quantification of doxorubicin.

3.2.7 Doxorubicin quantification with HPLC

For doxorubicin extraction, 125 μL of the homogenized blood, organs and standards were incubated with 50 μL AgNO_3 in water (1.94 M) for 10 minutes at room temperature. Subsequently, the doxorubicin was extracted by vigorous mixing with 1.25 mL chloroform/isopropanol (2:1 v/v). After centrifugation (10 min at 3600 rpm) the organic phase was transferred to a clean tube and evaporated to dryness at 40 $^\circ\text{C}$ under N_2 flow. The residue was dissolved in H_2O (200 μL), centrifuged and 50 μL was injected onto the HPLC column. The samples were analyzed on an Agilent Technologies HPLC system (1100 series) equipped with an autosampler and fluorescence detector with $\lambda_{\text{ex}} = 485 \text{ nm}$ and $\lambda_{\text{em}} = 590 \text{ nm}$. An Eclipse 5 μm , $4.6 \times 150 \text{ mm}^2$ XDB-C18 column (Agilent) was used. Doxorubicin and daunorubicin were eluted in 6 and 12 min respectively, using an isocratic flow of 1 mL/min with 30% (v/v) acetonitrile in H_2O containing 0.1% TFA(v/v). The amount of doxorubicin in the samples was calculated by comparing the dox/daun ratio measured for each sample with the calibration line prepared from the measured standards. The percentage of the injected dose was calculated per gram blood or tissue and as well as for the total blood and organs, assuming a total blood volume of 7% of the body weight.

3.2.8 Doxorubicin quantification with liquid scintillation counting

For LSC, the β -radiation emitted from the ^{14}C was quantified. Since scintillation counters do not directly measure the β -radiation, the use of a liquid scintillation cocktail is required, which contains scintillator and solvent molecules. After excitation of the solvent molecules by the β -radiation emitted from the ^{14}C -dox, the energy is transferred to the scintillator. The energy absorbed by the scintillator produces excited states of the electrons, which decay to the ground state and produce a characteristic light pulse. Finally, this light is detected by the photomultiplier tube (PMT) of the liquid scintillation counter (Figure 3.4).

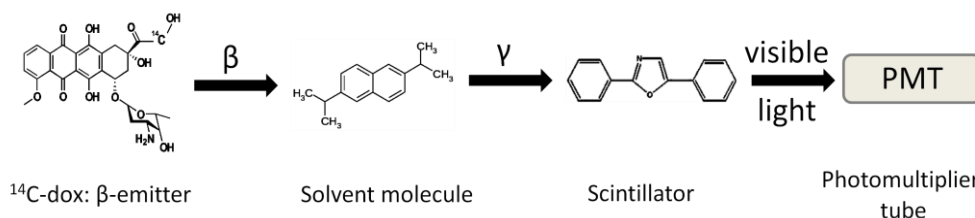


Figure 3.4. Principle of Liquid Scintillation Counting. Scintillation counters do not directly measure the β -radiation, but instead it measures light photons resulting from excitation of a scintillator, which is present in the scintillation cocktail.

First, 0.5 mL of the homogenized blood and tissue samples were dissolved in 1 mL solubilizer (SolvableTM) at 60 °C overnight. To avoid physical quenching, proper homogenization of the solution is important enabling optimal contact between the radioisotope and the scintillator. As color quenching occurs when the emitted light is absorbed by colored samples, a decolorization step is performed by overnight incubation at 60 °C after the addition of 0.3 mL of 30% hydrogen peroxide and 0.3 mL isopropanol. The isopropanol was added to reduce foaming. Finally, 10 mL scintillation cocktail (Ultima GoldTM) was added and the samples were counted with a liquid scintillation counter (Packard 2500 TR, 30 min/sample, energy window 4-156 keV). Standards of the injected TSLs were prepared in a similar fashion, except the hydrogen peroxide was replaced by H_2O .

3.2.9 Quench correction

Besides physical quenching and color quenching, the energy emitted by the radioisotopes can also be absorbed by compounds (e.g. chemicals added to the solution) that will not re-emit the energy. In this case, the energy of the ^{14}C will not reach the scintillator and consequently, no light will reach the detector. This phenomenon is termed chemical quench. Due to all types of quenching, the counting efficiency, defined as the ratio between the number of events counted by the instrument and the real quantity of disintegration events,

is reduced. To correct for quenching, the Spectral Index of the Transformed External standard spectrum (tSIE) was derived from the spectrum measured using a built-in gamma-source of ^{133}Ba external to the sample. The counting efficiency was obtained from the tSIE by using a standard quench curve of ^{14}C in Ultima Gold. The disintegrations per minute (DPM) were calculated using the formula $\text{DPM} = \text{CPM}/\text{efficiency}$, where CPM are the measured counts per minute.

3.2.10 Effect of indium on liquid scintillation counting

The presence of ^{111}In in the samples of group 3 contributed to the liquid scintillation counting results by photon interaction with the scintillation cocktail. Additionally, the $^{111}\text{InCl}_3$ which was used for the radiolabelling contained a fraction of $^{114\text{m}}\text{In}$, which was also detected by the scintillation counter. However, the ratio $^{111}\text{In}/^{114\text{m}}\text{In}$ is different for every batch of $^{111}\text{InCl}_3$. Therefore, it was necessary to perform a correction for the indium contribution to the LSC results.

To determine the CPM resulting from the two indium isotopes, different batches of $^{111}\text{InCl}_3$ were measured with an energy calibrated HpGe(Li) detector (Canberra DSA1000) to quantify the amount of ^{111}In and $^{114\text{m}}\text{In}$ in the samples, as well as with the liquid scintillation counter to quantify the total CPM. Subsequently, the ratio $^{111}\text{In}/^{114\text{m}}\text{In}$ was measured with the HpGe(Li) detector for one sample of group 3. Since all rats were injected with the same batch of ^{111}In -labeled TSLs, this ratio is the same for all samples of this group. The $^{111}\text{In}/^{114\text{m}}\text{In}$ ratio and the gamma counting results were used to calculate the absolute amount of ^{111}In and $^{114\text{m}}\text{In}$ for every sample of this group. Next, the CPM contribution of the two indium isotopes was calculated for each sample, and subtracted from the measured CPM. Finally, the DPM was calculated using the formula $\text{DPM}_{\text{corrected}} = (\text{CPM}_{\text{total}} - \text{CPM}_{\text{In-111}} - \text{CPM}_{\text{In-114m}})/\text{efficiency}$.

3.2.11 Doxorubicin quantification with both protocols

In order to compare both quantification methods on the same samples, the collected samples from group 2 and 3 were homogenized and divided. A schematic overview is shown in Figure 3.5 and the detailed SOP is provided at the end of this Chapter. When only the scintillation method is used, the blood and tissue samples do not need to be homogenized first, but they can be directly dissolved into the solubilizer.

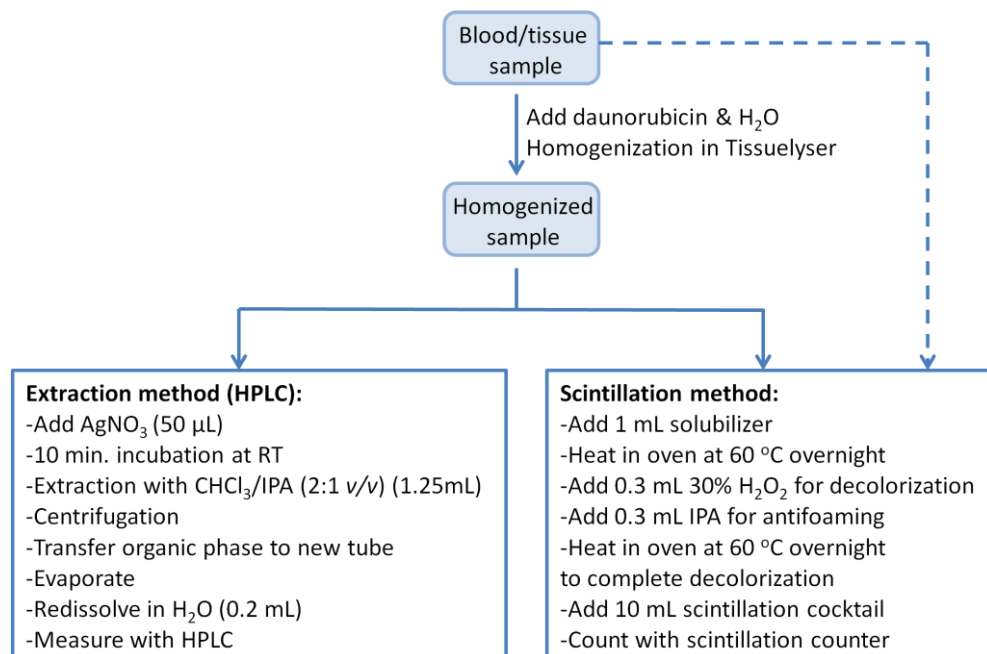


Figure 3.5. Sample preparation protocol for the two doxorubicin quantification methods. The blood and tissue samples were homogenized, divided and analyzed with both methods. The dotted line shows the shortcut in the case when only the scintillation method is used; the blood and tissue samples do not need to be homogenized first, but they can be directly dissolved into the solubilizer.

3.3 Results

3.3.1 Liposome preparation

TSLs were successfully prepared and loaded with doxorubicin, either cold or spiked with ^{14}C -doxorubicin. For the cold TSLs (group 1), the hydrodynamic radius was 63.7 nm (polydispersity index < 0.1) as determined by dynamic light scattering (DLS). The melting phase transition temperature (T_m), defined as the onset of the phase transition peak in the differential scanning calorimetry (DSC) spectrum, was $42.4 \pm 0.1^\circ\text{C}$. The phosphate, gadolinium, doxorubicin and ^{14}C concentrations of the liposomal solutions were determined by the methods described in section 3.2.2 and are shown in Table 3.1. For the samples containing ^{14}C -dox the hydrodynamic radius, T_m , phosphate and gadolinium concentrations were not determined, because these assays could not be performed due to radiosafety regulations.

Table 3.1. Phosphate, gadolinium, doxorubicin and ^{14}C concentrations of the three liposomal solutions. N.D. = not determined

Group	TSLs	[P] (mM)	[Gd] (mM)	[dox](mM)	[^{14}C](kBq/mL)
1	cold	46.5±2.5	24.3 ± 1.2	2.7 ± 0.1	-
2	^{14}C -dox	N.D.	N.D.	4.7 ± 0.2	59 ± 3
3	^{14}C -dox & ^{111}In	N.D.	N.D.	5.7 ± 0.1	72 ± 1

3.3.2 HPLC and LSC of samples spiked with ^{14}C -dox

Clean water and blood samples were spiked with different amounts of ^{14}C -dox solution ([dox]=2 mg/mL, [^{14}C] = 0.5 Bq/mL), homogenized and analyzed with HPLC and LSC, as described in section 3.2.11. Every sample was analyzed in triplicate. The results of both quantification methods are shown in Figure 3.6. Both methods showed a straight line for the different concentrations and the results for the water and blood samples were overlapping. However, the HPLC showed larger standard deviations (average standard deviation was 7.6% of the measured values) than the LSC results, where the standard deviations were only 2.2% of the measured values, indicating that the HPLC method resulted in larger deviations between the three analyzed samples at each concentration.

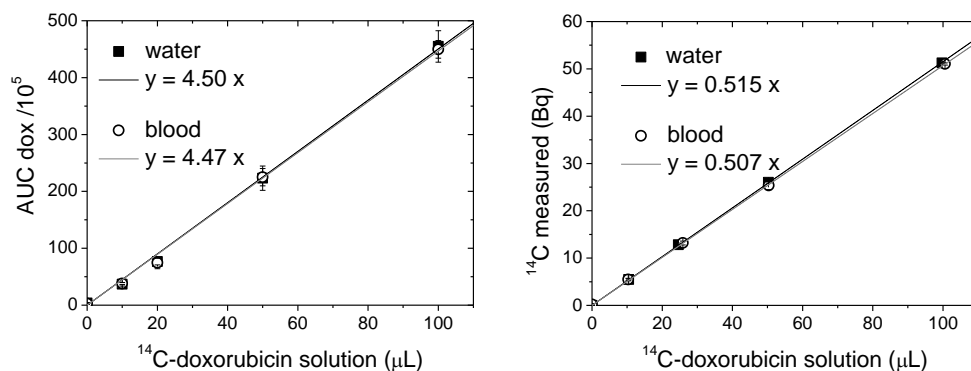


Figure 3.6. Results of HPLC analysis (left) and LSC analysis (right) of water and blood samples spiked with ^{14}C -doxorubicin solution. The x-axis indicates the amount of ^{14}C -doxorubicin ([dox] = 2 mg/mL, [^{14}C] = 0.5 Bq/mL) solution in the analyzed sample.

3.3.3 HPLC and LSC of blood and tissue samples from in vivo experiment

Figure 3.7 shows the doxorubicin concentrations in the blood and tissue samples of group 2 as determined with HPLC and LSC. In Figure 3.8 the LSC results were plotted against the HPLC results, showing a good correlation between the quantification results of the two different methods with a correlation coefficient of 0.965 for the biodistribution and 0.999 for

the blood samples. However, LSC showed $19 \pm 11\%$ higher values for blood samples compared to HPLC, while for the organs even $30 \pm 12\%$ higher values were found. When taking a closer look at the relative deviation between LSC and HPLC results (Figure 3.9) an increase was observed over time.

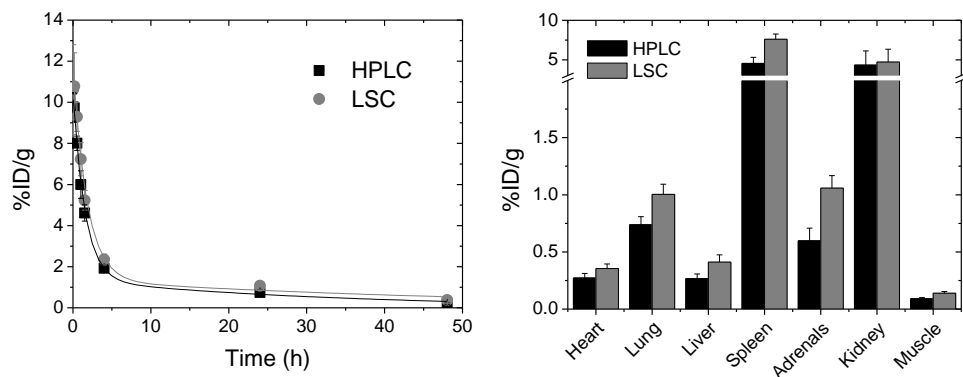


Figure 3.7. Doxorubicin quantification results from HPLC and LSC of blood (left) and tissue (right) samples of rats injected with ^{14}C -dox-TSLs (group 2). Biodistribution was performed 48h after injection.

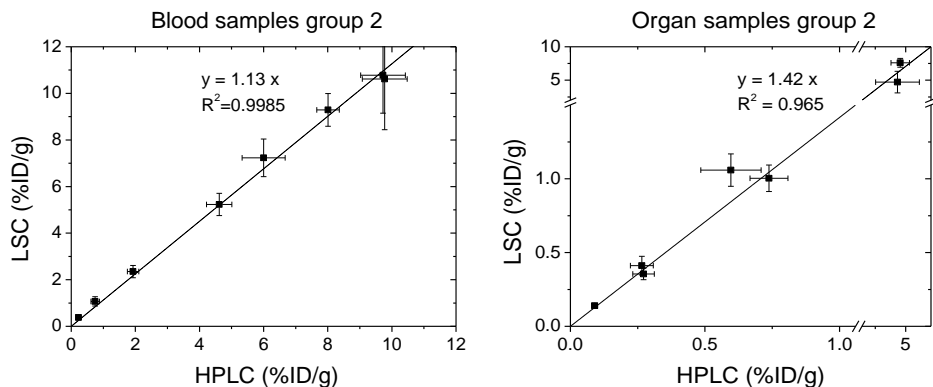


Figure 3.8. Correlation plots of results of doxorubicin quantification with HPLC plotted against the results of doxorubicin quantification with LSC of blood samples (left) and organs (right) of rats injected with ^{14}C -dox-TSLs (group 2).

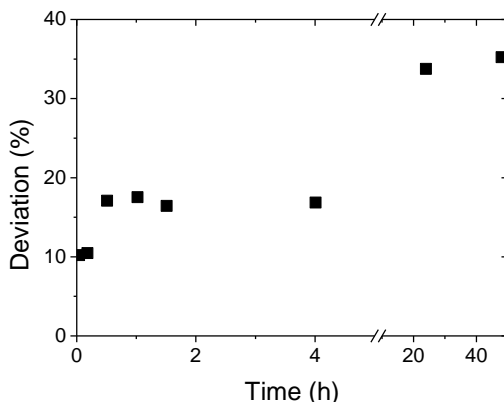


Figure 3.9. Relative deviation between doxorubicin quantification with HPLC and LSC method ($(LSC-HPLC)/LSC \times 100\%$) of blood samples taken at different time points after injection.

3.3.4 Dual labeled liposomes

For group 3, the amount of ^{111}In and doxorubicin were determined of the blood samples collected over time after *i.v.* injection. To correct for the contribution of the indium isotopes to the LSC a correction needed to be performed (see section 3.2.10). The two indium isotopes showed a linear contribution to the cpm in liquid scintillation counting as a function of the concentration, which was 13193 cpm/kBq for ^{111}In and 18442 cpm/kBq for $^{114\text{m}}\text{In}$. The effect of the In correction method is dependent on the amount of indium isotopes present in the samples. An example is shown in Figure 3.10.

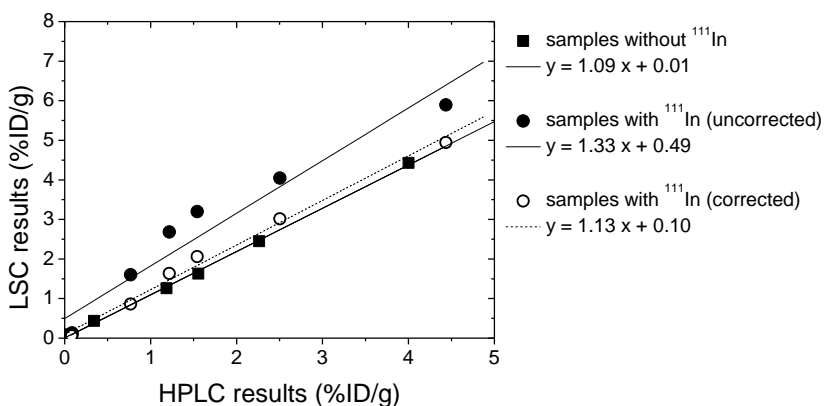


Figure 3.10. Effect of indium correction on LSC results. Without correction, the samples containing ^{111}In showed higher amounts of ^{14}C -dox. After correction, the results are similar to the results for samples without ^{111}In .

The injected dose per gram blood (%ID/g) of ^{111}In and doxorubicin as a function of time is depicted in Figure 3.11. Doxorubicin was cleared faster than its ^{111}In -labeled liposomal carrier, suggesting that the drug leaks out of the liposomes at physiological conditions, followed by rapid clearance of the free small molecules. This drug leakage from temperature-sensitive liposomes was already observed in earlier studies.⁴²⁻⁴⁴ The biodistribution (Figure 3.11) showed the highest liposome uptake by the liver and the spleen as expected, since these organs are part of the mononuclear phagocyte system (MPS), which is typically responsible for filtering out liposomes from the blood circulation.⁴⁵⁻⁴⁷ Interestingly, doxorubicin concentrations found in these organs were lower than the liposome concentrations. This can be explained by the excretion and metabolism of doxorubicin in these organs,¹⁷ as well as uptake of half-filled liposomes over time.

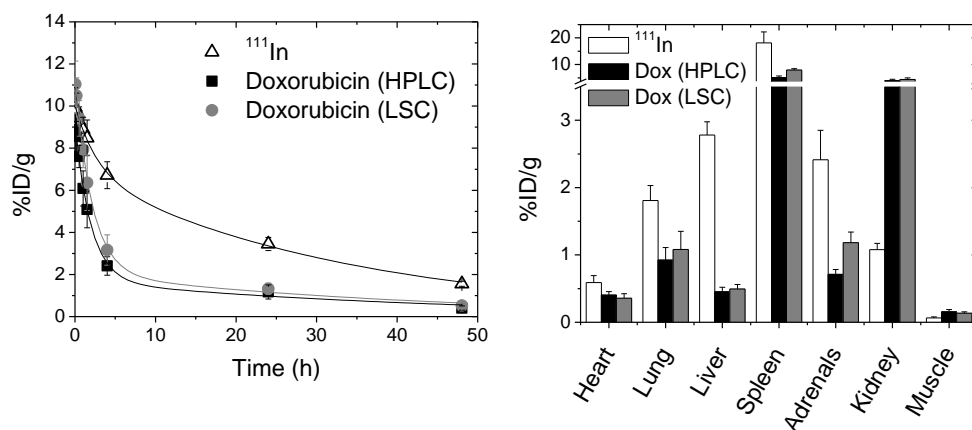


Figure 3.11. ^{111}In -labeled liposome and ^{14}C -doxorubicin quantification results from gamma counting, HPLC and LSC of blood (left) and organ (right) samples of rats injected with ^{14}C -dox- ^{111}In -TSLs (group 3). Biodistribution was performed 48h after injection. LSC results were corrected for indium contributions.

3.3.5 Multi-centre comparison

The homogenized samples of group 1 were used for a multi-centre comparison of the doxorubicin concentration by HPLC and were therefore divided in three aliquots. These aliquots were distributed and analyzed in three different labs: Lab A (our own lab), Lab B (UHM) and Lab C (NIH). Figures 3.12 and 3.13 show the comparison between the quantification results of the three labs. A few samples with low concentrations showed large deviations up to $\pm 50\%$, but the absolute differences were small ($< 0.04\% \text{ID/g}$). The average difference with Lab A, indicating a systemic deviation, was -0.8% for Lab B and -15% for Lab C. The standard deviation of the differences is a measure for the random fluctuations around this mean, which was 22% for both labs.

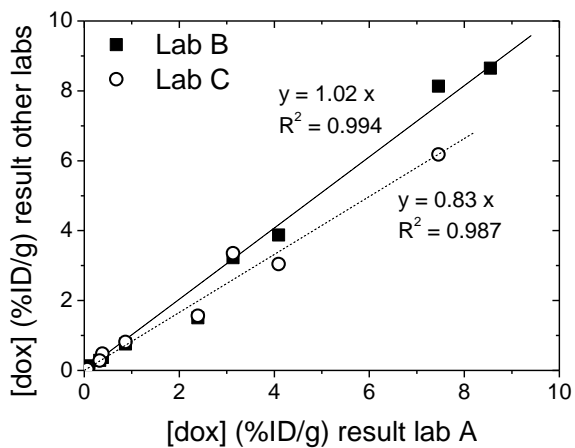


Figure 3.12. Results of lab A plotted against the results of the two other labs. An $R^2 > 0.98$ was found for both labs, indicating a strong relation between the results from the different labs.

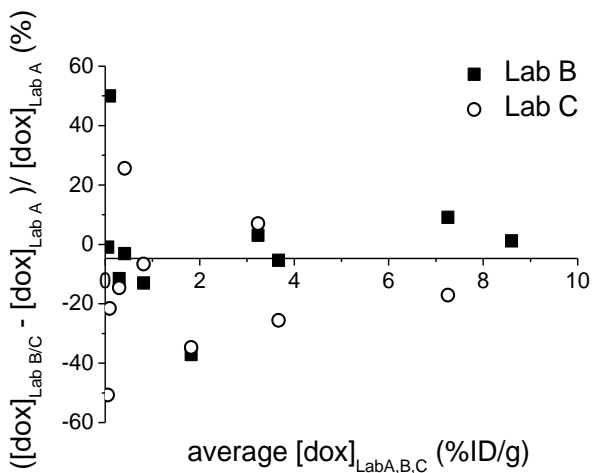


Figure 3.13. Relative difference for Labs B and C with Lab A plotted against the average of the results of the three labs.

3.4 Discussion

In the study presented here, two different protocols for quantification of doxorubicin in tissue and blood samples were compared. One is based on the quantification of doxorubicin with HPLC followed by fluorescent detection after chemical extraction from tissue and blood samples with an organic solvent, while with the other method the amount of β -emission from ^{14}C -labeled doxorubicin was quantified with Liquid Scintillation Counting (LSC). Additionally, a dual labeling method was presented where the liposomes were labeled with ^{111}In allowing the quantification of the liposomal carrier as well as the encapsulated doxorubicin. An advantage of this approach is that a correction on the injected dose could be performed when during the tail vein injection a part of the liposomes is accidentally injected subcutaneously instead of intravenously by measuring the amount of ^{111}In present in the tail. Quantification of doxorubicin as well as the drug carrier provided important information about leakage of the drug from the carrier system at body temperature, which is a necessary insight for the optimization of carrier-based strategies for local drug delivery.

In literature, different methods for sample preparation have been used for LSC of ^{14}C -doxorubicin in blood and tissue samples, such as combustion of the sample in an oxygen-rich atmosphere followed by the collection of $^{14}\text{CO}_2$,^{37, 48} chemical extraction from homogenized tissues,³⁶ or solubilization of the sample.⁴⁹ In this study, the blood and tissue samples were solubilized with Solvable[®], which is an easy and reliable method without the need for any special equipment such as a combustion chamber.

The analysis of spiked samples showed larger deviations between triplicate samples for the HPLC method in comparison with the LSC method, indicating a better reproducibility for the latter. Nevertheless, results from both methods showed a reproducible linear correlation with the concentration. An overview of the advantages and disadvantages of the two methods is shown in Table 3.2. An advantage of the LSC method is that most kinds of tissue can be quantified, in contrast to the HPLC method, where the required homogenization for this method is challenging to perform for some structures (e.g. muscle/tendons, skin and bone) without damaging the doxorubicin itself. Additionally, the same LSC protocol can be widely used for quantification of other ^{14}C -labeled molecules in blood and tissue samples, while the presented HPLC method is specifically for doxorubicin. Another advantage of the LSC method is that the sample preparation is less labor-intensive than the chemical extraction procedure for the HPLC analysis. Obviously, the LSC method requires a radiochemical lab and can therefore not be performed in standard analytical laboratories, nor can it easily be combined with other analytical techniques for radiochemical safety. Above consideration also triggered the here performed comparative study of LSC with an HPLC based protocol performed in three different centers. Similar results were found, showing a good reproducibility of the results obtained with the HPLC protocol between different labs.

Table 3.2. Advantages and disadvantages of the HPLC and LSC method for quantification.

	HPLC method	LSC method
Time needed for analysis	-	+
Applicable for all tissues	-	+
Applicable for other drugs	-	+
Possible to perform in a standard analytical lab	+	-

Typical concentrations that were found in the ~100 mg samples from the *in vivo* experiments were 0.5 – 5 µg doxorubicin (10-100 Bq ¹⁴C) in blood and 0.05-3.5 µg doxorubicin (1-70 Bq ¹⁴C) in organs. These quantities were still well detectable by both methods. However, in the case that a study requires the analysis of smaller samples, the sensitivity may become an issue. For LSC, sensitivity problems can easily be circumvented by increasing the ratio of ¹⁴C-doxorubicin to cold doxorubicin loaded into the liposomes, thereby increasing the amount of injected ¹⁴C, which was approximately 15 kBq ¹⁴C/rat in this study. In contrast, the amount of injected doxorubicin (5 mg/kg) cannot be increased tremendously, since this will lead to serious side effects of this cytotoxic drug.

It is important to keep in mind that the two quantification methods may not give the same results, due to metabolism of doxorubicin in the body. HPLC will only detect the intact doxorubicin molecules, while LSC will detect the amount of ¹⁴C in the sample, so also ¹⁴C-containing radio-metabolites will be included in this quantification.

In our study, LSC indeed showed higher values than HPLC, with an average difference of $19 \pm 11\%$ for the blood samples and $30 \pm 12\%$ for the organs (Figure 3.8). For the blood samples, an increase in the difference between LSC and HPLC was observed over time. We hypothesized that at shorter time points the ¹⁴C-doxorubicin was not yet metabolized and therefore the differences between both methods were small ($\approx 10\%$). Over time, doxorubicin metabolism occurred and therefore ¹⁴C-containing metabolites were detected with LSC, but not with the HPLC method, leading to larger differences between the two methods. This finding is in correspondence with earlier publications from Israel *et al.* They found that serum radioactivity decayed at a much slower rate than fluorescence after *i.v.* administration of ¹⁴C-labeled N-trifluoroacetyl Adriamycin-14-valerate (AD 32).³⁵ Already at 1h after *i.v.* injection, levels of radioactivity appeared to be higher than fluorescence in pancreas, spleen, heart and skeletal muscle (average deviation was 37%).³⁶ Although doxorubicin is a different molecule and the liposomal encapsulation can prevent rapid metabolism, a similar trend can be expected and the differences at 48h after injection will be much more pronounced than at short time points.

Another explanation might be that the extraction method did not recover all the doxorubicin. For example, it might be possible that the efficiency of doxorubicin extraction was lower for drug taken up by cells, then for extracellular drug. Due to slow leakage from liposomes at body temperature, the cellular uptake of doxorubicin also increases over time,

so this hypothesis also fits the time-dependent deviations between the two methods. In summary, both methods are complementary and extensive analysis using both methods provides the most information about metabolism processes and/or cellular uptake.

3.5 Conclusion

¹⁴C-Doxorubicin was quantified in tissue and blood samples with Liquid Scintillation Counting as well as with HPLC after chemical extraction. Both methods were reproducible and showed a linear correlation with the concentration. Complementary information was obtained when both methods were performed on the same samples. Additionally, a dual labeling method was presented where liposomes encapsulating ¹⁴C-doxorubicin were labeled with ¹¹¹In, to quantify the liposomal carrier as well as the encapsulated doxorubicin. This method provided important information about blood kinetics and biodistribution of the different compounds, feeding back into the optimization of carrier-based strategies for local drug delivery.

3.6 Acknowledgements

We thank Sandra van den Bosch, Katia Donato and Katrin Bitter (Philips Research Eindhoven) for their help with the experiments. For the setup of liquid scintillation counting in our lab we would like to thank Perkin Elmer for the technical support and Suzanne Kivits and Katia Donato (Philips Research Eindhoven) for the cooperation regarding the safety regulations. Martin Hossann and Lars Lindner (University Hospital Munich) and Ayele Negussie, Matthew Dreher and Brad Wood (National Institutes of Health) are acknowledged for their collaboration for the multi-centre comparison of the doxorubicin quantification protocols.

3.7 SOP: Doxorubicin quantification with HPLC & LSC

Sample collection

- Collect blood and tissue (~100 mg) samples in preweighed 2mL eppendorf cups
- Weigh the cups again

Calibration line

- Dilute the original injected solution 20x (determine the dilution factor exactly by weighing)
 - o 190 μ L H₂O + 10 μ L dox-solution (=injected liposomes)
- Put 2, 5, 10, 25 & 50 μ L of the diluted solution in preweighed 2 mL eppendorf cups
- Weigh the cups again

Process blood, tissue and calibration samples together:

Homogenisation

- Add 1.5mL daunorubicin in H₂O (0.5 μ g/mL daunorubicin)
- Weigh cups again
- Add 1 ball (stainless steel beads, Qiagen, 5mm)
- Homogenisation with TissueLyser: 2-20 min at 30Hz

HPLC method

- Transfer 125 μ L sample to preweighed 2 mL eppendorf cups
- Weigh cups again and store at -80 °C until further processing
- Add 50 μ L 1.94 M silver nitrate solution & vortex
- 10 min. incubation at room temperature
- Add 1.25 mL chloroform/isopropanol (2:1 v/v) – Vortex & shake for 5 minutes
- Centrifuge 10 min at 3600 r/min at room temperature
- Transfer the organic (lower) phase to glass tube (Duran, 12 x 75 mm)
- Evaporate (40 °C, N₂-flow)
- Dissolve in 2 x 100 μ L H₂O
- If necessary (dirty sample) transfer sample to 1.5 mL eppendorf cup and centrifuge
- Transfer clean sample to HPLC cup and measure with HPLC

LSC method

- Put 0.5 mL sample in preweighed plastic scintillation cups (super polyethylene vial, 20 mL, Perkin Elmer)
- Weigh scintillation cups
- Add 1 mL solubilizer (Solvable®, Perkin Elmer)
- Heat in oven at 60 °C overnight (leave caps a bit open to let gas out)
- Add 0.3 mL 30% H₂O₂ for decolorization (3 x 0.1 mL) (H₂O for standards)
- Add 0.3 mL IPA for antifoaming
- Heat in oven at 60 °C overnight to complete decolorization (leave caps a bit open to let gas out)
- Add 10 mL scintillation cocktail (Ultima Gold™, Perkin Elmer)
- Temperature and light adapt for at least one hour before counting
- Measure in liquid scintillation counter: 30 min/sample, record dpm (4-156 keV)

References

1. Bonadonna G, Monfardini S, de Lena M, et al. Clinical evaluation of adriamycin, a new antitumour antibiotic. *British Medical Journal*. 1969;3:503-6.
2. Lown JW. Discovery and development of anthracycline antitumour antibiotics. *Chemical Society Reviews*. 1993;22(3):165-76.
3. Licata S, Saponiero A, Mordente A, et al. Doxorubicin metabolism and toxicity in human myocardium: Role of cytoplasmic deglycosidation and carbonyl reduction. *Chem Res Toxicol* 2000;13:414-20.
4. Olson RD, Mushlin PS. Doxorubicin cardiotoxicity: analysis of prevailing hypotheses. *The FASEB Journal*. 1990;4(13):3076-86.
5. Gabizon A. Pharmacokinetics of PEGylated liposomal doxorubicin. *Clinical Pharmacokinetics*. 2003;42:419-36.
6. Abraham SA, D.N. Waterhouse, D. Lawrence, D. Mayer, P.R. Cullis, T.D. Madden, M.B. Bally. The liposomal formulation of doxorubicin. *Methods Enzymol*. 2005;391:71-97.
7. Gabizon A, R. Catane, B. Uziely, B. Kaufman, T. Safra, R. Cohen, F. Martin, A. Huang, Y. Barenholz. Prolonged circulation time and enhanced accumulation in malignant exudates of doxorubicin encapsulated in poly-ethylene-glycol coated liposomes. *Cancer Res*. 1994;54:987-92.
8. Gaber MH, Wu NZ, Hong K, et al. Thermosensitive liposomes: extravasation and release of contents in tumor microvascular networks. *Int J Radiat Oncol Biol Phys* 1996;36(5):1177-87.
9. Matsumura Y, H. Maeda. A new concept for macromolecular therapeutics in cancer chemotherapy: mechanism of tumoritropic accumulation of proteins and the antitumor agent smancs. *Cancer Res*. 1986;46:6387-92.
10. Yatvin MB, Weinstein JN, Dennis WH, et al. Design of liposomes for enhanced local release of drugs by hyperthermia. *Science*. 1978;202:1290-3.
11. Weinstein JN, Magin RL, Yatvin MB, et al. Liposomes and local hyperthermia- selective delivery of methotrexate to heated tumors. *Science*. 1979;204(4389):188-91.
12. de Smet M, Langereis S, van den Bosch S, et al. Temperature-sensitive liposomes for doxorubicin delivery under MRI guidance. *Journal of Controlled Release*. 2010;143(1):120-7.
13. Needham D, Anyarambhatla G, Kong G, et al. A new temperature-sensitive liposome for use with mild hyperthermia: characterization and testing in a human tumor xenograft model. *Cancer Res*. 2000;60:1197-201.
14. Lindner LH, Eichhorn ME, Eibl H, et al. Novel temperature-sensitive liposomes with prolonged circulation time. *Clin Cancer Res*. 2004;10:2168-78.
15. Charrois GJR, Allen TM. Drug release rate influences the pharmacokinetics, biodistribution, therapeutic activity, and toxicity of pegylated liposomal doxorubicin formulations in murine breast cancer. *Biochimica et Biophysica Acta*. 2004;1663:167-77.
16. Shinozawa S, Mimaki Y, Araki Y, et al. Determination of the concentration of adriamycin and its metabolites in the serum and tissues of ehrlich carcinoma-bearing mice by high-performance liquid chromatography. *Journal of Chromatography*. 1980;196:463-9.
17. Arnold RD, Slack JE, Straubinger RM. Quantification of doxorubicin and metabolites in rat plasma and small volume tissue samples by liquid chromatography/electrospray and tandem mass spectroscopy. *Journal of Chromatography B*. 2004;808:141-52.

18. Shinozawa S, Mimaki Y, Tomano H, et al. Determination of adriamycin in liposomes by high-performance liquid chromatography using a fluorescence detector. *Journal of Chromatography*. 1980;190:498-2.
19. van Asperen J, van Tellingen O, Beijnen JH. Determination of doxorubicin and metabolites in murine specimens by high-performance liquid chromatography. *Journal of Chromatography B*. 1998;712:129-43.
20. Alvarez-Cedron L, Sayalero ML, Lanao JM. High-performance liquid chromatographic validated assay of doxorubicin in rat plasma and tissues. *Journal of Chromatography B*. 1999;721:271-8.
21. Cox SK, Wilke AV, Frazier D. Determination of adriamycin in plasma and tissue biopsies. *Journal of Chromatography*. 1991;564:322-9.
22. Zhou Q, Chowbay B. Determination of doxorubicin and its metabolites in rat serum and bile by LC: application to preclinical pharmacokinetic studies. *Journal of Pharmaceutical and Biomedical Analysis*. 2002;30:1063-74.
23. Mazuel C, Grove J, Gerin G, et al. HPLC-MS/MS determination of a peptide conjugate prodrug of doxorubicin, and its active metabolites, leucine-doxorubicin and doxorubicin, in dog and rat plasma. *Journal of Pharmaceutical and Biomedical Analysis*. 2003;33:1093-102.
24. Cummings J, C.S. McArdle. Studies on the in vivo disposition of adriamycin in human tumours which exhibit different responses to the drug. *Br J Cancer*. 1986;53:835-8.
25. de Bruijn P, Verweij J, Loos WJ, et al. Determination of doxorubicin and doxorubicinol in plasma of cancer patients by High-Performance Liquid Chromatography. *Analytical Biochemistry*. 1999;266:216-21.
26. Kümmerle A, Krueger T, Dusmet M, et al. A validated assay for measuring doxorubicin in biological fluids and tissues in an isolated lung perfusion model: matrix effect and heparin interference strongly influence doxorubicin measurements. *Journal of Pharmaceutical and Biomedical Analysis*. 2003;33:475-94.
27. Laginha KM, Verwoert S, Charrois GJR, et al. Determination of doxorubicin levels in whole tumor and tumor nuclei in murine breast cancer tumors. *Clinical Cancer Research*. 2005;11(19):6944-9.
28. Liu Y, Yang Y, Liu X, et al. Quantification of pegylated liposomal doxorubicin and doxorubicinol in rat plasma by liquid chromatography/electrospray tandem mass spectroscopy: Application to preclinical pharmacokinetic studies. *Talanta*. 2008;74:887-95.
29. Schwartz HS. A fluorometric assay for daunomycin and adriamycin in animal tissues. *Biochemical medicine*. 1973;7:396-404.
30. Wei G, Xiao S, Si D, et al. Improved HPLC method for doxorubicin quantification in rat plasma to study the pharmacokinetics of micelle-encapsulated and liposome-encapsulated doxorubicin formulations. *Biomedical chromatography*. 2008;22:1252-8.
31. Zagotto G, Gatto B, Moro S, et al. Anthracyclines: recent developments in their separation and quantitation. *Journal of Chromatography B*. 2001;764:161-71.
32. Fogli S, Danesi R, Innocenti F, et al. An improved HPLC method for therapeutic drug monitoring of daunorubicin, idarubicin, doxorubicin, epirubicin, and their 13-dihydro metabolites in human plasma. *Therapeutic Drug Monitoring*. 1999;21(3):367.
33. Lachâtre F, Marquet P, Ragot S, et al. Simultaneous determination of four anthracyclines and three metabolites in human serum by liquid chromatography-electrospray mass spectrometry. *Journal of Chromatography B*. 2000;738:281-91.

34. Katzenmeyer JB, Eddy CV, Arriaga EA. Tandem laser-induced fluorescence and mass spectrometry detection for High-Performance Liquid Chromatography analysis of the in vitro metabolism of doxorubicin. *Analytical Chemistry*. 2010;82:8113-20.
35. Israel M, Karkowsky AM, Pegg WJ. Pharmacologic studies with radiolabeled N-trifluoroacetyl Adriamycin-14-valerate (AD 32). Comparison of total anthracycline fluorescence and radioactivity in mouse serum and urine. *Cancer Chemotherapy and Pharmacology*. 1980;4:79-82.
36. Israel M, Karkowsky AM, Khetarpal VK. Distribution of radioactivity and anthracycline-fluorescence in tissues of mice one hour after [¹⁴C]-labeled AD 32 administration. *Cancer Chemotherapy and Pharmacology*. 1981;6:25-30.
37. Verdun C, Brasseur F, Vranckx H, et al. Tissue distribution of doxorubicin associated with polyisohexylcyanoacrylate nanoparticles. *Cancer Chemotherapy and Pharmacology*. 1990;26:13-8.
38. Hak S, Sanders H, Agrawal P, et al. A high relaxivity Gd(III)DOTA-DSPE-based liposomal contrast agent for magnetic resonance imaging. *European Journal of Pharmaceutics and Biopharmaceutics*. 2009;72(2):397-404.
39. Rouser G, Fleische S, Yamamoto A. 2 Dimensional thin layer chromatographic separation of polar lipids and determination of phospholipids by phosphorus analysis of spots. *Lipids*. 1970;5(5):494.
40. Hossann M, Wiggenhorn M, Schwerdt A, et al. In vitro stability and content release properties of phosphatidylglyceroglycerol containing thermosensitive liposomes. *Biochimica Et Biophysica Acta-Biomembranes*. 2007;1768:2491-9.
41. Ranjan A, Jacobs GC, Woods DL, et al. Image-guided drug delivery with magnetic resonance guided high intensity focused ultrasound and temperature sensitive liposomes in a rabbit Vx2 tumor model. *Journal of Controlled Release*. 2012;158:487-94.
42. Gasselhuber A, Dreher MR, Negussie A, et al. Mathematical spatio-temporal model of drug delivery from low temperature sensitive liposomes during radiofrequency tumour ablation. *International Journal of Hyperthermia*. 2010;26(5):499-513.
43. Poon RTP, Borys N. Lyso-thermosensitive liposomal doxorubicin: a novel approach to enhance efficacy of thermal ablation of liver cancer. *Expert Opinion on Pharmacotherapy*. 2009;10(2):333-43.
44. de Smet M, Langereis S, van den Bosch S, et al. SPECT/CT imaging of temperature-sensitive liposomes for MR-image guided drug delivery with High Intensity Focused Ultrasound. submitted.
45. Allen TM, Hansen C. Pharmacokinetics of stealth versus conventional liposomes: effect of dose. *Biochimica et Biophysica Acta*. 1991;1068:133-41.
46. Ishida T, Harashima H, Kiwada H. Liposome clearance. *Bioscience Reports*. 2002;22(2):197-224.
47. Drummond DC, C.O. Noble, M.E. Hayes, J.W. Park, D.B. Kirpotin. Pharmacokinetics and In Vivo drug release rates in liposomal nanocarrier development. *J Pharm Sci*. 2008;97(11):4696-740.
48. Cheung WK, Aiache M, Yacobi A, et al. Changes in tissue concentrations of ¹⁴C-doxorubicin caused by mitoxantrone, mithramycin A and vinblastine in the rat. *Research Communications in Chemical Pathology and Pharmacology*. 1988;59(1):61-8.
49. Al-Jamal WT, Al-Ahmady ZS, Kostarelos K. Pharmacokinetics & tissue distribution of temperature-sensitive liposomal doxorubicin in tumor-bearing mice triggered with mild hyperthermia. *Biomaterials*. 2012;33:4608-17.

Chapter 4

Blood kinetics and biodistribution of temperature-sensitive liposomes for MR-image guided drug delivery with High Intensity Focused Ultrasound

Abstract

In this Chapter, the blood kinetics and biodistribution of temperature-sensitive liposomes (TSLs) for MR image-guided drug delivery was investigated. The co-encapsulated doxorubicin and [Gd(HPDO3A)(H₂O)] as well as the ¹¹¹In-labeled liposomal carrier were quantified in blood and organs of tumor bearing rats. After TSL injection, mild hyperthermia (T = 42 °C) was induced in the tumor using MR-HIFU. The biodistribution of the radiolabeled TSLs was investigated using SPECT/CT imaging, where the highest uptake of ¹¹¹In-labeled TSLs was observed in the spleen and liver. The MR-HIFU-treated tumors showed 4.4 times higher liposome uptake after 48 h in comparison with controls, while the doxorubicin concentration was increased with a factor of 7.9. These effects of HIFU-treatment are promising for applications in liposomal drug delivery to tumors.

Based on:

M. de Smet, S. Langereis, S. van den Bosch, K. Bitter, N.M. Hijnen, E. Heijman and H. Gröll. *SPECT/CT imaging of temperature-sensitive liposomes for MR-image guided drug delivery with High Intensity Focused Ultrasound*. Submitted

4.1 Introduction

Local drug delivery using temperature-sensitive liposomes (TSLs) holds great promise to improve the therapeutic window of chemotherapeutic treatments.¹⁻⁴ By using TSLs in combination with local heating of the tumor, the encapsulated drug is rapidly released from the TSL into the tumor microvasculature. Consequently, the drug becomes bioavailable at a cytotoxic concentration at the surrounding tumor cells.⁵⁻⁷ In the remaining (unheated) part of the body, the drug stays encapsulated in the TSL, thereby reducing the side effects in non-tumorous tissue. MR image-guided drug delivery and drug quantification can be performed using TSLs co-encapsulating drugs and MRI contrast agents (CAs).⁸⁻¹² The biodistribution of doxorubicin and [Gd(HPDO3A)(H₂O)] is well known,¹³⁻¹⁵ however encapsulation into liposomes changes the blood kinetics and biodistribution of these compounds thoroughly.¹⁶⁻¹⁷ Altered biodistribution of the drug and the MRI contrast agent, coupled with tissue-dependent differences in metabolism of these compounds, could play an important role in therapeutic effects and the toxicity profiles of the chemotherapeutic drug. Therefore, it is important to study the blood kinetics and biodistribution of the TSL as well as the individual encapsulated compounds. Additionally, the influence of HIFU on the uptake of TSLs and their encapsulated compounds in non-tumorous tissue is an important aspect, which has not been addressed yet.

In this Chapter, the blood kinetic and biodistribution of radiolabeled TSLs co-encapsulating doxorubicin and [Gd(HPDO3A)(H₂O)] (Figure 4.1) have been investigated in rats. First, the blood kinetics and biodistribution of the three liposomal systems described in Chapter 2 (LTSL, TTSL and NTSL) were studied. Subsequently, the biodistribution of ¹¹¹In-labeled TTSLs was monitored using SPECT/CT imaging and the effect of local MR-HIFU mediated hyperthermia of the tumor on the biodistribution of the liposomes, doxorubicin and [Gd(HPDO3A)(H₂O)] has been studied in detail.

4.2. Materials and Methods

4.2.1 Materials

1,2-Dipalmitoyl-*sn*-glycero-3-phosphocholine (DPPC) and hydrogenated-*L*- α -phosphatidylcholine (HSPC) were kindly provided by Lipoid (Germany). 1,2-Dipalmitoyl-*sn*-glycero-3-phosphoethanolamine-*N*-[methoxy(polyethyleneglycol)-2000] (DPPE-PEG2000), 1-stearoyl-*sn*-glycero-3-phosphocholine (MSPC) and cholesterol were purchased from Avanti Polar Lipids (USA). DOTA-DSPE was synthesized according to the literature procedure described by Hak *et al.*¹⁸ Doxorubicin hydrochloride was purchased from AvaChem Scientific (USA), [Gd(HPDO3A)(H₂O)] (ProHance®) from Bracco Diagnostics (Italy) and ¹¹¹InCl₃ was obtained from Perkin Elmer (USA).

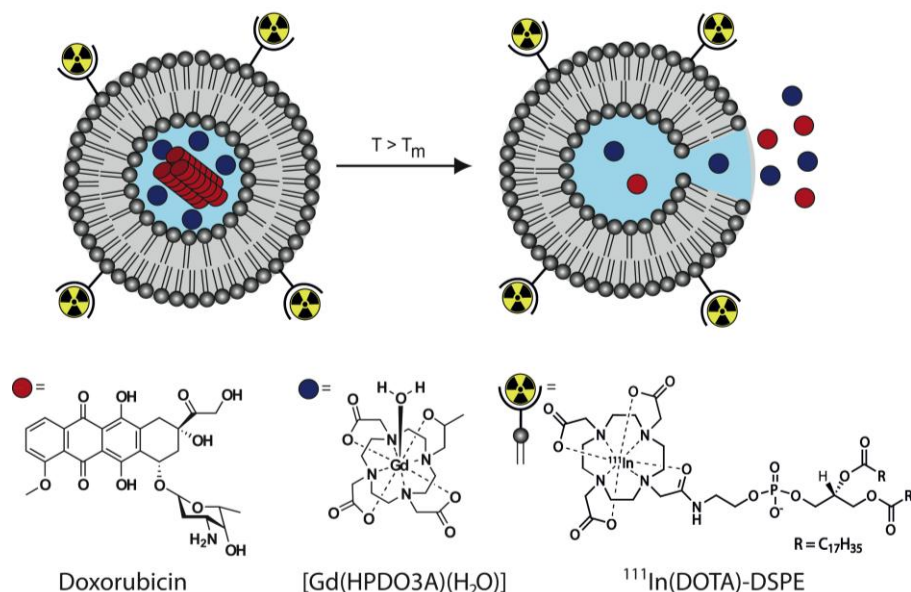


Figure 4.1. ¹¹¹In-labeled temperature-sensitive liposomes encapsulating doxorubicin and [Gd(HPDO3A)(H₂O)]. The co-encapsulated MRI contrast agent and the drug are released upon heating.

4.2.2 Radiolabeled temperature-sensitive liposomes

The liposomes were prepared by lipid film hydration followed by extrusion in a similar fashion as described in Chapter 2. A small fraction of DOTA-DSPE was incorporated in the liposomal bilayer to enable radiolabeling. The liposomal formulations used for the blood kinetics and biodistribution studies presented in this Chapter are shown in Table 4.1.

Table 4.1. Liposomal formulations used for blood kinetics and biodistribution studies.

Liposome	Composition (molar ratio)	Encapsulated compounds
Dox-LTSL	DPPC:MSPC:DPPE-PEG2000:DOTA-DSPE (86:10:4:5)	Doxorubicin
Dox-TTSL	DPPC:HSPC:Chol:DPPE-PEG2000:DOTA-DSPE (50:25:15:3:5)	Doxorubicin
Dox-NTSL	HSPC:Chol:DPPE-PEG2000:DOTA-DSPE (75:50:3:5)	Doxorubicin
Dox/Gd-TTSL	DPPC:HSPC:Chol:DPPE-PEG2000:DOTA-DSPE (50:25:15:3:1)	Doxorubicin and [Gd(HPDO3A)(H ₂ O)]

The phospholipids and cholesterol were dissolved in CHCl_3 :MeOH (4:1 v/v). Subsequently, the organic solvents were removed *in vacuo* and a lipid film was formed, which was further dried overnight under a nitrogen flow. For Dox-TSLs, the lipid film was hydrated at 60 °C in 240 mM $(\text{NH}_4)_2\text{SO}_4$ buffer (pH 5.4). For Dox/Gd-TTSL encapsulating doxorubicin and $[\text{Gd}(\text{HPDO3A})(\text{H}_2\text{O})]$, 120 mM $(\text{NH}_4)_2\text{SO}_4$ buffer (pH 5.4) containing 250 mM $[\text{Gd}(\text{HPDO3A})(\text{H}_2\text{O})]$ was used for the hydration. The liposomal suspensions were extruded at 60 °C successively through a polycarbonate filter of 200 nm (two times), and 100 nm (six times). Subsequently, the extraliposomal buffer was replaced by HEPES Buffered Saline (HBS) (20 mM HEPES and 137 mM NaCl at pH 7.4) by gel filtration through a PD-10 column. A solution of doxorubicin in HBS (5 mg/mL) was added to the liposomes and incubated at 37 °C overnight. Finally, the TSLs were passed through a 0.22 μm filter and a second PD-10 column in order to remove any non-encapsulated doxorubicin. The doxorubicin-loaded liposomes were concentrated using an Amicon Ultra-4 Centrifugal Filter Unit (100 kDa MWCO, Millipore).

For characterization, the hydrodynamic radius of the liposomes in HBS was determined using dynamic light scattering (DLS; ALV/CGS-3 Compact Goniometer System, ALV-GmbH, Langen, Germany). The doxorubicin concentration was determined fluorimetrically with a spectrophotometer (Perkin Elmer LS55, $\lambda_{\text{ex}} = 485$ nm and $\lambda_{\text{em}} = 590$ nm) in a solution of isopropyl alcohol:H₂O (1:1 v/v). The phospholipid concentration was determined according to the Rouser assay¹⁹ and the gadolinium concentration was determined by inductively coupled plasma- mass spectrometry (ICP-MS).

In order to determine the blood kinetics and biodistribution of the liposomal carriers, TSLs were radiolabeled with $^{111}\text{InCl}_3$ in ammonium acetate buffer (95 mM) at pH 4.5 by overnight incubation at 30 °C. The NTSLs were radiolabeled with $^{177}\text{LuCl}_3$, instead of $^{111}\text{InCl}_3$, in ammonium acetate buffer at pH 7.5. The radiolabeling yield was determined with radio-TLC (running buffer: 200 mM EDTA in saline) before and after incubation with 0.1 mM DTPA for 10 minutes. The crude mixture was passed through a Zeba Desalt Spin column (MWCO = 7 kDa) pre-equilibrated with HBS (pH 7.4) in order to remove unbound isotopes and to exchange the ammonium acetate buffer. The final radiolabeled TSLs were obtained with a radiolabeling yield of > 95%, as determined with radio-TLC.

4.2.3 *In vitro* stability and release

The *in vitro* release of doxorubicin and $[\text{Gd}(\text{HPDO3A})(\text{H}_2\text{O})]$ from the Dox/Gd-TTSLs was determined by addition of 125 μL liposomal solution to 3 mL preheated FBS at 37 °C, 40 °C and 42 °C. Samples of 250 μL were taken over time and immediately mixed with 250 μL ice-cold FBS. Samples were stored at -20 °C until analysis with a spectrophotometer and a clinical MRI scanner (3T) to quantify doxorubicin and $[\text{Gd}(\text{HPDO3A})(\text{H}_2\text{O})]$ release, respectively.

For quantification of the doxorubicin release from the Dox/Gd-TTSL samples, the intensity of fluorescence ($\lambda_{\text{ex}} = 485 \text{ nm}$ and $\lambda_{\text{em}} = 590 \text{ nm}$) was measured of 40 μL sample in HBS (2 mL). At the end of each measurement, 5 μL of a 10% v/v solution of Triton X-100 was added to the solution, to afford quantitative release of doxorubicin. The percentage of doxorubicin release was calculated according to: $(I_t - I_0) / (I_{100} - I_0) \times 100\%$, in which I_t is the intensity of the fluorescence at a specific time (t), I_0 is the intensity of the fluorescence immediately after mixing of the sample with FBS at 37 °C and I_{100} is the intensity of the fluorescence after the addition of Triton X-100.

For quantification of the [Gd(HPDO3A)(H₂O)] release, the longitudinal relaxation time (T_1) of the samples was measured at 3T using a Look-Locker sequence²⁰ (FA = 10°; TR/TE=9.3/3.5 ms; interval time = 100 ms; time of inversion repetition = 6 s; EPI factor = 5; field of view (FOV) = 140 mm × 72 mm; matrix = 64 × 65; slice thickness = 5 mm; acquisition time = 84 s). One sample was heated for 30 min at 45 °C in order to obtain quantitative release of [Gd(HPDO3A)(H₂O)] from the TSL.²¹ Release of [Gd(HPDO3A)(H₂O)] was calculated by $(R_{1,t} - R_{1,0}) / (R_{1,100} - R_{1,0}) \times 100\%$, in which $R_{1,t}$ is the $1/T_1$ of the sample taken at time (t), $R_{1,0}$ is the $1/T_1$ of the sample taken immediately after mixing with FBS at 37 °C and $R_{1,100}$ is the $1/T_1$ of the heated sample.

4.2.4 Animal model

Subcutaneous 9L gliosarcoma tumors in Fisher 344 rats (age 5-7 weeks, Charles River) were established by subcutaneous injection of 1×10^6 9L cells in 100 μL PBS on the hind leg. Tumor dimensions were determined by measuring the length (l), width (w) and depth (d) using a caliper, from which the tumor volume was calculated by $0.5 \times l \times w \times d$. Animal studies were performed with tumor volumes between 400 – 1600 mm^3 , typically 14-28 days after tumor cell injection.

4.2.5 Blood kinetics and biodistribution

The blood circulation time of the liposomes was investigated by injecting ¹¹¹In-labeled TSLs (4 MBq/mL, ~2 MBq/rat, 5 mg doxorubicin/kg bodyweight) via the tail vein of Fisher rats. Blood samples were taken via the vena saphena of awake animals, at various time points between 2 minutes and 48 h after injection. The blood samples and standards of the radiolabeled liposomes were weighed and their radioactivity was counted with a 1480 Automatic Gamma Counter (Wizard™ 3", Perkin Elmer). Subsequently, doxorubicin and gadolinium in the blood samples was quantified according to the procedure described in section 4.2.8. The percentage of the injected dose (%ID) in the total blood was calculated assuming a total blood volume of 7% of the body weight. Blood kinetics were fitted in Origin (Origin 7.5, OriginLab Corporation, Northampton, USA) according to the bi-exponential equation: $\%ID/\text{total blood} = A \cdot \exp(-t/\tau_1) + B \cdot \exp(-t/\tau_2)$. At 48 hours after the injection,

the rats were euthanized by cervical dislocation. Subsequently, organs were dissected, weighed and the amount of radioactivity was quantified with the gamma counter.

4.2.6 MR-HIFU hyperthermia treatment

All MR-HIFU experimental procedures were conducted while the animals were anesthetized with isoflurane (induction 3%, maintenance 1-3%) in medical air (flow 0.4-0.6 L/min). Local hyperthermia treatment was applied with an MR-HIFU, integrated into a 3T human MR scanner (Philips Achieva, Best, the Netherlands).^{11,22} All animals received Rimadyl® (carprofen, 4 mg/kg bodyweight) as a precautional pain suppressor prior to MR-HIFU treatment. Ultrasound gel (Aquasonic 100, Parker Laboratories, Fairfield, USA) was applied onto the shaven and depilated leg and tumor to ensure acoustic coupling and to prevent air bubbles from sticking to the skin. The animal was placed into a dedicated multichannel small animal MR receiver coil that was used as an add-on to a clinical MR-HIFU system (Philips Sonalleve, Vantaa, Finland).²² The respiration rate and body temperature of the animal were monitored continuously. The treatment was planned on T_2 -weighted images acquired with a turbo spin echo scan. Subsequently, an ellipsoidal-shaped HIFU treatment volume (diameter \approx 4 mm, length \approx 10 mm) was positioned in the centre of the tumor. Several test sonications (continuous wave ultrasound, acoustic frequency = 1.44 MHz, acoustic power = 5-10 W, duration = 20 s, typical temperature elevation of 1-2 °C) were performed prior to therapeutic sonication to correct for misregistration between the heated area and planned treatment location. During sonications, proton resonance frequency shift (PRFS) based MR thermometry was used to monitor the temperature change in the target region by continuous acquisition of one slice perpendicular and one slice parallel to the ultrasonic beam axis, all centred on the target area (RF-spoiled gradient echo with EPI readout, FA = 19.5°; TR/TE=52/19.5 ms; EPI-factor = 7; SENSE factor 1.8; field of view = 250 × 250 mm²; matrix = 176 × 169; slice thickness = 4 mm; number of averages = 4; fat suppression = SPIR; dynamic scan time = 4.8 s). For prolonged hyperthermia (acoustic power 8 W), the heating was controlled using a binary feedback control algorithm,^{22,23} switching the transducer power on or off accordingly, when pre-defined temperatures were reached. The temperature images were corrected for baseline drift by subtracting the drift measured in a non-heated reference region from the actual temperature images.

4.2.7 SPECT/CT imaging

¹¹¹In-labeled Dox/Gd-TTSLs (79.9 ± 19.5 MBq/mL liposome solution, 39.9 ± 1.6 MBq/rat) were injected via the tail vein of the 9L tumor bearing rats (n=8), of which 4 received hyperthermia treatment with HIFU. The control rats were not treated with HIFU, but were directly after the injection scanned with single photon emission computed tomography (SPECT) (24 projections, 15 s/projection, scan time = 9 min) over time for 1 hour, followed

by an X-ray computed tomography (CT) scan for anatomical information (180 projections, pitch=1, tube voltage = 55 kV, scan time= 14 min) using a dedicated small animal SPECT/CT system equipped with four detector heads and converging multi-pinhole collimators (9 pinholes/collimator, pinhole diameter = 2.5 mm, NanoSPECT/CT®, Bioscan, USA). For both the HIFU-treated and the control group, the rats were sacrificed with an i.p. pentobarbital injection 48 h after Dox/Gd-TTSL injection and post-mortem SPECT/CT scans were acquired (SPECT: 36 projections, 500 s/projection, scan time = 10 ± 2 h, CT: 240 projections, tube voltage = 55 kV, scan time = 48 ± 3 min). After the SPECT/CT scans the tumors and organs were dissected, weighed and the amount of ^{111}In was quantified with the gamma counter. Subsequently, doxorubicin and gadolinium concentrations were determined as described in section 4.2.8. A schematic overview of the experimental procedures is shown in Figure 4.2.

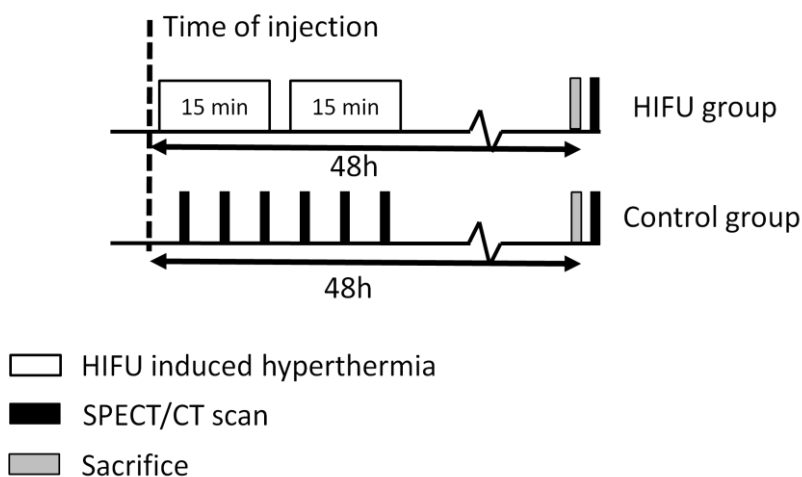


Figure 4.2. Schematic overview of the SPECT/CT imaging and biodistribution protocol. HIFU-mediated hyperthermia was applied on the tumors of the experimental group immediately after intravenous Dox/Gd-TTSL injection. For the control group, no hyperthermia was applied, SPECT/CT imaging was performed instead. Animals were sacrificed 48 h after injection, followed by a post-mortem SPECT/CT scan and biodistribution.

4.2.8 Quantification of doxorubicin and gadolinium in blood and tissue

Blood samples (~ 50 μL /sample), pieces of organs (~ 100 mg/organ) and complete tumors obtained during the blood kinetics and biodistribution experiments were analysed for their doxorubicin and gadolinium concentrations. To all samples, an aqueous solution of daunorubicin (0.5 $\mu\text{g}/\text{mL}$ in 1.5 mL H_2O) was added as an internal standard for doxorubicin quantification, followed by homogenization for 5-20 min at 30 Hz in a Qiagen TissueLyser.

The homogenized samples were divided in two aliquots: *i*) for the determination of the gadolinium concentration by ICP-MS and *ii*) for the determination of the doxorubicin concentration by using the HPLC protocol as described in Chapter 3.

4.3 Results

4.3.1 Temperature-sensitive liposomes

TSLs were successfully prepared using the lipid film hydration technique followed by sequential extrusion through polycarbonate filters. An overview of the hydrodynamic radius, and the phosphorus, doxorubicin and gadolinium concentrations of the four liposomal formulations is shown in Table 4.2. For the three dox-liposomes (LTSL, TTSL and NTSL), the same doxorubicin and phosphate concentrations were obtained by dilution in HBS and the addition of liposomes without doxorubicin.

Table 4.2 Hydrodynamic radius and phosphorus, doxorubicin and gadolinium concentrations of the different TSL formulations used for blood kinetics and biodistribution experiments.

Liposome	r_h (nm)	[P] (mM)	[dox] (mM)	[Gd] (mM)
Dox-LTSL	61 (PDI<0.1)	30 ± 1	2.6 ± 0.1	-
Dox-TTSL	72 (PDI<0.1)	30 ± 1	2.6 ± 0.1	-
Dox-NTSL	86 (PDI<0.1)	30 ± 1	2.6 ± 0.1	-
Dox/Gd-TTSL	64 (PDI<0.1)	65 ± 2	3.3 ± 0.1	15.6 ± 0.8

4.3.2 Blood kinetics and biodistribution of Dox-TSLs

First a pilot study was performed to study the blood kinetics of the three liposomal formulations discussed in Chapter 2. Therefore, LTSL, TTSL and NTSL were prepared containing 5 mol% DOTA-DSPE in the liposomal bilayer and were subsequently loaded with doxorubicin. After injection of the radiolabeled liposomal carriers, the blood kinetics and biodistribution of the three liposomal systems were studied. NTSL showed the longest blood circulation, followed by TTSL, and finally LTSL, which showed the fastest clearance (Figure 4.5). Figure 4.6 shows the liposomes as well as the doxorubicin in the blood after injection of the three different formulations. The LTSL and TTSL displayed higher blood concentrations for the radiolabeled liposomal carriers compared to the doxorubicin, implying premature leakage of the encapsulated drug from the aqueous lumen of the TSL at physiological temperatures (37-38 °C)²⁴ followed by a rapid blood clearance of this small molecule. For LTSL, doxorubicin was cleared from the blood within 30 minutes (<0.5 %ID/total blood), indicating a fast leakage of doxorubicin from these liposomes. In contrast, the TTSL showed

a much slower leakage, with 55% of the injected doxorubicin still present in the blood after 30 minutes. For NTSL, doxorubicin showed the same blood clearance as the liposomes, indicating no significant leakage at body temperature. The blood clearance of radiolabeled TSLs and doxorubicin over time were fitted with a biexponential function (Table 4.3).

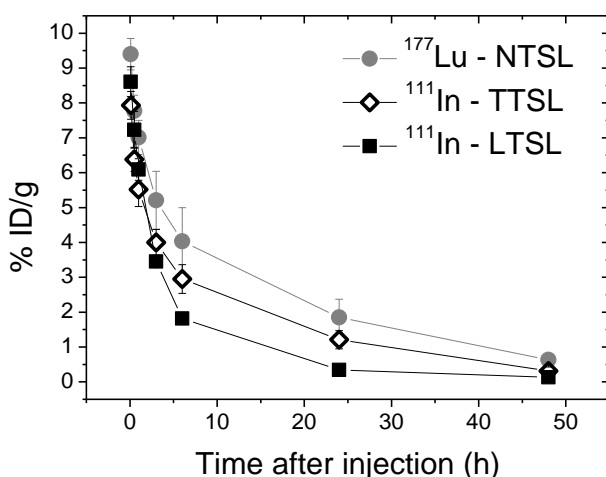


Figure 4.5. Blood kinetics of radiolabeled liposomes: NTSL, TTSL and LTSL (n=4 per group)

Table 4.3. Parameters (\pm errors) from biexponential fit on blood clearance curves of radiolabeled liposomes and doxorubicin for three different liposomal formulations.

Fitted values	A	τ_1	B	τ_1
LTSL, liposomes	24.1 \pm 5.2	12.3 \pm 3.3	76.2 \pm 4.9	1.68 \pm 0.17
LTSL, dox	0.36 \pm 0.04	3.26 \pm 0.65	13.7 \pm 0.7	0.11 \pm 0.01
TTSL, liposomes	50.8 \pm 4.1	18.1 \pm 3.1	46.2 \pm 4.5	0.94 \pm 0.20
TTSL, dox	9.48 \pm 3.40	24.1 \pm 19.8	78.8 \pm 3.7	1.04 \pm 0.11
NTSL, liposomes	64.2 \pm 3.8	21.8 \pm 2.4	48.6 \pm 4.1	1.11 \pm 0.22
NTSL, dox	54.9 \pm 41.9	26.4 \pm 19.5	38.9 \pm 40.0	3.57 \pm 4.92

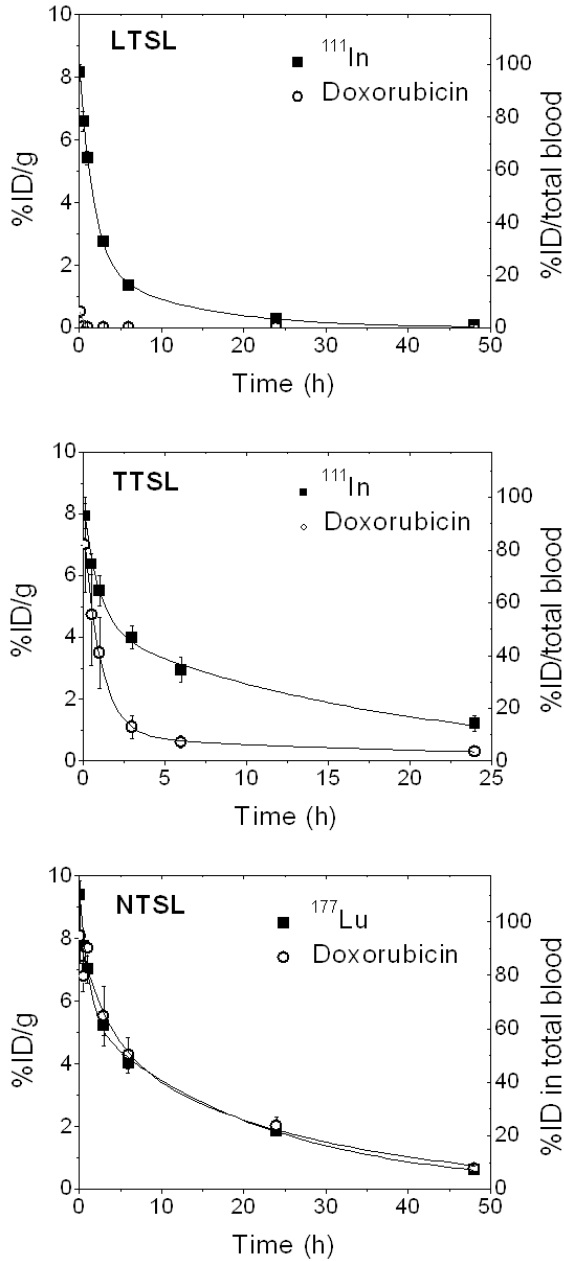


Figure 4.6. Blood kinetics of radiolabeled liposomes and doxorubicin of LTSL, TTSL and NTSL ($n=4$ per group).

At 48h after injection, the rats were sacrificed and organs were collected. The biodistribution of the radiolabeled liposomes is shown in Figure 4.7. The highest uptake was observed for the liver and spleen, however, for each liposomal formulation the liver/spleen ratio was different. For LTSL and TTSL, an increased uptake by the kidneys was observed, which can be caused by unbound ^{111}In . Similarly, the increased uptake by the bone found for the NTSL, can be caused by free ^{177}Lu .

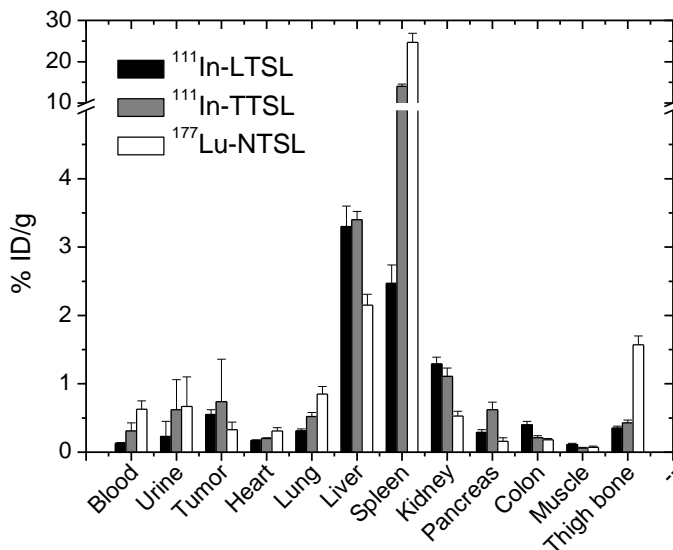


Figure 4.7. Biodistribution of LTSL, TTSL and NTSL at 48h after injection.

Due to the relatively low doxorubicin leakage at body temperature, the TTSL formulation was chosen as the most suitable temperature-sensitive formulation for hyperthermia-mediated drug delivery. This formulation was prepared co-encapsulating doxorubicin and $[\text{Gd}(\text{HPDO3A})(\text{H}_2\text{O})]$ and the amount of DOTA-DSPE was decreased to 1 mol%. The *in vitro* release as well as the blood kinetics and biodistribution of the liposomes, doxorubicin and $[\text{Gd}(\text{HPDO3A})(\text{H}_2\text{O})]$ is presented in the next sections of this Chapter. Additionally, the biodistribution of these ^{111}In -labeled dox/Gd-TTSLs was monitored using SPECT/CT imaging and the effect of local MR-HIFU mediated hyperthermia of the tumor was investigated.

4.3.3 *In vitro* release of doxorubicin and [Gd(HPDO3A)(H₂O)] from Dox/Gd-TTSL

In Chapter 2, simultaneous release of doxorubicin and [Gd(HPDO3A)(H₂O)] in HBS was already shown for these liposomal systems without DOTA-lipid in the liposomal bilayer. Since components in plasma might affect the release kinetics,²⁵⁻²⁶ the *in vitro* release of doxorubicin and [Gd(HPDO3A)(H₂O)] from the aqueous lumen of the TTSLs containing 1 mol% DOTA-DSPE was determined at 37 °C, 40 °C and 42 °C in fetal bovine serum (FBS). The longitudinal relaxivity (r_1) of TSLs encapsulating 250 mM [Gd(HPDO3A)(H₂O)] is limited by the transmembrane water exchange.^{11, 27} Upon release of the contrast agent, a decrease in the longitudinal relaxation time was observed. As a consequence, the release of [Gd(HPDO3A)(H₂O)] from the TSL can be probed by the change in the longitudinal relaxation rate ($R_1 = 1/T_1$). At 37 °C, [Gd(HPDO3A)(H₂O)] remained compartmentalized in the lumen of the TSL, while fast and quantitative release of the MRI contrast agent was observed at 42 °C (Figure 4.8). Moreover, a similar trend was observed for the co-release of doxorubicin, implying that drug release could be performed under MR image-guidance.

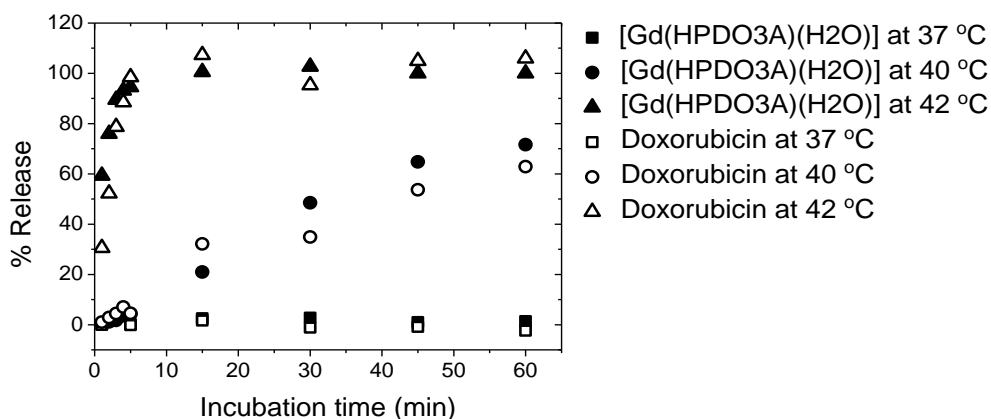


Figure 4.8. *In vitro* release of Prohance® and doxorubicin from Dox/Gd-TTSLs in FBS.

4.3.4 Blood kinetics of dox/Gd-TTSLs

The blood kinetics of radiolabeled TSLs, doxorubicin and [Gd(HPDO3A)(H₂O)] were determined by collecting blood samples over time followed by quantification of ¹¹¹In, doxorubicin and gadolinium. The percentage of the injected dose in total blood (%ID/total blood) of the TSLs over time is depicted in Figure 4.9. The %ID/total blood was calculated assuming a blood volume of 0.07*body weight of the rat. The radiolabeled TSLs displayed a more prolonged blood circulation time with higher blood concentrations compared to doxorubicin and [Gd(HPDO3A)(H₂O)], implying premature leakage of the encapsulated structures from the aqueous lumen of the TSL already at body temperature (37-38 °C)²⁴

followed by a rapid blood clearance of these small molecules. The blood clearance of radiolabeled TSLs, doxorubicin and [Gd(HPDO3A)(H₂O)] over time was fitted with a biexponential function (Table 4.4), demonstrating that at t=0, the liposomes, doxorubicin and gadolinium were distributed over the total blood volume (average of ¹¹¹In, doxorubicin and Gd = 98.9 ± 6.4 %ID/total blood).

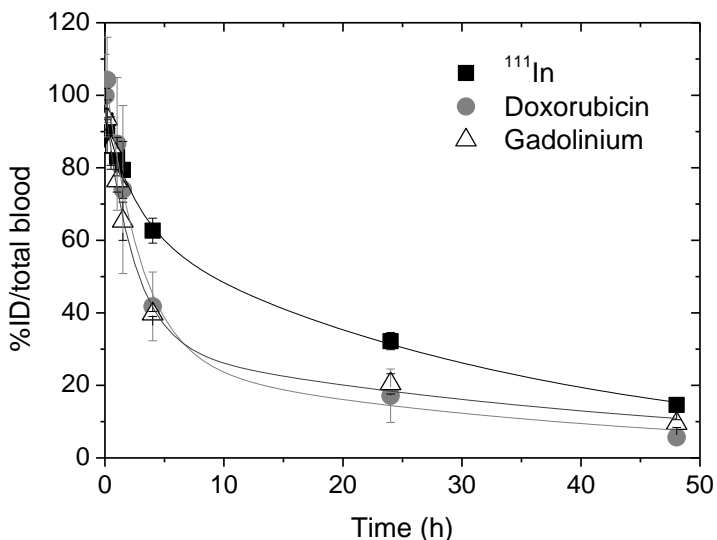


Figure 4.9. Blood kinetics of ¹¹¹In-labeled Dox/Gd-TTSLs, doxorubicin and [Gd(HPDO3A)(H₂O)] in Fisher rats (n=4).

Table 4.4. Parameters (± errors) of the blood kinetics fitted with a biexponential function:

$$\%ID/total\ blood = A \cdot \exp(-t/\tau_1) + B \cdot \exp(-t/\tau_2).$$

	A	τ₁	B	τ₂
¹¹¹ In-labeled TSL	64.1 ± 4.8	33.6 ± 3.0	29.5 ± 4.6	2.75 ± 0.65
Doxorubicin	27.0 ± 21.8	38.2 ± 39.0	79.0 ± 21.2	3.00 ± 1.17
Gadolinium	31.1 ± 8.4	45.8 ± 18.8	66.1 ± 8.0	2.47 ± 0.52

4.3.5 SPECT/CT imaging

The biodistribution of radiolabeled Dox/Gd-TTSL in tumor bearing rats in the absence of HIFU within the first hour was monitored with SPECT/CT imaging (Figure 4.10). Since the blood clearance of the TSLs is low within the first hour (Figure 4.9), the majority of the ^{111}In activity was observed in the heart and large blood vessels. Moreover, accumulation of ^{111}In -labeled TSLs in the spleen and liver was observed over time. Any significant accumulation in the unheated tumor was not visible during this first hour.

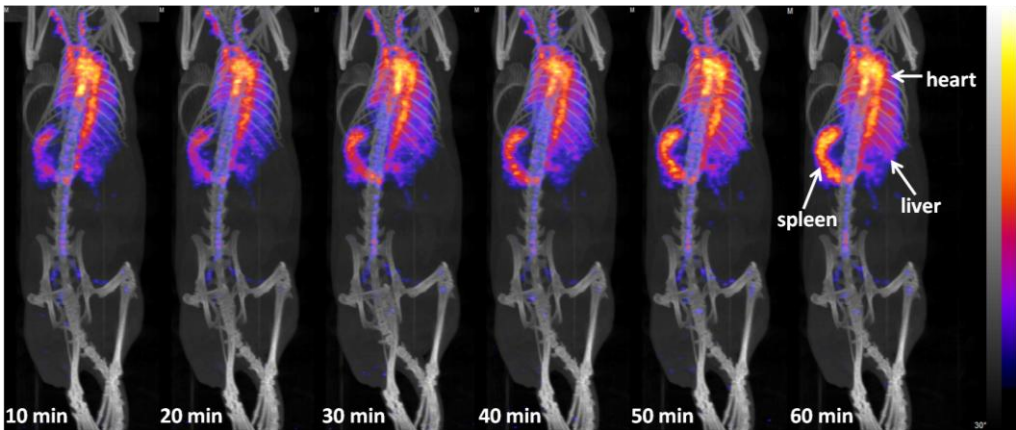


Figure 4.10. SPECT/CT images (maximum intensity projections) over time after the intravenous injection of ^{111}In -labeled Dox/Gd-TTSLs in tumor bearing rats without MR-HIFU treatment.

4.3.6 SPECT/CT imaging and biodistribution of radiolabeled Dox/Gd-TTSL at 48 h p.i.

The influence of MR-HIFU mediated hyperthermia of the 9L tumor on the biodistribution of ^{111}In -labeled TSLs was investigated 48 hours after administration. Local mild hyperthermia of the tumor on the hind leg was applied for two times 15 minutes after the intravenous injection of the radiolabeled TSL co-encapsulating doxorubicin and $[\text{Gd}(\text{HPDO3A})(\text{H}_2\text{O})]$ (Figure 4.2). Control experiments ($n=4$) were performed with ^{111}In -labeled TSLs without MR-HIFU treatment of the tumor. After 48 h, the animals were sacrificed and post-mortem SPECT/CT scans were recorded (Figure 4.11). The SPECT/CT images showed clearly that the radiolabeled TSLs were mainly cleared by the liver and spleen. Importantly, a high amount of radioactivity was observed in the tumors of the MR-HIFU treated animals ($n=4$) in comparison with the control group ($n=4$), implying tumor uptake of the TSLs. Furthermore, a high amount of ^{111}In in muscle close to the femur of the MR-HIFU treated animal was observed as well as increased radioactivity in the adrenals for some of the MR-HIFU treated animals. (Figure 4.11)

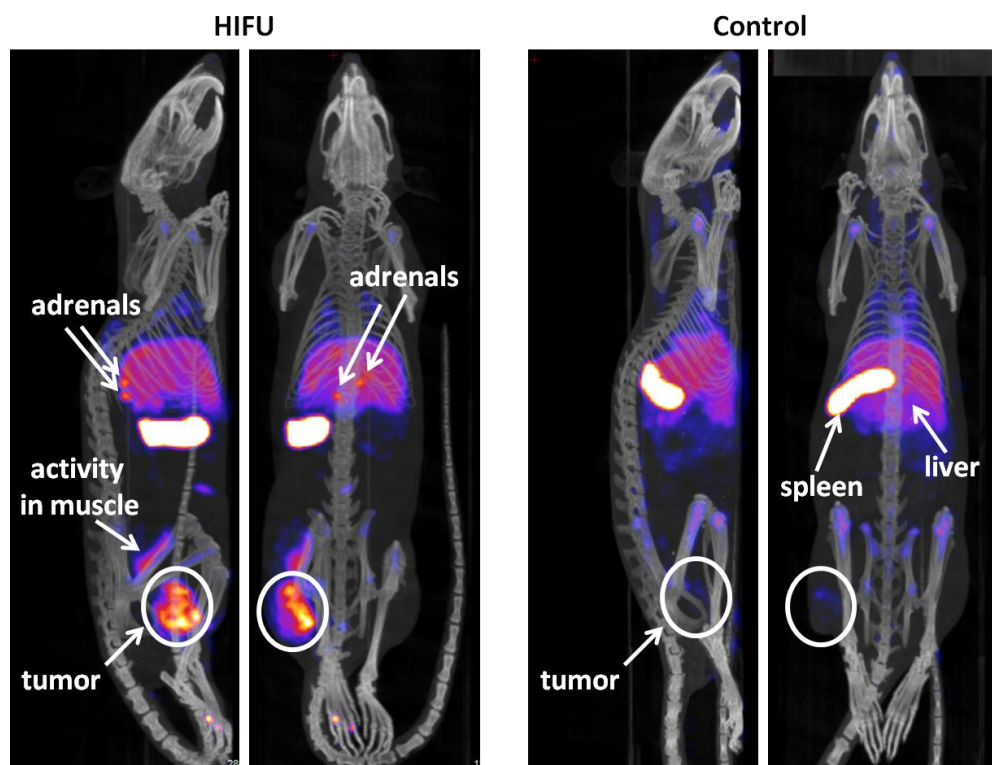


Figure 4.11. SPECT/CT images (maximum intensity projections) of tumor bearing rats at 48 hours after liposome injection. HIFU-mediated hyperthermia of the 9L tumor in combination with radiolabeled Dox/Gd-TTSL (left) and a control experiment with radiolabeled Dox/Gd-TTSL only (right).

Occasionally, some rats showed a high amount of ^{111}In in the lungs on the SPECT images (Figure 4.12), for both the HIFU-treated and the control group.

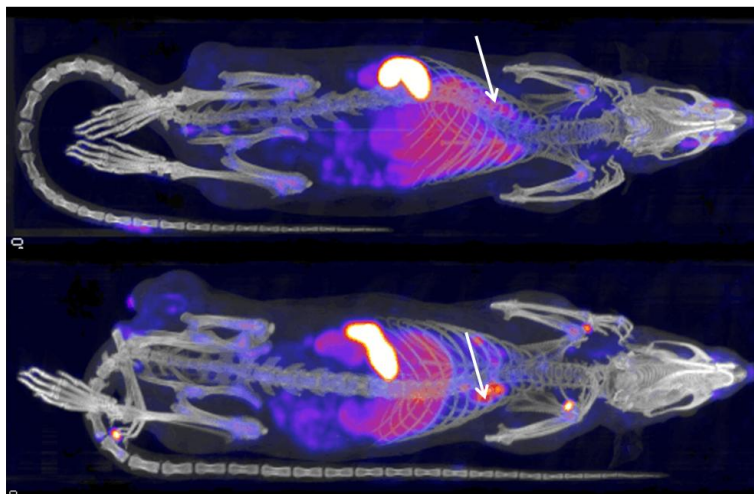


Figure 4.12. Occasional lung uptake of ^{111}In -labeled Dox/Gd-TTSL observed on SPECT scans. Two examples are given, upper image: homogeneous uptake in the lungs, lower image: inhomogeneous uptake in the lungs. The activity detected in the lungs is indicated with a white arrow.

After the post-mortem SPECT/CT scans of the animals, the organs of interest were excised, weighed and analyzed for quantification of the liposome, doxorubicin and gadolinium content (Figure 4.13). The biodistribution showed a similar trend for the HIFU treated and control rats, except for the tumor and the radioactivity in the adrenals, where a higher uptake in the HIFU-treated group was observed. Corresponding to the SPECT images, the highest uptake of ^{111}In -labeled TSLs was observed in the spleen (14.7 ± 3.8 %ID/g, $n=8$). Also the liver had an important contribution to the clearance of liposomes, since for this big organ the uptake of 2.1 ± 0.3 %ID/g ($n=8$) corresponds to 13.4 ± 1.9 % uptake of the injected dose in the total organ. Interestingly, the content of doxorubicin and gadolinium in these organs was lower than the amount of ^{111}In . This can be caused by uptake of liposomes that already lost part of their contents, as well as metabolism and outwash of doxorubicin and gadolinium over time. Figure 4.14 shows the decreasing gadolinium concentrations in liver, spleen and kidney over time. One month after injection of Gd/Dox-TTSL the amount of gadolinium was $\leq 0.3\%$ of the injected dose for these three analysed organs.

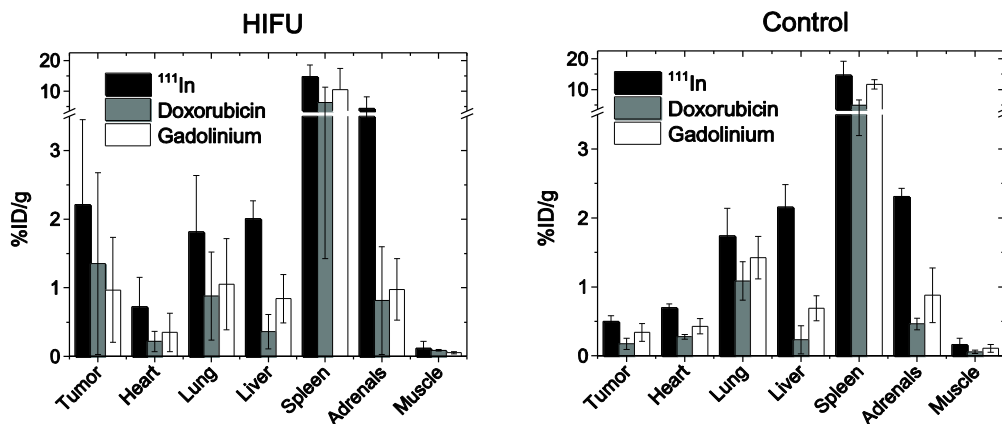


Figure 4.13. The biodistribution of ^{111}In , doxorubicin and gadolinium at 48 h after injection of radiolabeled Dox/Gd-TTSL. HIFU-mediated hyperthermia of the tumor (2x15 min) in combination with TSLs (left) and a control experiment with TSLs in the absence of HIFU-mediated hyperthermia (right). The analyzed muscle was the calf muscle of the untreated leg.

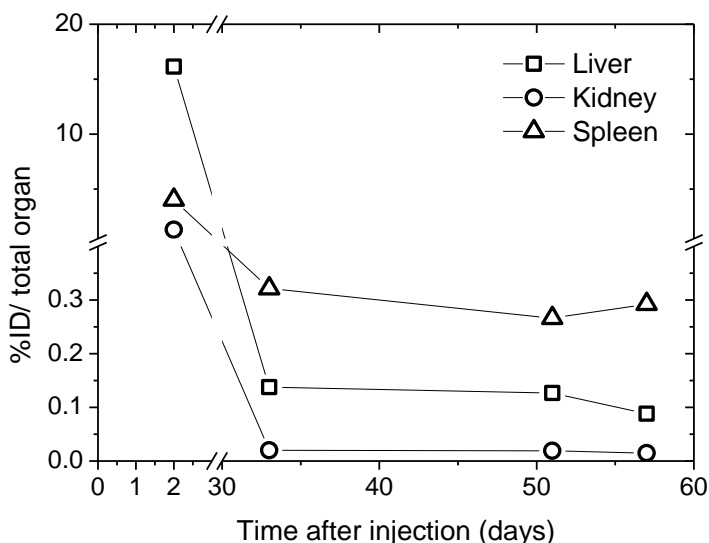


Figure 4.14. Gadolinium concentrations over time in lung, liver, spleen and kidney after injection with Dox/Gd-TTSL. The amount of gadolinium present in the organs after 1 month is $\leq 0.3\%$ of the injected dose for all organs.

The most interesting observation was that MR-HIFU-mediated hyperthermia of the tumor caused a 4.4 fold increase in liposomal tumor uptake from 0.50 ± 0.08 %ID/g without HIFU to 2.2 ± 1.2 %ID/g with HIFU, whereas a 7.9 fold increase in doxorubicin content was observed (0.17 ± 0.08 %ID/g without HIFU versus 1.35 ± 1.32 %ID/g with HIFU). The amount of gadolinium in the tumor was slightly higher than the doxorubicin content in the control (0.34 ± 0.13 %ID/g) and slightly lower for the MR-HIFU-treated tumors (0.97 ± 0.76 %ID/g). In this case, MR-HIFU-mediated hyperthermia of the tumor led to a gadolinium increase by a factor of 2.9. ^{111}In , doxorubicin and gadolinium concentrations in HIFU-treated tumors showed large variations, resulting in high standard deviations for the average concentrations. However, in tumors with high amounts of ^{111}In , also higher doxorubicin concentrations were found (Figure 4.15).

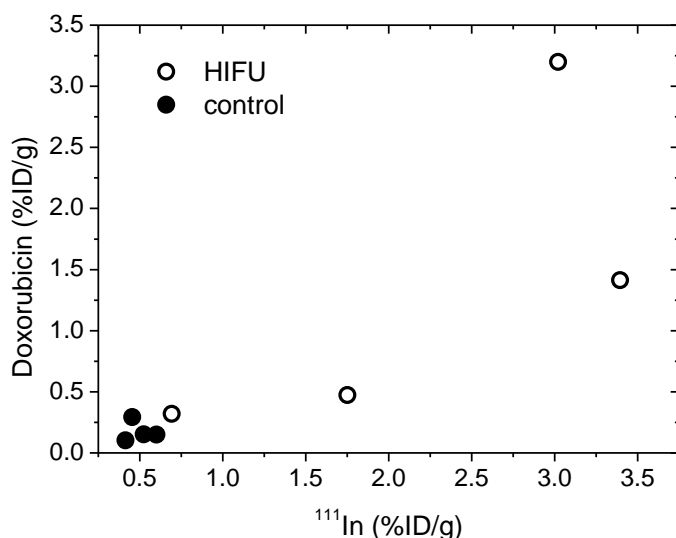


Figure 4.15. Amount of ^{111}In plotted against the amount of doxorubicin measured in the HIFU-treated and control tumors. Large variations were found between the HIFU-treated tumors. However, high amounts of ^{111}In also resulted in high amounts of doxorubicin.

4.4 Discussion

The pharmacokinetic behavior of TSLs encapsulating doxorubicin and $[\text{Gd}(\text{HPDO3A})(\text{H}_2\text{O})]$ was investigated with and without MR-HIFU induced hyperthermia of the tumor. The radiolabeled liposomes showed long blood circulation times, which is favorable for the MR-HIFU mediated drug delivery approach with intravascular release. For *in vivo* experiments, the stability of TSLs at physiological temperatures is of utmost importance in order to avoid

premature drug leakage. The perfect temperature-sensitive liposomal formulation has no doxorubicin leakage at 37 °C, and fast release at 42 °C. Although many research efforts have been made so far,²⁸⁻³⁰ this liposomal formulation has not been discovered yet, and these two prerequisites might even be mutually exclusive. Based on the blood kinetics measurements presented in section 4.3.2, we decided to proceed with the TTSL formulation for the *in vivo* drug delivery experiments performed in this thesis.

In vitro studies with dox/Gd-TTSLs co-encapsulating doxorubicin and [Gd(HPDO3A)(H₂O)] showed no leakage in FBS over 1 hour at 37 °C (Figure 4.8). However, *in vivo* studies showed a faster blood clearance of doxorubicin and [Gd(HPDO3A)(H₂O)] compared to the radiolabeled liposomal carrier, indicating that premature leakage of the encapsulated drug and MRI contrast agent already occurred at body temperature. Apparently, the experimental *in vitro* conditions do not seem to mimic the *in vivo* situation completely. However, one hour after injection, 88 % of the initial liposome concentration and 78 % of the doxorubicin was still present in the blood. These high concentrations are beneficial for localized MR-HIFU mediated drug delivery.

For clinical translation of MR-HIFU mediated drug delivery using TSLs, fundamental insight on the effect of HIFU on the biodistribution of the liposomal drug carrier is essential. Preclinical evaluation of radiolabeled TSLs with SPECT provides essential information on the biodistribution, revealing insights which might be overseen by a regular 'cut and count' biodistribution experiment. Side effects from the liposomes and the encapsulated doxorubicin are expected to be similar to clinically approved non-temperature sensitive liposomal formulation of doxorubicin (e.g. Caelyx®). However, the addition of the MRI contrast agent in the aqueous lumen of the TSL for MR-image guidance of the drug delivery as well as the influence of MR-HIFU mediated hyperthermia on the biodistribution has to be investigated carefully.

The clinically approved MRI contrast agent used in this study, [Gd(HPDO3A)(H₂O)] (Prohance®), is in its free form rapidly eliminated from the body through the kidneys.¹⁵ However, liposomal encapsulation not only increases the blood half-life from minutes to hours, but also changes the route of elimination from the body to clearance by the liver and spleen instead of the kidney. One point of concern is that long term tissue retention in the liver and spleen leads to release of Gd³⁺ from the chelate leading to nephrogenic systemic fibrosis (NSF).³¹⁻³² ICP-MS measurements of organs collected one month after injection of the TSLs containing [Gd(HPDO3A)(H₂O)] showed that the amount of gadolinium was ≤ 0.3% of the injected dose in all analyzed organs (Figure 4.14) indicating that significant clearance occurred compared to the 48 h time point.

SPECT imaging and biodistribution studies were used to investigate the liposome clearance and the influence of the MR-HIFU treatment hereon. The biodistribution showed the highest uptake by the liver and the spleen and was similar for the MR-HIFU treated and

control rats, except for the tumor and adrenals that showed a higher uptake due to the MR-HIFU treatment. The high liver and spleen uptake was expected, as these organs are part of the mononuclear phagocyte system (MPS), which is typically responsible for filtering out liposomes from the blood circulation.³³⁻³⁵ Doxorubicin and gadolinium concentrations found in these organs were lower than the liposome concentrations, which was expected as liposomes in the blood stream lose their [Gd(HPDO3A)(H₂O)] and doxorubicin payload by leakage over time but keep circulating "empty" until they are taken up by the MPS. Secondly, the extensive metabolism in liver and spleen may cause a more rapid organ clearance for [Gd(HPDO3A)(H₂O)] and doxorubicin compared to the ¹¹¹In-labeled liposomes.³⁶

The increased uptake in the adrenals in the MR-HIFU treated animals was observed for the liposomes as well as for doxorubicin and gadolinium. One of the functions of the adrenals is the release of hormones (e.g. adrenaline) in response to stress. However, no explanation was found why these organs would have an increased liposome uptake due to the MR-HIFU treatment. Furthermore, SPECT imaging revealed an increased liposomal uptake in non-tumor tissue close to the femur of the HIFU-treated, tumor-bearing leg (Figure 4.11). This is probably caused by some unintentional heating of the muscle caused by the interaction of the ultrasound waves in the far field with the bone, leading to liposome accumulation in the heated areas. However, for possible later clinical translation we do not consider this as a problem, as it will be easier in humans to avoid bone with the ultrasound beam due to the larger dimensions. An unexpected observation was the occasional high uptake in the lungs, independent of the HIFU treatment. This lung uptake showed a large variation between the animals. In some cases a homogeneous uptake was observed, while in other rats a heterogeneous uptake was seen (Figure 4.12) or almost no lung uptake was observed as shown in Figure 4.11.

For tumors, MR-HIFU induced hyperthermia led to an increase in liposome accumulation by a factor of 4.4. Though, large intertumoral variations were observed. This can be most likely attributed to differences in vascularization, tumor permeability and/or the presence of a necrotic core in this tumor model.^{5, 11} Various factors of the MR-HIFU treatment may play a role in the increased liposome accumulation. For example increased blood flow, increased permeability of the tumor and increased extravasation are reported effects of hyperthermia. Recently, Al Jamal *et al.* observed a two times higher liposome accumulation in a B16F10 tumor 24 h after injection, in which a water bath was used to heat the tumor bearing leg.³⁷ This increase is lower than the 4.4 fold increase found in our study, which can probably be explained by the differences in tumor model and/or the heating method with a water bath instead of HIFU. In their work, a liposomal uptake of approximately 6 %ID/g in the unheated B16F10 tumors was found, while our control experiments in the absence of HIFU on the 9L tumors showed only 0.50 ± 0.08 %ID/g. Thus, tumors that are well vascularized and show a considerable uptake of liposomes via the

enhanced permeability and retention (EPR) effect to start with, such as the B16F10, may profit from hyperthermia less than tumors with a poor EPR effect. Considering the heating method, ultrasound may have some additional effects on liposome accumulation in comparison with water bath heating. The observed increase in liposome accumulation in the tumor upon MR-HIFU mediated hyperthermia is of general importance to applications in liposomal drug delivery. Both temperature-sensitive and non-temperature-sensitive liposomal drugs may benefit from this effect when combined with local heating.

Comparison of the doxorubicin concentration between the MR-HIFU treated and the control tumors 48 h after injection showed an increase by a factor of 7.9 due to HIFU-treatment, which is even larger than the increased uptake of liposomes. The additional drug accumulation due to increased extravasation and uptake of long circulating TSLs with subsequent release of doxorubicin was so far not systematically investigated. The doxorubicin concentration in heated tumors over 48 h is therefore likely a combined effect of the intravascular release of doxorubicin, the increased accumulation of doxorubicin-filled liposomes and the wash-out and/or metabolism of doxorubicin. The observed drug leakage at 37 °C from the TSLs used in this study will reduce the beneficial effect of the increased accumulation of liposomes at extended periods of time, since the amount of doxorubicin encapsulated inside the liposomes during the extravasation process determines the additional effect. A good alternative to consider would be a combined injection with TSL and a non-temperature sensitive liposomal formulation, which stably encapsulates the drug.

4.5 Conclusion

Radiolabeled TSLs co-encapsulating doxorubicin and [Gd(HPDO3A)(H₂O)] showed a long blood circulation time of the liposomal carrier and premature release of the drug and the MRI contrast agent at physiological temperatures in Fisher rats. Fundamental insights on the effect of HIFU on the biodistribution of TSLs and their encapsulating compounds are essential for clinical translation of MR-HIFU mediated drug delivery. SPECT/CT images and biodistribution studies showed high uptake of the liposomes in the spleen and the liver for both the control and HIFU-treated rats. Although a large intratumoral variation was found, HIFU-mediated hyperthermia of the tumor resulted in a 4.4-fold higher uptake of the radiolabeled TSL in the tumor (t = 48 h) compared to control experiments in the absence of HIFU, while the doxorubicin concentration was increased by a factor 7.9. This increased accumulation of doxorubicin-filled liposomes at longer time points may have an important contribution to the therapeutic outcome of MR-HIFU mediated drug delivery.

References

1. Ganta S, H. Devalapally, A. Shahiwala, M. Amiji. A review of stimuli-responsive nanocarriers for drug and gene delivery. *J Control Release*. 2008;126:187-204.
2. Banerjee R. Trigger-responsive nanoparticles: control switches for cancer therapy. *Nanomedicine*. 2011;6(10):1657-60.
3. Yatvin MB, Weinstein JN, Dennis WH, et al. Design of liposomes for enhanced local release of drugs by hyperthermia. *Science*. 1978;202:1290-3.
4. Weinstein JN, Magin RL, Yatvin MB, et al. Liposomes and local hyperthermia- selective delivery of methotrexate to heated tumors. *Science*. 1979;204(4389):188-91.
5. de Smet M, Hijnen NM, Langereis S, et al. Magnetic Resonance guided High Intensity Focused Ultrasound (MR-HIFU) mediated hyperthermia improves the intratumoral distribution of temperature-sensitive liposomal doxorubicin. submitted.
6. Manzoor AA, Lindner LH, Landon CD, et al. Overcoming limitations in nanoparticle drug delivery: Triggered, intravascular release to improve drug penetration into tumors. . *Cancer Research*. 2012;72(21):5566-75.
7. Staruch RM, Ganguly M, Tannock IF, et al. Enhanced drug delivery in rabbit VX2 tumours using thermosensitive liposomes and MRI-controlled focused ultrasound hyperthermia. *International Journal of Hyperthermia*. 2012;28(8):776-87.
8. Ponce AM, Viglianti BL, Yu D, et al. Magnetic Resonance Imaging of temperature-sensitive liposome release: Drug dose painting and antitumor effects. *J Natl Cancer Inst* 2007;99:53-63.
9. Viglianti BL, A.M. Ponce, C.R. Michelich, D. Yu, S.A. Abraham, L. Sanders, P.S. Yarmolenko, T. Schroeder, J.R. MacFall, D.P. Barboriak, O.M. Colvin, M.B. Bally, M.W. Dewhirst. Chemodosimetry of in vivo tumor liposomal drug concentration using MRI. *Magn Reson Med*. 2006;56:1011-8.
10. Negussie AH, Yarmolenko PS, Partanen A, et al. Formulation and characterisation of magnetic resonance imageable thermally sensitive liposomes for use with magnetic resonance-guided high intensity focused ultrasound. *International Journal of Hyperthermia*. 2011;27(2):140-55.
11. de Smet M, Heijman E, Langereis S, et al. Magnetic resonance imaging of high intensity focused ultrasound mediated drug delivery from temperature-sensitive liposomes: An in vivo proof-of-concept study. *Journal of Controlled Release*. 2011;150(1):102-10.
12. Tagami T, Foltz WD, Ernsting MJ, et al. MRI monitoring of intratumoral drug delivery and prediction of the therapeutic effect with a multifunctional thermosensitive liposome. *Biomaterials*. 2011;32(27):6570-8.
13. Gustafson DL, Rastatter J, Colombo T, et al. Doxorubicin pharmacokinetics: macromolecule binding, metabolism, and excretion in the context of a physiologic model. *Journal of Pharmaceutical Sciences*. 2002;91(6):1488-501.
14. Raduchel B, Schmitt-Willich H, Platzek J, et al. Synthesis and characterization of novel dendrimer-based gadolinium complexes as MRI contrast agents for the vascular system. *Polymeric Materials Science and Engineering*. 1998;79:516-7.
15. Eakins MN, Eaton SM, Fisco RA, et al. Physicochemical properties, pharmacokinetics and biodistribution of Gadoteridol injection in rats and dogs. *Acad Radiol*. 1995;2:584-91.
16. Unger E, Cardenas D, Zerella A, et al. Biodistribution and clearance of liposomal gadolinium-DTPA. *Investigative Radiology*. 1990;25(6):638-44.

17. Gabizon A. Pharmacokinetics of PEGylated liposomal doxorubicin. *Clinical Pharmacokinetics*. 2003;42:419-36.
18. Hak S, Sanders H, Agrawal P, et al. A high relaxivity Gd(III)DOTA-DSPE-based liposomal contrast agent for magnetic resonance imaging. *European Journal of Pharmaceutics and Biopharmaceutics*. 2009;72(2):397-404.
19. Rouser G, Fleische S, Yamamoto A. 2 Dimensional thin layer chromatographic separation of polar lipids and determination of phospholipids by phosphorus analysis of spots. *Lipids*. 1970;5(5):494.
20. Look DC, Locker DR. Time saving in measurement of NMR and EPR relaxation times. *Review of Scientific Instruments*. 1970;41(2):250-1.
21. de Smet M, Langereis S, van den Bosch S, et al. Temperature-sensitive liposomes for doxorubicin delivery under MRI guidance. *Journal of Controlled Release*. 2010;143(1):120-7.
22. Hijnen NM, Heijman E, Köhler MO, et al. Tumour hyperthermia and ablation in rats using a clinical MR-HIFU system equipped with a dedicated small animal set-up. *International Journal of Hyperthermia*. 2012;28(2):141-55.
23. Enholm JK, Köhler MO, Quesson B, et al. Improved volumetric MR-HIFU ablation by robust binary feedback control. *IEEE Trans Biomed Eng*. 2010;57(1):103-13.
24. Briese E. Normal body temperature of rats: the setpoint controversy. *Neuroscience and Biobehavioral Reviews*. 1998;22(3):427-36.
25. Hosokawa T, Sami M, Kato Y, et al. Alteration in the temperature-dependent content release property of thermosensitive liposomes in plasma. *Chem Pharm Bull*. 2003;51(11):1227-32.
26. Hossann M, Syunyaeva Z, Schmidt R, et al. Proteins and cholesterol lipid vesicles are mediators of drug release from thermosensitive liposomes. *Journal of Controlled Release*. 2012;162:400-6.
27. Fossheim SL, A.K. Fahlvik, J. Klaveness, R.N. Muller Paramagnetic liposomes as MRI contrast agents: influence of liposomal physicochemical properties on the in vitro relaxivity. *Magnetic Resonance Imaging*. 1999;17(1):83-9.
28. Lindner LH, Eichhorn ME, Eibl H, et al. Novel temperature-sensitive liposomes with prolonged circulation time. *Clin Cancer Res*. 2004;10:2168-78.
29. Tagami T, Ernsting MJ, Li S-D. Optimization of a novel and improved thermosensitive liposome formulated with DPPC and a Brij surfactant using a robust in vitro system. *Journal of Controlled Release*. 2011;154(3):290-7.
30. Landon CD, Park J, Needham D, et al. Nanoscale drug delivery and hyperthermia: The materials design and preclinical and clinical testing of low temperature-sensitive liposomes used in combination with mild hyperthermia in the treatment of local cancer. *The Open Nanomedicine Journal*. 2011;3:38-64.
31. Penfield JG. Nephrogenic systemic fibrosis and the use of gadolinium-based contrast agents. *Pediatr Nephrol*. 2008;23:2121-9.
32. MacNeil S, Bains S, Johnson C, et al. Gadolinium contrast agent associated stimulation of human fibroblast collagen production. *Investigative Radiology*. 2011;46:711-7.
33. Allen TM, Hansen C. Pharmacokinetics of stealth versus conventional liposomes: effect of dose. *Biochimica et Biophysica Acta*. 1991;1068:133-41.
34. Ishida T, Harashima H, Kiwada H. Liposome clearance. *Bioscience Reports*. 2002;22(2):197-224.
35. Drummond DC, C.O. Noble, M.E. Hayes, J.W. Park, D.B. Kirpotin. Pharmacokinetics and In Vivo drug release rates in liposomal nanocarrier development. *J Pharm Sci*. 2008;97(11):4696-740.

36. Arnold RD, Slack JE, Straubinger RM. Quantification of doxorubicin and metabolites in rat plasma and small volume tissue samples by liquid chromatography/electrospray and tandem mass spectroscopy. *Journal of Chromatography B*. 2004;808:141-52.
37. Al-Jamal WT, Al-Ahmady ZS, Kostarelos K. Pharmacokinetics & tissue distribution of temperature-sensitive liposomal doxorubicin in tumor-bearing mice triggered with mild hyperthermia. *Biomaterials*. 2012;33:4608-17.

Chapter 5

Magnetic Resonance Imaging of High Intensity Focused Ultrasound mediated drug delivery from temperature-sensitive liposomes; an *in vivo* proof-of-concept study

Abstract

Temperature-sensitive liposomes (TSLs) co-encapsulating doxorubicin and 250 mM [Gd(HPDO3A)(H₂O)] were evaluated for HIFU-mediated drug delivery under MR image guidance. *In vitro* studies showed simultaneous and quantitative release of the drug and the MRI contrast agent from the lumen of the TSLs at 42 °C, while no leakage was observed over 1 hour at 37 °C. In a proof-of-concept study, local hyperthermia has been applied for 30 minutes in 9L rat tumors using a clinical MR-HIFU system. The local temperature-triggered release of [Gd(HPDO3A)(H₂O)] was monitored with interleaved T_1 mapping of the tumor tissue. A good correlation between the ΔR_1 , the uptake of doxorubicin and the gadolinium concentration in the tumor was found, implying that the *in vivo* release of doxorubicin from TSLs can be probed *in situ* with the longitudinal relaxation time of the co-released MRI contrast agents.

Based on:

M. de Smet, E. Heijman, S. Langereis, N.M. Hijnen and H. Gröll. *Magnetic Resonance Imaging of High Intensity Focused Ultrasound mediated drug delivery from temperature-sensitive liposomes: an in vivo proof-of-concept study*. *Journal of Controlled Release* 2011; 150(1): 102-110

5.1 Introduction

In this Chapter, the concept of HIFU-mediated doxorubicin delivery from temperature-sensitive liposomes (TSLs) under MR image guidance was explored *in vitro* and *in vivo*. The traditional temperature-sensitive liposomal formulation (TTSL from Chapter 2) co-encapsulating doxorubicin and 250 mM [Gd(HPDO3A)(H₂O)] were evaluated for HIFU-mediated drug delivery under MR image guidance. *In vitro* studies were performed to study the release kinetics of the drug and the MRI contrast agent from the lumen of the TSLs during heating. The MRI monitoring of HIFU-induced release of [Gd(HPDO3A)(H₂O)] from the TSLs was tested *in vitro* on a gelphantom containing TSLs that were homogeneously distributed across a gel.

In an *in vivo* proof-of-concept study, local hyperthermia has been applied for 30 minutes in tumor bearing rats using a clinical MR-HIFU system at 3T. The local temperature-triggered release of [Gd(HPDO3A)(H₂O)] was monitored with interleaved T_1 mapping of the tumor tissue and correlated with the co-release of doxorubicin.

5.2 Materials and Methods

5.2.1 Materials

1,2-Dipalmitoyl-*sn*-glycero-3-phosphocholine (DPPC) and hydrogenated-*L*- α -phosphatidylcholine (HSPC) were provided by Lipoid. 1,2-Dipalmitoyl-*sn*-glycero-3-phosphoethanolamine-*N*-[methoxy(polyethyleneglycol)-2000] (DPPE-PEG2000) and cholesterol were purchased from Avanti Polar Lipids (USA). Doxorubicin hydrochloride was purchased from AvaChem Scientific (USA). [Gd(HPDO3A)(H₂O)] (ProHance®) was obtained from Bracco Diagnostics (Italy).

5.2.2 Preparation and characterization of liposomes

Temperature-sensitive liposomes composed of DPPC:HSPC:Chol:DPPE-PEG2000 = 50:25:15:3 (molar ratio) were prepared by lipid film hydration followed by extrusion, in a similar fashion as described in Chapter 2. The main difference is the increased intraliposomal [Gd(HPDO3A)(H₂O)] concentration from 60 mM to 250 mM for the liposomes used in this study.

In short, the phospholipids and cholesterol were dissolved in a solution of chloroform/methanol (4:1 *v/v*). The organic solvents were removed *in vacuo* until a thin lipid film was formed, which was further dried overnight under a nitrogen flow. The lipid film was hydrated at 60 °C in 120 mM (NH₄)₂SO₄ buffer (pH 5.4) containing 250 mM [Gd(HPDO3A)(H₂O)]. The suspension was extruded at 60 °C successively through a polycarbonate filter of 400 nm (two times), 200 nm (two times), and 100 nm (six times).

Subsequently, the extraliposomal buffer was replaced by HEPES Buffered Saline (HBS) (20 mM HEPES and 137 mM NaCl at pH 7.4) by gel filtration through a PD-10 column. Subsequently, a solution of doxorubicin in HBS (5 mg/mL) was added to the liposomes at a phospholipid to doxorubicin molar ratio of 17.5:1 and the TSLs were incubated at 37 °C for 24 hours. During incubation, 20 μ L samples were taken over time to follow the doxorubicin loading with fluorescence measurements. Finally, the TSLs were passed through a second PD-10 column. The liposomes were concentrated using an Amicon Ultra-4 Centrifugal Filter Unit (100 kDa MWCO, Millipore).

The doxorubicin concentration was determined fluorimetrically (Perkin Elmer LS55, $\lambda_{\text{ex}} = 485$ nm and $\lambda_{\text{em}} = 590$ nm) after destruction of the doxorubicin-loaded liposomes with Triton X-100. Gadolinium concentrations were determined by means of Inductively Coupled Plasma-Mass Spectrometry (ICP-MS, DRCII, Perkin Elmer) after the destruction of the TSLs with nitric acid and perchloric acid at 180 °C. The phospholipid concentration was measured by phosphate determination according to Rouser *et al.*¹ The hydrodynamic radius of the liposomes was determined using dynamic light scattering (DLS) and the phase transition temperature (T_m) of the liposomal membrane was determined with differential scanning calorimetry (DSC) as described in Chapter 2.

5.2.3 *In vitro* release of doxorubicin and [Gd(HPDO3A)(H₂O)] from TSLs

The release of doxorubicin from TSLs was determined by measuring the intensity of fluorescence ($\lambda_{\text{ex}} = 485$ nm and $\lambda_{\text{em}} = 590$ nm) as a function of the temperature. Experiments were performed on a solution of TSLs (2 μ L) in HBS (2 mL) during heating from 30 < T/ °C < 50 (heating rate = 0.5 K/min). At the end of each measurement, 5 μ L of a 10% v/v solution of Triton X-100 was added to afford quantitative release of doxorubicin. The doxorubicin release (%) was calculated according to: $(I_t - I_0) / (I_{100} - I_0) \times 100\%$; in which I_t is the intensity of the fluorescence at a specific time (t), I_0 is the intensity of the fluorescence at t=0, I_{100} is the intensity of the fluorescence after the addition of Triton X-100.

The release of [Gd(HPDO3A)(H₂O)] from TSLs in HBS was studied by measuring the longitudinal relaxation time (T_1) as a function of the temperature at 7 T (Bruker Avance 300 MHz). The NMR experiments were performed during heating from 30 < T/ °C < 50 (heating rate = 0.5 K/min) followed by cooling down from 50 > T/ °C > 30 (-0.5 K/min). The longitudinal relaxivity (r_1) was calculated according to $r_1 = [(1/T_1) - (1/T_{1,0})]/[\text{Gd}]$, in which T_1 is the longitudinal relaxation time, $T_{1,0}$ is the longitudinal relaxation time of HBS buffer and [Gd] is the concentration of [Gd(HPDO3A)(H₂O)] in mM.

5.2.4 *Magnetic Resonance Imaging and High Intensity Focused Ultrasound on gelphantom*

Temperature-induced release experiments were performed on gel phantoms using a clinical MR-HIFU system (Sonalleve MR-HIFU, Philips Healthcare, Vantaa, Finland). In this system, the HIFU transducer is embedded in the patient bed of a clinical 3T MRI scanner (Achieva 3.0 T, Philips Healthcare, Best, The Netherlands), where the MRI provides spatial and temperature feedback to the ultrasound transducer.² Gel phantoms were prepared from low gelling temperature agarose (Sigma, Steinheim, Germany) (2% w/w) and silicon dioxide (2% w/w) and homogenously mixed with TSLs (1.25% v/v). The liposomes were added to the gel once the temperature was sufficiently below T_m in order to avoid any thermal release of the liposomal contents during the gel preparation. The gel phantom was positioned between gel pads in a water bath at 37 °C above the HIFU transducer. A part of the gel was heated to mild hyperthermia ($T = 42$ °C) for 15 min with an approximately cylindrical sonication volume with either a diameter of $d = 12$ mm and height of $h \approx 30$ mm, or $d = 4$ mm and $h \approx 10$ mm respectively.³ Sonications were controlled by a binary feedback loop with a modified algorithm to maintain the desired temperature, using temperature maps which were continuously acquired by an MR thermometry sequence during the sonication.² The MR thermometry sequence was a single slice gradient echo sequence with the parameters: flip angle = 19.5°; TR/TE=52/19.5 ms; EPI-factor = 7; SENSE factor 1.8; field of view = 250 × 250 mm²; matrix = 176 × 169; slice thickness = 4 mm; number of averages = 8; fat suppression = SPIR; acquisition time = 5.09 s. R_1 maps were acquired using a single slice steady state inversion-recovery Look-Locker sequence⁴⁻⁵ with parameters: flip angle = 10°; TR/TE=9.0/3.4 ms; interval time = 100 ms; time of inversion repetition = 6 s; EPI-factor = 5; field of view = 50 mm × 169 mm; matrix = 64 × 165; half scan = 80%; slice thickness = 5 mm; number of averages = 1; fat suppression = SPIR; acquisition time = 3 min, 18 s.

5.2.5 *Animal model*

Subcutaneous 9L gliosarcoma tumors in Fisher 344 rats (Charles River, age 5-7 weeks) were established by subcutaneous injection of 5×10^6 9L cells (in 100 μ L) on the hind leg. This tumor model was characterized in detail by Dynamic Contrast Enhanced (DCE)-MRI and PET. DCE-MRI was performed using the low molecular weight contrast agent gadopentetate dimeglumine (Gd-DTPA, Magnevist®, Bayer Schering, Germany). A pre-contrast reference scan was performed (single shot 3D gradient-echo, TR/TE: 4.1/1.74 ms, FA: 3°, FOV: 80x80x42 mm³, voxel size: 0.7x0.7x0.7 mm³, number of averages: 4, acquisition time: 28.4 s) to calculate a pre-contrast T_1 -map required for quantitative analysis of the uptake kinetics. Gd-DTPA was injected via a tail vein catheter using an infusion pump (0.2 mmol/kg bw, 0.2 mL/min) after the 10th dynamic scan during a dynamic scan series (single shot 3D gradient-echo, TR/TE: 4.1/1.74 ms, FA: 13°, FOV: 80x80x42 mm³, voxel size:

0.7x0.7x0.7 mm³, number of averages: 1, dynamic scan time: 10.7 s, number of dynamics: 90, acquisition time: 16:05 min). The uptake kinetics of Gd-DTPA were analysed on a voxel-by-voxel basis using the 2-parameter Tofts and Kermod model.⁶ The model was fitted to the measured voxel concentration–time curves and used for the calculation of quantitative parametric maps of the transfer constant k_{trans} (min⁻¹), the rate constant k_{ep} (min⁻¹) and the volume of extra-vascular extracellular space per unit volume of tissue v_e (unitless) using an IDL-based software tool (IDL 6.3, ITT Visual Information Solutions, Boulder, CO).

PET scanning was performed using a small animal PET scanner (Philips Mosaic, spatial resolution \approx 3 mm at full-width-half-maximum). 20-25 MBq ¹⁸F-FDG (GE Healthcare, Eindhoven, the Netherlands) was injected i.v. via the tail vein just after starting the dynamic PET acquisition (duration = 1h16min).

Tumor dimensions were determined by measuring the length (l), width (w) and depth (d) using a caliper and the tumor volume was calculated by $0.5 \times l \times w \times d$. Animal studies were performed with tumor volumes between 400 – 1000 mm³, typically 14-20 days after tumor cell injection.

5.2.6 *In vivo* Magnetic Resonance Imaging and High Intensity Focused Ultrasound

The release of doxorubicin and [Gd(HPDO3A)(H₂O)] from TSLs at hyperthermia was studied in a group ($n = 5$; weight 183 ± 17 g) of 9L tumor bearing rats (tumor size 980 ± 450 mm³). TSLs were intravenously injected with an injection pump (injection speed = 0.2 mL/min) into the tail vein at the moment when the local temperature in the tumor reached 42 °C. The dose was kept at 5 mg doxorubicin/kg bodyweight. The tumors of the control group ($n = 4$; weight 181 ± 8 g; tumor size 770 ± 219 mm³) received exactly the same treatment, except for the heating with HIFU.

All experimental procedures were conducted while the animals were anesthetized with isoflurane (induction 3%, maintenance 1-3%) in medical air (flow 0.4-0.6 L/min). Rimadyl (3 mg/kg) was injected subcutaneously as a precautional pain suppressor at least 30 minutes before treatment. Ultrasound gel (Aquasonic 100, Parker Laboratories, Fairfield, USA) was applied onto the shaven leg and tumor to ensure acoustic coupling and to prevent air bubbles from sticking to the skin. The animal was placed into a dedicated multichannel small animal coil (Philips Healthcare, Vantaa, Finland) mounted on the ultrasound transducer.⁷ During the whole experiment the respiration rate and body temperature of the animal was monitored.

The measurement protocol for the experimental group and the control group is schematically shown in Figure 2. The Sonalleve 3T MR-HIFU system was used to induce local hyperthermia, using an approximately cylindrical sonication volume (diameter = 4 mm, height \approx 10 mm) which was positioned in the centre of the tumor. Two 15-minute hyperthermia treatments were performed using 8W acoustical power. For temperature

monitoring and calculation of T_1 -maps, the MR thermometry and Look-Locker sequences were used respectively, using the same parameters as for the *in vitro* gelphantom experiment described in section 5.2.4 except for the Look-Locker field of view = 50×69 mm; matrix = 64 × 65; number of averages = 2; acquisition time = 2 min, 36 s. At $t = 89 \pm 5$ min after the intravenous injection of TSLs, the rats were euthanized and the tumor was dissected.

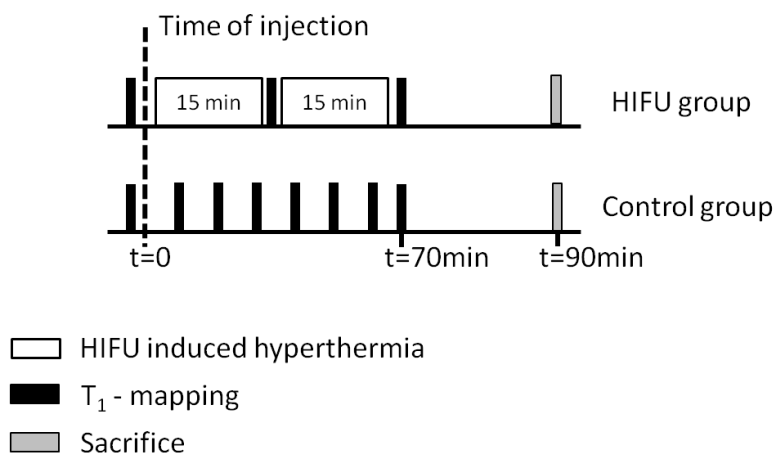


Figure 5.1. MR-HIFU protocol for the experimental (HIFU) and control group. The experimental group received intravenous TSL injection once the local temperature in the tumor reached 42 °C ($t = 0$). For the control group no hyperthermia was applied, instead, T_1 -mapping was performed continuously. Animals were sacrificed at $t = 89 \pm 5$ min, followed by collection of tumors.

5.2.7 Determination of doxorubicin and gadolinium concentration in blood and tumors

Dissected tumors were divided in pieces (~100 mg), which were homogenized with a stainless steel ball in 1.5 mL water/methanol (1:2 v/v) for 5 min at 30 Hz with a Qiagen TissueLyser. The homogenized tumor tissue was divided in two aliquots: I) for the determination of the gadolinium concentration by ICP-MS (see section 5.2.2) and II) for the determination of the doxorubicin concentration.⁸⁻⁹

For doxorubicin quantification, the homogenized solutions were incubated with 200 μ L AgNO₃ in water (33% w/v) for 10 minutes at room temperature. Subsequently, the doxorubicin was extracted by vigorous mixing with 5 mL chloroform/isopropanol (2:1 v/v). After centrifugation (10 min at 3600 rpm) the organic phase was transferred to a clean tube and evaporated to dryness at 40 °C under N₂ flow. The residue was dissolved in H₂O (200 μ L), centrifuged and 50 μ L was injected onto the HPLC column. The samples were analysed on an Agilent Technologies HPLC system (1100 series) equipped with an

autosampler and fluorescence detector with $\lambda_{\text{ex}} = 485 \text{ nm}$ and $\lambda_{\text{em}} = 590 \text{ nm}$. An Eclipse $5 \mu\text{m}$, $4.6 \times 150 \text{ mm}^2$ XDB-C18 column (Agilent) was used. The doxorubicin was eluted in 20 min with a gradient of 5 – 95% (v/v) acetonitrile in 0.1% (v/v) aqueous TFA, using a flow rate of 1 mL/min. With above protocol, $91\% \pm 7\%$ of doxorubicin was recovered in extraction experiments from tissues containing known doxorubicin concentrations in the range 2.5 to $5 \mu\text{g/mL}$. All samples were analysed in triplo.

5.3 Results

5.3.1 Temperature-sensitive liposomes containing doxorubicin and $[\text{Gd}(\text{HPDO3A})(\text{H}_2\text{O})]$

Temperature-sensitive liposomes (TSLs) composed of DPPC:HSPC:Chol:DPPE-PEG2000 = 50:25:15:3 (molar ratio) and encapsulating 250 mM $[\text{Gd}(\text{HPDO3A})(\text{H}_2\text{O})]$ were prepared using the lipid film hydration technique followed by sequential extrusion. The remote loading of doxorubicin performed at $37 \text{ }^\circ\text{C}$ with a transmembrane gradient of ammonium sulfate to yield TSLs containing $[\text{Gd}(\text{HPDO3A})(\text{H}_2\text{O})]$ and doxorubicin was followed over time. Figure 5.2 shows the fluorescence intensity of samples taken during the doxorubicin loading. After overnight loading (22 hours) no further decrease of the fluorescence intensity was observed, indicating that the doxorubicin loading was finished. The mean average hydrodynamic radius of the TSLs was 57.9 nm (polydispersity index < 0.1) as determined by DLS. The melting phase transition temperature (T_m) was $41.9 \text{ }^\circ\text{C}$ as evidenced from DSC. The concentration of phosphorus, gadolinium and doxorubicin was $58.9 \pm 2.2 \text{ mM}$, $14.2 \pm 0.7 \text{ mM}$, and $3.1 \pm 0.1 \text{ mM}$, respectively.

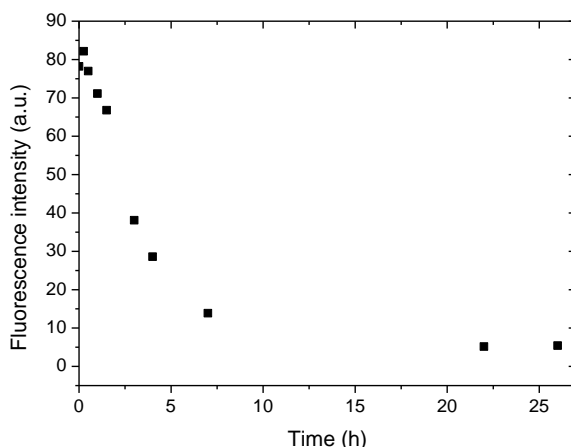


Figure 5.2. Fluorescence intensity of samples taken during the doxorubicin loading of TSL. Active loading of doxorubicin into TSLs was finished after overnight loading.

5.3.2 *In vitro* release of doxorubicin and [Gd(HPDO3A)(H₂O)]

The temperature-induced release of doxorubicin and [Gd(HPDO3A)(H₂O)] from the aqueous lumen of the TSLs was monitored from 30 °C to 50 °C applying a constant heating rate of 0.5 K/min (Figure 5.3). The release of doxorubicin was studied fluorimetrically, while the release of [Gd(HPDO3A)(H₂O)] was probed using the longitudinal relaxivity (r_1). Quantitative release of doxorubicin from the TSLs was observed at 42 °C. The longitudinal relaxivity (r_1) of [Gd(HPDO3A)(H₂O)] inside the TSLs was significantly lower than the corresponding r_1 of non-encapsulated [Gd(HPDO3A)(H₂O)] at 30 °C, which can be explained in terms of limited transmembrane water exchange.¹⁰⁻¹² Upon heating to 40 °C ($T < T_m$), the r_1 increased steadily with temperature, implying an increase in the transmembrane water exchange rate. A rapid increase in r_1 was observed between 40 - 42 °C. This effect was attributed to the release of [Gd(HPDO3A)(H₂O)] from the lumen of the TSLs. Upon cooling, the observed r_1 was similar to the r_1 of [Gd(HPDO3A)(H₂O)], which was taken as experimental evidence for the quantitative release of the MRI contrast agent from the TSLs. It is important to note that the co-release of [Gd(HPDO3A)(H₂O)] and doxorubicin from the TSLs occurred at the same temperature.

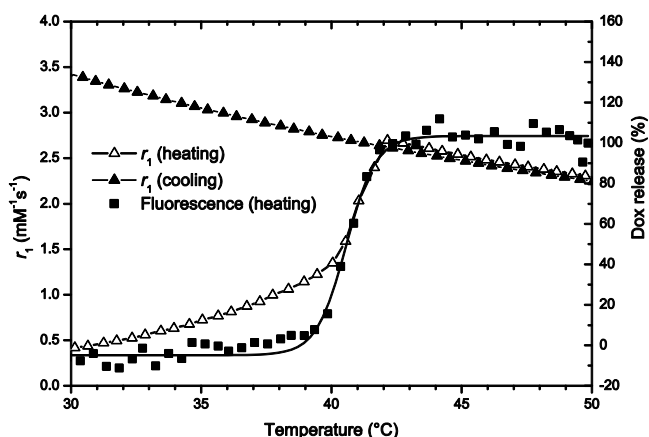


Figure 5.3. Fluorescence and T_1 relaxivity of TSLs in HBS during a linear temperature increase (0.5 K/min) from 30 °C to 50 °C and cooling back to 30 °C.

5.3.3 HIFU mediated release in a gel phantom

An *in vitro* experiment was performed for testing the MRI monitoring of HIFU-induced release of [Gd(HPDO3A)(H₂O)] from the TSLs. The TSLs were homogeneously distributed across a gelphantom, which was placed in a water bath kept at a temperature of 37 °C. Two cylindrical shaped volumes were heated with HIFU to 42 °C for a period of 15 minutes; one with a diameter of 4 mm and the other with $d=12$ mm. Temperature images were acquired

during the HIFU sonication (Figure 5.4 A and B). A temperature gradient developed from the heated area extending into the surrounding gel due to heat diffusion. After the HIFU application Look-Locker scans were performed for calculation of R_1 maps (Figure 5.4 D and E). The heated areas showed a significant increase of the R_1 from $0.91 \pm 0.13 \text{ s}^{-1}$ before heating to $1.23 \pm 0.05 \text{ s}^{-1}$ after heating. Spatial profiles of temperature and ΔR_1 resulting from the 4 mm sonication are shown in Figure 5.4 C and F, respectively. Overlay of the temperature and R_1 map showed that release of $[\text{Gd}(\text{HPDO3A})(\text{H}_2\text{O})]$ was induced in gel regions where temperatures reached 40°C and above.

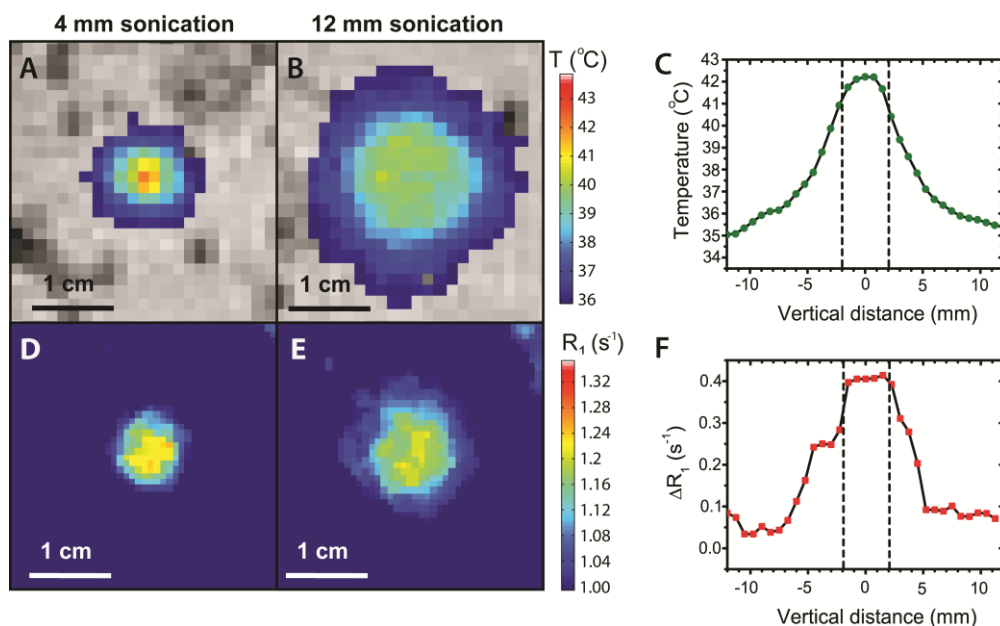


Figure 5.4. MR images of a gel phantom containing TSLs. Temperature maps during hyperthermia with a sonication volume with a diameter of 4 mm (A) and 12 mm (B), R_1 maps after HIFU treatment with the sonication volume with $d = 4 \text{ mm}$ (D) and $d = 12 \text{ mm}$ (E). Spatial profiles of temperature (C) and ΔR_1 (F) with the sonication volume with $d = 4 \text{ mm}$.

5.3.4 Tumor characterization

9L tumors were obtained by s.c. injection of 9L tumor cells in the hind leg of Fisher rats. This tumor model was characterized with MRI and ^{18}F FDG-PET, of which some typical results are shown in Figure 5.5. With PET homogeneous ^{18}F FDG uptake was observed in some tumors, while other tumors showed no uptake in the core. T_2 -weighted and DCE-MRI of a 9L tumor over time showed the formation of a less-permeable core. Therefore, different tumor morphologies might be expected when using this tumor model.

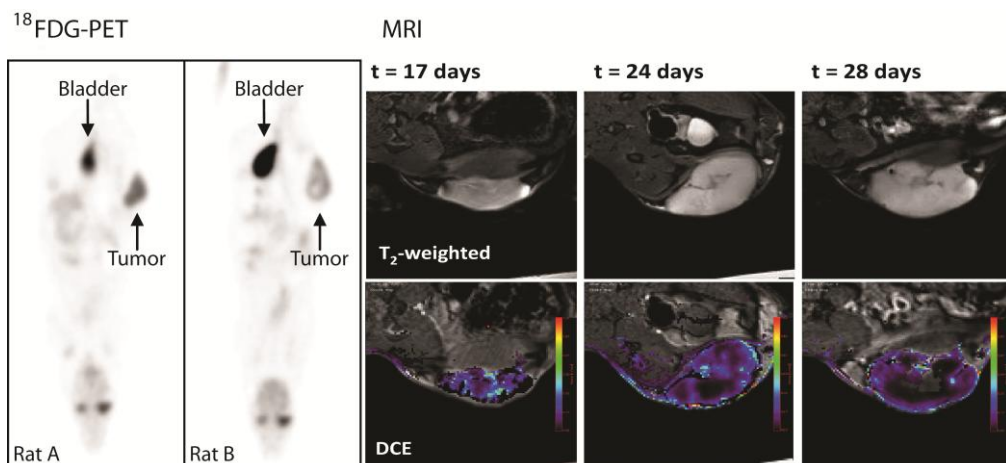


Figure 5.5. Characterization of 9L tumors on Fisher rats. Left: ^{18}F FDG-PET of a rat with a homogeneous tumor (rat A) and with an inhomogeneous tumor (rat B). Right: T_2 -weighted and DCE-MRI of a 9L tumor over time showing the formation of a less-permeable core.

5.3.5 *In vivo* HIFU-mediated release of doxorubicin and $[\text{Gd}(\text{HPDO3A})(\text{H}_2\text{O})]$ from TSLs

In our proof-of-concept study for MR image-guided drug delivery, the release of doxorubicin from the lumen of the TSLs in tumor bearing rats was probed using the longitudinal relaxation time of $[\text{Gd}(\text{HPDO3A})(\text{H}_2\text{O})]$. *In vivo* studies were performed in Fisher rats bearing a subcutaneous 9L tumor on the hind leg. For planning of the HIFU target area, anatomical MR images of the tumor were acquired (Figure 5.6 A). HIFU-mediated hyperthermia of the tumor was accomplished for two times 15 minutes interrupted for ca. 8 minutes for cooling and the acquisition of a T_1 map. During local hyperthermia, temperature maps were acquired of the target area perpendicular to the acoustic beam axis (Figure 5.6 B). The local heating of the tumor was clearly visible on the corresponding temperature maps. As shown in Figure 5.6 C, the mean temperature of the treatment cell (positioned in the centre of the tumor) was maintained between 41 - 42 °C due to the binary feedback control of the HIFU.

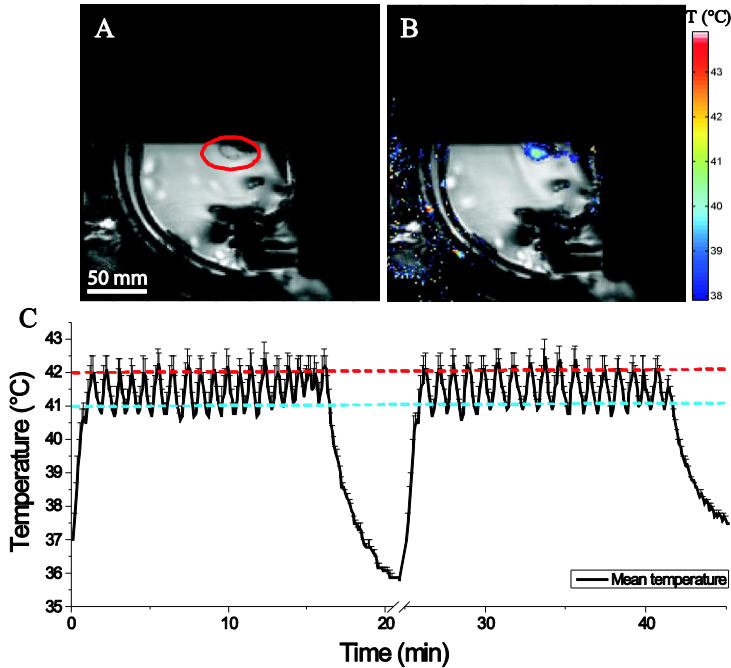


Figure 5.6. A) Anatomical MR image with saturation slab on the rat's body to prevent image artifacts. Tumor is indicated with the red circle. B) MR image overlaid with the calculated temperature map at $t=40$ min. C) The mean temperature within the 4 mm treatment cell during the two hyperthermia periods of 15 min each. The positive error bars indicate the maximum temperature in the treatment cell. The dotted red line and dotted blue line are the major and minor limits, respectively, of the binary feedback loop of the MR-HIFU system.

In this study, five animals received hyperthermia in combination with the administration of TSLs (rat 1-5). Control experiments were performed with four animals in which TSLs were administered without the application of HIFU (rat 6-9). T_1 -maps of the tumor and the surrounding muscle were acquired before the administration of the TSLs and directly after the first and second local hyperthermia treatment (Figure 5.7). Before the administration of the TSLs, the tumor could be clearly discriminated from the surrounding muscle ($T_{1,muscle} = 745 \pm 24$ ms, $T_{1,tumor} = 1120 \pm 28$ ms). The administration of TSLs in combination with mild hyperthermia induced significant changes in the T_1 of the tumor, whereas the T_1 values of the muscle hardly changed.

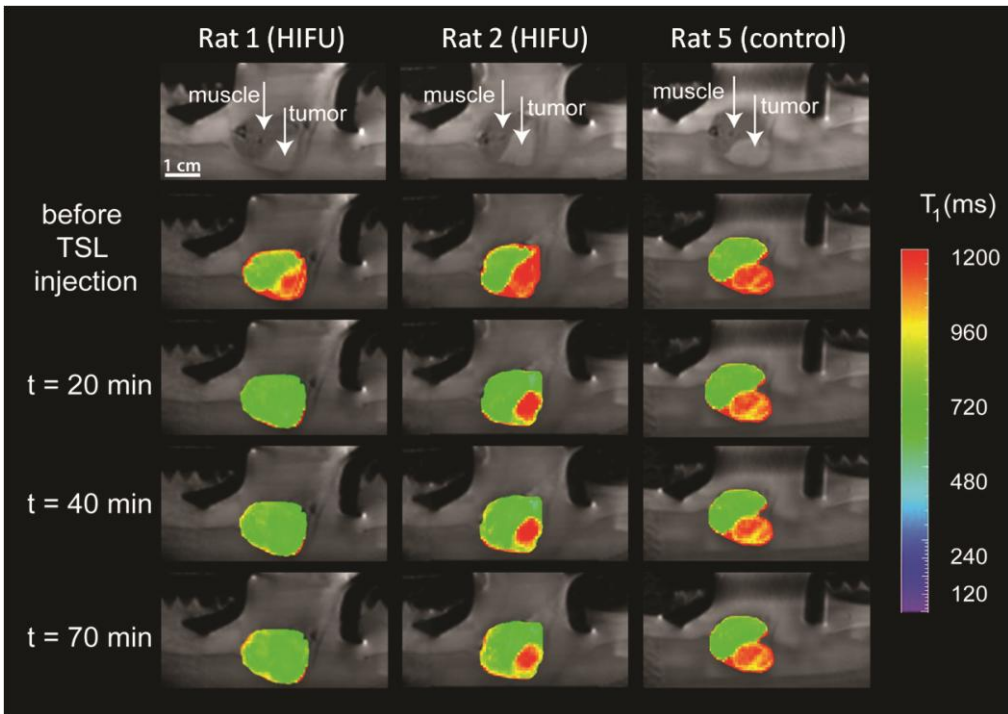


Figure 5.7. Anatomical MR images of tumor bearing rats in the small animal HIFU setup (upper row) and T_1 maps of the tumor and leg overlaid on the anatomical images at different time points: before the TSL injection, after the first hyperthermia period ($t = 20$ min), after the second hyperthermia period ($t = 40$ min) and 70 min after TSL injection. Left; HIFU treated tumor showing a large T_1 response (rat 1), middle; HIFU treated tumor showing a less sensitive response (rat 2) and right; untreated tumor (control, rat 5).

Interestingly, rat 1 showed a distinct decrease of the T_1 over the whole tumor region, while rat 2 showed a much lower response. Here, especially the tumor rim displayed a pronounced T_1 change while the core of the tumor showed barely any change at $t = 40$ min. In-wash of $[\text{Gd}(\text{HPDO3A})(\text{H}_2\text{O})]$ from the outer rim to the core of the tumor was only observed at $t = 70$ min. The control experiments with tumor bearing rats that were not treated with HIFU (e.g. rat 5) showed only a minor decrease in T_1 upon injection of the TSLs.

The ΔR_1 was obtained from the difference in T_1 values averaged over the whole tumor in the MR image slice before and at different time points after TSL injection. ΔR_1 of the tumors over time is shown in Figure 5.8 of the five HIFU-treated (rat 1-5) and the four control (rat 6-9) rats. During HIFU treatment no T_1 measurements could be performed, resulting in missing data points at these time slots. The graph clearly shows that the HIFU-treated tumors showed a larger change in R_1 than the controls. Interestingly, the tumors of

rat 2 and 3 showed a much lower ΔR_1 than the other three HIFU-treated rats. The increase in R_1 observed after HIFU-treatment was quiet stable over time for most of the rats, except for rat 5 which showed a significant decrease of ΔR_1 over time.

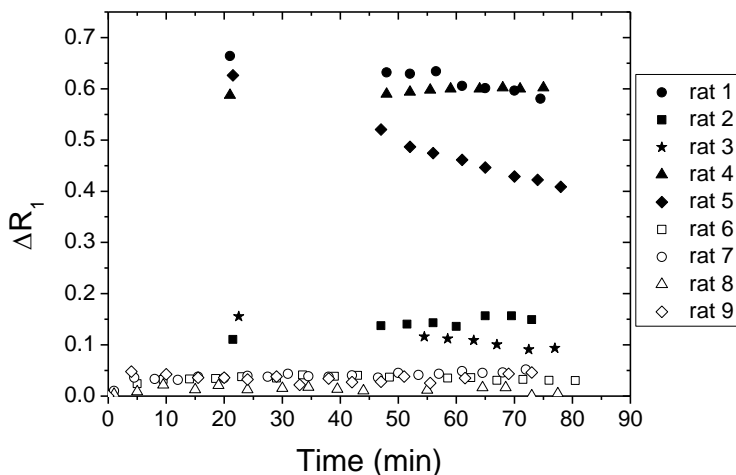


Figure 5.8. ΔR_1 (1/s) of the tumors over time of HIFU treated (rat 1-5; closed symbols) and control (rat 6-9; open symbols) rats.

At the end of the protocol ($t = 89 \pm 5$ min) the rats were sacrificed and the tumors were dissected for analysis. The concentration of gadolinium and doxorubicin in the tumor samples as well as the change in the longitudinal relaxation rate ($\Delta R_1 = \Delta(1/T_1)$) is shown in Figure 5.9. The ΔR_1 shown in this figure is from the scan 70 min after TSL injection.

The tumors that received local HIFU-mediated hyperthermia (rat 1-5) showed higher concentrations of gadolinium and doxorubicin compared to the control group (rat 6-9). Interestingly, the uptake of doxorubicin (average = 2.5 ± 1.5 %ID/g) and gadolinium (average = 1.3 ± 0.4 %ID/g) in the tumors of rats 1, 4 and 5 was relatively high, while rat 2 (dox = 0.36 ± 0.04 %ID/g, Gd = 0.43 ± 0.02 %ID/g) and rat 3 (dox = 0.53 ± 0.07 %ID/g, Gd = 0.37 ± 0.02 %ID/g) showed a lower uptake. Additionally, rat 1, 4 and 5 showed a large change in R_1 (average $\Delta R_1 = 0.53 \pm 0.11$ s⁻¹) while the other two HIFU treated tumors (rat 2 and 3) showed a much lower response on the MR image ($\Delta R_1 = 0.09$ and 0.15 s⁻¹, respectively). The control experiments revealed low concentrations of doxorubicin (0.19 ± 0.08 %ID/g) and gadolinium (0.21 ± 0.08 %ID/g) in the tumors. Moreover, hardly any changes in R_1 were observed ($\Delta R_1 = 0.03 \pm 0.02$ s⁻¹).

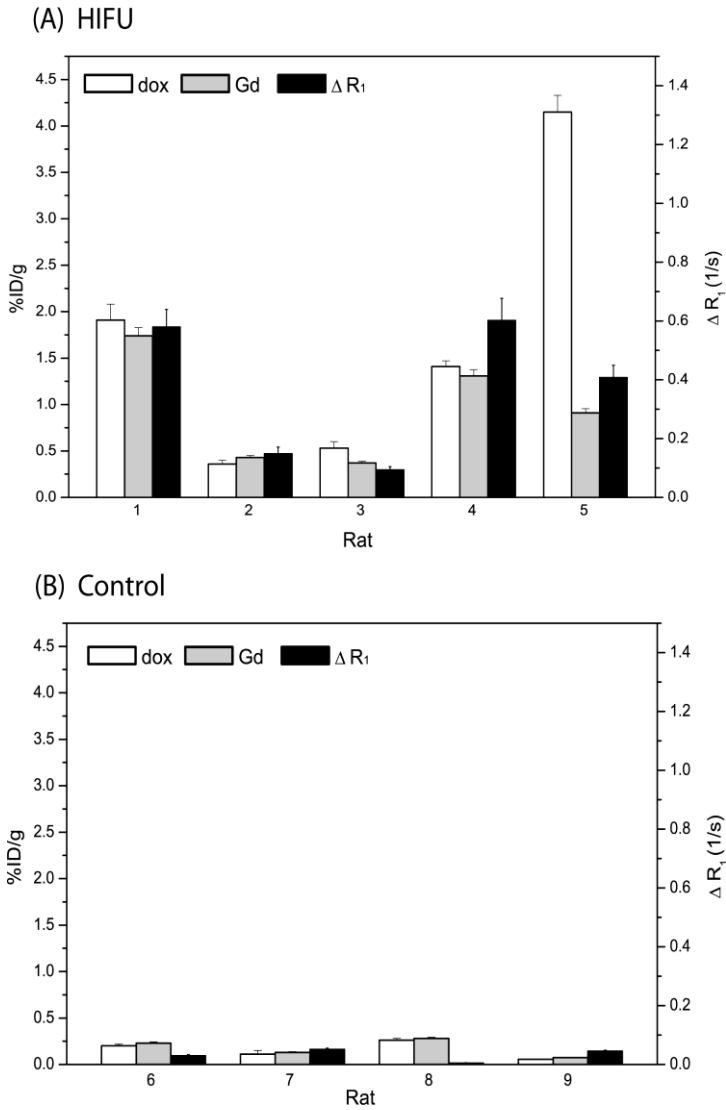


Figure 5.9. Doxorubicin and gadolinium concentrations (expressed in % injected dose/g) and ΔR_1 (1/s) in the tumor of HIFU treated (A) and control (B) rats 70 minutes after time of injection. The error bars show the standard deviation of the doxorubicin extraction ($n=3$ per sample), ICP-MS analysis ($\pm 5\%$ error) and the standard deviation of the ΔR_1 within the region of interest.

For MR image guided doxorubicin delivery at the tumor region, the release of [Gd(HPDO3A)(H₂O)], reflected in the observed change in R₁, should correlate with the concentration of doxorubicin. In fact, HIFU-mediated hyperthermia in combination with TSLs showed a good relation between the ΔR_1 and the doxorubicin concentration from the tumor tissue after dissection. For instance, hyperthermia-treated tumors with a relatively low ΔR_1 (i.e. rats 2 and 3) showed a relatively low uptake of doxorubicin. Moreover, the relatively high tumor uptake of doxorubicin observed for rats 1, 4 and 5 was accompanied by a relatively large ΔR_1 . A similar correlation is found for ΔR_1 and gadolinium concentration. A low uptake of doxorubicin and gadolinium was found in non-treated tumors accompanied by only a subtle change in R₁.

In figure 5.10 the doxorubicin concentration was plotted against ΔR_1 for the tumors of the nine rats injected with TSLs. For all rats, a good correlation was found between [dox], [Gd] and ΔR_1 , except for rat 5, which showed a much higher doxorubicin concentration in comparison to the measured gadolinium concentration and ΔR_1 .

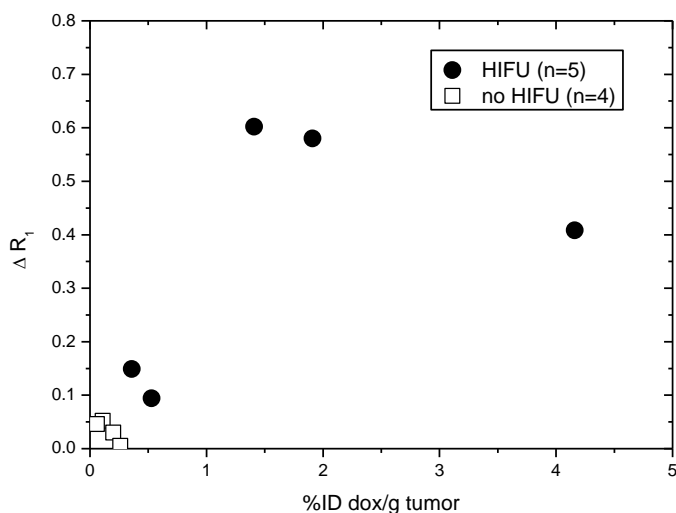


Figure 5.10. Doxorubicin concentrations plotted against ΔR_1 for the tumors of the HIFU-treated (closed symbols) and non-HIFU-treated (open symbols) rats injected with TSLs.

In Figure 5.11 the ΔR_1 data are plotted against the corresponding Gd concentrations for the five HIFU-treated animals. The slope of a linear fit through these data points showed that the longitudinal relaxivity of $4.5 \text{ mM}^{-1}\text{s}^{-1}$ was obtained. For comparison, the relaxivity of free [Gd(HPDO3A)(H₂O)] in HBS was measured *in vitro* (Figure 5.12).

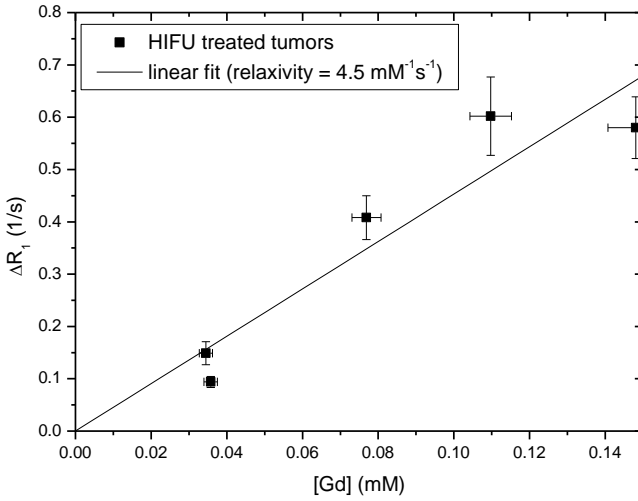


Figure 5.11. ΔR_1 of the five HIFU treated tumors as function of the gadolinium concentrations. The slope of the graph shows the relaxivity of $4.5 \text{ mM}^{-1}\text{s}^{-1}$.

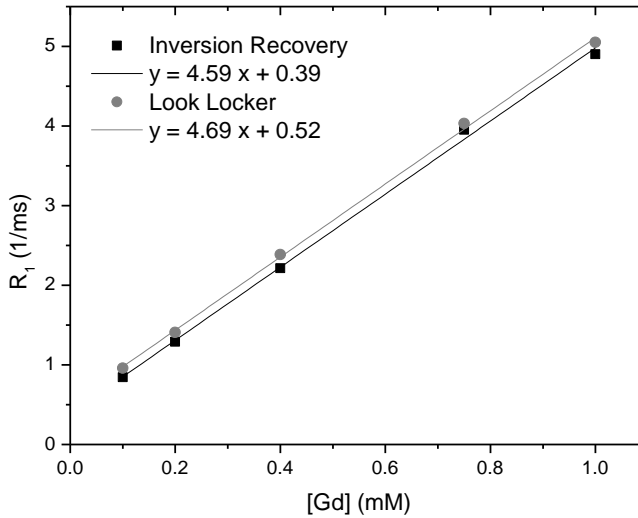


Figure 5.12. R_1 vs $[Gd]$ of $[Gd(HPDO3A)(H_2O)]$ in FBS at $37 \text{ }^\circ\text{C}$ measured at 3T with the Look-Locker sequence and Inversion Recovery sequence. The slope of the graphs shows the relaxivity of $4.6 \text{ mM}^{-1}\text{s}^{-1}$.

5.4. Discussion

In this Chapter, TSLs containing doxorubicin and [Gd(HPDO3A)(H₂O)] were exploited as temperature activatable drug delivery vehicles for HIFU-mediated drug delivery. The underlying concept is that co-encapsulated drug and MRI contrast agent remain in the aqueous lumen of the liposome at body temperature, while HIFU-mediated local hyperthermia induces the release of the encapsulated solutes.

As shown in Chapter 2, the release kinetics of the encapsulated doxorubicin and [Gd(HPDO3A)(H₂O)] strongly depends on the composition of the liposomal membrane. Since the MRI contrast enhancement upon release scales with the concentration of the paramagnetic complex, we increased in difference to the liposomes described in Chapter 2 the intraliposomal [Gd(HPDO3A)(H₂O)] concentration from 60 mM to 250 mM. Temperature-dependent NMR measurements (Figure 5.3) on TSLs loaded with 250 mM [Gd(HPDO3A)(H₂O)] revealed an increase in longitudinal relaxivity r_1 of the encapsulated paramagnetic complex already at temperatures below T_m , which can be attributed to an temperature-dependant increase of the transmembrane water exchange rate.¹¹ The higher intraliposomal [Gd(HPDO3A)(H₂O)] concentration of 250 mM did not affect the water permeability nor the longitudinal relaxivity per liposome at $T < T_m$. Moreover, simultaneous release of doxorubicin and [Gd(HPDO3A)(H₂O)] has been observed and is not affected by the increased intraliposomal [Gd(HPDO3A)(H₂O)] concentration, implying that the release of doxorubicin from these TSLs can be probed by means of the longitudinal relaxivity. The latter was tested in gel-phantom experiments showing that HIFU-mediated hyperthermia induced the release of [Gd(HPDO3A)(H₂O)] from the TSLs. The changes in R_1 observed with MRI were congruent with the temperature map, where temperatures exceeded the liposomal release temperature of approximately 40 °C (Figure 5.4).

As a proof-of-concept study, we performed temperature mediated local drug delivery experiments in tumor bearing rats. Intravenous administration of TSLs in combination with HIFU mediated hyperthermia led to higher uptake of doxorubicin and [Gd(HPDO3A)(H₂O)] in HIFU treated tumors compared to the control group. Although the number of animals in this proof-of-concept study was rather small, a correlation between the ΔR_1 , the uptake of doxorubicin, and the gadolinium concentration in the tumor was found. By combining the ΔR_1 data with the corresponding Gd concentrations for the treatment group, a longitudinal relaxivity of 4.5 mM⁻¹s⁻¹ was obtained (Figure 5.11). This relaxivity corresponds to the r_1 of non-encapsulated [Gd(HPDO3A)(H₂O)] at 3T (Figure 5.12) and is taken as evidence that the contrast agent was indeed released from the liposomes. The observed high intertumoral variation was observed can be most likely attributed to differences in vascularization and/or tumor permeability as well as the presence of a necrotic core (Figure 5.5).¹³

An important point to take into account is that the pharmacokinetic properties of the encapsulated agents prior to release from the lumen of the TSLs are governed by the liposomal carrier. Upon release, however, the different pharmacokinetic and pharmacodynamic (PK/PD) behavior of the chemotherapeutic drug and the MRI contrast agent leads to different biodistribution profiles and tumor uptake, respectively. The high free volume of distribution of doxorubicin will lead to a rapid distribution in the interstitial space across the tumor upon its local release, associated with sticking of doxorubicin to compounds present in the interstitial space and cellular uptake.¹⁴⁻¹⁶ As opposed to doxorubicin, [Gd(HPDO3A)(H₂O)] will distribute across the extracellular space¹⁷ and its intratumoral concentration is a balance between tumor inflow and wash out. For most of the measured rat tumors, the washout of [Gd(HPDO3A)(H₂O)] was low within the measured time span. Therefore, we found a good correlation between the averaged ΔR_1 changes across the tumor and the amount of doxorubicin deposited in the tumor based on two T_1 maps acquired before and after treatment for these tumors. Though our analysis was based on tumor averaged values, the T_1 maps shown in Figure 5.7 are quite likely congruent to dose maps even on a voxel level. Only for rat 5 a high washout of [Gd(HPDO3A)(H₂O)] was observed. Pharmacokinetic modeling taking the PK/PD properties of the drug and the MRI contrast agent into account, next to properties of the drug carrier and parameters related to the tumor biology, will therefore be required to predict the amount of doxorubicin delivered to this tumor based on MR imaging. Real time T_1 and simultaneous temperature mapping during the hyperthermia treatment will be the next step in image guided drug delivery allowing for a dose painting approach during the therapy.¹⁸

Previously, temperature-sensitive liposomes containing doxorubicin in combination with mild hyperthermia showed an improved treatment efficacy in comparison with the free drug.^{16,19} Our results suggest that the deposited amount of drug depends on the type and morphology of tumor, for example the presence of a necrotic core, vascularization and permeability. Image guided therapy enables a way to quantify and monitor the drug delivery process *in situ* and may serve as a tool in clinical decision making to personalize treatments.

5.5. Conclusion

In this proof-of-concept study, we explored local doxorubicin delivery from TSLs under MR image guidance mediated by ultrasound induced hyperthermia in tumor bearing rats. The local temperature-triggered release of [Gd(HPDO3A)(H₂O)] was monitored with interleaved T₁ mapping of the tumor tissue and linearly correlated with the co-release of doxorubicin as well as the gadolinium concentration in the tumor. The combination of hyperthermia with TSLs resulted in higher concentrations of doxorubicin and [Gd(HPDO3A)(H₂O)] by a factor between 2 to 27 (average factor = 11), depending on the nature of the tumor. Imaging of the drug release of temperature-sensitive liposomes will be an important tool in order to monitor and control the drug delivery process.

5.6 Acknowledgements

We would like to thank Philips Healthcare (Vantaa, Finland) for all technical support regarding the Sonalleve 3T MR-HIFU system. Iris Verel (Life Science Facility, Philips Research Eindhoven) and Charles Sio (Biomolecular Engineering, Philips Research Eindhoven) are acknowledged for the contributions to the 9L tumor model characterization and Roland van de Molengraaf (Life Science Facility, Philips Research Eindhoven) for his assistance with the MR-HIFU system. We thank Jeroen Pikkemaat (Materials Analysis - MiPlaza, Philips Research Eindhoven) for the NMR measurements at 300 MHz and Jeannette Smulders (MiPlaza Test, Measurement & Analysis, Philips Research Eindhoven) for the ICP-MS measurements.

References

1. Rouser G, Fleische S, Yamamoto A. 2 Dimensional thin layer chromatographic separation of polar lipids and determination of phospholipids by phosphorus analysis of spots. *Lipids*. 1970;5(5):494.
2. Enholm JK, Köhler MO, Quesson B, et al. Improved volumetric MR-HIFU ablation by robust binary feedback control. *IEEE Trans Biomed Eng*. 2010;57(1):103-13.
3. Köhler MO, Mougnot C, Quesson B, et al. Volumetric HIFU ablation under 3D guidance of rapid MRI thermometry. *Medical Physics*. 2009;36(8):3521-35.
4. Shin W, Gu H, Yang Y. Fast high-resolution T1 mapping using inversion-recovery Look-Locker echo-planar imaging at steady state: optimization for accuracy and reliability. *Magnetic Resonance in Medicine*. 2009;61:899-906.
5. Look DC, Locker DR. Time saving in measurement of NMR and EPR relaxation times. *Review of Scientific Instruments*. 1970;41(2):250-1.
6. Tofts PS, Kermode AG. Measurement of the blood-brain barrier permeability and leakage space using dynamic MR imaging. 1. Fundamental concepts. *Magn Reson Med*. 1991;17(2):357-67.
7. Hijnen NM, Heijman E, Köhler MO, et al. Tumour hyperthermia and ablation in rats using a clinical MR-HIFU system equipped with a dedicated small animal set-up. *International Journal of Hyperthermia*. 2012;28(2):141-55.
8. Cummings J, C.S. McArdle. Studies on the in vivo disposition of adriamycin in human tumours which exhibit different responses to the drug. *Br J Cancer*. 1986;53:835-8.
9. Hossann M, Wiggenhorn M, Schwerdt A, et al. In vitro stability and content release properties of phosphatidylglycerol containing thermosensitive liposomes. *Biochim Biophys Acta*. 2007;1768:2491-9.
10. de Smet M, Langereis S, van den Bosch S, et al. Temperature-sensitive liposomes for doxorubicin delivery under MRI guidance. *Journal of Controlled Release*. 2010;143(1):120-7.
11. Fossheim SL, A.K. Fahlvik, J. Klaveness, R.N. Muller Paramagnetic liposomes as MRI contrast agents: influence of liposomal physicochemical properties on the in vitro relaxivity. *Magnetic Resonance Imaging*. 1999;17(1):83-9.
12. Unger E, D.K. Shen, G.L. Wu, T. Fritz. Liposomes as MR contrast agents: pros and cons. *Magn Reson Med*. 1991;22(2):304-8.
13. Mazurchuk R, Zhou R, Straubinger RM, et al. Functional Magnetic Resonance (fMR) Imaging of a rat brain tumor model: implications for evaluation of tumor microvasculature and therapeutic response. *Magnetic Resonance Imaging*. 1999;17(4):537-48.
14. Working PK, Newman MS, Huang SK, et al. Pharmacokinetics, biodistribution and therapeutic efficacy of doxorubicin encapsulated in stealth® liposomes (Doxil®). *J Liposome Res*. 1994;4(1):667-87.
15. Harashima H, Iida S, Urakami Y, et al. Optimization of antitumor effect of liposomally encapsulated doxorubicin based on simulations by pharmacokinetic/ pharmacodynamic modeling. *Journal of Controlled Release*. 1999;61:93-106.
16. Needham D, Anyarambhatla G, Kong G, et al. A new temperature-sensitive liposome for use with mild hyperthermia: characterization and testing in a human tumor xenograft model. *Cancer Res*. 2000;60:1197-201.
17. Eakins MN, Eaton SM, Fisco RA, et al. Physicochemical properties, pharmacokinetics and biodistribution of Gadoteridol injection in rats and dogs. *Acad Radiol*. 1995;2:584-91.

18. Hey S, de Smet M, Stehning C, et al. Simultaneous T1 measurements and proton resonance frequency shift based thermometry using variable flip angles. *Magn Reson Med*;67(2):457-63.
19. Kong G, Anyarambhatla G, Petros WP, et al. Efficacy of liposomes and hyperthermia in a human tumor xenograft model: importance of triggered drug release. *Cancer Res.* 2000;60:6950-7.

Chapter 6

MR-HIFU mediated hyperthermia improves the intratumoral distribution of temperature-sensitive liposomal doxorubicin

Abstract

The aim of this study was to investigate the intratumoral distribution of a temperature-sensitive liposomal carrier and its encapsulated compounds, doxorubicin and [Gd(HPDO3A)(H₂O)], after High Intensity Focused Ultrasound (HIFU)-mediated hyperthermia induced local drug release. The presence of the ¹¹¹In labeled liposomal carriers and the intratumoral distribution of doxorubicin were imaged *ex vivo* with autoradiography and fluorescence microscopy, respectively, for two different time points after injection (90 min and 48h). In hyperthermia treated tumors, radiolabeled liposomes were distributed more homogeneously across the tumor than in the control tumors. At 48h after injection, the liposomal accumulation in the tumor was enhanced in the hyperthermia group in comparison with the controls. Fluorescence images showed perivascular doxorubicin in control tumors while in the HIFU-treated tumors the delivered drug was spread over a much larger area and also taken up by tumor cells at a larger distance from blood vessels. HIFU hyperthermia treatment improved not only the immediate drug delivery, bioavailability and intratumoral distribution, it also enhanced liposomal accumulation over time. The sum of these effects may have a significant contribution to the therapeutic outcome.

This work has been published in:

M. de Smet, N.M. Hijnen, S. Langereis, A. Elevelt, E. Heijman, L. Dubois, P. Lambin and H. Gröll. *MR-HIFU mediated hyperthermia improves the intratumoral distribution of temperature-sensitive liposomal doxorubicin.* Investigative Radiology, 2013

6.1 Introduction

Treatment of solid tumors with chemotherapeutic drugs is often limited by poor drug penetration into the tumorous tissue.¹⁻⁴ Drug penetration is for example hindered by poor perfusion of the respective tissue, or barriers like fibrotic tissue. Therefore, mainly cells close to blood vessels receive adequate drug concentrations while tumor cells farther away remain at sub-therapeutic levels. Especially for larger-sized polymeric drug formulations or drug formulations based on nanoparticles such as Caelyx[®], with particle diameters around 100 nm, tumor penetration remains a challenge. Tumor hyperthermia is known to increase blood perfusion and its positive effect on drug extravasation from the vascular compartment into the interstitial space was explored earlier.⁵⁻⁶ However, it may take a considerable time span before drugs encapsulated within nanocarriers become bioavailable by passive release from its carrier. To address this problem, the strategy of hyperthermia triggered release from temperature-sensitive drug carriers was developed.⁷⁻⁸ Previous studies have demonstrated that hyperthermia-mediated drug delivery from TSLs resulted in increased drug concentrations in the tumor compared to levels achieved with systemic drug administration or non-temperature sensitive liposomal drug formulations.⁹⁻¹⁴ Recently, Staruch *et al.* demonstrated that the delivery of doxorubicin from TSLs induced by MR-HIFU results in enhanced intracellular uptake of bioavailable drug in heated tumors.¹⁵ Similar results were obtained by Ranjan *et al.*, showing an increased doxorubicin uptake in the tumor periphery as well as in the tumor core, suggesting an improved intra-tumoral distribution of the drug.¹¹ After the application of hyperthermia for 30 minutes, more than 60% of the injected dox-loaded TSLs was still present in the blood circulation. Their contribution to the overall drug uptake in the tumor over longer times remains unclear, as the effects of HIFU-mediated hyperthermia might show a considerable reminiscence leading to an additional uptake of drug-filled liposomes via the enhanced permeability and retention effect.

In this Chapter, we used ¹¹¹In-labeled temperature-sensitive liposomes encapsulating doxorubicin and [Gd(HPDO3A)(H₂O)] for hyperthermia triggered drug delivery under MR image guidance (see Chapter 4, Figure 4.1). The effect of local MR-HIFU mediated hyperthermia on the intratumoral distribution of the drug and the liposomal carrier was studied at 90 minutes and 48 hours after intravenous injection. At 90 minutes, a significant fraction of the TSLs is still circulating in the blood and, consequently, the effect of heat triggered release is measured against passive extravasation of drug-filled liposomes. After 48 hours, the combined effect of heat triggered release, possible hyperthermia reminiscence, and passive extravasation is obtained.

6.2 Materials and methods

6.2.1 Materials

1,2-Dipalmitoyl-*sn*-glycero-3-phosphocholine (DPPC) and hydrogenated-*L*- α -phosphatidylcholine (HSPC) were kindly provided by Lipoid (Germany). 1,2-Dipalmitoyl-*sn*-glycero-3-phosphoethanolamine-*N*-[methoxy(polyethyleneglycol)-2000] (DPPE-PEG2000) and cholesterol were purchased from Avanti Polar Lipids (USA). DOTA-DSPE was synthesized according to the procedure described by Hak *et al.*¹⁶ Doxorubicin hydrochloride was purchased from AvaChem Scientific (USA). [Gd(HPDO3A)(H₂O)] (ProHance®) was obtained from Bracco Diagnostics (Italy).

6.2.2. Preparation, characterization and radiolabeling of temperature-sensitive liposomes

Temperature-sensitive liposomes composed of DPPC:HSPC:Chol:DPPE-PEG2000:DOTA-DSPE (50:25:15:3:1 molar ratio) encapsulating doxorubicin and [Gd(HPDO3A)(H₂O)] were prepared, characterized and radiolabeled with ¹¹¹In in a similar fashion as described in Chapter 3.

6.2.3 Animal model

Syngeneic R1 rhabdomyosarcoma tumors were established on the hind leg of female Wag/Rij rats (n = 12) (Charles River, age 5-7 weeks) by subcutaneous implantation under anesthesia with pieces of donor tumor tissue (~1 mm³).¹⁷ This tumor model was compared with the previously used 9L tumor model by histology and DCE-MRI. The uptake kinetics of Gd-DTPA (0.2 mmol/kg bw) was analyzed on a voxel-by-voxel basis using the 2-parameter Tofts and Kermode model.¹⁸ The model was fitted to the measured voxel concentration-time curves and used for the calculation of quantitative parametric maps of the transfer constant k_{trans} (min⁻¹), the rate constant k_{ep} (min⁻¹) and the volume of extra-vascular extracellular space (EES) per unit volume of tissue v_e (unitless) using an IDL-based software tool (IDL 6.3, ITT Visual Information Solutions, Boulder, CO).

Tumor sizes were determined by measuring the length (l), width (w) and depth (d) using a caliper and the tumor volume was calculated by $0.5 \times l \times w \times d$. Animal studies were performed with tumor volumes between 300 – 1000 mm³, typically 14-20 days after tumor implantation.

6.2.4 MR-HIFU protocol

Local hyperthermia of the tumor was performed by MR-HIFU heating in a similar manner as described in Chapter 4. Maps of the longitudinal relaxation time (T_1) were acquired before and after the first 15 minutes of the hyperthermia treatment, using a single slice Look-Locker sequence¹⁹ (FA = 10°; TR/TE=9.0/3.4 ms; interval time = 100 ms; time of inversion repetition = 6 s; EPI-factor = 5; field of view = 50 × 69 mm²; matrix = 64 × 65; half scan =

80%; slice thickness = 2 mm; number of averages = 2; fat suppression = SPIR; acquisition time = 2 min, 36 s). The effective T_1 (T_1^*) was calculated from the signal recovery on a voxel-by-voxel basis using an in-house created IDL-based software tool (IDL version 6.3, RSI, Colorado, USA). Further data processing was performed in MATLAB (R2010a, MathWorks, Massachusetts, USA), in which the longitudinal relaxation rate R_1 was calculated from the effective R_1^* ($R_1^* = 1/T_1^*$, $R_1 = R_1^* + \ln(\cos(\alpha))/TR$, with $\alpha = 10^\circ$ and $TR = 100$ ms)²⁰ on a voxel-by-voxel basis.

Once the HIFU treatment was planned and co-registered, ^{111}In -labeled TSLs (20 ± 5 MBq ^{111}In , 0.50 ± 0.03 mL) were injected via a tail vein catheter at a dose of 5 mg/kg doxorubicin. Immediately after the injection, the HIFU-induced hyperthermia treatment was started. In the control group, animals received the same handling as the HIFU treated animals, except for the actual heating. Rats were sacrificed 90 min or 48 h after TSL injection. The treatment protocol is shown schematically in Figure 6.1.

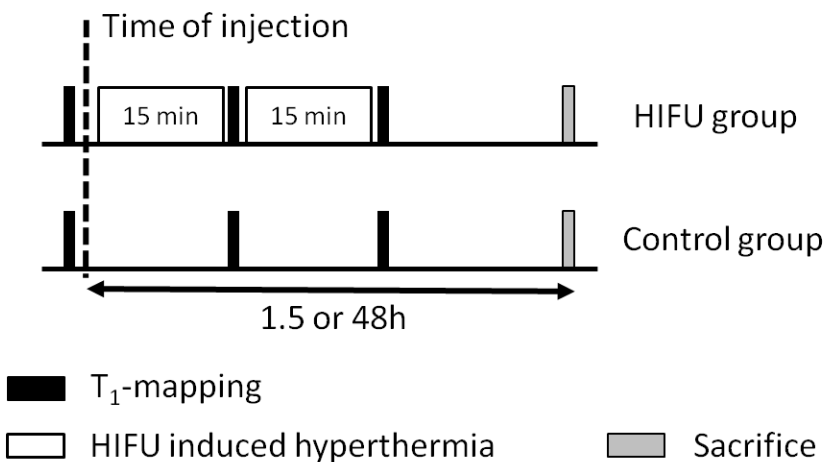


Figure 6.1. Timelines for the MR-HIFU group and the control experiment (without MR-HIFU). Animals were sacrificed either at 1.5 or 48 h after the administration of the TSLs.

6.2.5 Autoradiography

The activity in the entire, dissected tumor was measured using a dose calibrator (VDC-405, Veenstra Instruments). Subsequently, tumor slices of 2 mm thickness were cut from the middle of the tumor using a stainless steel tissue matrix (Ted Pella Inc.). Tissue dye was used to mark the tumor, in order to select the slice corresponding to the middle of the HIFU treatment cell. After weighing, the slices were exposed to a photostimulable phosphor plate for a time varying from 4 hours to 2 days, depending on the amount of radioactivity in the

tumor slice. The exposed plates were scanned using a phosphor imager (FLA-7000, Fujifilm). To quantify the homogeneity of the TSL distribution, the coefficient of variation (CV) was calculated of the histogram of pixel intensities from the autoradiographic images. Therefore, regions of interest were manually drawn around the tumor sections (ImageJ, NIH, Bethesda, MD). The CV's between the hyperthermia and control groups were compared statistically using a two-sided t-test (Statgraphics Centurion, version 16.0.05). Subsequently, the radioactivity of the tumor slices was quantified using γ -counting (WizardTM 3", Perkin Elmer). Known volumes of the injected TSLs were counted to serve as a reference. The decay corrected radioactivity in the slices was expressed as a percentage of the injected dose per gram tissue (%ID/g).

6.2.6 Histology

The tumor parts that were not used for autoradiography were snap frozen in 2-methyl butane and stored at -20 °C prior to histological analysis. The frozen tissue was cut into 6 μ m slices. Fluorescence images of the doxorubicin distribution were acquired with a fluorescence microscope (Leica, DM6000B, DFC310FX camera) equipped with a custom-made doxorubicin filter set (excitation: 480/40 nm, emission: 600/60 nm, dichroic: 505lp). Subsequently, the tissue slides were stained with CD31 and DAPI to mark respectively endothelial cells and cell nuclei. After fixation with ice-cold acetone (5 minutes at -20 °C), the slides were air-dried and washed in PBS. A blocking step was performed with 20% goat serum in PBS containing 1% BSA for 15 minutes to minimize non-specific staining. Primary incubation of mouse monoclonal anti-rat CD31 antibody (BD Pharmingen) was performed at a dilution of 1:50 in PBS containing 1% BSA for 2h at room temperature. Secondary incubation was performed using anti-mouse IgG-FITC antibody (F5387, Sigma) (1:100 in PBS containing 1% BSA and 5% goat serum) for 1h at room temperature. Finally, the sections were incubated with DAPI (Invitrogen, Molecular Probes) for 10 minutes at room temperature and mounted (Fluoromount F4680, Sigma). Between every step the sections were washed with PBS. Sections were examined with fluorescence microscopy (filters L5 [FITC] and R/G/B [DAPI]) and the different color channels were merged (ImageJ, <http://rsbweb.nih.gov>). For anatomical analysis, tissue slides were air dried briefly at room temperature and stained with Hematoxylin and Eosin (H&E). Cell viability was analyzed after nicotinamide adenine dinucleotide (NADH) diaphorase staining. For the latter, tissue slides were incubated at 37 °C for 1h in a Gomori-Tris-HCl buffer (pH 7.4, 10 mL) containing β -NAD reduced disodium salt hydrate (N8129, Sigma-Aldrich, St Louis, MO, 10 mg) and nitro blue tetrazolium (N5514, Sigma-Aldrich, 10 mg). Specimens were then washed and mounted for analysis with bright field microscopy.

6.3 Results

6.3.1 Radiolabeled temperature-sensitive liposomes

DOTA-functionalized TSLs encapsulating doxorubicin and $[\text{Gd}(\text{HPDO3A})(\text{H}_2\text{O})]$ with an average hydrodynamic diameter of 121.8 nm (polydispersity index < 0.1) have been prepared. The melting phase transition temperature (T_m), defined as the onset of the phase transition peak in the DSC thermogram, was $42.4 \pm 0.1^\circ\text{C}$. The phosphorus, gadolinium and doxorubicin concentrations of the TSL solution were 64.9 ± 1.8 mM, 15.6 ± 0.8 mM and 3.3 ± 0.1 mM, respectively. The incorporation of 1 mol% DOTA-DSPE in the phospholipid bilayer did not affect the stability of the liposomes at 37°C , nor the doxorubicin release at 42°C . Before injection, the DOTA-TSLs were labeled with ^{111}In (41 ± 10 MBq/mL), resulting in ^{111}In -labeled TSLs with a radiolabeling yield of $>95\%$.

6.3.2 Tumor characterization

The subcutaneously implanted rhabdomyosarcoma tumor model was compared with the previously used 9L tumors, obtained by s.c. cell injection, by means of histology and DCE-MRI. Histology shows well-structured blood vessels in the rhabdomyosarcoma, while the 9L tumor shows regions with very large and disorganized blood vessels (Figure 6.2). DCE-MRI shows different permeability properties for the two tumors, with $k_{\text{trans}} = 0.05 \text{ min}^{-1}$, $k_{\text{ep}} = 0.26 \text{ min}^{-1}$ and $v_e = 0.21$ for the rhabdomyosarcoma and $k_{\text{trans}} = 0.25 \text{ min}^{-1}$, $k_{\text{ep}} = 0.37 \text{ min}^{-1}$ and $v_e = 0.66$ for the 9L tumor (Figure 6.3).

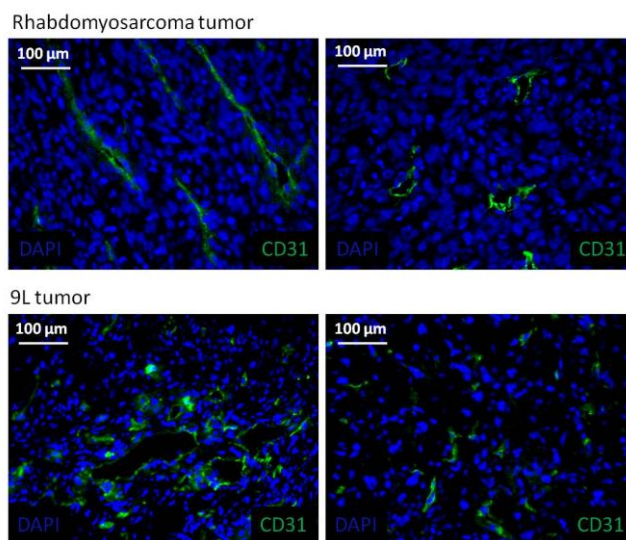


Figure 6.2. Cryosections of rhabdomyosarcoma tumor (above) and 9L tumor (below) stained with DAPI (cell nuclei) and CD31 (endothelial cells).

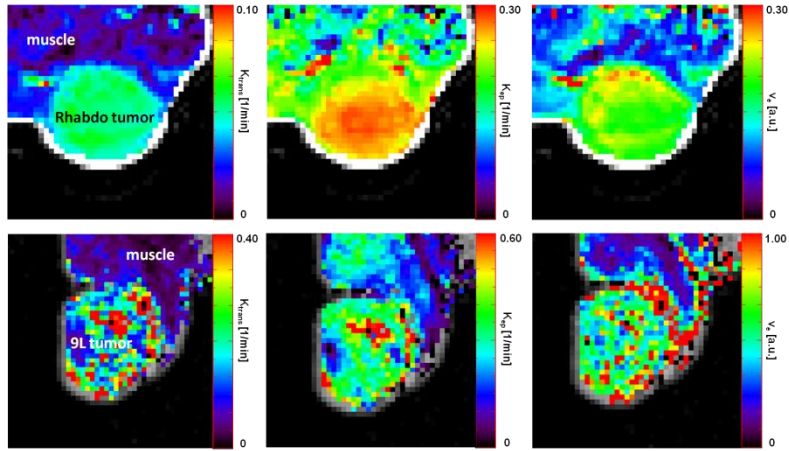


Figure 6.3. DCE-MRI results from Rhabdomyosarcoma tumor (above) and 9L tumor (below).

6.3.3 MR-HIFU treatment

HIFU-mediated hyperthermia of the tumor was applied immediately after the administration of TSLs. The therapy planning and the temperature maps of the MR-HIFU treatment over time are shown in Figure 6.4. Although the HIFU treatment cell volume of approximately 85 mm^3 was smaller than the tumor volume of approximately 500 mm^3 , mild hyperthermia of the majority of the tumor volume was achieved two minutes after the onset of HIFU-sonication due to heat diffusion (Figure 6.4). Furthermore, gradual warming of the muscle surrounding the tumor was observed over time, with some areas reaching similar temperatures as the center of the tumor. During the hyperthermia treatments (two times 15 minutes), the heating was monitored and controlled using a binary feedback control algorithm, obtaining an average temperature in the treatment cell of $41 \pm 2 \text{ }^\circ\text{C}$. Based on previous *in vitro* measurements, the temperature-sensitive liposomes are expected to show quantitative release of the encapsulated doxorubicin and $[\text{Gd}(\text{HPDO3A})(\text{H}_2\text{O})]$ within a few minutes at these temperatures.²¹

Maps of the longitudinal relaxation rate (R_1) were acquired before TSL injection and directly after the hyperthermia treatments in order to probe the release of the MRI contrast agent from the liposomal carrier (Figure 6.5). The combination of TSLs and HIFU-induced hyperthermia resulted in an increase in tumor R_1 ($\Delta R_{1,\text{tumor } 15\text{min}} = 0.15 \pm 0.10$, p-value = 0.022, two-sided paired t-test), while the R_1 values of the adjacent muscle remained constant ($\Delta R_{1,\text{muscle } 15\text{min}} = 0.02 \pm 0.07$, p-value = 0.628, two-sided paired t-test). The second hyperthermia treatment did not result in a further R_1 increase ($\Delta R_{1,\text{tumor } 30\text{min}} = 0.15 \pm 0.11$, p-value = 0.934, two-sided paired t-test). Control experiments in rats with TSLs without HIFU treatment showed similar R_1 changes in tumor as in surrounding muscle upon injection of

the TSLs, suggesting that the liposomal content was not actively released from the TSLs in the unheated tumors. At the end of the protocol (90 minutes or 48 hours after TSL injection), the rats were sacrificed. The tumors were dissected for further analysis using a dose calibrator, autoradiography, and histology.

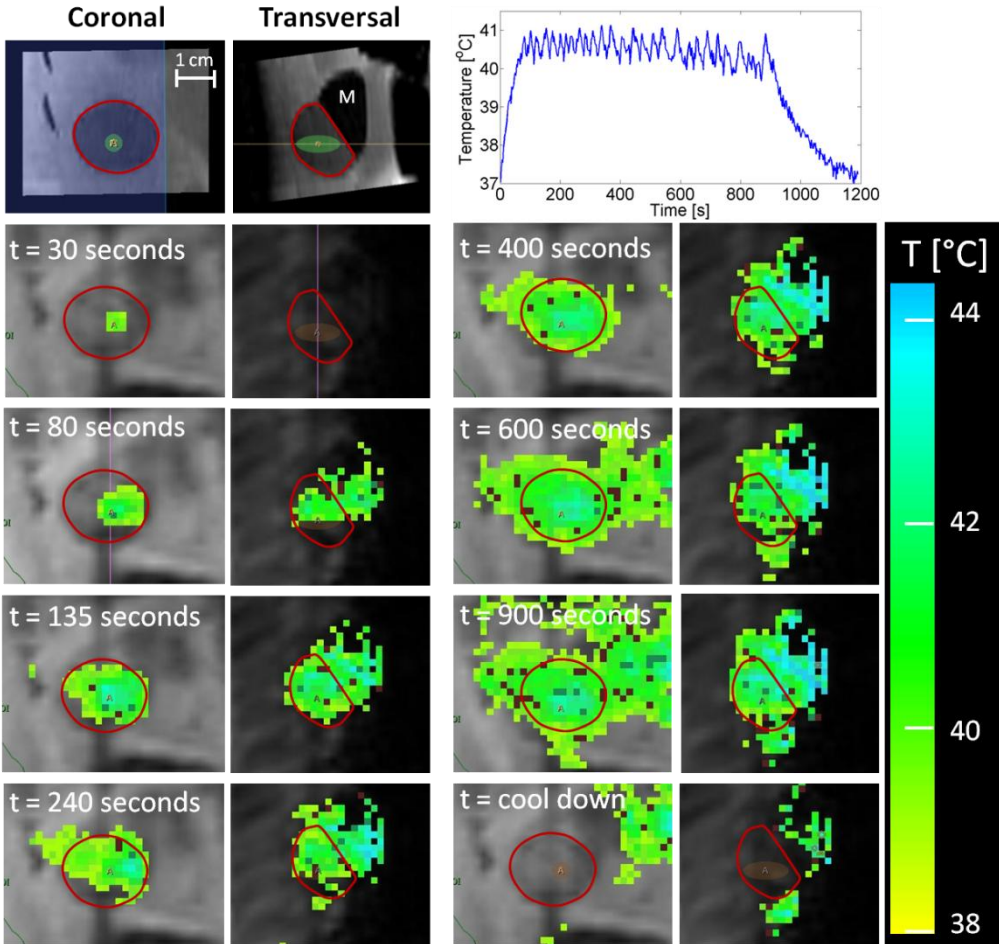


Figure 6.4. MR-HIFU therapy planning and temperature maps. On the top left, anatomical images are shown with an overlay of the planned treatment volume (green ellipsoid). The red contours indicate the tumor area. M indicates the leg muscle. Temperature maps are shown perpendicular to the ultrasound beam path (left images, coronal) and parallel to the beam path (right images, transversal) over time (t) during hyperthermia treatment. On the top right, the mean temperature of the treatment cell is plotted against time.

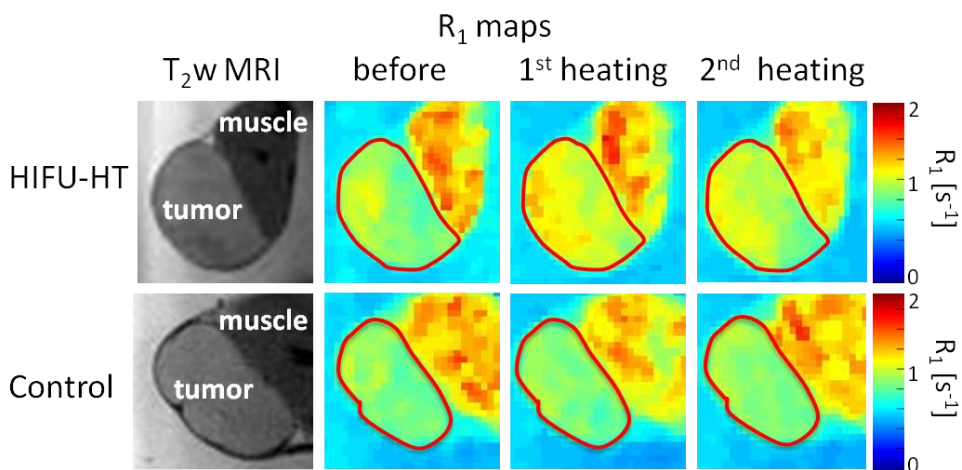


Figure 6.5. *T₂-weighted MR image and R₁ maps before TSL injection and after each heating period, with HIFU-mediated hyperthermia (upper row) and control (lower row). On the R₁ maps, the tumor is delineated with a red line.*

6.3.4 Autoradiography

The intratumoral distribution of the ¹¹¹In-labeled TSLs was investigated using autoradiography. Figures 6.6 and 6.7 show the autoradiography images of all investigated tumor slices, as well as the images scaled to the same %ID/g, of the 90 min and 48 h groups respectively. At 90 min post injection, the high TSL concentration in the blood (>50% of the injected dose²²) contributed to a large extent to the activity observed on autoradiography. In control tumors, most activity was present in major blood vessels, the tumor rim and the supporting tissue layer between skin and tumor (Figure 6.6). Table 6.1 shows the amount of radioactivity in the tumor slices as well as in the whole tumor. At 90 minutes after injection, the ¹¹¹In uptake was not increased due to hyperthermia treatment in comparison with the controls (t-test whole tumor_{90min} hyperthermia vs control: p-value = 0.684). However, the distribution of radioactivity over the tumor was different, as areas in the core of the heated tumors showed higher uptake (Figure 6.6). In the hyperthermia treated tumors the coefficient of variation (CV) of the activity distribution was significantly lower than for the control tumors (t-test, p-value = 0.002), suggesting a more homogeneous activity distribution over the tumors after HIFU hyperthermia treatment. This effect was maintained 48 hours after injection (t-test p-value = 0.037, Figure 6.7). After 48 hours, also an activity increase was observed in the hyperthermia group (Table 6.1), suggesting enhanced liposome accumulation and extravasation after the heating has finished.

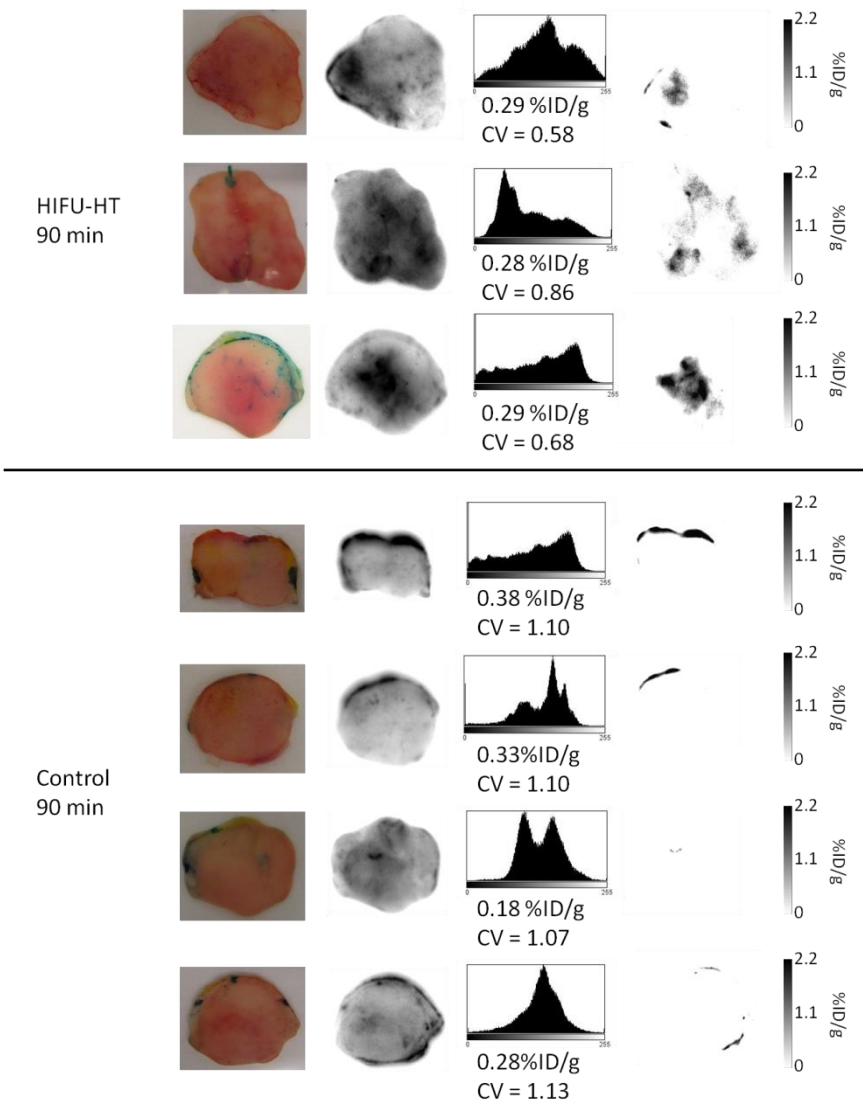


Figure 6.6. Each row shows the result of one tumor slice of HIFU-treated and control tumors 90 minutes after TSL injection. From left to right: picture, non-scaled autoradiographic image, histogram of non-scaled autoradiographic image, and autoradiographic image scaled to the total %ID/g activity uptake in the slice.

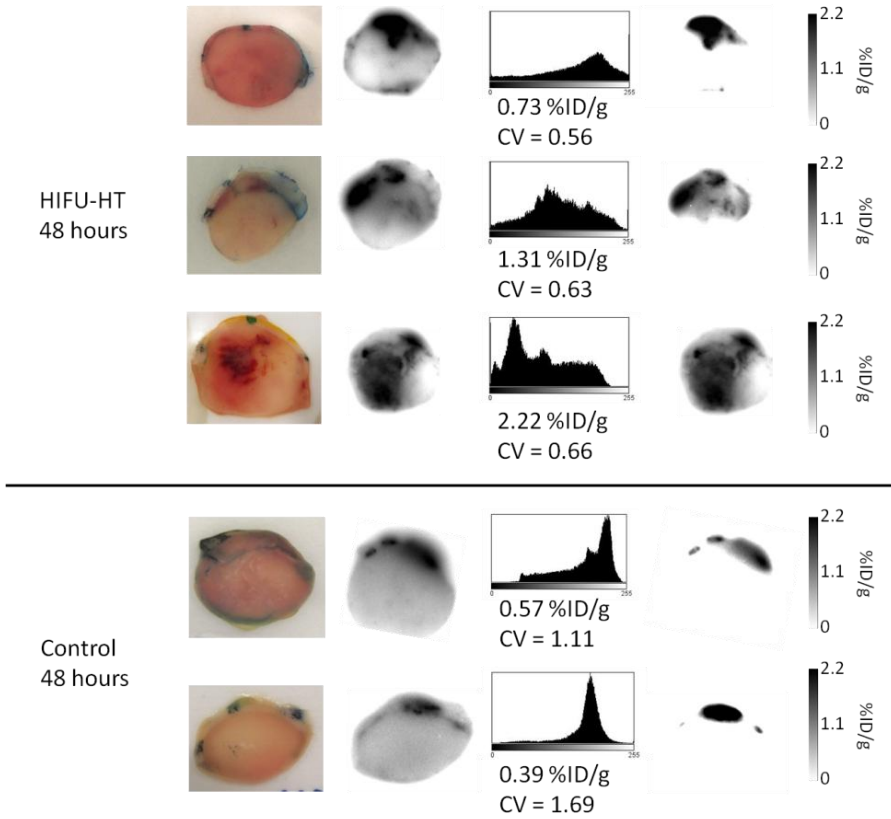


Figure 6.7. Each row shows the result of one tumor slice of HIFU-treated and control tumors 48 hours after TSL injection. From left to right: picture, non-scaled autoradiographic image, histogram of non-scaled autoradiographic image, and autoradiographic image scaled to the total %ID/g activity uptake in the slice.

Table 6.1. Coefficient of variation and the amount of ^{111}In in the tumor slice and the amount of ^{111}In in the whole tumor for the four groups.

Group	Coefficient of variation	^{111}In in tumor slice (%ID/g)	^{111}In in whole tumor (%ID/g)
HIFU-HT 90 min	0.7 ± 0.2	0.29 ± 0.01	0.55 ± 0.31
Control 90 min	1.1 ± 0.2	0.29 ± 0.08	0.64 ± 0.24
HIFU-HT 48h	0.6 ± 0.1	1.42 ± 0.75	4.21 ± 1.41
Control 48h	1.4 ± 0.4	0.48 ± 0.13	1.99 (n=1)

6.3.5 Histology

The intratumoral distribution of doxorubicin was examined by fluorescence microscopy. In control tumors ($t = 90$ min), doxorubicin uptake was only visible in the endothelial cells. For the HIFU-treated tumors, the delivered drug was spread over a larger area (Figure 6.8). Furthermore, the doxorubicin was co-localized with tumor cell nuclei indicating cellular uptake even at relatively large distances ($\approx 50 \mu\text{m}$) from blood vessels. On DAPI (cell nuclei), CD31 (endothelial cell) and H&E staining, the hyperthermia treated tumor appeared similar as control tumor tissue; showing a tight packing of cell nuclei and a large amount of well-structured blood vessels distributed over the entire tumor. NADH-diaphorase staining for cell viability showed viable tumor tissue 90 minutes after TSL injection in both the HIFU treated and control group, indicating that there was no instant effect of the therapy on the cell viability.

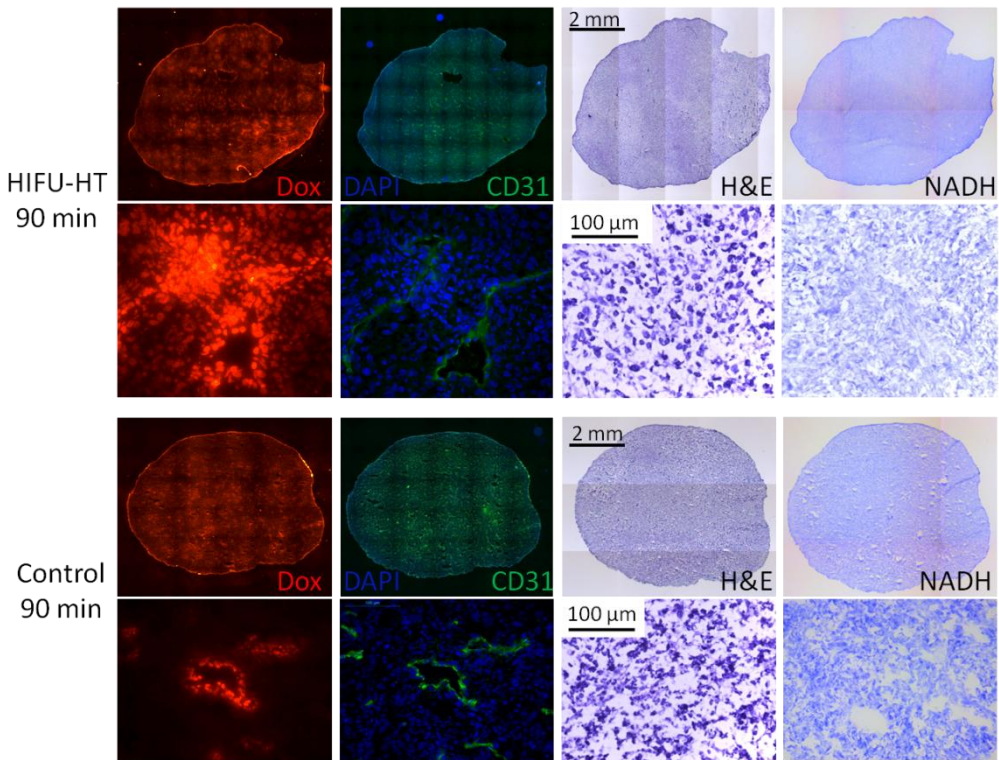


Figure 6.8. Histology of HIFU-mediated hyperthermia treated and control tumor tissue 90 minutes after TSL injection. Of each staining an overview image of the whole tumor slice as well as a 40x zoom is shown. Shutter times for doxorubicin were 3s (overview) and 1s (40x zoom). On NADH-diaphorase staining, viable cells appear blue whereas non-viable cells would remain colorless.

After 48h, cellular uptake of doxorubicin was observed in the control tumors, however, to a smaller extent compared to the hyperthermia treated ones (Figure 6.9). In the hyperthermia group, areas that showed a high liposome accumulation on autoradiography also showed high fluorescence on the fluorescence microscopy (Figure 6.10). Interestingly, these areas were congruent with the areas that showed no cell viability on NADH-diaphorase staining. Although a contribution of autofluorescence of necrotic tissue to the signal cannot be fully excluded, the high fluorescent signal observed in this area most likely results from a high doxorubicin uptake. Outside the high intensity area, the doxorubicin signal was comparable to that in control tumors and viable according to the NADH-diaphorase staining.

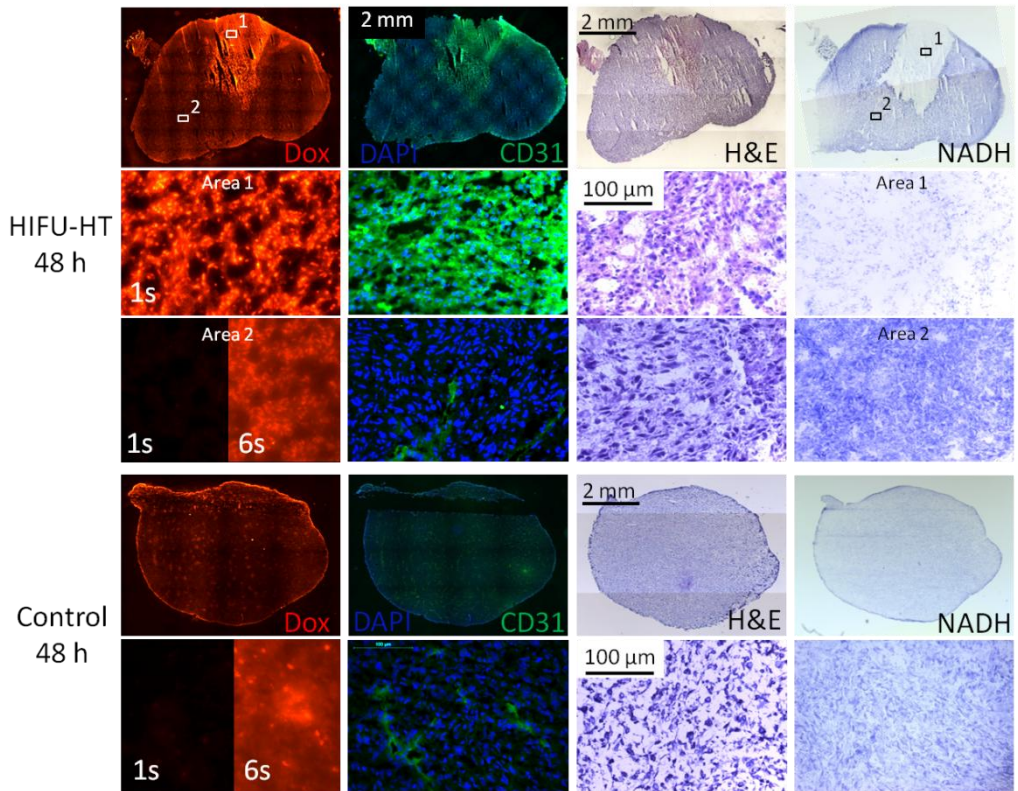


Figure 6.9. Histology of HIFU-mediated hyperthermia treated and control tumor tissue 48 hours after TSL injection. Shutter times for doxorubicin were 3s (overview) and 1s (40x zoom). For the control tumor and Area 2 of the hyperthermia treated tumor, the doxorubicin signal intensity was very low. Therefore, images were acquired both with the standard shutter time of 1s as well as with a longer shutter time of 6s (indicated in the images). The small boxes indicate where the enlarged images were taken (Area 1 and 2). Area 1 shows high signal in the dox channel, as well as in the FITC channel.

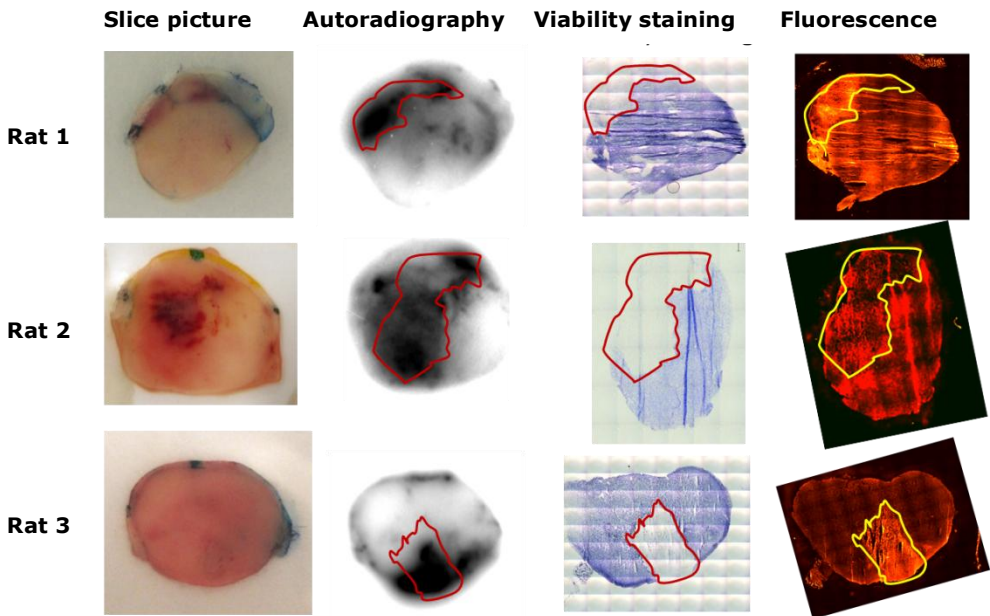


Figure 6.10. Pictures, autoradiography, viability NADH-staining, and fluorescence signal intensity in the dox-channel of all tumors dissected 48 hours after hyperthermia treatment. The red contour indicates the necrotic area as determined based on the NADH-staining, which is overlaid on the autoradiographic image and on the fluorescence image taken from the same histology slice.

6.4 Discussion

In this Chapter, the effect of HIFU-mediated hyperthermia on the intratumoral distribution of temperature-sensitive liposomes, as well as for the released doxorubicin and MRI contrast agent, has been investigated at different time points after injection. The localization of the TSLs and the cellular uptake of doxorubicin were studied using autoradiography and fluorescent microscopy, respectively. Moreover, the *in situ* release of doxorubicin from the TSLs was probed with MRI by measuring the change in relaxation times induced by the co-release of [Gd(HPDO3A)(H₂O)].

Radiographic images of the control tumors showed highest radioactivity along the rim of the tumor, which is usually well-perfused or surrounded by large blood vessels. For the MR-HIFU treated tumors, elevated radioactivity was not restricted to the tumor rim, but more spread over the entire tumor. In our previous work, we found more than 50% of ¹¹¹In-TSLs still being present in the blood circulation after 90 min.²² Therefore, it is hard to distinguish between tumor uptake of TSLs and liposomes circulating in the blood at this time point. However, as the high radioactivity in non-heated tumors coincides with the vascularized tumor rim, TSLs present in the blood circulation are the most likely explanation

for this observation. Although there was no increase in the absolute amount of radioactivity present in the HIFU-treated tumors after 90 min compared to control, the activity was distributed differently over the tumor tissue. This suggests a rebalance of perfusion between the tumor periphery and core due to the increased perfusion of the heated tumor areas. The radioactivity was measured in a single slice taken from the tumor center, as well as in the whole tumor volume. Taking into account that more than 50% of the radiolabeled TSLs are still present in the blood circulation after 90 min, the absolute amount of radioactivity is heavily affected by the blood volume distribution in the selected tumor slice. The blood distribution, as well as tumor heterogeneity in general, also explains the difference in absolute activities found in the whole tumors as compared to tumor slices. On the other hand, with less than 5% of ^{111}In -TSLs present in the blood after 48h, the autoradiography images at this time point reflect radiolabeled liposomes accumulated in the tumor. The heated and control tumors after 48h showed an increased %ID/g of TSL in comparison with the autoradiographic images at 90 min. The ^{111}In -TSL accumulation in the MR-HIFU treated tumors was higher in comparison with non-heated tumors, which was not yet observed after 90 min. These results suggest that HIFU-based hyperthermia has caused long lasting effects, which enhanced liposomal uptake over a much longer time period compared to the hyperthermia treatment itself. These findings are consistent with earlier experiments published by Kong *et al.* showing that hyperthermia increases the extravasation of liposomes due to a further enhanced permeability and retention effect in tumors.⁹ These effects of hyperthermia on extravasation extended to several hours after administration. As a consequence, doxorubicin levels in the tumor may further increase beyond the amount observed directly after intravascular release triggered by hyperthermia due to further but slow accumulation of drug-filled temperature-sensitive liposomes that are still circulating. These results are of general importance to applications in liposomal drug delivery, because both temperature-sensitive and commercially available non-temperature sensitive liposomal drugs (e.g. Doxil[®], Caelyx[®]) will benefit from the increased extravasation due to HIFU-mediated hyperthermia.

The intratumoral distribution of doxorubicin for the different time points and groups was studied using fluorescence microscopy. At 90 min after injection, doxorubicin uptake in HIFU-treated tumors was observed in cells at a much larger distance from blood vessels in comparison to the control tumors where doxorubicin uptake was visible only in the vicinity of blood vessels. Recently, Manzoor *et al.* showed similar results after electric heating in a window-chamber model; they observed an increase in drug penetration distance after intravascular release from TSLs.²³ Two days after TSL injection, the doxorubicin was spread throughout the tumor for both the control and HIFU-treated group. Also this observation corresponds with findings from previous studies with non-temperature sensitive liposomes, where the drug initially appeared to be restricted to the perivascular space, most likely still

encapsulated inside the liposome, but spread throughout the tumor 24-48h later.²⁴⁻²⁵ The limited bioavailability of the drug at early time points due to slow release from these non-temperature sensitive liposomes, and subsequent diffusion driven distribution across the tumor may be the underlying reason for the observed sub-optimal anti-tumor efficacy in the clinic.²⁶⁻²⁸ In our study, the fluorescence intensity was much higher for the HIFU treated tumors as opposed to controls, suggesting an increased amount of drug uptake by the heated tumors. Furthermore, doxorubicin becomes directly bioavailable to tumor cells after the temperature-triggered release from the TSLs.

In Chapter 4, we have shown that mild hyperthermia of paramagnetic TSLs containing doxorubicin and [Gd(HPDO3A)(H₂O)] leads to a simultaneous release of the encapsulated molecules. The change in R_I was found to be proportional to the amount of drug delivered in 9L gliosarcoma tumors in rats (Chapter 5).²² In this study, an increase in the R_I was observed immediately after HIFU treatment in a rat rhabdomyosarcoma tumor model, while no distinct effect was visible in the control tumor. No further increase in R_I was measured after the second time of hyperthermia treatment, indicating that equilibrium was reached between washout and release of the MRI contrast agent. Overall, the observed ΔR_I due to [Gd(HPDO3A)(H₂O)] release from TSLs during HIFU treatment in the rhabdomyosarcoma tumor model was smaller than the effect observed previously in 9L gliosarcoma tumors²². Histological examination of both tumor models showed better structured and more homogeneously formed blood vessels in the rhabdomyosarcoma model in comparison to the 9L tumor (Figure 6.2). As expected, the different blood vessel structures also resulted in differences in vessel permeability as measured by Dynamic Contrast Enhanced (DCE) MRI, showing $k_{trans} = 0.05 \text{ min}^{-1}$, $k_{ep} = 0.26 \text{ min}^{-1}$ and $v_e = 0.21$ for the rhabdomyosarcoma tumor and $k_{trans} = 0.25 \text{ min}^{-1}$, $k_{ep} = 0.37 \text{ min}^{-1}$, $v_e = 0.66$ for the 9L tumor (Figure 6.3). It is important to note that the pharmacokinetic properties of the encapsulated agents prior to release from the lumen of the TSLs are determined by the liposomal carrier. Upon release, however, the doxorubicin and [Gd(HPDO3A)(H₂O)] will show different biodistribution profiles and tumor uptake. The high permeability of doxorubicin across different barriers will result in a rapid distribution in the interstitial space and cellular uptake across the tumor upon its local release.^{10, 23, 29-30} On the other hand, [Gd(HPDO3A)(H₂O)] will distribute across the extracellular space³¹ and its intratumoral concentration is a balance between tumor inflow and wash out. Therefore, the smaller ΔR_I change observed in the rhabdomyosarcoma model can most likely be explained with the considerably lower k_{trans} and v_e in this tumor compared to the 9L tumor. Quantitative measurements of the doxorubicin and gadolinium concentrations and a comparison with ΔR_I were not performed in this study as the tumors were used for histology and autoradiography exams.

As discussed before, mild hyperthermia can be used to improve liposomal chemotherapy in two ways. First, hyperthermia leads to an increase of vascular permeability and therefore increasing levels of liposome accumulation, and secondly, hyperthermia can be used for a triggered drug release from temperature-sensitive liposomes.³² In a recent review by Grüll *et al.*,³³ studies on MR-HIFU-induced delivery from temperature-sensitive liposomes have been summarized, reporting a heating-induced 2.3-4.9 fold enhancement in tumor doxorubicin concentrations at early time points. This enhancement effect was mainly due to the intravascular release of doxorubicin during heating. Any additional drug accumulation due to extravasation and uptake of long circulating TSLs and subsequent release of doxorubicin was so far not systematically investigated. Dromi *et al.* investigated doxorubicin uptake in tumors at 24h after TSL injection followed by pulsed-HIFU exposures.³⁴ They did not observe a difference between HIFU-exposed and untreated tumors, but this may be attributed to the relatively short exposure of 2 min per pulsed-HIFU raster point. Although quantitative measurements of doxorubicin concentrations were not performed in our study, it is quite likely that the measured increase in TSL uptake in heated tumors over two days will lead to a further increase in doxorubicin concentrations beyond the level found directly after hyperthermia treatment. In this study we observed that the HIFU-treated tumors showed necrotic areas at 48h after the treatment, corresponding to the areas where large amounts of radioactivity were detected. This observation suggested that the doxorubicin uptake in these areas exceeded the concentrations necessary for cell necrosis. Since no necrosis was detected at 90 min after the treatment, it can be assumed that the observed cell death in these tumors was a long term effect.

6.5 Conclusion

HIFU-induced hyperthermia was shown to increase drug release from temperature-sensitive liposomes during hyperthermia and to increase uptake of liposomal drug delivery carriers in the time period following the hyperthermia. In the hyperthermia group, intravascular release of doxorubicin led to a homogeneous drug coverage of large areas within the tumor. Additionally, liposome accumulation and penetration was increased due to the HIFU hyperthermia treatment. These accumulated liposomes will slowly release the drug throughout the tumor over a longer time period, resulting in even more bioavailable drug present at the tumor site. Both the intravascular release of doxorubicin and the increased accumulation of doxorubicin filled liposomes may have an important contribution to the therapeutic outcome.

References

1. Tunggall JK, Cowan DSM, Shaikh H, et al. Penetration of anticancer drugs through solid tissue: A factor that limits the effectiveness of chemotherapy for solid tumors. *Clinical Cancer Research*. 1999;5:1583-6.
2. Tannock IF, Lee CM, Tunggall JK, et al. Limited penetration of anticancer drugs through tumor tissue: A potential cause of resistance of solid tumors to chemotherapy. *Clinical Cancer Research*. 2002;8:878-84.
3. Minchinton AI, Tannock IF. Drug penetration in solid tumours. *Nature Reviews Cancer*. 2006;6:583-92.
4. Primeau AJ, Rendon A, Hedley D, et al. The distribution of the anticancer drug doxorubicin in relation to blood vessels in solid tumors. *Cancer Therapy: Preclinical*. 2005;11(24):8782-8.
5. Kong G, Braun RD, Dewhirst MW. Characterisation of the effect of hyperthermia on nanoparticle extravasation from tumor vasculature. *Cancer Research*. 2001;61:3027-32.
6. Kong G, Dewhirst MW. Hyperthermia and liposomes. *Int J Hyperthermia*. 1999;15(5):345-70.
7. Laginha KM, Verwoert S, Charrois GJR, et al. Determination of doxorubicin levels in whole tumor and tumor nuclei in murine breast cancer tumors. *Clinical Cancer Research*. 2005;11(19):6944-9.
8. Seynhaeve ALB, Hoving S, Schipper D, et al. Tumor necrosis factor alpha mediates homogeneous distribution of liposomes in murine melanoma that contributes to a better tumor response. *Cancer Research*. 2007;67(19):9455-62.
9. Kong G, Anyarambhatla G, Petros WP, et al. Efficacy of liposomes and hyperthermia in a human tumor xenograft model: importance of triggered drug release. *Cancer Res*. 2000;60:6950-7.
10. Needham D, Anyarambhatla G, Kong G, et al. A new temperature-sensitive liposome for use with mild hyperthermia: characterization and testing in a human tumor xenograft model. *Cancer Res*. 2000;60:1197-201.
11. Ranjan A, Jacobs GC, Woods DL, et al. Image-guided drug delivery with magnetic resonance guided high intensity focused ultrasound and temperature sensitive liposomes in a rabbit Vx2 tumor model. *Journal of Controlled Release*. 2012;158:487-94.
12. Aoki H, Kakinuma K, Morita K, et al. Therapeutic efficacy of targeting chemotherapy using local hyperthermia and thermosensitive liposome: evaluation of drug distribution in a rat glioma model. *Int J Hyperthermia*. 2004;20(6):595-605.
13. Dromi S, Frenkel V, Luk A, et al. Pulsed-High Intensity Focused Ultrasound and Low Temperature-Sensitive Liposomes for enhanced targeted drug delivery and antitumor effect. *Clin Cancer Res*. 2007;13(9):2722-7.
14. Gasselhuber A, Dreher MR, Rattay F, et al. Comparison of conventional chemotherapy, stealth liposomes and temperature-sensitive liposomes in a mathematical model. *PLoS One*. 2012;7(10):e47453.
15. Staruch RM, Ganguly M, Tannock IF, et al. Enhanced drug delivery in rabbit VX2 tumours using thermosensitive liposomes and MRI-controlled focused ultrasound hyperthermia. *Int J Hyperthermia*. 2012;28(8):776-87.
16. Hak S, Sanders HM, Agrawal P, et al. A high relaxivity Gd(III)DOTA-DSPE-based liposomal contrast agent for magnetic resonance imaging. *Eur J Pharm Biopharm*. 2009;72(2):397-404.
17. Dubois LJ, Lieuwes NG, Janssen MH, et al. Preclinical evaluation and validation of [¹⁸F]HX4, a promising hypoxia marker for PET imaging. *Proc Natl Acad Sci*. 2011;108(35):14620-5.
18. Tofts PS, Kermode AG. Measurement of the blood-brain barrier permeability and leakage space using dynamic MR imaging. 1. Fundamental concepts. *Magn Reson Med*. 1991;17(2):357-67.

19. Look DC, Locker DR. Time saving in measurement of NMR and EPR relaxation times. Review of Scientific Instruments. 1970;41(2):250-1.
20. Shin W, Gu H, Yang Y. Fast high-resolution T1 mapping using inversion-recovery Look-Locker echo-planar imaging at steady state: optimization for accuracy and reliability. Magnetic Resonance in Medicine. 2009;61:899-906.
21. de Smet M, Langereis S, van den Bosch S, et al. Temperature-sensitive liposomes for doxorubicin delivery under MRI guidance. Journal of Controlled Release. 2010;143(1):120-7.
22. de Smet M, Heijman E, Langereis S, et al. Magnetic resonance imaging of high intensity focused ultrasound mediated drug delivery from temperature-sensitive liposomes: An in vivo proof-of-concept study. Journal of Controlled Release. 2011;150(1):102-10.
23. Manzoor AA, Lindner LH, Landon CD, et al. Overcoming Limitations in Nanoparticle Drug Delivery: Triggered, Intravascular Release to Improve Drug Penetration into Tumors. Cancer Res. 2012;72(21):5566-75.
24. Forssen EA, Malé-Brune R, Adler-Moore JP, et al. Fluorescence imaging studies for the disposition of daunorubicin liposomes (DaunoXome) within tumor tissue. Cancer Research. 1996;56:2066-75.
25. Uster PS, Working PK, Vaage J. Pegylated liposomal doxorubicin (Doxil (R), Caelyx (R)), distribution in tumour models observed with confocal laser scanning microscopy. International Journal of Pharmaceutics. 1998;162:77-86.
26. Judson I, Radford JA, Harris M, et al. Randomised phase II trial of pegylated liposomal doxorubicin (DOXIL^(R)/CAELYX^(R)) versus doxorubicin in the treatment of advanced or metastatic soft tissue sarcoma: a study by the EORTC Soft Tissue and Bone Sarcoma Group. Eur J Cancer. 2001;37:870-7.
27. Harris L, Batist G, Belt R, et al. Liposome-encapsulated doxorubicin compared with conventional doxorubicin in a randomized multicenter trial as first-line therapy of metastatic breast carcinoma. Cancer. 2002;94(1):25-36.
28. O'Brien MER, Wigler N, Inbar M, et al. Reduced cardiotoxicity and comparable efficacy in a phase III trial of pegylated liposomal doxorubicin HCl (CAELYXTM/Doxil^(R)) versus conventional doxorubicin for first-line treatment of metastatic breast cancer. Ann Oncol. 2004;15:440-9.
29. Working PK, Newman MS, Huang SK, et al. Pharmacokinetics, biodistribution and therapeutic efficacy of doxorubicin encapsulated in stealth[®] liposomes (Doxil[®]). J Liposome Res. 1994;4(1):667-87.
30. Harashima H, Iida S, Urakami Y, et al. Optimization of antitumor effect of liposomally encapsulated doxorubicin based on simulations by pharmacokinetic/ pharmacodynamic modeling. Journal of Controlled Release. 1999;61:93-106.
31. Eakins MN, Eaton SM, Fisco RA, et al. Physicochemical properties, pharmacokinetics and biodistribution of Gadoteridol injection in rats and dogs. Acad Radiol. 1995;2:584-91.
32. Koning GA, Eggermont AM, Lindner LH, et al. Hyperthermia and thermosensitive liposomes for improved delivery of chemotherapeutic drugs to solid tumors. Pharm Res. 2010;27(8):1750-4.
33. Grull H, Langereis S. Hyperthermia-triggered drug delivery from temperature-sensitive liposomes using MRI-guided high intensity focused ultrasound. J Control Release. 2012;161(2):317-27.
34. Dromi S, Frenkel V, Luk A, et al. Pulsed-high intensity focused ultrasound and low temperature-sensitive liposomes for enhanced targeted drug delivery and antitumor effect. Clin Cancer Res. 2007;13(9):2722-7.

Chapter 7

Therapeutic effect of MR-HIFU mediated local drug delivery using temperature-sensitive liposomes

Abstract

The therapeutic effect of HIFU-hyperthermia mediated local drug delivery from temperature-sensitive liposomes was investigated by measuring the tumor growth over time after the treatment. For comparison, doxorubicin and the clinically available non-temperature sensitive doxorubicin liposomes, Caelyx®, were used. Saline injection was used as a control. The tumor growth of the four different groups (TSL, Caelyx®, doxorubicin and saline) were all tested in combination with and without HIFU-hyperthermia treatment. TSL+HIFU showed a 2 to 4-fold increase in the time to reach two times the initial tumor size in comparison with the other groups. Furthermore, a correlation was found between the MRI contrast change (ΔR_1) and the relative tumor size after 7 days, showing that the MR measurements can be used as a prediction for the therapeutic effect.

7.1 Introduction

Mild hyperthermia of tissues in the range of 40-43 °C causes a number of effects on tissue as well as on cellular level that acts synergistically with systemic chemotherapy and radiation therapy. On tissue level, hyperthermia increases blood flow, improves perfusion, enhances oxygenation and increases permeability of blood vessels.^{1, 2} On a cellular level, cells become more susceptible to chemotherapeutic drugs or radiation by heat-induced up or down-regulation of pathways, or inhibition of certain proteins, e.g. proteins responsible for radiation induced DNA repair.³⁻⁵ Many of these effects are enhanced for tumor tissue compared to normal tissue, which is exploited clinically in treatment schemes combining hyperthermia with chemo and radiotherapy.⁶⁻⁹ For example, Issels *et al.* showed in a randomized phase 3 multicentre study that regional hyperthermia enhanced the benefit of chemotherapy, consisting of etoposide, ifosfamide and doxorubicin (EIA), for patients with high-risk soft tissue sarcoma.⁹ For liposomal drugs, local heating of the tumor has additional advantages, such as increased permeability and extravasation from the microvasculature.¹⁰⁻¹³ In a clinical setting, Caelyx® was administered in combination with reirradiation and local hyperthermia treatment in patients with recurrent breast cancer. A significant correlation between the clinical response to Caelyx® and the temperatures reached during the hyperthermia treatments was observed.¹⁴ However, in the case of these non-temperature sensitive liposomes, the bioavailability of the drug was still limited due to the poor drug release from these nanoparticles. The triggered release of drugs from a temperature-sensitive liposomal formulation will enhance their bioavailability to tumor cells, which might even further improve the therapeutic response. Furthermore, the intravascular release of doxorubicin from TSLs during heating increases the amount of delivered drug and improves the intratumoral distribution.¹⁵⁻¹⁸

Many preclinical studies investigated the therapeutic effect of hyperthermia-mediated doxorubicin delivery with TSLs (see Table 1.2 in Chapter 1). One of the difficulties in comparing these different studies is the lack of uniform study setup, experimental conditions and read-out parameters. The majority of preclinical studies were performed with the LTSL formulation originating from Needham *et al.*¹⁹ An impressive therapeutic effect was obtained by Kong and Needham using LTSL in combination with waterbath heating for 1h at 42 °C in mice bearing a *s.c.* FaDu tumor on the hind leg. Complete regression was accomplished for 6 out of 9 treated tumors in the first study and for all the 11 treated tumors in the second study.^{20, 21} Dromi *et al.* used the same liposomal formulation, but performed 15-20 min hyperthermia with pulsed-HIFU.²² Tumors receiving LTSL and pulsed-HIFU exposures grew significantly slower than tumors in all control groups. However, no complete regression was observed with this protocol. Yarmolenko *et al.* tested the therapeutic effect of LTSL + heat in five different tumormodels.²³ SKOV-3 was the most sensitive tumor model; only 50% of the tumors reached 5x the initial volume within 60 days.

Recently, Tagami *et al.* found a larger therapeutic effect for their developed Brij-liposomes (50% cure) than for the LTSL systems (25% cure) in murine EMT-6 tumors.²⁴

In this thesis, we have used HIFU-mediated hyperthermia as a trigger for local drug delivery from temperature-sensitive liposomes. Promising results of this strategy were already shown in earlier Chapters. In Chapter 5, HIFU-mediated local delivery of doxorubicin using TSLs demonstrated an 11-fold increase of drug concentrations at 90 min after injection in 9L tumors. The long-term effect was investigated in Chapter 4, where a 4.4-fold increase in liposome accumulation and a 7.8-fold increase in doxorubicin concentrations was found at 48h after TSL injection, in comparison with the unheated control tumors. Additionally, the drug was spread over a much larger area and was also taken up by tumor cells at a larger distance from blood vessels in comparison with unheated tumors (Chapter 6).

The 9L tumor model used for the quantification experiments in Chapters 4 and 5, was obtained by subcutaneous tumor cell injection and appeared to be unsuitable for therapeutic studies due to variable tumor growth rates between different rats and occasional tumor shrinkage even without treatment. Therefore, a rhabdomyosarcoma tumor model was used for this study, which was obtained by subcutaneous implantation with syngeneic pieces of donor tumor tissue. Without treatment, this tumor model showed similar tumor growth curves for all rats and was therefore a suitable model for this therapeutic study. Unfortunately, the quantification experiments performed on 9L tumors cannot be directly compared to the therapeutic effects found in this study, however, similar effects of the hyperthermia treatment can be expected.

During HIFU treatment, MRI plays a crucial role in the treatment planning as well as for providing temperature and spatial feedback. Additionally, MR imaging can provide a tool for quantification and monitoring of the drug release process, as shown in Chapter 5, where the change in the relaxation rate (ΔR_1) upon release of an MRI contrast agent together with the drug from TSLs correlated with the amount of drug taken up in the 9L tumors.

In this Chapter, the therapeutic effect of doxorubicin delivery from TSLs using HIFU-mediated hyperthermia was investigated by measuring the tumor growth over time. For comparison, two formulations which are currently available in the clinic were used; free doxorubicin and Caelyx®. Saline injection was used as a control. The tumor growth of the four different groups (TSL, Caelyx®, doxorubicin and saline) were all tested with and without HIFU-hyperthermia treatment. Additionally, the potential of MR imaging to predict and monitor the response to the treatment was investigated.

7.2 Materials and Methods

7.2.1 Materials

1,2-Dipalmitoyl-*sn*-glycero-3-phosphocholine (DPPC) and hydrogenated-*L*- α -phosphatidylcholine (HSPC) were kindly provided by Lipoid (Germany). 1,2-Dipalmitoyl-*sn*-glycero-3-phosphoethanolamine-*N*-[methoxy(polyethyleneglycol)-2000] (DPPE-PEG2000) and cholesterol were purchased from Avanti Polar Lipids (USA). Doxorubicin hydrochloride was purchased from AvaChem Scientific (USA). [Gd(HPDO3A)(H₂O)] (ProHance®) was obtained from Bracco Diagnostics (Italy). Caelyx® was purchased from Schering-Plough (Germany) and saline (0.9% NaCl) from B Braun Melsungen AG (Germany).

7.2.2 Temperature-sensitive liposomes

TSLs, composed of DPPC:HSPC:Chol:DPPE-PEG2000 = 50:25:15:3 (molar ratio), encapsulating doxorubicin and 250 mM [Gd(HPDO3A)(H₂O)], were prepared as described in Chapter 4. The only difference was that these liposomes did not contain DOTA-DSPE lipids for radiolabeling. The hydrodynamic radius of the liposomes was determined in HEPES Buffered Saline (HBS) using Dynamic Light Scattering (DLS) and the melting phase transition temperature (T_m) of the liposomal membrane was determined with Differential Scanning Calorimetry (DSC) (Chapter 2). The doxorubicin concentration was determined fluorimetrically with a spectrophotometer (Perkin Elmer LS55, λ_{ex} = 485 nm and λ_{em} = 590 nm) in an isopropyl alcohol:H₂O (1:1 v/v) solution and the phospholipid concentration was measured by phosphate determination according to Rouser *et al.*²⁵

7.2.3 Animal model

R1 rhabdomyosarcoma tumors were established on the hind leg of female Wag/Rij rats (Charles River, age 5-7 weeks) by subcutaneous implantation under anesthesia with syngeneic pieces of donor tumor tissue ($\sim 1 \text{ mm}^3$).⁴ Tumor dimensions were determined by measuring the length (l), width (w) and depth (d) using a caliper and the tumor volume was calculated by $0.5 \times l \times w \times d$. Animal studies were performed as soon as a tumor volume of 400 mm^3 was reached, typically 20-30 days after tumor implantation.

7.2.4 Anti tumor efficacy study

An overview of the treatment protocol is shown in Figure 7.1. Animals were randomly divided in one of the eight treatment groups: TSL, doxorubicin, Caelyx® or saline, with or without hyperthermia treatment with HIFU. TSLs were prepared as described in Section 7.2.2, doxorubicin HCl was dissolved in HBS pH7.4 (2 mg/mL) and Caelyx® and saline were used as purchased, without any further preparation. The prepared TSL and doxorubicin solutions were kept at -20 °C until use. All experimental procedures were conducted while the animals were anesthetized with isoflurane (induction 3%, maintenance 1-3% in medical

air (flow 0.6 L/min)). The solutions were injected via a tail vein catheter (dose = 2 mg doxorubicin/ kg bodyweight or a comparable volume of saline). Immediately after the injection, the HIFU-induced hyperthermia treatment was started (Section 7.2.5). Animals in the groups without HIFU were kept under anesthesia for 1h after the injection. The bodyweight and tumor size were measured just before the treatment (t=0) and three times per week after the treatment. The relative tumor size was calculated by dividing the measured tumor size with the tumor size at t=0.

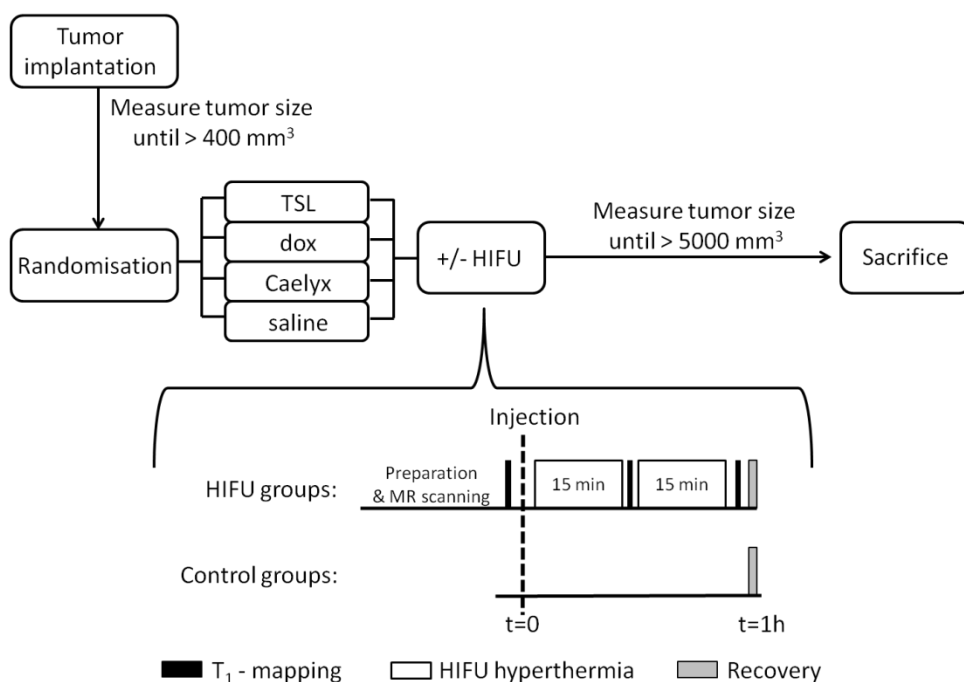


Figure 7.1. Schematic overview of the therapy study protocol. Animals were randomly divided in one of the eight treatment groups: TSL, doxorubicin, Caelyx® or saline, with or without hyperthermia treatment with HIFU.

7.2.5 MR-HIFU treatment

Local HIFU-mediated hyperthermia treatment was performed as described in Chapter 4, using an acoustical power of 5-10 W.²⁶ The heating was controlled using a binary feedback control algorithm in order to keep the temperature between 41 and 42 °C for 2 times 15 minutes. The temperature images were corrected for baseline drift by subtracting the drift calculated from a reference region from the actual temperature images.

7.2.6 T_1 mapping

Maps of the longitudinal relaxation time (T_1) were acquired before, in between and after the two 15 minute-periods of the hyperthermia treatment, using a single slice Look-Locker sequence²⁷ (FA = 10°; TR/TE=9.0/3.4 ms; interval time = 100 ms; time of inversion repetition = 6 s; EPI-factor = 5; field of view = 50 mm × 69 mm; matrix = 64 × 65; half scan = 80%; slice thickness = 2 mm; number of averages = 2; fat suppression = SPIR; acquisition time = 2 min, 36 s). The effective T_1 (T_1^*) was calculated from the signal recovery on a voxel-by-voxel basis using an in-house created IDL-based software tool (IDL version 6.3, RSI, Colorado, USA). Further data processing was performed in MATLAB (R2010a, MathWorks, Massachusetts, USA), in which the longitudinal relaxation rate R_1 was calculated from the effective R_1^* ($R_1^* = 1/T_1^*$, $R_1 = R_1^* + \ln(\cos(\alpha))/TR$, with $\alpha = 10^\circ$ and TR = 100 ms)²⁸ on a voxel-by-voxel basis.

7.2.7 Data analysis

Growth curves were fitted in Origin (Origin 7.5, OriginLab Corporation, Northampton, USA) according to the bi-exponential equation $S_t = A e^{Bt} + C e^{Dt} + S_0$ for the TSL+HIFU group. The other groups showed a mono-exponential behaviour and were therefore fitted with $S_t = A e^{Bt} + S_0$. In order to calculate an average growth curve for every group, the relative tumor size for every rat was calculated for each day by using the fitted equation. Subsequently, the average and standard deviation for each day was calculated from the tumor sizes of all the rats in the treatment group. The time to reach two times the initial tumor size was calculated from the fitted equation by using a numerical method ('fsolve') in Matlab. On the obtained time points a one-way analysis of variance (ANOVA) statistical test was performed with Origin, followed by Bonferroni's post-hoc multiple comparisons tests.

7.3 Results

Tumor-bearing animals were divided randomly in one of the eight treatment groups: TSL, doxorubicin, Caelyx® or saline, with or without hyperthermia treatment with HIFU. As soon as a tumor volume of 400 mm³ was reached, the experiment was performed. Table 7.1 gives an overview of the group sizes and average tumor sizes at the time of the treatment (t=0).

Table 7.1. Overview of rats used in the therapy study

Group	Group size	Tumor size at treatment [mm ³]
TSL + HIFU	n=6	669 ± 229
TSL	n=6	734 ± 276
Doxorubicin + HIFU	n=6	822 ± 316
Doxorubicin	n=6	769 ± 256
Caelyx® + HIFU	n=6	794 ± 238
Caelyx®	n=6	788 ± 368
Saline + HIFU	n=5	670 ± 123
Saline	n=5	828 ± 157

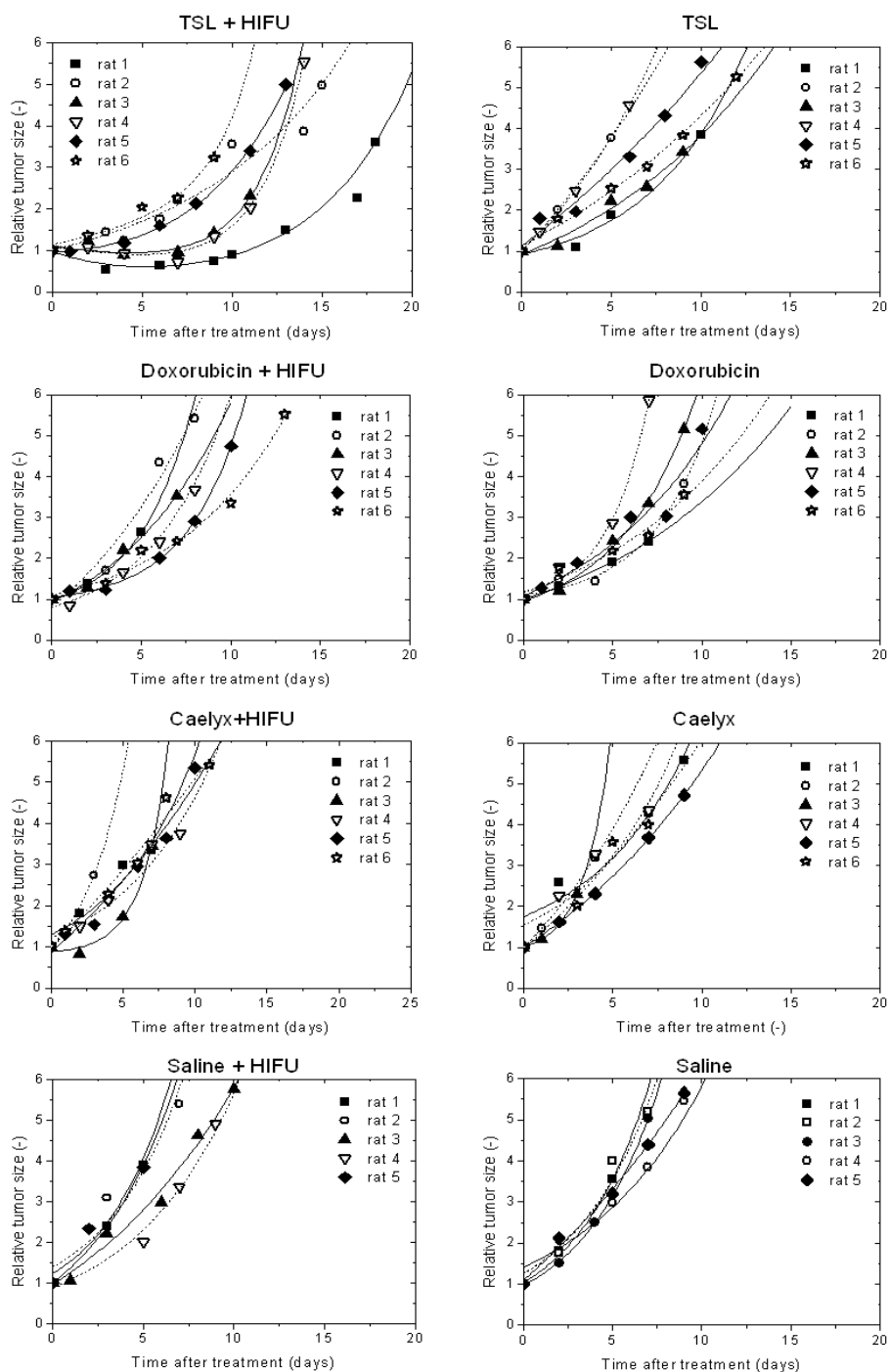


Figure 7.2. Growth curves for all treated animals, fitted with an exponential equation.

In Figure 7.2, the relative tumor sizes over time for all rats of the eight different treatment groups; TSL, doxorubicin, Caelyx®, and saline, with and without HIFU-hyperthermia treatment are shown. No obvious differences were observed between the different groups, except the tumors in the TSL+HIFU group showed delayed growth. For three tumors in this group, even a decrease in tumor size was observed at the first days after the treatment. To be able to fit the decrease in tumor size, the curves in this group were fitted with the biexponential equation $S_t = A e^{Bt} + C e^{Dt} + S_0$, while for all the other groups the growth showed a mono-exponential time dependence. For every group, an average growth curve was calculated, which is shown in Figure 7.3. The TSL+HIFU group clearly showed a slower tumor growth than all other groups.

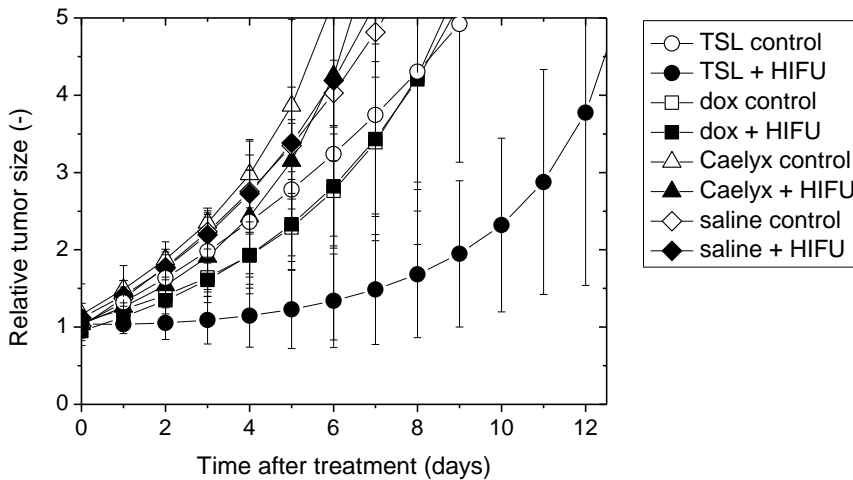


Figure 7.3. Average tumor growth of all treatment groups. Average tumor size \pm standard deviation was calculated for each day from the fitted curves.

In Figure 7.4, the time to reach two times the initial tumor size is shown for the different groups. Obviously, this time was longer for the tumors of the TSL+HIFU group (9.4 ± 3.5 days, $n=6$) than for the tumors of the other groups (3 ± 2 days, $n=40$). A one-way ANOVA test showed that the tumor doubling times of the different groups were significantly different, $F(7,38)=10.96$, $p<0.00001$. Post hoc analysis using Bonferroni's post-hoc multiple comparisons tests indicated that only the TSL+HIFU group was significantly different from the other 7 groups on a 0.01 level.

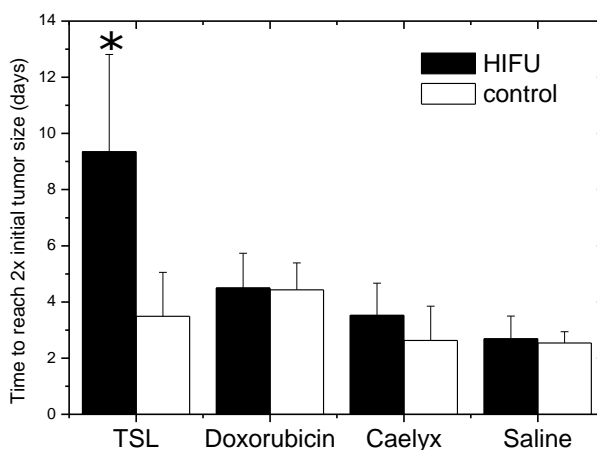


Figure 7.4. Average tumor doubling time for the eight different groups. The error bars represent the standard deviation. The star indicates the significant difference between the TSL+HIFU group and the other groups ($p < 0.01$).

In order to monitor the animal wellness and detect possible side effects of the treatment, the animal body weight was measured over time. In figure 7.5 the average and standard deviation of the relative body weights at 7 days after the treatment (=body weight $t=7$ days / body weight $t=0$) is shown for the different treatment groups. Without treatment, the relative body weight would be higher than 1 because of animal growth over time. However, for all groups the average body weights were slightly below 1, indicating an effect of the performed procedure on the body weight. The HIFU-treated groups showed a weight loss of $6.2 \pm 5.3\%$ ($n=23$), which was larger than the weight loss of the control groups ($1.4 \pm 3.6\%$, $n=23$). For each group, a one-sample t-test was performed to test whether the weight loss was significant (hypothesis: average body weight < 1) with a significance level of 0.05 (Table 7.2). The weight loss was significant for all HIFU-treated animals, except for the 'saline + HIFU' group. For the control groups no significant weight losses were found. The 'doxorubicin + HIFU' group showed the largest weight loss of $8.4 \pm 5.0\%$. Some rats were sacrificed within 1 week after treatment, therefore group sizes were slightly smaller than the initial group sizes (Table 7.1 and 7.2).

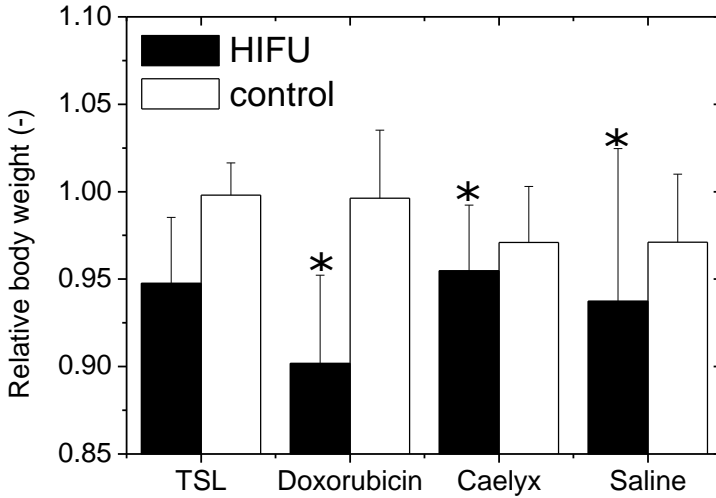


Figure 7.5. Relative body weights after 1 week of the rats in the eight treatment groups. The stars indicate the groups of which the body weights are significant lower than 1 with $p < 0.05$.

Table 7.2. Results of one-sample t -test for all groups with hypothesis bodyweight < 1 and p -value = 0.05.

Group	HIFU	Control
TSL	Yes (P=0.010, n=6)	No (P=0.457, n=5)
Doxorubicin	Yes (P=0.015, n=4)	No (P=0.412, n=6)
Caelyx	Yes (P=0.027, n=5)	No (P=0.084, n=4)
Saline	No (P=0.123, n=4)	No (P=0.090, n=4)

During the MR-HIFU treatment after injection of TSL, the change in T_1 relaxation rate can be used to image the release of the drug from the liposomes. T_1 maps were obtained using a Look-Locker sequence before and after HIFU-mediated hyperthermia, of which the R_1 maps were calculated. Figure 7.6 shows two examples of T_2 -weighted MR images, which were obtained for tumor localization and therapy planning, and the corresponding R_1 maps. In figure 7.6A an example is shown of a tumor that showed a relatively large ΔR_1 of 0.12 s^{-1} , while in figure 7.6B almost no change in relaxation rate was observed ($\Delta R_1 = 0.01 \text{ s}^{-1}$).

The average ΔR_1 was $0.06 \pm 0.04 \text{ s}^{-1}$ for the six tumors of the TSL+HIFU group, while there was no significant R_1 change for the control groups injected with saline, doxorubicin or Caelyx® without MR contrast agent (average $\Delta R_1 = -0.01 \pm 0.04 \text{ s}^{-1}$, $n=17$).

For each rat treated with TSL + HIFU, the relative tumor size reached after 7 days was calculated from the fitted exponential curve on an individual bases; $S_{7\text{days}} = S_0 + A e^{7*B} + C e^{7*D}$. Figure 7.7 shows the $S_{7\text{days}}$ plotted against the ΔR_1 measured during the MR-HIFU treatment. An inverse correlation was found between the ΔR_1 and the relative tumor size after one week: the larger the change in the relaxation rate, the smaller the tumor size after one week.

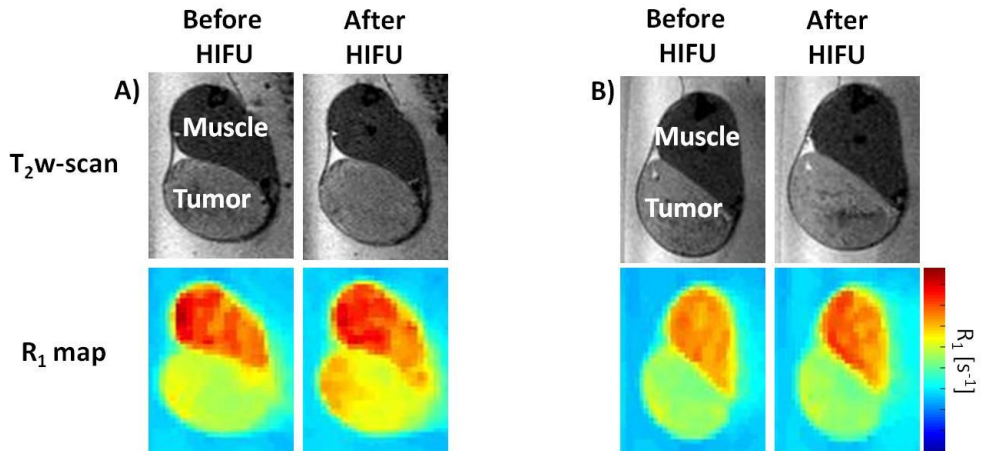


Figure 7.6. MRI scans before and after MR-HIFU treatment of two rats injected with TSL. Images at the upper row are T_2 -weighted scans of the hind limb with tumor and muscle, the lower row shows the corresponding R_1 maps. A) Tumor showed a relatively large ΔR_1 of 0.12 s^{-1} . B) Tumor showed a low ΔR_1 of 0.01 s^{-1} .

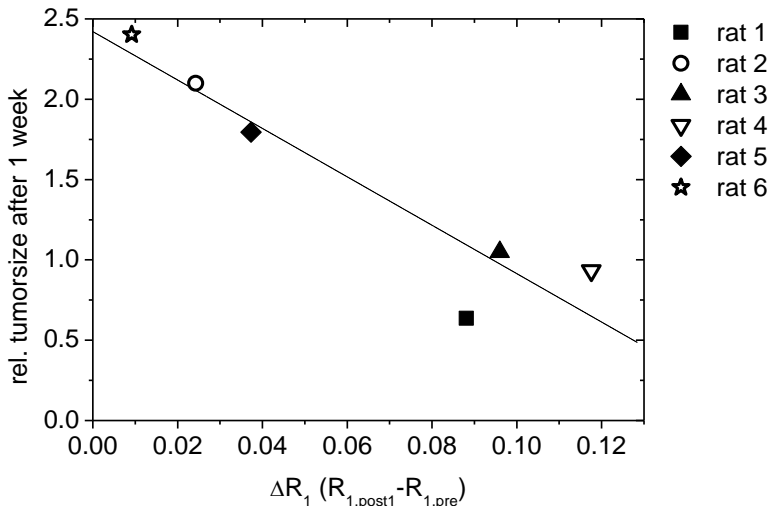


Figure 7.7. Change in R_1 of the six rats treated with TSL+HIFU plotted against the relative tumor size after 7 days.

7.4 Discussion

The therapeutic effect of HIFU-hyperthermia mediated local drug delivery from temperature-sensitive liposomes was investigated by measuring the tumor growth over time. Four different groups (TSL, Caelyx®, doxorubicin and saline) were tested with and without HIFU-hyperthermia treatment.

In order to avoid side effects due to the systemic toxicity of doxorubicin, a low dose of 2 mg doxorubicin/kg body weight was administered. However, still some decrease in body weight was observed due to the treatment. Besides doxorubicin toxicity, also the anesthesia used during the treatment can affect the body weight. This effect will be larger for HIFU-treated rats than for the controls, because of the longer anesthesia time needed for animal preparation and MRI scanning for HIFU treatment planning (about 3 hours anesthesia for HIFU groups vs 1 hour for the control groups). Although the liposomal encapsulation of doxorubicin should decrease the toxicity profile of doxorubicin, no significant differences in toxicity were found between Caelyx®, TSL and free doxorubicin. However, as expected due to the low dose the weight losses were very small, with a maximum weight loss of 8.4 ± 5.0 % for the dox+HIFU group at 1 week after treatment. Therefore, small differences in toxicity profiles between the different groups will not be detected with this method.

Morita et al.²⁹ reported a tumor growth delay of 2.2 days using a dose of 2.5 mg/kg free doxorubicin in R1 rhabdomyosarcoma tumors, which is similar to our results where the time reach two times the initial tumor size was 4.4 ± 0.96 days for the doxorubicin group and 2.5 ± 0.4 days for the saline group. As expected, HIFU-hyperthermia treatment alone did not show an effect. However, in combination with doxorubicin or Caelyx® the HIFU-treatment did not show an additional effect on the tumor growth either, while different other groups have shown a synergistic effect of hyperthermia on doxorubicin and/or Caelyx® efficacy.^{4, 14, 29-31} Apparently, the amount of (bioavailable) doxorubicin in these tumors was too low to show a significant effect on the tumor growth.

For TSL administration in combination with HIFU-mediated hyperthermia, already promising results were obtained showing an increase in doxorubicin concentration at early time points due to intravascular release (Chapter 5), as well as increased accumulation of liposomes over longer time points (Chapters 4 and 6). Additionally, bioavailability of the drug and a good distribution over the tumor were shown in Chapter 6. The combined effect of the intravascular release of doxorubicin during heating, bioavailability and deep penetration of the drug, and the additional increased accumulation of doxorubicin-filled liposomes, may have an important contribution to the therapeutic outcome of HIFU-mediated drug delivery. As expected, a decrease in tumor growth in the TSL+HIFU group was observed, while no effect was found for TSL injection only. However, no complete regression was achieved in any of the rats. In Chapter 6 we observed on histology that only a part of the tumor became necrotic after 48h. These findings have implications for a therapeutic study as the remaining

viable part of the tumor will continue growing. This explains the delayed tumor growth or decreasing tumor size directly after treatment, followed by recurrence of the tumor growth. Repeated treatments, an increased injected dose, and/or optimized treatment schedules can be considered to further increase the therapeutic effect.

In Chapter 5, we have shown that the change in the relaxation rate (R_1) correlated with the amount of delivered drug in 9L tumors. In this rhabdomyosarcoma model, the effect on R_1 was much lower than found in the previous experiments with 9L tumors. As discussed extensively in Chapter 6, this difference can most probably be explained due to the lower permeability and higher perfusion of the R1 compared to 9L tumors leading to less extravasation and a more rapid washout of the Gd contrast agent. However, still a good correlation was found between the ΔR_1 and the relative tumor size after 7 days, showing that the MR measurements can be used as a surrogate marker for a therapeutic effect.

7.5 Conclusion

The therapeutic effect of HIFU-hyperthermia mediated local drug delivery from temperature-sensitive liposomes was investigated by measuring the tumor growth over time after treatment. TSL+HIFU showed a significant increase in the time to reach two times the initial tumor size in comparison with all other tested groups (TSL, Caelyx®, doxorubicin and saline, with and without HIFU-hyperthermia). A good correlation was found between the signal change on the MR measurements and the relative tumor size after one week, showing that MR imaging offers a tool to predict the successfulness of the treatment.

References

1. Horsman MR. Tissue physiology and the response to heat. *International Journal of Hyperthermia*. 2006;22(3):197-203.
2. Vaupel PW, Kelleher DK. Pathophysiological and vascular characteristics of tumours and their importance for hyperthermia: Heterogeneity is the key issue. *International Journal of Hyperthermia*. 2010;26(3):211-23.
3. Hildebrandt B, Wust P, Ahlers O, et al. The cellular and molecular basis of hyperthermia. *Critical Reviews in Oncology Hematology*. 2002;43(1):33-56.
4. Issels RD. Hyperthermia adds to chemotherapy. *European Journal of Cancer*. 2008;44(17):2546-54.
5. Krawczyk PM, Eppink B, Essers J, et al. Mild hyperthermia inhibits homologous recombination, induces BRCA2 degradation, and sensitizes cancer cells to poly (ADP-ribose) polymerase-1 inhibition. *Proc Natl Acad Sci*. 2011;108:9851-6.
6. Overgaard J, González González D, Hulshof MCCM, et al. Randomized trial of hyperthermia as adjuvant to radiotherapy for recurrent or metastatic malignant melanoma. *Lancet*. 1995;345(8949):540-3.
7. van der Zee J, González González D, van Rhoon GC, et al. Comparison of radiotherapy alone with radiotherapy plus hyperthermia in locally advanced pelvic tumours: a prospective, randomised, multicentre trial. *Lancet*. 2000;355(9210):1119-25.
8. Jones EL, Oleson JR, Prosnitz LR, et al. Randomized trial of hyperthermia and radiation for superficial tumors. *Journal of Clinical Oncology*. 2005;23(13):3079-85.
9. Issels RD, Lindner LH, Verweij J, et al. Neo-adjuvant chemotherapy alone with regional hyperthermia for localised high-risk soft-tissue sarcoma: a randomised phase 3 multicentre study. *Lancet oncology*. 2010;11(6):561-70.
10. Koning GA, Eggermont AMM, Lindner LH, et al. Hyperthermia and thermosensitive liposomes for improved delivery of chemotherapeutic drugs to solid tumors. *Pharm Res*. 2010;27:1750-4.
11. Deckers R, Rome C, Moonen CTW. The role of ultrasound and Magnetic Resonance in Local Drug Delivery. *Journal of Magnetic Resonance Imaging*. 2008;27:400-9.
12. Kong G, Braun RD, Dewhirst MW. Characterisation of the effect of hyperthermia on nanoparticle extravasation from tumor vasculature. *Cancer Research*. 2001;61:3027-32.
13. Gaber MH, Wu NZ, Hong K, et al. Thermosensitive liposomes: extravasation and release of contents in tumor microvascular networks. *Int J Radiat Oncol Biol Phys* 1996;36(5):1177-87.
14. Kouloulias VE, Dardoufas CE, Kouvaris JR, et al. Liposomal doxorubicin in conjunction with reirradiation and local hyperthermia treatment in recurrent breast cancer: A phase I/II trial. *Clinical Cancer Research*. 2002;8:374-82.
15. de Smet M, Heijman E, Langereis S, et al. Magnetic resonance imaging of high intensity focused ultrasound mediated drug delivery from temperature-sensitive liposomes: An in vivo proof-of-concept study. *Journal of Controlled Release*. 2011;150(1):102-10.
16. de Smet M, Hijnen NM, Langereis S, et al. Magnetic Resonance guided High Intensity Focused Ultrasound (MR-HIFU) mediated hyperthermia improves the intratumoral distribution of temperature-sensitive liposomal doxorubicin. *Investigative Radiology*. accepted.
17. Gasselhuber A, Dreher MR, Rattay F, et al. Comparison of conventional chemotherapy, stealth liposomes and temperature-sensitive liposomes in a mathematical model. *PLoS ONE*. 2012;7(10):e47453.

18. Manzoor AA, Lindner LH, Landon CD, et al. Overcoming limitations in nanoparticle drug delivery: Triggered, intravascular release to improve drug penetration into tumors. . *Cancer Research*. 2012;72(21):5566-75.
19. Needham D, Dewhirst MW. The development and testing of a new temperature-sensitive drug delivery system for the treatment of solid tumors. *Advanced Drug Delivery Reviews*. 2001;53(3):285-305.
20. Kong G, Anyarambhatla G, Petros WP, et al. Efficacy of liposomes and hyperthermia in a human tumor xenograft model: importance of triggered drug release. *Cancer Res*. 2000;60:6950-7.
21. Needham D, Anyarambhatla G, Kong G, et al. A new temperature-sensitive liposome for use with mild hyperthermia: characterization and testing in a human tumor xenograft model. *Cancer Res*. 2000;60:1197-201.
22. Dromi S, Frenkel V, Luk A, et al. Pulsed-High Intensity Focused Ultrasound and Low Temperature-Sensitive Liposomes for enhanced targeted drug delivery and antitumor effect. *Clin Cancer Res*. 2007;13(9):2722-7.
23. Yarmolenko PS, Zhao Y, Landon C, et al. Comparative effects of thermosensitive doxorubicin-containing liposomes and hyperthermia in human and murine tumors. *International Journal of Hyperthermia*. 2010;26(5):485-98.
24. Tagami T, Ernsting MJ, Li S-D. Efficient tumor regression by a single and low dose treatment with a novel and enhanced formulation of thermosensitive liposomal doxorubicin. *Journal of Controlled Release*. 2011;152(2):303-9.
25. Rouser G, Fleische S, Yamamoto A. 2 Dimensional thin layer chromatographic separation of polar lipids and determination of phospholipids by phosphorus analysis of spots. *Lipids*. 1970;5(5):494.
26. Hijnen NM, Heijman E, Köhler MO, et al. Tumour hyperthermia and ablation in rats using a clinical MR-HIFU system equipped with a dedicated small animal set-up. *International Journal of Hyperthermia*. 2012;28(2):141-55.
27. Look DC, Locker DR. Time saving in measurement of NMR and EPR relaxation times. *Review of Scientific Instruments*. 1970;41(2):250-1.
28. Shin W, Gu H, Yang Y. Fast high-resolution T1 mapping using inversion-recovery Look-Locker echo-planar imaging at steady state: optimization for accuracy and reliability. *Magnetic Resonance in Medicine*. 2009;61:899-906.
29. Morita K, Zywiets F, Kakinuma K, et al. Efficacy of doxorubicin thermosensitive liposomes (40°C) and local hyperthermia on rat rhabdomyosarcoma. *Oncology reports*. 2008;20:365-72.
30. Hahn GM, Braun J, Har-Kedar I. Thermochemotherapy: Synergism between hyperthermia (42-43°) and Adriamycin (or Bleomycin) in mammalian cell inactivation *Proc Natl Acad Sci USA*. 1975;72(3):937-40.
31. van Bree C, Krooshoop JJ, Rietbroek RC, et al. Hyperthermia enhances tumor uptake and antitumor efficacy of thermostable liposomal daunorubicin in a rat solid tumor. *Cancer Research*. 1996;56:563-8.

Chapter 8

General discussion

8.1 Treatment strategies for drug delivery with temperature-sensitive liposomes

Local drug delivery using temperature-sensitive liposomes (TSLs) is an attractive option for the treatment of localized tumors. Nevertheless, for performing hyperthermia-mediated drug delivery with TSLs, different treatment schedules may be considered. Hyperthermia treatment schedules as well as a combination of hyperthermia with pressure-mediated drug delivery are discussed in this Section.

8.1.1 Hyperthermia treatment schedules

The strategy used in this thesis was to inject TSLs just prior to the hyperthermia treatment, resulting in immediate release of their contents upon arrival in the heated tumor area. This treatment scheme is usually referred to as the intravascular release strategy (Figure 8.1A). Another approach is to exploit the EPR effect followed by heating e.g. 48 hours after injection to make the drug bioavailable (Figure 8.1B). Besides optimization of the treatment schedule, also the TSL formulation should be optimized for each treatment strategy, since every approach comes with different requirements for the liposomes.

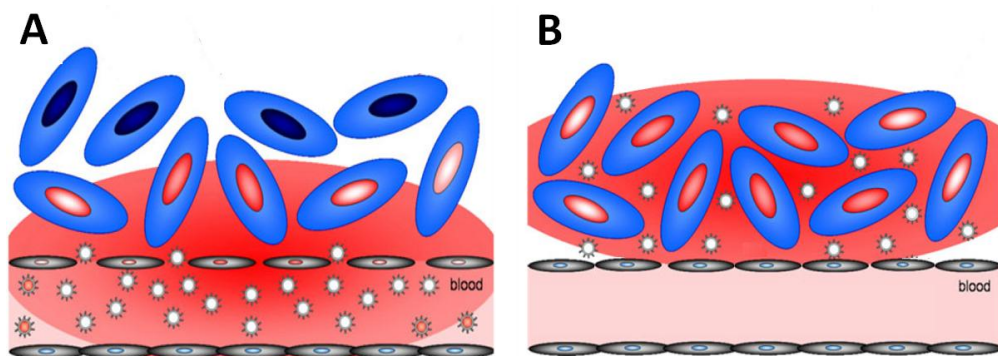


Figure 8.1. Heating strategies for drug delivery with TSLs. A) Intravascular release, B) Extravascular release (heating after extravasation). Figures adapted from Koning et al.¹

In case of the intravascular release treatment strategy (Figure 8.1A), the amount of delivered drug scales with the time where hyperthermia is applied, the plasma concentration of the liposomal drug carrier, the drug-payload per carrier, and the perfusion of the tumor tissue. The drug release from the liposomal carrier and subsequent uptake into the tumor tissue needs to be relatively fast to compete against downstream wash-out. This approach requires TSLs that do not show fast leakage at body temperature, but rapidly release their

drug payload at mild hyperthermia (39-42 °C). Furthermore, the concentration of the drug-loaded TSLs in the blood should be as high as possible during the application of the heat treatment, thus rapid clearance by the reticuloendothelial system (RES) should be prevented. By using the intravascular release approach in combination with a fast-releasing TSL, approximately 30 times higher peak intracellular drug concentrations in the tumor can be obtained in comparison with the free drug.² Additionally, intravascular release from TSLs overcomes heterogeneity in vascular permeability, since it creates high intravascular drug concentrations that drive drug uptake by cells and increase drug penetration to reach more tumor cells at a larger distance from vessels.^{3,4}

For the extravascular release (Figure 8.1B), stability and prolonged circulation time of the liposomes becomes even more important. Additionally, the size of the liposomes needs to be optimized in order to have an optimal extravasation. Solid tumors often have poorly differentiated vasculature that in contrast to the vasculature in healthy tissues, allows for the extravasation of nanocarriers. Together with the lack of functional lymphatics, and therefore the inability to eliminate extravasated liposomes, this increase in vascular permeability allows long-circulating nanoparticles to accumulate in tumors over time. This effect is called the enhanced permeability and retention (EPR) effect.⁵ To ensure that the liposomes still contain high drug payloads at the time of extravasation, a process that typically proceeds for 1-3 days, low drug leakage from the TSLs at body temperature is of high importance. On the other hand, fast drug release is less relevant, because the extravasated liposomes will not be washed out during the heating period. Harrington *et al.* quantified the amount of extravasated liposomes in various human tumors (breast, head and neck, lung, brain and cervical cancer) at 72 hours after injection. The liposome uptake varied from 0.5 to 3.5% of the injected dose, depending on the type of the malignancy.⁶ For the extravascular release approach, the maximum amount of delivered drug to the tumors can never exceed the amount of drug present in the accumulated liposomes. According to a mathematical model by Gasselhuber *et al.*, a 5-fold increase in peak intracellular tumor drug concentrations can be obtained in comparison with free doxorubicin, assuming a stable TSL formulation.² In the case of drug leakage from the liposomes at body temperature before extravasation has occurred, the amount of drug delivered to the tumors will be even lower. Another shortcoming is that the relatively large size of the liposomes limits their penetration depth to 1-2 cell layers from blood vessels, preventing drug uptake by tumor cells at a larger distance from the vasculature.⁷⁻⁹ Overall, for doxorubicin delivery, the intravascular release seems more promising than the extravascular release in terms of tumor treatment efficacy.

Since hyperthermia has also shown to improve liposome extravasation in tumor areas,⁹⁻¹¹ combinations of the intravascular and extravascular release strategy might result in even higher amounts of bioavailable drug in the tumor.¹ In this case, the first hyperthermia treatment can be applied for intravascular release as well as to increase tumor

vascular permeability, after which the administered TSLs can extravasate into the tumor area. Upon reaching optimal liposome accumulation levels in the tumor, a second hyperthermia treatment can be applied to release the drug from the extravasated liposomes. This combination of both heating strategies looks promising, as the first heating has a double effect; it immediately causes intravascular release and it enhances the liposome extravasation over longer time periods. Additionally, all the drug encapsulated by the extravasated liposomes will become bioavailable due to the second heating step. This strategy will have the most optimal effect when combined with the administration of two different liposomes; one with a fast release for effective intravascular release and the other one with a high stability to ensure accumulation of drug-filled liposomes over longer time points. However, in clinical practice it may be unpractical to apply two heating periods. Therefore, the additional effect of the second heating period should be carefully investigated and weighed against the discomfort and costs of the extra hyperthermia treatment.

8.1.2 Ultrasound-mediated drug delivery for cell-impermeable drugs

The hyperthermia-mediated delivery strategies discussed above, are applicable for the delivery of a drug with high permeability across different barriers (e.g. doxorubicin). After the release from TSL, this high permeability results in a rapid distribution in the interstitial space and cellular uptake across the tumor upon its local release.¹²⁻¹⁵ However, for drugs that are cell-impermeable but have an intracellular target, another approach is needed. Besides heat production, ultrasound can be utilized to locally break biological barriers and as a consequence enable the internalization of molecules.^{16,17} A two-step protocol for intracellular delivery of cell-impermeable molecules has been developed by Yudina *et al.*^{18,19} In this protocol, ultrasound-induced permeabilization is followed by hyperthermia-mediated release of a model drug (TO-PRO-3) from temperature-sensitive liposomes (Figure 8.2).

The efficacy of this approach was evaluated *in vivo* by fluorescence imaging followed by histological analysis. A 2.4-fold increase of fluorescence signal was observed and intracellular delivery of TO-PRO-3 was confirmed by a characteristic nuclear staining. Possible applications of this two-step protocol include local and controlled intracellular delivery of molecules with otherwise limited bioavailability.

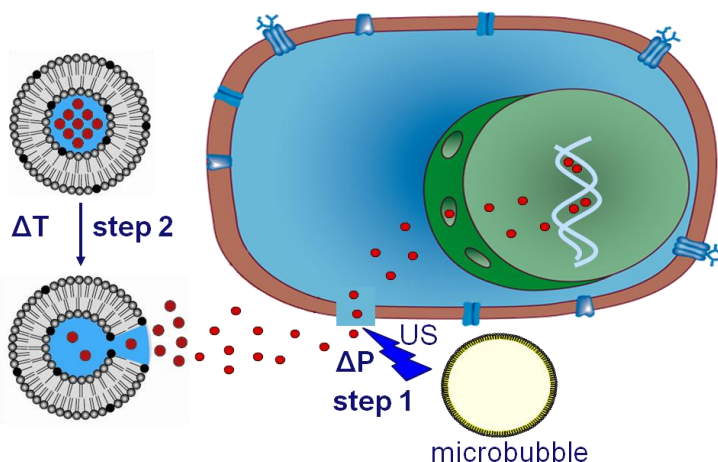


Figure 8.2. Schematic representation of an intracellular drug delivery protocol combining ultrasound-mediated cell-membrane permeabilization in the presence of microbubbles (step 1) and release of the drug from TSLs (step 2).

8.2 Liposomal formulations

As discussed in Section 8.1, the optimal temperature-sensitive liposomal formulation for the intravascular release approach has no doxorubicin leakage at 37 °C and fast release at 42 °C. Although many research efforts have been made so far,²⁰⁻²² this liposomal formulation has not been discovered yet, and these two prerequisites might even be mutually exclusive. In this thesis, two temperature-sensitive liposomal formulations were investigated; low temperature-sensitive liposomes (LTSL)²³ and traditional temperature-sensitive liposomes (TTSL).²⁴ *In vitro* experiments with these liposomal systems (Chapter 2) showed fast release of doxorubicin from the LTSL in HBS at 42 °C, with quantitative release of doxorubicin within 1 min. This fast release may originate from the lysolipids present in the lipid bilayer of this formulation, which enhances the doxorubicin release occurring via grain boundary permeabilization (Chapter 1).^{22, 25} The TTSL showed a slower release of doxorubicin in comparison with the LTSL formulation, but still all doxorubicin was released within a few minutes. Besides the release kinetics at hyperthermia, the stability at 37 °C of the two liposomal systems was investigated as well. The LTSL showed considerable doxorubicin leakage in fully supplemented DMEM containing 10% Fetal Bovine Serum (FBS) at 37 °C. In this medium, approximately 30% of the doxorubicin was released in 1 hour, while no release was observed in pure HBS solution at this physiological temperature (Chapter 2). Apparently, the interaction of the LTSL with compounds present in the fully supplemented

DMEM, such as albumin, alters the release properties. In contrast, the TTSL formulation did not show doxorubicin leakage under the same conditions.

Subsequently, the *in vivo* behavior of both liposomal systems was investigated (Chapter 4). After injection, the blood kinetics of the radiolabeled liposomes as well as of the encapsulated doxorubicin was measured. For both systems, the blood clearance of doxorubicin was faster compared to the liposomal carriers, implying premature leakage of the encapsulated drug from the aqueous lumen of the TSL at physiological temperatures, followed by a rapid blood clearance of this small molecule. For LTSL, doxorubicin was cleared from the blood within 30 minutes (<0.5 %ID/total blood), indicating a fast leakage of doxorubicin from these liposomes. In contrast, the TTSL showed a much slower leakage, with 55% of the injected doxorubicin still present in the blood after 30 minutes.

The question is whether the faster doxorubicin release from LTSL at hyperthermia outweighs the increased leakage at body temperature of these systems compared to the TTSL formulation. Additionally, for TTSL the long-term extravasation will contribute to drug accumulation in the tumor, while for LTSL this effect will be negligible, since most of the liposomes will already be empty at the time of extravasation. The amount of delivered drug to the tumor over time can be predicted using pharmaceutical models. Gasselhuber *et al.* published a mathematical model for predicting the amount of doxorubicin delivered to tumors, using stability and release properties of TSLs based on *in vitro* measurements.² Their calculations showed that fast releasing TSL lead to higher peak values as well as the area under the curve of bioavailable drug concentrations in the tumor in comparison with a slow releasing TSL. However, the doxorubicin leakage at 37 °C of TSL formulations used in this model was lower than the *in vivo* doxorubicin leakage from LTSL and TTSL as measured in this thesis (Chapter 3). Accurate knowledge of doxorubicin release kinetics from TSL formulations *in vivo* is needed as an input, in order to provide a reliable output. Doxorubicin leakage at physiological temperatures can be determined by measuring the blood kinetics of the liposomes as well as for the doxorubicin (Chapter 3). However, no methods are currently available to accurately determine the release kinetics at hyperthermic temperatures *in vivo*. Effects of plasma components and exchange of lysolipids from LTSLs with lipids present in biological membranes, leads *in situ* to differences in the drug release kinetics of TSLs,^{26, 27} making predictions of *in vivo* drug release kinetics based on *in vitro* measurements even more challenging. Based on the blood kinetic measurements presented in Chapter 3, we decided to proceed with the TTSL formulation for the *in vivo* drug delivery experiments performed in this thesis. This formulation showed promising results for MR monitoring of the drug release and for the therapeutic effect in rat tumor models.

8.3 MR-HIFU-mediated hyperthermia

For the application of local hyperthermia, different methods are available, such as the use of radiofrequency (RF) applicators,^{28, 29} microwave (MW) applicators,^{30, 31} lasers,^{32, 33} hot water baths,³⁴ and ultrasound.^{17, 35} Drawbacks of some of these methods are the lack of spatial and temporal accuracy and/or the limited penetration depth. In terms of basic physics, ultrasound has the best combination for non-invasive heating of small wavelengths and corresponding attenuation coefficient, which allows penetration to deep sites with the ability to focus power into small regions. For example, the High Intensity Focused Ultrasound (HIFU) system used for the experiments in this thesis has an ellipsoidal shaped focus point with dimensions 1x1x7 mm³.³⁵ The small size of the focal point is advantageous for accurate heating of small lesions, but on the other hand it complicates heating of larger areas. Köhler *et al.* developed a volumetric sonication method for heating of larger areas by electronic steering the focal point, reaching trajectories with a diameter of 16 mm.³⁵ Due to heat diffusion, the area experiencing a significant temperature increase will be larger than the directly heated area. However, for hyperthermia of human tumors the possibility for homogeneous heating of much larger regions will be required. Therefore, the development of specific ultrasound transducers might be required. The primary limitation of the use of ultrasound for heating is the inability to penetrate through air filled organs (e.g. lung and bowel) and structures such as bone can absorb or reflect an ultrasound beam. Therefore, certain lesion locations are not accessible for HIFU treatment.

A drawback of clinically used RF and MW heating methods for hyperthermia, is the lack of temperature imaging during the treatment. Usually, a CT scan recorded several days to weeks before the hyperthermia treatment, is used for the therapy planning. Temperature monitoring is performed based on calculations and modeling using the CT scan as an input, instead of *in situ* temperature measurements. For HIFU, the integration with magnetic resonance imaging (MRI) is a major advantage. Using this MR-HIFU technique, MR imaging of the target area is performed just prior to the hyperthermia treatment enabling accurate treatment planning. Additionally, MR also allows dynamic mapping of the HIFU-induced temperature change. These temperature measurements provide direct feedback to the ultrasound control unit, creating the possibility to maintain tissues at local mild hyperthermia for long time periods in a controlled manner.³⁶⁻³⁸

As shown in Chapter 5, temperature-induced drug delivery from TSLs is most effective in well-perfused tumor areas. Less perfused areas (e.g. a necrotic core) are difficult to treat, since the liposomes circulating in the blood cannot reach these areas. Combined treatment of local drug delivery from TSLs with ablation of less-perfused regions may offer an extremely efficient treatment solution. This combination of ablation with TSLs is already used in clinical trials using Thermadox® with RF ablation (Figure 8.3). An advantage of using

HIFU for local heating, is that the same equipment and setup can be used for hyperthermia as well as for thermal ablation in the same therapy session.

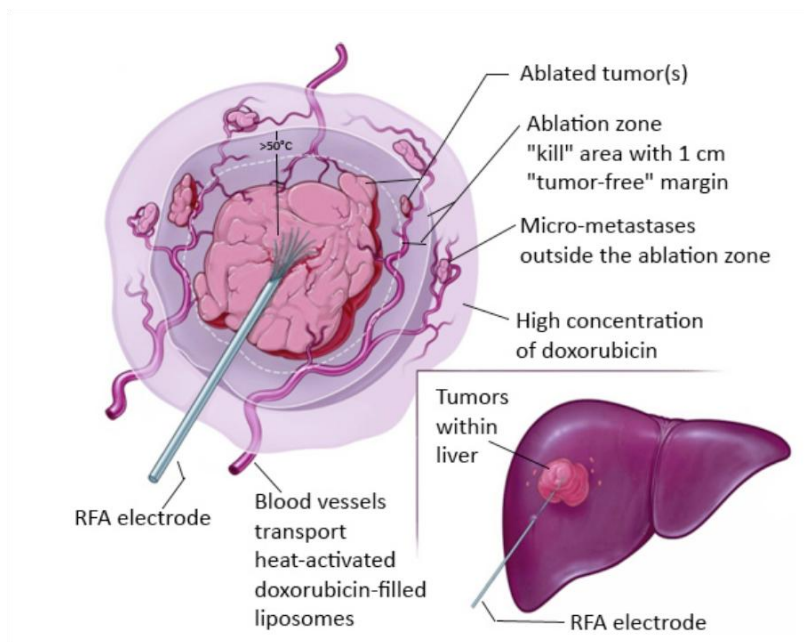


Figure 8.3. RF ablation combined with ThermoDox®. Figure from Landon et al.³

8.3 Image guidance of drug delivery

In drug delivery, imaging can be used for monitoring the delivery, release and/or efficacy of the drug.³⁹ Nuclear imaging of radiolabeled drug carriers is a commonly used method to image accumulation of drug carriers in tumors.^{6, 11} Nevertheless, this imaging modality cannot be used to image the release of the drug, because the contrast enhancing properties of the radioactive agents are the same for the encapsulated and the released form. MRI to this respect has the advantage of being able to probe both liposome accumulation and drug release when a co-encapsulated MRI contrast agent is released together with the drug.⁴⁰⁻⁴²

In Chapter 2, it was shown that mild hyperthermia of paramagnetic TSLs containing doxorubicin and [Gd(HPDO3A)(H₂O)] leads to a simultaneous release of the encapsulated molecules. In 9L gliosarcoma tumors in rats, the change in R_1 was found to be proportional to the amount of drug delivered (Chapter 5). It is important to note that the pharmacokinetic properties of the encapsulated agents prior to release from the lumen of the TSLs are determined by the liposomal carrier. Upon release, however, the doxorubicin and [Gd(HPDO3A)(H₂O)] will show different biodistribution profiles and tumor uptake. The high

free volume of distribution of doxorubicin will lead to a rapid distribution in the interstitial space and cellular uptake across the tumor upon its local release.¹²⁻¹⁴ On the other hand, [Gd(HPDO3A)(H₂O)] will distribute across the extracellular space⁴³ and its intratumoral concentration is a balance between tumor inflow and outwash. In the 9L tumor model the ΔR_1 was measured over time, showing that the wash-out of [Gd(HPDO3A)(H₂O)] was slow in most of these tumors (Chapter 5). Therefore, the ΔR_1 at 70 minutes post injection showed a good correlation with the doxorubicin concentrations found at 90 minutes post injection. In the rhabdomyosarcoma tumor model however, the observed ΔR_1 after HIFU treatment was smaller than the effect observed in 9L gliosarcoma tumors (Chapter 6). Histological examination and DCE-MRI measurements of both tumor models showed obvious differences in blood vessel distribution and structure as well as a considerably lower k_{trans} and v_e in the rhabdomyosarcoma model in comparison to the 9L tumor (Chapter 6). Therefore, the smaller ΔR_1 observed in the rhabdomyosarcoma model can most likely be explained by a higher wash-out from [Gd(HPDO3A)(H₂O)]. The amount of doxorubicin delivered to these tumors was not yet investigated, but histology and therapeutic efficacy (Chapters 6 and 7) suggest high amounts of delivered drug. Possibly, the ratio of the ΔR_1 at 70 min. after injection to the doxorubicin concentration at 90 min. after injection is different for this tumor model than for the 9L tumors. In order to predict the amount of delivered drug based on MR imaging for all different tumors, a solution would be to measure the ΔR_1 over time during the complete hyperthermia protocol, which can be used as an input for pharmacokinetic modeling of the drug and contrast agent.^{2, 45, 46} Currently, this was not possible because during HIFU-treatment the MRI was occupied with performing temperature measurements, which were needed to control the heating with HIFU. In the mean time, progress has been made in sequence development for simultaneous temperature and T_1 mapping.⁴⁴ After implementation of these sequences in the MR-HIFU system, real time T_1 mapping during HIFU treatment in combination with pharmacokinetic modeling may allow a better estimation of the drug delivered to highly perfused tumors.

Besides [Gd(HPDO3A)(H₂O)], also other MRI contrast agents might be considered for the image guidance of the drug release. As discussed in Chapter 1, TSLs containing manganese (Mn²⁺) and doxorubicin were investigated for drug delivery and dose painting.^{40,47} In contrast to [Gd(HPDO3A)(H₂O)], Mn²⁺ can bind to doxorubicin.⁴⁸⁻⁵⁰ This complexation can be an advantageous characteristic for drug dose painting, because co-release of the MRI contrast agent and doxorubicin from the liposomes is guaranteed. Another important aspect is the different pharmacokinetic properties of the MRI contrast agent. In a phospholipid-rich environment *in vivo*, after release from the TSL, Mn²⁺ might interact with for example the cellular membrane, which may result in longer Mn²⁺ retention time at tumor sites and longer contrast enhancement to localize drug delivery. However, besides complexation of Mn²⁺ to doxorubicin, an interaction between Mn²⁺ and the

phospholipid bilayer exists as well.⁵¹ Recently, Yeo *et al.* showed that the incorporation of Mn²⁺ reduced the stability of the TSLs, while [Gd(HPDO3A)(H₂O)] had less influence on the stability of TSLs.⁵² Furthermore, cellular toxicity has always been a setback for clinical applications of Mn²⁺.^{53, 54} To date, only Mn-DPDP (Teslascan®) has been approved for clinical applications.^{55, 56} In contrast, the contrast agent used in this thesis, [Gd(HPDO3A)(H₂O)] (Prohance®), is a clinically approved MRI contrast agent, which may facilitate the clinical translation of these systems. [Gd(HPDO3A)(H₂O)] is generally safe to use and in its free form rapidly eliminated from the body through the kidneys.⁴³ However, the liposomal encapsulation increases the blood half-life from minutes to hours and the route of elimination from the body is changed to clearance by the liver and spleen. One point of concern is that long term tissue retention in the liver and spleen leads to release of Gd³⁺ from the chelate leading to nephrogenic systemic fibrosis (NSF).^{57, 58} ICP-MS measurements of organs collected one month after injection of the TSLs containing [Gd(HPDO3A)(H₂O)] showed that the amount of gadolinium was ≤ 0.3% of the injected dose in all analyzed organs (Chapter 4). Additional investigation needs to be performed to test whether this amount is low enough regarding all safety issues, i.e. does not induce NSF. When safety is guaranteed, the addition of an MRI contrast agent will enable monitoring of drug distribution and prediction of the therapeutic outcome, creating the possibility for optimization of personalized treatments.

References

1. Koning GA, Eggermont AMM, Lindner LH, et al. Hyperthermia and thermosensitive liposomes for improved delivery of chemotherapeutic drugs to solid tumors. *Pharm Res.* 2010;27:1750-4.
2. Gasselhuber A, Dreher MR, Rattay F, et al. Comparison of conventional chemotherapy, stealth liposomes and temperature-sensitive liposomes in a mathematical model. *PLoS ONE.* 2012;7(10):e47453.
3. Manzoor AA, Lindner LH, Landon CD, et al. Overcoming limitations in nanoparticle drug delivery: Triggered, intravascular release to improve drug penetration into tumors. *Cancer Research.* 2012;72(21):5566-75.
4. de Smet M, Hijnen NM, Langereis S, et al. Magnetic Resonance guided High Intensity Focused Ultrasound (MR-HIFU) mediated hyperthermia improves the intratumoral distribution of temperature-sensitive liposomal doxorubicin. *Investigative Radiology.* accepted.
5. Maeda H. Tumor-Selective Delivery of Macromolecular Drugs via the EPR Effect: Background and Future Prospects. *Bioconjugate Chemistry.* 2010;21(5):797-802.
6. Harrington KJ, Mohammadtaghi S, Uster PS, et al. Effective targeting of solid tumors in patients with locally advanced cancers by radiolabeled pegylated liposomes. *Clinical Cancer Research.* 2001;7(2):243-54.
7. Yuan F, Leunig M, Huang SK, et al. Microvascular permeability and interstitial penetration of sterically stabilized (stealth) liposomes in a human tumor xenograft. *Cancer Research.* 1994;54:3352-6.

8. Dreher MR, Liu W, Michelich CR, et al. Tumor vascular permeability, accumulation, and penetration of macromolecular drug carriers. *J Natl Cancer Inst.* 2006;98:335-44.
9. Kong G, Braun RD, Dewhirst MW. Characterisation of the effect of hyperthermia on nanoparticle extravasation from tumor vasculature. *Cancer Research.* 2001;61:3027-32.
10. Kong G, M.W. Dewhirst. Review Hyperthermia and liposomes. *Int J Hyperthermia.* 1999;15(5):345-70.
11. de Smet M, Langereis S, van den Bosch S, et al. SPECT/CT imaging of temperature-sensitive liposomes for MR-image guided drug delivery with High Intensity Focused Ultrasound. submitted.
12. Needham D, Anyarambatla G, Kong G, et al. A new temperature-sensitive liposome for use with mild hyperthermia: characterization and testing in a human tumor xenograft model. *Cancer Res.* 2000;60:1197-201.
13. Working PK, Newman MS, Huang SK, et al. Pharmacokinetics, biodistribution and therapeutic efficacy of doxorubicin encapsulated in stealth® liposomes (Doxil®). *J Liposome Res.* 1994;4(1):667-87.
14. Harashima H, Iida S, Urakami Y, et al. Optimization of antitumor effect of liposomally encapsulated doxorubicin based on simulations by pharmacokinetic/ pharmacodynamic modeling. *Journal of Controlled Release.* 1999;61:93-106.
15. Manzoor AA, Lindner LH, Landon CD, et al. Overcoming Limitations in Nanoparticle Drug Delivery: Triggered, Intravascular Release to Improve Drug Penetration into Tumors. *Cancer Res.* 2012;72(21):5566-75.
16. van Wamel A, Kooiman K, Hartevelde M, et al. Vibrating microbubbles poking individual cells: Drug transfer into cells via sonoporation. *Journal of Controlled Release.* 2006;112(2):149-55.
17. Deckers R, Rome C, Moonen CTW. The role of ultrasound and magnetic resonance in local drug delivery. *Journal of Magnetic Resonance Imaging.* 2008;27:400-9.
18. Yudina A, de Smet M, Lepetit-Coiffe M, et al. Ultrasound-mediated intracellular drug delivery using microbubbles and temperature-sensitive liposomes. *Journal of Controlled Release.* 2011;155(3):442-8.
19. Yudina A, Lepetit-Coiffé M, de Smet M, et al. *In vivo* temperature controlled ultrasound-mediated intracellular delivery of cell-impermeable compounds. *Journal of Controlled Release.* 2012;161:90-7.
20. Lindner LH, Eichhorn ME, Eibl H, et al. Novel temperature-sensitive liposomes with prolonged circulation time. *Clin Cancer Res.* 2004;10:2168-78.
21. Tagami T, Ernsting MJ, Li S-D. Optimization of a novel and improved thermosensitive liposome formulated with DPPC and a Brij surfactant using a robust in vitro system. *Journal of Controlled Release.* 2011;154(3):290-7.
22. Landon CD, Park J, Needham D, et al. Nanoscale drug delivery and hyperthermia: The materials design and preclinical and clinical testing of low temperature-sensitive liposomes used in combination with mild hyperthermia in the treatment of local cancer. *The Open Nanomedicine Journal.* 2011;3:38-64.
23. Anyarambatla GR, D. Needham. Enhancement of the phase transition permeability of DPPC liposomes by incorporation of MPPC: A new temperature-sensitive liposome for use with mild hyperthermia. *J Liposome Res.* 1999;9(4):491-506.
24. Gaber MH, K. Hong, S.K. Huang, D. Papahadjopoulos. Thermosensitive sterically stabilized liposomes: formulation and in vitro studies on mechanism of doxorubicin release by bovine serum and human plasma. *Pharm Res.* 1995;12(10):1407-16.

25. Ickenstein LM, M.C. Arfvidsson, D. Needham, L.D. Mayer, K. Edwards. Disc formation in cholesterol-free liposomes during phase transition. *Biochimica et Biophysica Acta - Biomembranes*. 2003;1614:135-8.
26. Banno B, Ickenstein LM, Chiu GNC, et al. The functional roles of Poly(Ethylene Glycol)-lipid and lysolipid in the drug retention and release from lysolipid-containing thermosensitive liposomes in vitro and in vivo. *Journal of Pharmaceutical Sciences*. 2009.
27. Sandstrom MC, Ickenstein LM, Mayer LD, et al. Effects of lipid segregation and lysolipid dissociation on drug release from thermosensitive liposomes. *J Control Release*. 2005;107:131-42.
28. Paulides MM, Bakker JF, Neufeld E, et al. The HYPERcollar: A novel applicator for hyperthermia in the head and neck. *International Journal of Hyperthermia*. 2007;23(7):567-76.
29. Fatehi D, van der Zee J, de Bruijne M, et al. RF-power and temperature data analysis of 444 patients with primary cervical cancer: Deep hyperthermia using the Sigma-60 applicator is reproducible. *International Journal of Hyperthermia*. 2007;23(8):623-43.
30. Johnson JE, Neuman DG, Maccarini PF, et al. Evaluation of a dual-arm Archimedean spiral array for microwave hyperthermia. *International Journal of Hyperthermia*. 2006;22(6):475-90.
31. Juang T, Stauffer PR, Neuman DG, et al. Multilayer conformal applicator for microwave heating and brachytherapy treatment of superficial tissue disease. *International Journal of Hyperthermia*. 2006;22(7):527-44.
32. Carpentier A, Chauvet D, Reina V, et al. MR-guided laser-induced thermal therapy (LITT) for recurrent glioblastomas. *Lasers in Surgery and Medicine*. 2012;44:361-8.
33. McNichols RJ, Kangasniemi M, Gowda A, et al. Technical developments for cerebral thermal treatment: water-cooled diffusing laser fibre tips and temperature-sensitive MRI using intersecting image. *International Journal of Hyperthermia*. 2004;20(1):45-56.
34. Boreham DR, Gasmann HC, Mitchel REJ. Water bath hyperthermia is a simple therapy for psoriasis and also stimulates skin tanning in response to sunlight. *International Journal of Hyperthermia*. 1995;11(6):745-54.
35. Köhler MO, Mougnot C, Quesson B, et al. Volumetric HIFU ablation under 3D guidance of rapid MRI thermometry. *Medical Physics*. 2009;36(8):3521-35.
36. Hokland SL, Pedersen M, Salomir R, et al. MRI-Guided focused ultrasound: Methodology and applications. *IEEE Transactions on Medical Imaging*. 2006;25(6):723-31.
37. Dromi S, Frenkel V, Luk A, et al. Pulsed-High Intensity Focused Ultrasound and Low Temperature-Sensitive Liposomes for enhanced targeted drug delivery and antitumor effect. *Clin Cancer Res*. 2007;13(9):2722-7.
38. Partanen A, Yarmolenko PS, Viitala A, et al. Mild hyperthermia with magnetic resonance-guided high-intensity focused ultrasound for applications in drug delivery. *International Journal of Hyperthermia*. 2012;28(4):320-36.
39. Lammers T, Aime S, Hennink WE, et al. Theranostic nanomedicine. *Accounts of Chemical Research*. 2011;44(10):1029-38.
40. Ponce AM, Viglianti BL, Yu D, et al. Magnetic Resonance Imaging of temperature-sensitive liposome release: Drug dose painting and antitumor effects. *J Natl Cancer Inst* 2007;99:53-63.
41. Peller M, A. Schwerdt, M. Hossann, H.M. Reinl, T. Wang, S. Sourbron, M. Ogris, L.H. Lindner. MR characterization of mild hyperthermia-induced gadodiamide release from thermosensitive liposomes in solid tumors. *Investigative Radiology*. 2008;43(12):877-92.

42. Langereis S, Keupp J, van Veldhoven JLJ, et al. A temperature-sensitive liposomal 1H CEST and 19F contrast agent for MR Image-guided drug delivery. *J Am Chem Soc.* 2009;131:1380-1.
43. Eakins MN, Eaton SM, Fisco RA, et al. Physicochemical properties, pharmacokinetics and biodistribution of Gadoteridol injection in rats and dogs. *Acad Radiol.* 1995;2:584-91.
44. Hey S, de Smet M, Stehning C, et al. Simultaneous T1 measurements and proton resonance frequency shift based thermometry using variable flip angles. *Magn Reson Med*;67(2):457-63.
45. ten Eikelder HMM, de Smet M, Grüll H. Modelling drug and MRI contrast agent concentrations during local drug delivery with temperature-sensitive liposomes. 12th European Symposium on Controlled Drug Delivery. Egmond aan Zee, the Netherlands 2012.
46. Gasselhuber A, Dreher MR, Negussie A, et al. Mathematical spatio-temporal model of drug delivery from low temperature sensitive liposomes during radiofrequency tumour ablation. *International Journal of Hyperthermia.* 2010;26(5):499-513.
47. Viglianti BL, A.M. Ponce, C.R. Michelich, D. Yu, S.A. Abraham, L. Sanders, P.S. Yarmolenko, T. Schroeder, J.R. MacFall, D.P. Barboriak, O.M. Colvin, M.B. Bally, M.W. Dewhirst. Chemodosimetry of in vivo tumor liposomal drug concentration using MRI. *Magn Reson Med.* 2006;56:1011-8.
48. Abraham SA, K. Edwards, G. Karlsson, S. MacIntosh, L.D. Mayer, C. McKenzie, M.B. Bally. Formation of transition metal-doxorubicin complexes inside liposomes. *Biochim Biophys Acta.* 2002;1565:41-54.
49. Abraham SA, D.N. Waterhouse, D. Lawrence, D. Mayer, P.R. Cullis, T.D. Madden, M.B. Bally. The liposomal formulation of doxorubicin. *Methods Enzymol.* 2005;391:71-97.
50. Chiu GNC, S.A. Abraham, L.M. Ickenstein, R. Ng, G. Karlsson, K. Edwards, E.K. Wasan, M.B. Bally. Encapsulation of doxorubicin into thermosensitive liposomes via complexation with the transition metal manganese. *J Control Release.* 2005;104:271-88.
51. Viglianti BL, S.A. Abraham, C.R. Michelich, P.S. Yarmolenko, J.R. MacFall, M.B. Bally, M.W. Dewhirst. In vivo monitoring of tissue pharmacokinetics of liposome/drug using MRI: illustration of targeted delivery. *Magn Reson Med.* 2004;51:1153-62.
52. Yeo SY. Temperature-sensitive paramagnetic liposomes for image-guided drug delivery: Mn²⁺ versus [Gd(HPDO3A)(H₂O)]. in preparation.
53. Koretsky AP, A.C. Silva. Manganese-enhanced magnetic resonance imaging (MEMRI). *NMR Biomed.* 2004;17:527-31.
54. Silva AC, J.H. Lee, I. Aoki, A.P. Koretsky. Manganese-enhanced magnetic resonance imaging (MEMRI): methodological and practical considerations. *NMR Biomed.* 2004;17:532-43.
55. Federle MP, Chezmar JL, Rubin DL, et al. Safety and efficacy of Mangafodipir Trisodium (MnDPDP) injection for hepatic MRI in adults: Results of the U.S. multicenter phase III clinical trials (safety). *Journal of Magnetic Resonance Imaging.* 2000;12(1):186-97.
56. Karlsson JO, Adolfsson K, Thelin B, et al. First clinical experience with the magnetic resonance imaging contrast agent and superoxide dismutase mimetic mangafodipir as an adjunct in cancer chemotherapy - a translational study. *Translational Oncology.* 2012;5(1):32-8.
57. Penfield JG. Nephrogenic systemic fibrosis and the use of gadolinium-based contrast agents. *Pediatr Nephrol.* 2008;23:2121-9.
58. MacNeil S, Bains S, Johnson C, et al. Gadolinium contrast agent associated stimulation of human fibroblast collagen production. *Investigative Radiology.* 2011;46:711-7.

Ethical paragraph

Cancer is one of the leading causes of death worldwide and according to the World Health Organization the number of deaths are projected to continue rising, with an estimated 13.1 million deaths in 2030 (www.who.int). Therefore, research to explore new cancer treatments is of utmost importance in order to improve the treatment efficacy and reduce the treatment burden on patients. In this thesis, a new non-invasive treatment of tumors using a temperature-sensitive drug delivery system for local chemotherapy was investigated. As much as possible, all assays were developed and used *in vitro* avoiding unnecessary animal studies. However, for clinical translation of these new developed drug delivery systems, it is essential to gain knowledge about their behavior *in vivo*. For medical and ethical reasons, these new systems cannot be tested directly into humans; therefore the use of an animal model was the only option for the final tests.

All preclinical studies performed for this thesis were approved by the animal welfare committee of Maastricht University (the Netherlands). For each experiment, the amount of animals used, as well as the discomfort they experienced, was weighed against the importance of the obtained data. The maintenance and care of the experimental animals was in compliance with the guidelines set by the institutional animal care committee, accredited by the National Department of Health.

Summary

In this thesis, temperature-sensitive liposomes co-encapsulating the chemotherapeutic drug doxorubicin and the MRI contrast agent [Gd(HPDO3A)(H₂O)] were investigated for the use of Magnetic Resonance-guided High Intensity Focused Ultrasound (MR-HIFU)-mediated local drug delivery.

In **Chapter 2**, the preparation and *in vitro* characterization of different liposomal formulations is discussed. Two temperature-sensitive systems (LTSL and TTSL) were investigated and non-temperature sensitive liposomes were used as a control. The co-release of doxorubicin together with [Gd(HPDO3A)(H₂O)], a paramagnetic MRI contrast agent, from the aqueous lumen of liposomes was studied in great detail. The composition of the lipid bilayer determined the leakage of doxorubicin at body temperature as well as the release kinetic at elevated temperatures. The LTSL showed a higher leakage of doxorubicin at 37 °C, but a faster release of doxorubicin at 42 °C compared to the TTSL system.

The biodistribution of free doxorubicin and [Gd(HPDO3A)(H₂O)] is well known, however encapsulation into liposomes alters the biodistribution of these compounds radically. Altered drug and contrast agent distribution, coupled with tissue-dependent differences in metabolism of these compounds, could play an important role in therapeutic effects and toxicity. Therefore, it is important to study the biodistribution of all the injected compounds. In **Chapter 3**, two different methods for quantification of doxorubicin in blood and tissue samples were setup and validated. One is based on the quantification of doxorubicin fluorescence with High Performance Liquid Chromatography (HPLC) after chemical extraction. The other method requires the use of ¹⁴C-labeled doxorubicin, which is a β-emitter that can be quantified with Liquid Scintillation Counting.

Subsequently, the blood kinetics and biodistribution of ¹¹¹In-labeled temperature-sensitive liposomes and their encapsulated compounds, doxorubicin and the MRI contrast agent [Gd(HPDO3A)(H₂O)], was investigated in **Chapter 4**. The influence of HIFU-mediated local hyperthermia of the tumor on the biodistribution was studied using SPECT/CT imaging. The highest uptake of ¹¹¹In-labeled TSLs was observed in the spleen and liver and was similar for the control and HIFU-treated rats. Although a large intratumoral variation was found, HIFU-mediated hyperthermia of the tumor resulted in a 4.4-fold higher uptake of the radiolabeled TSL in the tumor (t = 48h) compared to control experiments without HIFU, while the doxorubicin concentration was increased by a factor 7.9. This increased accumulation of doxorubicin-filled liposomes at longer time points may have an important contribution to the therapeutic outcome of HIFU-mediated drug delivery.

In **Chapter 5**, an *in vivo* proof-of-concept study for image-guided local drug delivery was performed. The local temperature-triggered release of [Gd(HPDO3A)(H₂O)] was monitored with interleaved T_1 mapping of the tumor tissue and correlated with the co-release of doxorubicin. A good correlation between the ΔR_1 , the uptake of doxorubicin and the gadolinium concentration in the tumor was found, implying that the *in vivo* release of doxorubicin from TSLs can be probed *in situ* with the longitudinal relaxation time of the co-released MRI contrast agents. Furthermore, an increase with a factor of 11 of doxorubicin concentrations in the tumor at 90 min after TSL injection was observed due to HIFU treatment.

In **Chapter 6**, the intratumoral distribution of the TSLs and their encapsulated compounds was investigated, after HIFU-mediated hyperthermia induced local drug release. The presence of radiolabeled liposomal carriers and the intratumoral distribution of doxorubicin were imaged *ex vivo* with autoradiography and fluorescence microscopy, respectively. In hyperthermia treated tumors, liposomes were distributed more homogeneously across the tumor than in the control tumors. At 48h after injection, the liposomal accumulation in the tumor was enhanced in the hyperthermia group in comparison with the controls. In control tumors, doxorubicin uptake was observed in endothelial cells only, while in the HIFU-treated tumors the delivered drug was spread over a much larger area and was also taken up by tumor cells at a larger distance from blood vessels.

Finally, the therapeutic effect of the HIFU-mediated hyperthermia treatment with administration of TSLs was studied and compared with saline, free doxorubicin and clinically available non-temperature sensitive liposomal doxorubicin (Caelyx®) (**Chapter 7**). TSL+HIFU showed a 2 to 4-fold increase in the time to reach two times the initial tumor size in comparison with the other groups. Furthermore, a correlation was found between the ΔR_1 and the relative tumor size after 7 days, showing that the MR measurements can be used as a prediction for the therapeutic effect.

Dankwoord

Werk je nu voor de TU of voor Philips? Dat is een vraag die ik de afgelopen vier jaar ontelbare keren heb moeten beantwoorden. Toch was het wat mij betreft een ideale situatie om bij zowel een universiteit als een bedrijf mijn promotieonderzoek te kunnen doen. Ik heb veel kunnen leren over het bedrijfsleven, maar kon ook altijd rekenen op de steun van de TU/e voor een goed verloop van mijn promotietraject. Bovendien ben ik verwend met een buitengewoon luxe laboratorium en er stonden altijd overal mensen klaar om me te helpen. Ik maak graag van deze gelegenheid gebruik om iedereen te bedanken die aan mijn mooie promotietijd heeft bijgedragen. Een aantal mensen zou ik in het bijzonder willen vermelden.

Holger, ik ben heel dankbaar dat jij mijn professor was. Met al je enthousiasme sta je altijd open voor nieuwe ideeën. Ik heb van jou geleerd om niet te denken in problemen, maar in oplossingen. Voor bijna elk experiment dat we bedachten werd er wel een manier gevonden om het uit te kunnen voeren. Ik heb het altijd erg gewaardeerd dat je je AIOs overal zoveel mogelijk bij betreft. Mede hierdoor zijn we ook een gezellige en hechte groep geworden. We hebben ontelbare leuke dingen samen meegemaakt. Ik heb de afgelopen vier super mooie jaren van mijn leven voor een groot deel aan jou te danken!

Sander, heel erg bedankt voor alle hulp. Ik heb veel geleerd van je energieke en enthousiaste manier van werken, maar ook van je vermogen om dingen te relativiseren. Voor artikelen, abstracts en hoofdstukken voor mijn boekje heb ik altijd kunnen rekenen op jouw kritische blik. Gezellig biertjes drinken in München, hardlopen op het strand in Egmond aan Zee of langs de rivier in Tours, roeien op een idyllisch meer in Bled; het zijn allemaal mooie momenten die we de afgelopen vier jaar samen hebben meegemaakt en die ik niet snel zal vergeten!

Ik heb erg genoten van de samenwerking, besprekingen en gezelligheid die ik heb beleefd met onze eigen AIO groep. Onze reisjes naar Cochem en Dresden waren geweldig, we hebben samen de halve marathon gerend en de voetbal en volleybal toernooitjes konden altijd rekenen op onze deelname. Maar daarnaast kon ik ook onze samenwerking in het lab erg waarderen. Iedereen was altijd bereid om iemand anders te helpen en dit creëerde een hele fijne werksfeer. Nicole, bedankt voor alle keren dat ik een beroep op je kon doen als de HIFU weer eens niet deed wat ik wilde. Onze reis naar Japan was een mooie belevenis. Ik heb altijd met veel plezier met je samengewerkt, hopelijk kunnen we dit nog afsluiten met een mooi artikel over onze supercombi behandeling. Pedro, we had so much fun at the Sonodrugs meetings. You were the best social committee member! Luc, jouw kritische blik gaf vaak weer nieuwe inzichten. Bedankt daarvoor. Tiemen, je was een gezellige kamergenoot. Bedankt voor de leuke achtergrond muziek en sorry dat ik altijd de verwarming zo hoog zette. Sin Yuin, about 4 years ago you performed your external internship project with me. I am very happy that one year later you returned as a PhD

student in our group. I am looking forward to the next clash of the cultures dinner. Sander, bedankt voor alle tips voor het maken van dit boekje en ik wens je veel succes met je postdoc in de VS. Anke, jij was altijd de mama van de groep en het grote voorbeeld van ons allemaal. Bedankt voor alle gezelligheid en goede raad. Esther, ik heb van je genoten om te zien met hoeveel enthousiasme en doorzettingsvermogen je je afstuderen hebt afgerond en vind het heel leuk dat je nu ook begonnen bent als AIO bij ons in de groep. Met veel vertrouwen draag ik het stokje aan je over.

Met heel veel plezier heb ik samengewerkt met vele mensen van Philips Research Eindhoven. Allemaal erg bedankt voor alle gezelligheid in en buiten het lab! Edwin, hartelijk bedankt voor je hulp met de HIFU experimenten. Sandra, ik ben blij dat jij voor AMIGDD bent komen werken. Met een gerust hart laat ik de *in vivo* liposoom experimenten aan jou over. Katia, thanks for your help with the SPECT experiments and with the setup of the liquid scintillation counting. Rolf, bedankt voor de MRI tips en sorry voor alle scantijd die ik van je heb afgepakt. Raffa, thanks a lot for your valuable advices for the radiolabeling experiments and for all your efforts to keep the RC-lab tidy. Tilman, bedankt voor de gezelligheid in het lab, helaas was ons gelabelde doxorubicin experiment geen groot succes. Johan en Erica, bedankt voor alle scheikunde bijlessen en het maken van lipiden, zonder jullie was het chemielab vast niet zo netjes. Marc, bedankt voor je commentaar op hoofdstuk 3 van dit boekje. Ik wens je veel succes met je bedrijf. Marcel, jij was de allerleukste werkpakket leider. Als ik het ooit nog eens koud heb, dan weet ik wat me te doen staat. Charles, je hebt ons goed onder de duim gehouden als Sonodrugs projectleider. Bedankt voor alle aanmoediging (lees 'reminders') en het zorgvuldig afronden van het project. Gerry, Dirk, Frenk en Andy, bedankt dat ik altijd met vragen bij jullie terecht kon en voor de ondersteuning in het lab. Suzanne, bedankt voor de hulp met het opzetten van de ¹⁴C experimenten en sorry dat je zo vaak voor mij moest poetsen. Jeroen en Daniëlle bedankt voor de NMR metingen, Jeannette en Carry voor de ICP-MS analyses en Marcel en Monja voor de Cryo-TEM experimenten.

Een groot deel van de resultaten in dit boekje heb ik te danken aan een groep gezellige meiden; Caren, Carlijn, Melanie, Monique en Marleen; dankzij jullie hulp heb ik efficiënt en nauwkeurig mijn dieren experimenten kunnen uitvoeren. Zonder jullie was dit boekje behoorlijk leeg geweest. Iris, heel erg bedankt voor alle hulp en adviezen voor de DEC protocollen en ontelbare wijzigingen die ik heb aangevraagd.

Biomedical NMR groep, het grootste deel van de tijd zaten we in verschillende gebouwen en zagen we elkaar alleen op de vakgroepmeeting. Desondanks hebben we toch veel gezellige dingen samen meegemaakt, zoals kroegentochten, kerstdiners, het weekend in de Ardennen en natuurlijk de zeskamp! Klaas, met veel plezier heb ik mijn afstudeerproject bij u gedaan. Tijdens mijn promotie was u altijd erg geïnteresseerd in mijn

onderzoek. Bedankt voor al uw kritische vragen en nieuwe ideeën die tijdens MIB's en groepmeetings naar boven kwamen, deze hebben vaak weer tot nieuwe inzichten geleid.

I would like to thank all members of the Sonodrugs project. I appreciated the interactions and collaborations between the different partners and I always enjoyed the Sonodrugs meetings. Chrit, bedankt dat ik een paar maanden welkom was op uw lab in Bordeaux, ik heb er een leuke en leerzame tijd gehad. Anna, Silke and Matthieu, thanks for the fruitful collaboration. Kostas and Wafa, thanks for the interesting discussions we had within workpackage 3. Huub, bedankt voor je werk aan het farmacokinetisch model.

Ook buiten het werk heb ik de afgelopen jaren veel leuke dingen beleefd. Kitty, Michiel, Marnix, Gijs en Bram, jullie zijn top bestuursgenootjes en ik vind het heel gezellig dat we nog steeds af en toe een leuk weekendje er tussenuit gaan met z'n zessen. Bram, je was voor mij een goed voorbeeld en tegelijkertijd ook mijn grootste fan. Ik ben blij dat je mijn paranimf wilt zijn.

Pusphaira dames, bedankt voor alle gezelligheid op en buiten het voetbalveld. Altijd fijn om na een zware werkdag even lekker een balletje te trappen. Veel van jullie zijn naast mijn teamgenootjes ook goede vriendinnen geworden. Eef, we hebben samen veel leuke dingen meegemaakt, waaronder twee fantastische reizen naar Singapore/Maleisië/Thailand en Zuid-Afrika. Ik vind het heel leuk dat je mijn paranimf bent.

Papa en mama, bedankt dat jullie mij altijd de kans hebben geboden om te doen wat ik leuk vind. Ik ben heel blij dat ik zo'n lieve ouders heb.

Lieve Paul, bedankt dat je altijd achter me staat. Jij zorgt ervoor dat ik nooit vergeet dat het allerbelangrijkste is om zoveel mogelijk van het leven te genieten. Bedankt voor alles!

List of Publications**Full papers**

1. **M. de Smet**, S. Langereis, S. van den Bosch and H. Grüll. Temperature-sensitive liposomes for doxorubicin delivery under MRI guidance. *Journal of Controlled Release*. 2010; 143(1): 120-7.
2. **M. de Smet**, E. Heijman, S. Langereis, N.M. Hijnen and H. Grüll. Magnetic resonance imaging of high intensity focused ultrasound mediated drug delivery from temperature-sensitive liposomes: An in vivo proof-of-concept study. *Journal of Controlled Release*. 2011; 150(1): 102-10.
3. S. Hey, **M. de Smet**, C. Stehning, H. Grüll, J. Keupp, C.T.W. Moonen and M. Ries. Simultaneous T_1 measurements and proton resonance frequency shift based thermometry using variable flip angles. *Magnetic Resonance in Medicine*. 2011; 67: 457-3
4. A. Yudina, **M. de Smet**, M. Lepetit-Coiffe, S. Langereis, H. Grüll and C.T.W. Moonen. Ultrasound-mediated intracellular drug delivery using microbubbles and temperature-sensitive liposomes. *Journal of Controlled Release*. 2011; 155(3):442-8.
5. A. Yudina, M. Lepetit-Coiffe, **M. de Smet**, S.Langereis, H.Grüll and C.T.W. Moonen. In vivo temperature controlled ultrasound-mediated intracellular delivery of cell-impermeable compounds. *Journal of Controlled Release*. 2012; 161: 90-7
6. G.S. van Bochove, H.M.H.F. Sanders, **M. de Smet**, H.M.Keizer, W.J.M.Mulder, R.Krams, G.J.Strijkers and K.Nicolay. Molecular MR imaging of collagen in mouse atherosclerosis using paramagnetic CNA35-micelles. *European Journal of Inorganic Chemistry*. 2012; 12: 2115-25.
7. **M. de Smet**, N.M. Hijnen, S. Langereis, A. Elevelt, E. Heijman, L. Dubois, P. Lambin and H. Grüll. Magnetic Resonance guided High Intensity Focused Ultrasound (MR-HIFU) mediated hyperthermia improves the intratumoral distribution of temperature-sensitive liposomal doxorubicin. *Investigative Radiology*, accepted for publication, 2013
8. **M. de Smet**, S. Langereis, S. van den Bosch, K. Bitter, N.M. Hijnen, E. Heijman and H. Grüll. SPECT/CT imaging of temperature-sensitive liposomes for MR-image guided drug delivery with High Intensity Focused Ultrasound. Submitted
9. **M. de Smet**, S. van den Bosch, K. Donato, K. Bitter, M. Hossann, A.H. Negussie, M.R. Dreher, S. Langereis, B.J. Wood, L.H. Lindner and H. Grüll. Validation of doxorubicin quantification methods in tissue and blood samples – a multi-centre comparison. In preparation

Abstracts (first author only)

1. **M. de Smet**, A. Yudina, M. Lepetit-Coiffe, S. Langereis, R. Deckers, H. Gröll and C. Moonen. Temperature-controlled US-mediated intracellular delivery of a fluorescent cell-impermeant model drug using temperature sensitive liposomes and cavitation. WMIC 2009, Montreal, Canada.
2. **M. de Smet**, S. Langereis, R. van den Molengraaf, E. Heijman, N.M. Hijnen and H. Gröll. HIFU-mediated doxorubicin release from temperature-sensitive liposomes under MRI guidance. Biomedica Life Science Summit 2010, Aachen, Germany.
3. **M. de Smet**, S. Langereis, R. van den Molengraaf and H. Gröll. Temperature sensitive liposomes for drug delivery with MRI-HIFU. ISMRM Benelux 2010, Utrecht.
4. **M. de Smet**, S. Langereis, R. van den Molengraaf, E. Heijman, N.M. Hijnen and H. Gröll. Temperature sensitive liposomes for drug delivery with MRI-HIFU. ISMRM 2010, Stockholm.
5. **M. de Smet**, E. Heijman, S. Langereis, N.M. Hijnen and H. Gröll. Temperature-induced drug delivery under MR image guidance. ISMRM Benelux 2011, Roosendaal.
6. **M. de Smet**, S. Langereis, E. Heijman, N.M. Hijnen and H. Gröll. MRI-guided HIFU-mediated drug delivery to tumors with temperature-sensitive liposomes. TOPIM - ESMI Winter Conference 2011, Les Houches, France.
7. **M. de Smet**, S. Langereis, E. Heijman, N.M. Hijnen and H. Gröll. Local drug delivery with temperature sensitive liposomes under MR image guidance. Biomedica Life Science Summit 2011, Eindhoven.
8. **M. de Smet**, S. Langereis, E. Heijman, N.M. Hijnen and H. Gröll. HIFU-mediated local drug delivery under MR image guidance. European Society of Hyperthermic Oncology 2011, Aarhus, Denmark.
9. **M. de Smet**, S. Langereis, E. Heijman, N.M. Hijnen and H. Gröll. MR monitoring of HIFU-mediated local drug delivery with temperature sensitive liposomes. 6th European Molecular Imaging Meeting, 2011, Leiden.
10. **M. de Smet**, N.M. Hijnen, L. Dubois, P. Lambin and H. Gröll. Intratumoral distribution of doxorubicin after HIFU-mediated delivery with temperature sensitive liposomes. 12th European Symposium on Controlled Drug Delivery 2012, Egmond aan Zee.
11. **M. de Smet**, S. Langereis, N.M. Hijnen, E. Heijman and H. Gröll. Blood kinetics and biodistribution of temperature sensitive liposomes for image guided drug delivery with MR-HIFU. 12th European Symposium on Controlled Drug Delivery, 2012, Egmond aan Zee.

12. **M. de Smet**, N.M. Hijnen and H. Grüll. Combined tumor treatment with local drug delivery from temperature sensitive liposomes and High Intensity Focused Ultrasound ablation. Biomedica Life Science Summit 2012, Liege, Belgium.
13. **M. de Smet**, N.M. Hijnen, S. Langereis, E. Heijman and H. Grüll. Biodistribution of temperature-sensitive liposomes for MR-image guided drug delivery. The 11th International Congress of Hyperthermic Oncology 2012, Kyoto, Japan.
14. N.M. Hijnen, **M. de Smet** and H. Grüll. Improved intratumoral distribution of temperature-sensitive liposomes and doxorubicin after combined hyperthermia and ablation treatment. The 11th International Congress of Hyperthermic Oncology 2012, Kyoto, Japan.

Invited presentations

1. **M. de Smet**, N.M. Hijnen, S. Langereis, E. Heijman and H. Grüll. Image guided drug delivery with temperature sensitive liposomes using MR-HIFU. Annual meeting hyperthermia working party of the Dutch Cancer Society, 2011, Amsterdam.
2. **M. de Smet**, N.M. Hijnen, S. Langereis, E. Heijman and H. Grüll. Intratumoral distribution of temperature sensitive liposomal doxorubicin after HIFU-mediated local hyperthermia and ablation. KWF Hyperthermia working group meeting, 2012, Eindhoven.
3. **M. de Smet**, N.M. Hijnen, S. Langereis, E. Heijman and H. Grüll. Image-guided HIFU-mediated drug delivery using temperature-sensitive liposomes. Instituut Verbeeten, 2012, Tilburg.

Patent applications

1. H. Grüll, S. Langereis, **M. de Smet**, M. Bohmer, A. Yudina and C. Moonen. Two step ultrasound protocol for drug delivery. WO036619 A2, March 31, 2011
2. S. Langereis, H. Grüll, **M. de Smet**, E. Aussems-Custers and J. Lub. Temperature-sensitive systems containing mixed short/long chain phosphatidylcholines for IGDD. WO053047, July 8, 2011

Curriculum Vitae



Mariska de Smet was born on March 9th 1983 in Oostburg, the Netherlands. She completed her secondary education (VWO) in 2001 at the Zwin College in Oostburg. In the same year, she started studying Biomedical Engineering at the Eindhoven University of Technology. During this study, she spent one year in the board of the study association of Biomedical Engineering 'Protagoras'. Also, she performed an internship at the Robarts Research Institute in London, Ontario, Canada, under supervision of prof. Brian Rutt. In 2008, she obtained her MSc degree with great appreciation in the Biomedical NMR group of prof. Klaas Nicolay, where she

studied the use of CNA35-micelles for Magnetic Resonance Imaging of collagen in atherosclerotic plaques. Subsequently, she performed her PhD project with prof. Holger Gröll at the Biomedical NMR group of the TU Eindhoven in collaboration with the Minimally Invasive Healthcare group of Philips Research Eindhoven. During this period, she developed and tested temperature-sensitive liposomes for local drug delivery to tumors using High Intensity Focused Ultrasound heating under MR-image guidance. The most important results of her PhD research are described in this thesis. As of March 2013 she works at the Catharina Hospital in Eindhoven as a Medical Physicist trainee in the field of radiotherapy.